FABRICATION AND CHARACTERIZATION OF MODIFIED MACROPOROUS BIOCERAMICS FOR BONE REGENERATION

Isabel Alexandra Fernandes Lemos

Dissertação elaborada para a obtenção do Grau de Doutor em Ciências de Engenharia pela Faculdade de Engenharia da Universidade do Porto

FEUP, 2008

THIS THESIS WAS SUPERVISED BY:

Professor Doutor José Maria da Fonte Ferreira

Departamento de Engenharia Cerâmica e do Vidro da Universidade de Aveiro

Professor Doutor José Domingos da Silva Santos

Faculdade de Engenharia da Universidade do Porto

THE HOST INSTITUTIONS OF THIS THESIS WERE:

Departamento de Engenharia Cerâmica e do Vidro, DECV

Universidade de Aveiro, Portugal

Laboratório de Biomateriais, INEB - Instituto de Engenharia Biomédica

Universidade do Porto, Portugal

Departamento de Engenharia Metalúrgica e de Materiais, DEMM

Faculdade de Engenharia

Universidade do Porto, Portugal

… to the memory of my brother, Rui

… to my parents, Ana and Elias

… to my syster, Lisinha

THIS THESIS WAS BASED ON THE FOLLOWING PUBLICATIONS:

AF Lemos, D Arcos, M Vallet-Regí, and JMF Ferreira. Rietveld analysis and phase evolution with heat treatment temperature of calcium phosphates with different Ca/P ratios. Submitted to publication in Journal of the European Ceramic Society.

AF Lemos, D Arcos, M Vallet-Regí, and JMF Ferreira. Rietveld analysis of magnesium substituted biphasic mixtures and influence of heat treatment temperature on phase evolution. Submitted to publication in Journal of the European Ceramic Society.

AF Lemos, M Vallet-Regí, and JMF Ferreira. Rietveld analysis and phase evolution with heat treatment temperature of biological-like calcium phosphates. Submitted to publication in Journal of the European Ceramic Society.

AF Lemos and JMF Ferreira. Colloidal processing and mechanical performance of biological-like calcium phosphates. Submitted to publication in Journal of the American Ceramic Society.

AF Lemos and JMF Ferreira. Designing of porous calcium phosphate scaffolds for different orthopaedic applications. Submitted as feature article to publication in Journal of the American Ceramic Society.

AF Lemos, JD Santos and JMF Ferreira. Preparation and physicochemical characterisation of bone-like hydroxyapatite/PLGA hybrid materials for biomedical applications. Submitted to publication in Journal of Biomedical Materials Research.

AF Lemos, CB Machado, P Valério, AM Goes and JMF Ferreira. Comparison of osteoblast responses to macroporous biological-like apatites and to biological-like apatites/plga hybrid materials. Submitted to publication in Biomaterials.

ACKNOWLEDGMENTS

Along the most important moments of our life, there are a lot of persons that pass and leave deep marks that we will never forget. This was definitely one of the moments in which I felt the strong presence of several persons to whom I can not forget to acknowledge.

First I would like to thank Professor José Maria Ferreira, my supervisor, for the opportunity of working in the fascinating world of biomaterials, for his support, encouragement, patience, friendship and opportunities he gave me all over the years I have been working with him. Thanks for trusting me, leaving me always the freedom to fly alone.

I had the privilege of working in DECV where I found not only excellent researchers to share experiences and learn with, but also good friends that I will keep for life. I would like to thank to my laboratory colleagues, whose friendship goes beyond laboratory relationship and who have also provided me with a considerable enrichement of knowledge of my work due to their excellent competence. Thanks for the good moments that we had in laboratory, the support, patience, collaboration and friendship been expressed in a smile that sometimes persisted in do not appearing.

Thank you very much to ÁgoraMat for the willingness they gave me to proceed with this thesis, their trust, encouragement and support.

During my stage in Brazil I have found a lot of friends that I will keep always in my heart. To all of them I would like to express my gratitude for their hospitality, friendship, and crazy moments and for showing me the wonderful world of cells.

There are no words to express how much I am grateful to my wonderful family for the invaluable support, unconditional love and encouragement. Special thanks to my parents that I adore, for everything they do for me. I am very proud for being their daughter and to take part in their lives. Thanks for the strength, courage and determination they pass

me and for never let me give up of my dreams. Special thanks to my sister, which is my best friend, for her maturity and for show me all the time which is the best way to go.

Thank you very much Paulo for your infinite patience, for being always unconditionally present when I needed you most, for trusting and encouraging me and for giving me the willpower to carry on my work.

My last thanks goes to my brother that even if not present, always guide me, shinning strongly in the moments that I need him most. Thanks for be my guardian angel!

ABSTRACT

Biomaterials are all kinds of materials that interact with biological systems to treat, strengthen or replace tissue, an organ or a body function. There has been an ever increasing need for new biomaterials, products and surgical techniques. Some of the main motivations behind the development of new synthetic biomaterials include:

- The growth of life expectancy, resulting in increased incidence of degenerative diseases such as osteoporosis;
- Excessively sedentary lifestyles resulting in degenerative osteoarthritis;
- Increased participation in sports causing serious trauma injuries;
- The refusal of the public to tolerate the slightest limitations in mobility;
- Increasing awareness among patients and doctors of the numerous co-morbidities associated with autograft harvesting;
- The elevated regulatory scrutiny and recalls imposed on allograft tissue banks for distributing human bone and soft tissue products that were improperly screened for infectious diseases.

Bone is a live tissue with a macroporous structure consisting of a hybrid organic-inorganic matrix constituted mainly by inorganic calcium phosphates (~70%), and organic components (~30%) that include collagen fibres, marrow cells and osseous cells. The inorganic part is composed of carbonated calcium deficient hydroxyapatite, often represented by a biphasic mixture of stoichiometric hydroxyapatite [HA, $Ca_5[(PO_4)_3(OH)]$ and β-tricalciumphosphate [β-TCP, β-$Ca_3(PO_4)_2$]. Moreover, biological apatites contain trace elements that play essential roles in bone metabolism.

The actual trend towards shifting away from autografts to bone graft substitutes, and from cadaver allografts to synthetics faces the big challenge of mimicking the living tissue from the mechanical, chemical, biological and functional points of view. This challenge has been undertaken in the present work. Accordingly, co-substituted biphasic calcium phosphates (BCP) comprising biological like HA (BL-HA - mixtures of HA and β-TCP doped with some essential trace elements found in the biological apatite) were given preference as the inorganic part of the developed synthetic bone substitutes, in detriment of pure single-phase HA or β-TCP components, while biopolymers, including polylactic acid (PLA), polyglycolic acid (PGA), or their co-polymers (PLGA) were thought as potential substitutes for the organic part of the bone.

The overall work carried out comprised the preparation and full characterisation of calcium phosphate powders with different compositions, the preparation of high concentrated suspensions from the powders that were used to prepare dense bodies, porous parts granular materials, porous scaffolds resembling the cortical, the trabecular, or the complete bone structure via traditional and emerging consolidation techniques. Silane-coupling agents were used to efficiently bond the inorganic and organic phases through an electrostatic/chemical interaction and to obtain hybrid composite scaffolds with controlled porous structures aiming at obtaining synthetic substitutes for bone regeneration and systems for local controlled delivery of therapeutic molecules.

Sintered inorganic specimens and the hybrid composite scaffolds were characterised for their physical properties (mechanical strength, porosity fraction, pore sizes). The ability of BL-HA and of the BL-HA/PLGA hybrid materials to mineralise was investigated in simulated body fluids (SBF). It was observed that the immersion of these materials in SBF easily induced the formation of an apatitic carbonate layer on its surface. The *in vitro* biocompatibility of these synthetic substitutes evaluated in cultured osteoblastic cells, in terms of cytoxicity and cell proliferation revealed that BL-HA and BL-HA/PLGA hybrid materials are cytocompatible, promoting proliferation of osteoblastic cells, conferring them a good potential for bone regeneration and maxillofacial applications.

RÉSUMÉ

Biomatériaux ce sont tous les types de matériaux qui interagissent avec des systèmes biologiques pour guérir, renforcer ou remplacer un tissu, un organe ou une fonction corporelle. Il y a eu une croissance constante du besoin de nouveaux biomatériaux, de produits et de techniques chirurgicales. Les motivations qui se cachent derrière le développement de nouveaux matériaux synthétiques incluent :

- La croissance de l'espoir moyen de vie, dont le résultat est la croissance de l'incidence de maladies dégénératives tel que l'ostéoporose ;
- Des styles de vie excessivement sédentaires résultant en osteoartrite dégénérative ;
- La participation croissante dans des sports causant diverses blessures traumatiques ;
- Le refus du public d'accepter de légères limitations de mobilité ;
- La croissante prise de conscience entre patients et docteurs de nombreuses co-morbidités associées à l'utilisation d'autogreffes ;
- Le scrutin de plus en plus exigeant, et les reprises imposées de greffes de cadavre qui n'ont pas été contrôlées adéquatement par rapport aux maladies infectieuses.

L'os est un tissu vivant avec une structure macroporeuse consistant en une matrice hybride organique-inorganique constituée principalement par des phosphates de calcium inorganiques (~70%) et des composants organiques (~30%) qui incluent des fibres de collagène, des cellules de moelle et des cellules d'os. La partie inorganique est composée par hydroxiapatite carbonatée déficitaire en calcium, souvent représentée par un mélange biphasique d' hydroxiapatite stéchiométrique [HA, $Ca_5(PO_4)_3(OH)$] et β-phosphate tricalcique [β-TCP, β-$Ca_3(PO_4)_2$]. De plus, les apatites biologiques contiennent des éléments vestigiaux qui tiennent un rôle essentiel dans le métabolisme de l'os. La tendance actuelle dans le sens de l'éloignement des autogreffes face aux remplacements de greffes osseuses, et des allogreffes de cadavre par des synthétiques va à la rencontre du grand défi d'imiter le tissu vivant du point de vue mécanique, chimique, biologique et fonctionnel. Ce défi a été pris en considération dans le présent travail. Dans ce sens, nous avons donné préférence aux phosphates de calcium

biphasiques co-remplacés (BCP) comprenant HA type biologique (BL-HA – mélanges de HA et β-TCP dopé avec quelques éléments vestigiaux essentiels trouvés dans les apatites biologiques) comme la partie inorganique des remplacements osseux développés, en détriment de la HA ou β-TCP pures, tandis que biopolimères incluant l'acide polilactique (PLA), l'acide poliglicolique (PGA) ou ses copolimères (PLGA), ont été pensés comme de potentiels remplaçants de la partie organique de l'os.

Tout le travail développé comprend la préparation et complète caractérisation des poudres de phosphates de calcium à différentes compositions, la préparation de suspensions fortement concentrées qui ont été utilisées pour préparer des corps denses, des parties poreuses, des matériaux granulaires, des supports poreux qui ressemblent à la partie corticale, trabeculaire ou à la structure complète de l'os à travers des techniques traditionnelles et des techniques de consolidation émergentes.

Des agents d'accouplage du type silane ont été utilisés pour lier efficacement les phases organique et inorganique à travers des interactions éléctrostatiques/chimiques et pour obtenir des supports composites hybrides avec une structure poreuse contrôlée, visant obtenir des remplaçants synthétiques pour la régénération de l'os et des systèmes pour la libération locale contrôlée de molécules thérapeutiques.

Les propriétés physiques (résistance mécanique, fraction de porosité, taille des pores) des échantillons inorganiques frittage et de supports composites hybrides ont été évaluées. L'habilité de BL-HA et des matériaux hybrides BL-HA/PLGA pour minéraliser a été recherchée dans des fluides semblables aux fluides corporels (SBF). Nous avons vérifié que l'immersion de ces matériaux en SBF induit facilement la formation d'une couche apatitique carbonatée dans sa surface. La biocompatibilité *in vitro* de ces remplaçants synthétiques évaluée en culture d' osteoblastes, en thermes de citotoxicité et prolifération cellulaire, a révélé que BL-HA et les matériaux hybrides BL-HA/PLGA sont citocompatibles, favorisant la prolifération des osteoblastes, leur conférant un bon potentiel pour la régénération de l'os et la reconstruction maxilofaciale.

RESUMO

Biomateriais são todos os tipos de materiais capazes de interagir com sistemas biológicos para tratar, fortalecer ou substituir um tecido, um órgão ou uma função corporal. A necessidade de novos biomateriais, produtos e técnicas cirúrgicas tem vindo a crescer de forma contínua. Algumas das motivações para o desenvolvimento de novos biomateriais sintéticos incluem:

- O crescimento da esperança média de vida, resultando no crescimento da incidência de doenças degenerativas como a osteoporose;
- O sedentarismo, resultando em osteoartrite degenerativa;
- Participação crescente em desportos causando ferimentos traumáticos;
- A recusa do público para tolerar mesmo ligeiras limitações na sua mobilidade;
- O maior nível de consciencialização por parte dos pacientes e dos médicos acerca da morbidez associada à recolha de auto enxertos;
- O escrutínio cada vez mais exigente, e as retomas impostas de enxertos de cadáver que não tenham sido adequadamente controlados relativamente a doenças infecciosas.

O osso é um tecido vivo com uma estrutura macroporosa consistindo de uma matriz híbrida orgânica-inorgânica constituída principalmente por fosfatos de cálcio (~70%) e componentes orgânicos (~30%) que incluem fibras de colagénio, células da medula e células ósseas. A parte inorgânica é composta por hidroxiapatite carbonatada deficiente em cálcio, muitas vezes representada por uma mistura bifásica de hidroxiapatite estequiométrica [HA, $Ca_5[(PO_4)_3(OH)]$ e β-fosfato tricálcico [β-TCP, β-$Ca_3(PO_4)_2$]. Além disso, as apatites biológicas contêm elementos vestigiais que desempenham um papel essencial no metabolismo do osso. A tendência actual de substituir os auto enxertos por enxertos ósseos, e os enxertos de cadáver por materiais sintéticos, depara-se com o grande desafio de imitar o tecido vivo do ponto de vista mecânico, químico, biológico e funcional. Foi este desafio que motivou o presente trabalho. Neste sentido, deu-se preferência a fosfatos de cálcio bifásicos co-substituídos (BCP) com composição próxima da HA biológica (BL-HA – misturas de HA e β-TCP dopadas com os principais elementos vestigiais encontrados nas apatites biológicas) como a parte inorgânica, em detrimento da HA ou β-TCP puros, enquanto biopolímeros como o ácido

poliláctico (PLA), o ácido poliglicólico (PGA) ou os seus copolímeros (PLGA), foram usados como potenciais substitutos da parte orgânica do osso.

O trabalho realizado incluiu a preparação e a caracterização completa de pós de fosfato de cálcio com composições diferentes, a preparação de suspensões muito concentradas para a consolidação de corpos densos, porosos, materiais granulares, enxertos com estrutura porosas semelhantes às partes cortical, trabecular, ou à constituição completa do osso através de técnicas de consolidação tradicionais e emergentes. Agentes do tipo silano foram usados para acoplar de forma efectiva as fases inorgânicas e orgânicas através de interacções electrostáticas/químicas e para obter enxertos sintéticos compósitos híbridos de porosidade controlada para aplicações em cirurgias de substituição e regeneração do osso em sistemas de libertação controlada de drogas.

Determinaram-se as propriedades físicas (resistência mecânica, fracção de porosidade, tamanho de poro) dos materiais inorgânicos sinterizados e dos enxertos compósitos híbridos. A capacidade de mineralização da BL-HA dos materiais híbridos BL-HA/PLGA foi testada em fluído fisiológico simulado (SBF). A imersão em SBF induziu a formação rápida de uma camada superficial de apatite carbonatada. Os testes de biocompatibilidade *in vitro* em culturas de osteoblastos em termos de citoxicidade e proliferação de células revelaram que a BL-HA e os materiais híbridos BL-HA/PLGA são citocompatíveis, promovendo a proliferação das células osteoblásticas, conferindo-lhes um bom potencial para aplicações em regeneração óssea e maxilofacial.

TABLE OF CONTENTS

Chapter 1 ..... **1**
Introduction 1
Biomaterials overview 1
The bone 2
General aspects 2
Bone grafts 6
Autografts 7
Allografts 7
Synthetic bone-graft substitutes 8
Ceramics 9
Calcium phosphates for medical applications 10
Hydroxyapatite 10
Preparation methods 10
Structure of HA 11
Substitutions in the HA lattice 12
Effects on chemical and physical properties of apatites by the substitutions in the lattice 13
Substituents for Ca^{2+} 13
Substituents for OH 16
Biphasic calcium phosphates 16
Porous calcium phosphate ceramics 17
Calcium phosphate granules 18
Composite hybrid materials 19
Lactide-glycolide copolymers 19
Hybrid polymer/inorganic composite materials 21
References 23

Chapter 2 ..... **47**
Rietveld analysis and phase evolution with heat treatment temperature of calcium phosphates with different Ca/P ratios 49
Abstract 49
Introduction 50
Experimental 51
Synthesis 51
Sample characterisation 51
Rietveld refinement 52
Results and Discussion 53
Characterisation of the as prepared powders 53
X-Ray diffraction 53
FT-IR spectra 53
Physical characteristics 54
Thermal analysis 56
Microstructural analysis 57
Characterisation of the calcined powders 59
Phase identification and determination of phase content by X-Ray diffraction 59

Refinement of lattice parameters 62
Conclusions 65
References 66
Rietveld analysis of magnesium substituted biphasic mixtures and influence of heat treatment temperature on phase evolution 71
Abstract 71
Introduction 71
Experimental 73
Synthesis 73
Sample characterisation 74
Rietveld refinement 75
Results and Discussion 75
Structural characteristics of the as prepared powders 75
Thermal analysis and phase transformation 78
Determination of phase content 81
Refinement of lattice parameters 83
Conclusions 85
References 86
Biological-like calcium phosphates - Rietveld analysis and phase evolution with heat treatment temperature 91
Abstract 91
Introduction 91
Experimental 92
Synthesis 92
Sample characterisation 93
Rietveld refinement 94
Results and Discussion 95
Characterisation of the as prepared powders 95
X-Ray diffraction 95
FT-IR spectra 95
Physical characteristics 97
Thermal analysis 98
Microstructural analysis 100
Characterisation of the calcined powders 101
Elemental analysis 101
Phase identification and determination of phase content by X-Ray diffraction 102
Role of substituted elements 107
Conclusions 108
References 109

Chapter 3 115
Colloidal Processing and Mechanical Performance of Biological-like Calcium Phosphates Ceramics 117
Abstract 117
Introduction 117
Materials and Methods 119
Preparation 119
X-Ray diffraction 120
Zeta potential measurements 120

Rheological characterization 121
Samples preparation 122
Mechanical characterization of the samples 122
Results and Discussion 123
X-Ray diffraction 123
Zeta potential 124
Rheological characterization 126
Characterization of the sintered samples 129
Conclusions 133
References 134

Chapter 4 139
Design of porous calcium phosphate scaffolds for different orthopaedic applications 141
Abstract 141
Introduction 142
The bone model 142
General aspects 142
Biologically Derived Bone Grafts 144
Synthetic Bone Graft Substitutes 145
Calcium Phosphates 146
Powder Synthesis Methods 148
Composition versus Properties 149
Substituted Apatites 149
Biphasic Calcium Phosphates 150
Implantable Products Based on Calcium Phosphate Ceramics 150
Porous Scaffolds 150
Granular Materials 153
Experimental Procedure 154
Porous Scaffolds Prepared by the Polymeric Sponge Method 154
Complex Structures Produced by Miscelaneous Methods 157
Development of Porous Granules 157
Results and Discussion 158
Porous Scaffolds Produced by the Polymeric Sponge Method 158
Complex Structures Produced by Miscelaneous Methods 169
Porous Granules 171
Conclusions 173
References 174

Chapter 5 186
Preparation Route and Physicochemical Characterisation of Bone-Like Hydroxyapatite/PLGA Hybrid Materials for Bone Regeneration 188
Abstract 188
Introduction 188
Materials and methods 190
Preparation of inorganic materials 190
Silanization procedure 192
Preparation of hydrid materials 192
Materials characterization 193
Results and Discussion 193

Conclusions 200
References 200

Chapter 6 207
Osteoblast Response to Macroporous Biological-Like Apatites and Biological-Like Apatites/PLGA Hybrid Composites 209
Abstract 209
Introduction 210
Materials and characterization techniques 211
Materials 211
Preparation of the composite hybrid materials 212
Characterization techniques 212
Dissolution tests 213
In vitro tests with osteoblasts 214
Stimulation of osteoblasts with macroporous bodies 215
Cellular viability 215
Alkaline phosphatase activity 216
Collagen production 216
Results and Discussion 216
Conclusions 224
References 225

Chapter 7 231
Conclusions 233

Chapter 8 235
Prospects for future work 236

LIST OF FIGURES

Chapter 1

Figure 1. Structure of bone: (A) cortical (compact) bone; (B) trabecular bone (adapted from Sambrook[43]) 4
Figure 2. Crystal structure of carbonated hydroxyapatite. Powder X-ray diffraction patterns and infrared spectra of enamel, dentine and bone (adapted from Vallet-Regí *et al.* [44]). 5
Figure 3. Bone remodelling process (adapted from www.roche.com/pages/facets/11/ostedefe.htm). 6

Chapter 2

Figure 1. X-ray diffraction pattern for the as prepared powders, HA and Ca-def-HA. . 53
Figure 2. FT-IR spectra for as prepared powders, HA and Ca-def-HA 54
Figure 3. Particle size distribution of the as prepared powders, HA and Ca-def-HA. ... 55
Figure 4. Specific surface area and average pore diameter of the as prepared and calcined at 1100ºC powders, HA and Ca-def-HA. 55
Figure 5. TG and DTA plots for the different Ca/P ratio powders, HA and Ca-def-HA. 56
Figure 6. Microstructures of the samples HA (a) and Ca-def-HA (b) obtained by scanning electronic microscopy. 57
Figure 7. Transmission electronic microscopy results of the as prepared HA: (a) Powder diffraction cliché; (b) Particle size and morphology. 58
Figure 8. Transmission electronic microscopy results of the as prepared Ca-def-HA: (a) ED pattern; (b) Particle made up of crystallites and (c) Dark field image of single particles. 59
Figure 9. Crystalline phase evolution of HA powders with heat treatment temperatures. 59
Figure 10. Crystalline phase evolution of Ca-def-HA powders with heat treatment temperatures. 60
Figure 11. Crystallite size of the HA powders, as calculated for the (002) and (300) reflections. The dashed line represents the phase transformation. 64
Figure 12. Crystallite size of the Ca-def-HA powders, as calculated for the (002) and (300) reflections. The dashed line represents the phase transformation. 65

Figure 1. X-ray diffraction pattern for the as prepared powders, calcium deficient apatite (Ca-def-HA) and Mg doped calcium deficient apatite Mg-(Ca-def-HA). 76
Figure 2. FT-IR spectra for as prepared powders, calcium deficient apatite (Ca-def-HA) and Mg doped calcium deficient apatite Mg-(Ca-def-HA). 77
Figure 3. TG and DTA plots for the different Ca/P ratio powders, calcium deficient apatite (Ca-def-HA) and Mg doped calcium deficient apatite Mg-(Ca-def-HA). 78
Figure 4. Crystalline phase evolution of Ca-def-HA powders with heat treatment temperatures. 79
Figure 5. Crystalline phase evolution of Mg-(Ca-def-HA) powders with heat treatment temperatures. 81

Figure 1. X-ray diffraction patterns for the as prepared powders, BL-HA1 and BL-HA2. 96
Figure 2. FT-IR spectra of the as prepared powders, BL-HA1 and BL-HA2. 96
Figure 3. Particle size distribution of the as prepared powders, BL-HA1 and BL-HA2.98
Figure 4. Specific surface area and average pore diameter of the as prepared and calcined at 1100ºC powders, BL-HA1 and BL-HA2. 98
Figure 5. TG and DTA plots for the different Ca/P ratio powders, BL-HA1 and BL-HA2. 99
Figure 6. SEM microstructures of the samples BL-HA1 (a), and BL-HA2 (b). 100
Figure 7. Transmission electron microscopy results of the as prepared BL-HA1: (a) Powder diffraction cliché; (b) Particle size and morphology; (c) Agglomeration and size of particles; (d) High resolution of one crystallite. 100
Figure 8. Transmission electron microscopy results of the as prepared BL-HA2: (a) Powder diffraction cliché; (b) Particle size and morphology. 101
Figure 9. Crystalline phase evolution of BL-HA1 powders with heat treatment temperatures. 103
Figure 10. Crystalline phase evolution of BL-HA2 powders with heat treatment temperatures. 103
Figure 11. Evolution of crystallite sizes with heat treatment temperature of the BL-HA1 samples. 106
Figure 12. Evolution of crystallite sizes with heat treatment temperature of the BL-HA2 samples. 107

Chapter 3

Figure 1. X-ray diffraction patterns for the powders calcined at 1150ºC (Ca-def-HA) and at 1250ºC (HA, Mg-(Ca-def-HA), BL-HA1 and BL-HA2). 123
Figure 3. Equilibrium shear stress *versus* shear rate curves for the HA suspensions with 40 vol.% solids in the presence of different added amounts of dispersant and with 60 vol.% solids milled for different time periods. 127
Figure 4. Equilibrium shear stress *versus* shear rate curves for the Ca-def-HA, Mg-(Ca-def-HA), BL-HA1 and BL-HA2 suspensions with 40 vol.% solids in the presence of 0.2 wt.% of dispersant, Targon 1128. 128
Figure 5. Equilibrium shear stress *versus* shear rate curves for the Ca-def-HA, Mg-(Ca-def-HA) and BL-HA2 suspensions with 60 vol.% solids in the presence of the optimal amounts of dispersant, after milling for different time periods..... 128
Figure 6. Evolution of density with the sintering temperature for the different compositions studied. 130
Figure 7. Evolution of flexural strength with the sintering temperature for the different compositions studied. 130
Figure 8. Micrographs of the calcium phosphate samples sintered at 1150ºC: (a) (Ca-def-HA) and at 1250ºC [(b) HA; (c) Ca-def-HA; (d) Mg-(Ca-def-HA); (e) BL-HA1; (f) BL-HA2]. 131
Figure 9. Curves of probability of failure *vs.* ultimate bending strength..... 133

Chapter 4

Figure 1a. Crystal structure of hydroxyapatite after Wilson *et al.*[43] projected perpendicular to *c*-axis. 147
Figure 1b. Crystal structure of hydroxyapatite after Wilson *et al.*[43] projected on (001). 148
Figure 2. Typical porous microstructure of HA scaffolds obtained from hydrothermal transformation of cuttlefish bones.[98] 153
Figure 3. Machined cuttlefish bone derived porous HA scaffolds (scale in mm). 153
Figure 6. Macroporous HA structures obtained by the polymeric sponge method. 159
Figure 7. Comparison of compressive strength values vs. porosity of porous HA scaffolds for tissue engineering prepared by the polymeric sponge method achieved in the present work (◆) and reported in literature for the same preparation method, and for conventional and computer-assisted processing techniques. Each style of point corresponds to a different literature source.[112-115,117-127] 160
Figure 8. Elastic modulus (G') at a constant strain (10^{-3}) *versus* temperature for protein beaten solutions. 161
Figure 9. Elastic modulus (G') and viscous modulus (G'') of protein beaten solutions *versus* frequency at a constant temperature (25 ºC). 162
Figure 10. Elastic modulus (G'), at a constant strain (10^{-3}), versus temperature, of hydroxyapatite suspensions with different amounts of beaten protein solutions. 163
Figure 11. Elastic modulus (G') and viscous modulus (G''), at a constant temperature (25 ºC), versus frequency, of hydroxyapatite suspensions with different amounts of beaten protein solutions. 164
Figure 13. Microstructural details of sintered (1250ºC) porous samples prepared with egg-white as pore former and consolidator agent. 165
Figure 14. Estimated values of total porosity based on the measured apparent density. 167
Figure 15. Microstructure of the samples I to IV, sintered at 1250ºC (see Table 2 for sample codes). 167
Figure 16. Microstructure of the samples A, B and C with different FBC/SLS proportions, sintered at 1250ºC. 168
Figure 17. Compressive strength of the samples obtained by combining foaming and starch consolidation methods. 169
Figure 18. Macroporous HA structures of different shapes, obtained by different methods: (A) Starch consolidation with wax spheres; (B) Starch consolidation and foaming; (C) 1 - Slip casting and polymeric sponge; 2,4 - Polymeric sponge and 3 – Slip casting, starch consolidation and foaming; (D) Polymeric sponge using a partially soluble bioglass (cylinder) and polysaccharide (block) as setting agents. Samples C1 and C3 present outer high density and inner macroporosity. 170
Figure 19. Rheological behaviour of HA suspensions mixed with different weight ratios of HA powder/setting agent solution of 0.2 (solid line) and 0.4 (dashed line). 171
Figure 20. Digital pictures of some of the samples listed in Table 6 (B, C, E and G), showing the influence of the experimental parameters on the granule size and shape. 172
Figure 21. Microstructure of the sample D, sintered at 1250ºC. 173

Chapter 5

Figure 1. XRD patterns of the samples HA and BL-HA2 (straight line - HA phase, dashed line – β-TCP). 194
Figure 2. TG plots for HA samples, silanized and silanized and post-hybridized. 195
Figure 3. TG plots for BL-HA2 samples, silanized and silanized and post-hybridized. 195
Figure 4. FT-IR spectra for HA samples silanized by different methods..... 196
Figure 5. XPS spectra of HA silanized by solvent evaporation method using a 10 wt% γ -MPS solution showing the appearance of most significant peaks Si2p, C1s, O1s, Ca2p (2p3 and 2p1), P2p. 197
Figure 6. XPS spectra of BL-HA2 silanized by solvent evaporation method using a 10 wt% γ -MPS solution showing the appearance of most significant peaks Si2p, C1s, O1s, Ca2p (2p3 and 2p1), P2p. 198
Figure 7. Raman spectra of BL-HA2 surface treated with 10 wt.% of PLGA/ethyl lactate solution using the solvent evaporation method. 199
Figure 8. FTIR-ATR spectroscopic results of BL-HA2 surface treatment. 200

Chapter 6

Figure 1. XRD patterns of the samples HA, Mg-(Ca-def-HA), BL-HA2-1 and BL-HA2-1 (straight line - HA phase, dashed line – β-TCP). 217
Figure 2. Microstructure of the different samples after sintering at 1250ºC: (a) Mg-(Ca-def-HA); (b) BL-HA2; (c) magnification of a pore surface of Mg-(Ca-def-HA); (d) magnification of a pore surface of BL-HA2..... 218
Figure 3. Microstructures of the samples sintered at 1250ºC (a-e) and at 1400ºC (f) after immersion in SBF for different time periods: (a) HA, 3 days; (b) Ca-def-HA, 12 hours; (c) Ca-def-HA, 14 days; (d) Mg-(Ca-def-HA), 3 days; (e) BL-HA2, 30 days and (f) BL-HA2, 1 day. 218
Figure 4. XRD patterns of the sample Mg-(Ca-def-HA) sintered at 1250ºC before and after and immersed in SBF for different time periods (straight line - HA phase, dashed line – β-TCP). 219
Figure 5. FT-IR spectra for BL-HA2 sintered at 1250ºC before and after immersion in SBF for different time periods..... 220
Figure 6. Evolution of the ionic concentrations with the time of immersion in SBF the BL-HA2 sample sintered at 1250ºC. 220
Figure 7. (A) Viability/proliferation. (B) Alkaline phosphatase production. (C) Collagen secretion. $1x10^5$ osteoblasts were plated in the presence of HA, Mg-(Ca-def-HA) and BL-HA2 powders. After 72 h of incubation, viability and proliferation were evaluated by MTT assay (A), alkaline phosphatase production by NBT-BCIP assay (B), and the collagen present in the supernatant was measured by SIRCOL method (C). In (A), (B) and (C) results represent Mean±SD of triplicates from three separate experiments ($P<0.05$). Smooth columns-samples without surface treatment; squared columns-hybrid samples. 223
Figure 8. Photomicrographs (400x) of (a) control; (b) Mg-(Ca-def-HA) and (c) BL-HA2 at 1400ºC. 224

LIST OF TABLES

Chapter 2

Table 1. Determined Rietveld quantification result of stoichiometric (HA) and calcium deficient apatite (Ca-def-HA). 61
Table 2. Refined lattice parameters and calculated cell volume of HA phase for HA and Ca-def-HA. 62
Table 3. Refined lattice parameters and calculated cell volume of β-TCP phase for Ca-def-HA. 63
Table 4. Refined lattice parameters and calculated cell volume of α-TCP phase for HA and Ca-def-HA. 64

Table 1. Molar concentrations of the precursors Ca and P used in the synthesis. 74
Table 2. Experimental details of X-ray powder diffraction data collection. 75
Table 3. Comparison of diffraction angle (2θ) and *d*-spacing values of experimental X-ray patterns with respect to standard JCPDS values. 80
Table 4. Determined Rietveld quantification results of Ca-def-HA and Mg-(Ca-def-HA) biphasic mixtures. 82
Table 5. Refined lattice parameters and calculated cell volume of HA phase for Ca-def-HA and Mg-(Ca-def-HA) biphasic mixtures. 83
Table 6. Refined lattice parameters and calculated cell volume of β-TCP phase for Ca-def-HA and Mg-(Ca-def-HA) biphasic mixtures. 84
Table 7. Refined lattice parameters and calculated cell volume of α-TCP phase for Ca-def-HA and Mg-(Ca-def-HA) biphasic mixtures. 85

Table 1. Concentrations of the precursors used in the synthesis of the co-substituted calcium phosphates. 94
Table 2. Concentrations of the elements measured after heat treatment (HA-1200ºC; BL-HA1 and BL-HA2-1400ºC). 102
Table 3. Rietveld phase analysis quantification in the co-substituted calcium phosphates powders heat treated at different temperatures. 105

Chapter 3

Table 1. Concentration of the precursors used in the synthesis of the calcium phosphate samples. 120
Table 3. Vickers hardness (HV5) of the sintered bars at different temperatures. 131
Table 4. Weibull modulus of the samples sintered at different temperatures. 132

Chapter 4

Table 1. Generic formulation of apatite minerals, and potential substitutions in the three sublattices. 150
Table 2. Sample codes, total foaming agent (TFA) added and relative fractions of FBC and SLS. 156

Table 3. Sample codes (in capital bold) with respect to powder/setting agent ratio, nozzle diameter, flow rate and distance between the nozzle and the setting media. 158
Table 4. Apparent density, estimated porosity and compressive strength of the porous samples obtained through the polymeric sponge method. 159
Table 5. Apparent density, porosity values and compressive strength of the porous samples prepared by the foaming method using egg white as consolidator and foaming agent. 164
Table 6. Density and porosity of the sintered samples. 171

Chapter 5

Table 1. Concentration of the precursors used in the synthesis of the calcium phosphate samples..... 192

Chapter 6

Table 1. Concentration of the precursors used in the synthesis of the calcium phosphate samples..... 211
Table 2. Ionic concentrations of the SBF solutions and of the human plasma (adapted from[19])..... 214
Table 3. Rietveld quantification of phase compositions for samples HA, Mg-(Ca-def-HA) and BL-HA2 sintered at 1250ºC and of the BL-HA2 sintered at 1400ºC. 217

LIST OF ABBREVIATIONS

ACP -	amorphous calcium phosphate
ALP -	alkaline phosphatase
APD -	average pore diameter
BCP -	biphasic calcium phosphate
BL-HA -	biological-like hydroxyapatite
BMP -	bone morphogenetic proteins
Ca-def-HA -	calcium deficient hydroxyapatite
CaP -	calcium phosphate
DCC -	direct coagulation casting
DCPD -	dicalcium phosphate dihydrate or brushite
DTA -	differential thermal analysis
FBC -	foam-bath concentrate
FBS -	fetal bovine serum
FT-IR -	infrared spectroscopy by Fourier transformed
G -	glycolide
GA -	glycolide acid
HA -	hydroxyapatite
HAS -	hydrolysis assisted solidification
IEP -	isoelectric point
JCPDS -	Joint Committee on Powder Diffraction Standards
L -	lactide
LA -	lactide acid
Mg-(Ca-def-HA)-	magnesium substituted calcium deficient hydroxyapatite
MPS -	methacryloxypropyltrimethoxy-silane
MTT -	3(4,5 dimethylthiazol-2yl) 2,5 diphenyltetrazoliumbromide
NMR -	nuclear magnetic resonance spectroscopy
OCP -	octacalcium phosphate
PGA -	polyglicolic acid
PLA -	polylactic acid
PLGA -	poly(D,L-lactide-co-glycolide acid
PMAA -	polymethacrylic acid
PVB -	poly vinyl butyral
SBF -	simulated body fluid
SEM -	scanning electronic microscopy
SLS -	sodium lauril sulphate
SSA -	specific surface area
TCP -	tricalcium phosphate
TEM -	transmission electronic microscopy
TFA -	total foaming agent
TG–DTA -	thermo gravimetric and differential thermal analysis
XPS -	X-ray photoelectron spectroscopy
XRD -	X-ray diffraction
XRF -	X-ray fluorescence spectroscopy
XRPD -	X-ray powder diffraction
ZP -	zeta potential

AIM AND STRUCTURE OF THE THESIS

One of the purposes of this thesis was to develop calcium phosphate powders with cosubstituted elements in order to find a material that could act in specific situations as an alternative to traditional calcium phosphates. Another objective was to investigate the applicability of these powders on the colloidal processing and the preparation of hybrid macroporous structures suitable for bone regeneration/replacement. In order to develop a macroporous structure similar to that of the human cancelous bone, new techniques were developed based on the combination of traditional techniques for the preparation of porous structures and new consolidation techniques.

The first chapter of this thesis consists in a brief overview of bone and of calcium phosphate materials to be used in bone regeneration, giving emphasis to HA and biphasic calcium phosphates. Aspects like the cationic and anionic substitutions in the HA lattice are discussed. An overview of porous calcium phosphate ceramics and composite hybrid materials is made.

Chapters 2 to 6 describe the experimental work in the form of a compilation of papers submitted for publication in international refereed journals.

Chapter 2 consists in a compilation of three papers. In this chapter the investigation concerning the substitution of elements in the HA lattice is described and Rietveld refinement studies are used to determine the phase analysis and the structural parameters of the phases formed. The phases formed upon heating are identified and characterised.

Chapter 3 describes how a proper processing route can be used to develop strong calcium phosphate bioceramic materials for bone graft applications. The dispersion conditions of biphasic calcium phosphate powders were studied in aqueous media in the presence of two anionic dispersants and the mechanical properties of the samples were evaluated.

In chapter 4, the preparation and characterisation of porous calcium phosphate ceramics that can mimic the structure, the mineral composition and the properties of bone to be used as reliable synthetic bone grafts for orthopedic applications is described. A comprehensive review on the general aspects of bone model, biologically derived bone grafts, synthetic bone graft substitutes based especially on calcium phosphates, including powder synthesis methods and their composition *versus* properties is presented. The state-of-the-art about the techniques used to produce porous materials, especially porous ceramic scaffolds is presented.

The preparation and characterisation of macroporous composite hybrid materials is described in chapter 5. Different silanization procedures and the post-hybridization procedure are described. The macroporous composite hybrid materials are expected to find use in medical applications of bone regeneration and as drug delivery carrier for therapeutic molecules.

In Chapter 6 the capacity of the macroporous composite hybrid materials to mineralise was studied, as well as its cytotoxicity.

The thesis concludes with a general discussion (chapter 7) and future work perspectives (chapter 8).

Chapter 1

Introduction

Biomaterials overview

A biomaterial is defined as a material intended to interface with biological systems to evaluate, treat, augment or replace any tissue, organ or function of the body.[1]

Since the pre-Christian era that substitutions of bone parts for repairing seriously damaged portions of the human body have been reported, so the use of certain materials as constituents of surgical implants is not new. The historical trail of biomaterials science has known insightful changes through time and has evolved from one of clinical trial and error to a scientific discipline based upon the design and control of the interface between tissues and materials. Biomaterials are now in their third generation of existence.[2]

During the 1960s and 1970s appeared the first generation of biomaterials. During this period the implanted prostheses were based on materials selected from engineering practice. In 1980, Hench reported that the aim of this first generation of biomaterials was to "achieve a suitable combination of physical properties to match those of the replaced tissue with a minimal toxic response in the host",[3] being their biological inertness a common feature of most of the materials used.[2] Inert materials were used to produce implantable devices (e.g. alumina, metals and polymers) that could fullfil mechanical demands and be biologically safe, but which could not be integrated into the body.[4] Although these inert materials provide an effective immediate solution for many patients, their outcome was often time-limited[5] and the development of biomaterials with extended lifetime in-patients was needed.

As a consequence of the limitations of the first generation of biomaterials, research was carried out in order to develop materials more closely resembling the biological template.[5] By the mid-1970s the field of biomaterials began to shift and to producing bioactive components that could elicit a controlled interaction with the living organism instead.[6] Different types of bioactive materials, namely glasses, ceramics, glass ceramics and composites reached clinical use in several orthopaedic and dental applications.[7-23] In 1971, Hench *et al.* developed the first man-made material that was found to bind to living bone, consisting of a glass (Bioglass®) of the system Na_2O-CaO-SiO_2-P_2O_5.[18] This second generation of biomaterials had another important innovation that was the utilisation of synthetic hydroxyapatite $Ca_{10}(PO_4)_6(OH)_2$ in bone regeneration in the form of powders, porous implants and coatings on metallic prostheses. Composites, namely hydroxyapatite-polymer also began to be used as bone

grafts. The pioneer of this application was Bonfield *et al.* who developed hydroxyapatite-reinforced polyethylene composites,[8] tailor made to produce bone apposition rather than bone resorption at an implant surface, so as to provide matching deformation characteristics and superior fracture toughness to cortical bone.[4] In this period of biomaterials history other advances were registered, as the use of resorbable materials which are replaced by the regenerating tissues[7,15,21,23-25] and the development of controlled drug delivery systems.[26-28] In the group of the resorbable materials are included not only ceramics, such as β-TCP (β-tricalcium phosphate), but also polymers, as for instance polylactic (PLA) and polyglicolic (PGA) acids.

Although the second generation of biomaterials had achieved many progresses, revision surgery is still needed in many cases and failure rates are not satisfactory. At the present time, a third generation of biomaterials is being intended to stimulate specific cellular responses at the molecular level and the separate concepts of bioactive and resorbable materials have converged.[2] Two different alternative routes of repair are currently being adopted, based on tailored biomaterials, namely,[2] *in situ* tissue regeneration and tissue engineering. The approach of *in situ* tissue regeneration involves the use of bioactive materials in the form of gels, solutions, powders, granules, or microparticles to stimulate local tissue repair.[2] The biomaterials used can be loaded with different chemicals or growth factors as bone morphogenetic proteins (BMP) in order to stimulate cells and favour tissue regeneration. The approach of tissue engineering is a process whereby functional biological prostheses are created by seeding progenitor cells onto synthetic biodegradable substrates that act as scaffolds, and allow diffusion of nutrients to the cells and the cell-to-cell contact that leads to the formation of new tissue.[29] The tissue-engineered constructs are then implanted into the patients to replace diseased or damaged tissues.[2] Different tissues are being engineered using this route of repair, including fabricated artery, bladder, skin, cartilage, bone, ligament and tendon.[30]

The bone

General aspects

Bone is the major calcification present in a human body.[31] It serves as structural support for the body and as a major reservoir of calcium and phosphate ions necessary for a wide variety of metabolic functions. Precise knowledge of the physical, chemical, and mechanical properties of bone is critical for the development of new bone substitute materials.

Human bone is a complex, actively functioning, constantly varying system. The structural-functional unit of bone is an osteon, a microscopic system of osseous tubes (cylinders) inserted in one another. In the centre of the system, there is a nutrient canal 10 to 100 μm in diameter, containing a blood capillary. The number of osseous tubes constituting an osteon may vary from 4 to 20. Bone is covered with a thin layer of connective tissue (periosteum), containing vessels and nerves. The inner layer of perisosteum contains a large amount of osteoblasts, which are responsible for bone growth (Fig. 1).[32,33]

From the chemical point of view, bone is a ceramic-organic composite material consisting mainly of calcium phosphate (69%), collagen (20%) and water (9%). Other organic substances, such as proteins and polysaccharides, are present in small amounts. The physiological fluids present in bone acts as plasticizers.[34] Porosity is an important property of bone, since it allows the body fluids and cells to access all the parts of the osseous tissue, and also influence the mechanical anisotropy.[31,35-42]

The bone molecules are bonded forming linear chains which are in turn arranged in fibres, giving rise to various macroscopic structures. In Fig. 1 is represented a bone structure scheme. Bone, usually is composed by a relative dense outer layer, the cortical or compact bone, surround a less dense porous tissue, the spongy or cancellous bone. The voids are filled with a gel-like tissue kwon as bone marrow.[31,35-42]

Microscopically, bones are characterized by their composition, crystalline structure, morphology, particle size and orientation. The carbonate content of biological apatites ranges between 4% and 8% and tends to increase with age while the hydrogen phosphate ion decreases. The crystals are nanometer sized, with an average length of 50 nm, 25 nm in width and thicknesses of just 2–5 nm, scattered in the organic matrix. Their small size is a very important factor related to the solubility of biological apatites when compared with mineral apatites. Small dimensions and low crystallinity are two distinct features of biological apatites which, combined with their non-stoichiometric composition, inner crystalline disorder and presence of carbonate ions in the crystal lattice, allow explaining their special behaviour (Fig. 2).

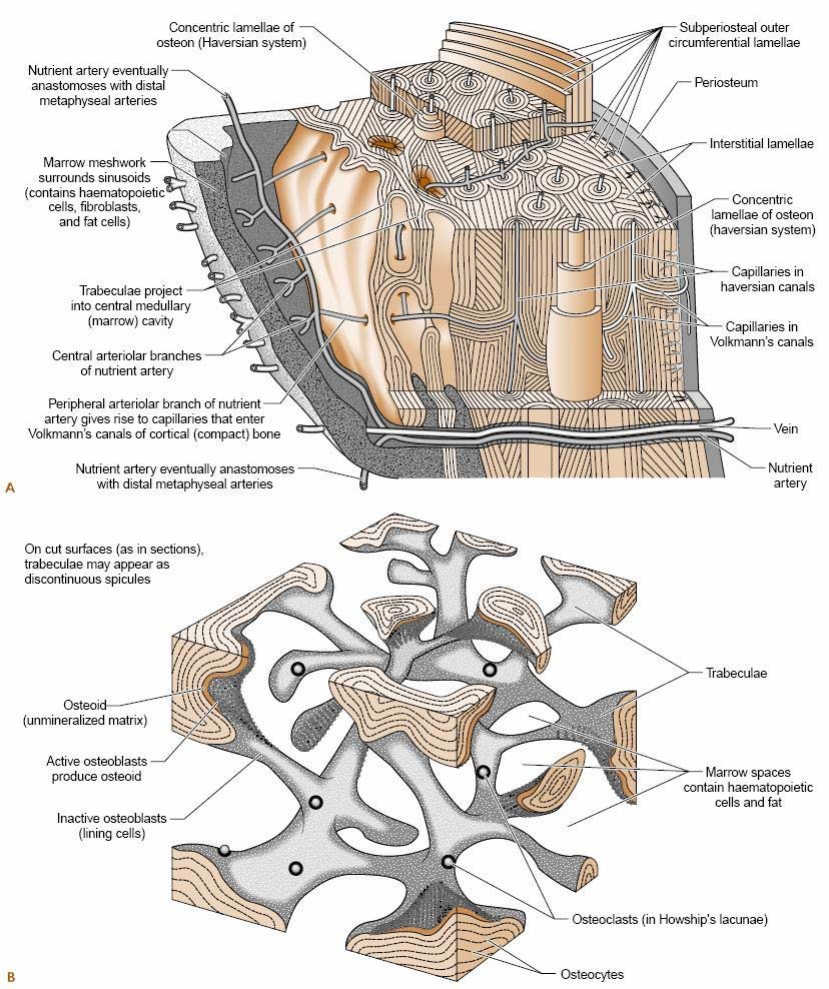

Figure 1. Structure of bone: (A) cortical (compact) bone; (B) trabecular bone (adapted from Sambrook[43])

The bones of vertebrates can be considered as ‘‘living biominerals’’ since there are cells inside them under permanent activity. The bone formation process starts by the action of osteoblasts, special cells that synthesize and release the collagen matrix, primarily composed of collagen Type I, in the form of a jelly substance, the osteoid, which is subsequently mineralized by controlled deposition of calcium phosphate. The osteoblasts remain trapped inside the mineral phase, evolving towards osteocytes which continuously maintain the bone formation activity.

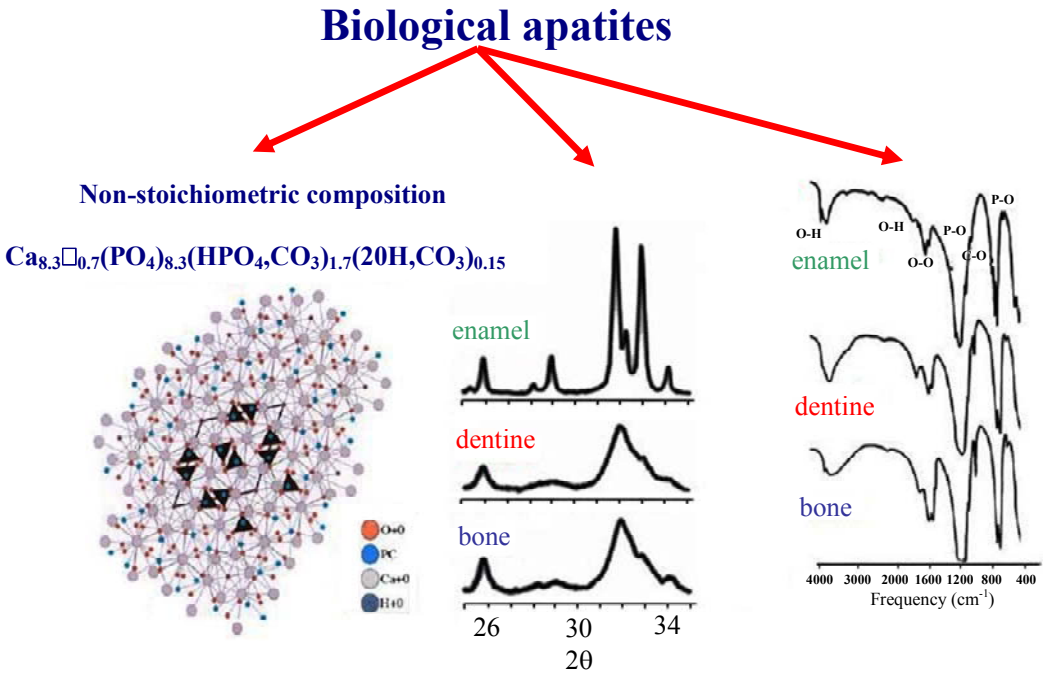

Figure 2. Crystal structure of carbonated hydroxyapatite. Powder X-ray diffraction patterns and infrared spectra of enamel, dentine and bone (adapted from Vallet-Regí *et al.* [44]).

Meanwhile, another type of cells, the osteoclasts, catabolise the bone by destroying it. This dynamic process of bone formation and destruction, bone remodelling (Fig. 3), accounts for its growth during the development stages of the body, preserving its shape and consistency, and enabling its regeneration in case of fracture. It also constitutes a storage and carrying mechanism for two essential elements, phosphorus and calcium, which are mainly stored in the bones.[44] An unbalanced ratio between the formation of new bone and the resorption of old bone, can lead to several osseous diseases, namely osteoporosis, osteopetrosis, and Paget's disease.

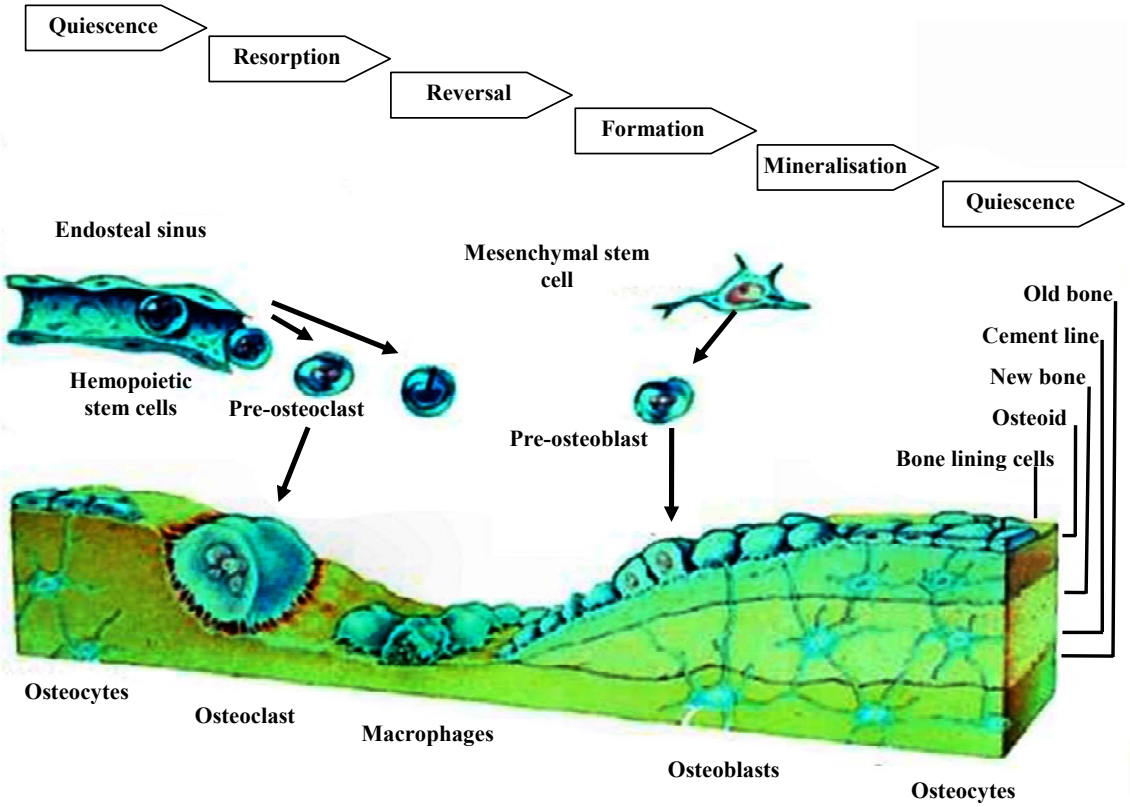

Figure 3. Bone remodelling process (adapted from www.roche.com/pages/facets/11/ostedefe.htm).

Bone grafts

Bone graft is the second most common transplantation tissue, with blood being by far the commonest.[45,46] More than 500,000 bone grafting procedures are happening annually in the United States and 2.2 million worldwide in order to repair bone defects in orthopaedics, neurosurgery and dentistry.[47,48]

Additionally, the treatment of posttraumatic skeletal complications, such as delayed unions, nonunions, malunions, are challenging.[49] Bone grafting is usually required to stimulate bone-healing. Moreover, spinal fusions, filling defects following removal of bone tumours and several congenital diseases may require bone grafting. Several methods for reconstructing bone defects are available namely using autografts, allografts, demineralised bone matrix, calcium phosphates, autologous bone marrow aspirates and bone morphogenetic proteins.

At the moment, the gold standard of bone grafting is harvesting autologous cortical and cancelous bone from iliac crest. All other forms of bone grafting have disadvantages compared to autograft and as such their use is suboptimal. However, technological

evolution along with better understanding of bone-healing biology, have lead to the development of several bone graft substitutes that are currently available to the orthopaedic surgeons.[50,51]

As mentioned before, autologous bone is the gold standard that all alternatives must meet or exceed, but the autographs have significant limitations, including donor site morbidity, inadequate amount, and inappropriate form.[50,52,53] These limitations have prompted increasing interest in alternative bone grafts, designedly allografts. These may be cancellous, cortical, or a combination of each. Even if they are attractive sources, there are several problems encountered in using them, including the risk of disease transmission, immunogenicity,[54,55] loss of biologic and mechanical properties secondary to its processing, increased cost, and non-availability world-wide due to financial and religious concerns. Consequently, significant efforts are being made to develop ideal bone graft substitutes.

Autografts

Autologous bone provides optimal osteoconductive, osteoinductive, and osteogenic properties.[56] Iliac crest is the most frequently chosen donor site as it provides easy access to good quality and quantity of cancellous autograft. However, this procedure is not easy, could be very painful for the patient and has some cosmetic disadvantages.[50,51,57] Moreover, it may fail in clinical practice as most of the cellular (osteogenic) elements do not survive transplantion.[58] Other limitations include old or paediatric patients and patients with malignant disease.[59-61]

In addition autograft harvesting is associated with a 8.5—20% of complications including haematoma formation, blood loss, nerve injury, hernia formation, infection, arterial injury, ureteral injury, fracture, pelvic instability, cosmetic defects, tumour transplantation, and sometimes chronic pain at the donor site.[50,52,62-65]

Allografts

Bone allograft transplantation has been performed in humans for more than one hundred and twenty years. The use of allograft tissue has increased and changed since the mid 1980's. Prior to the 1980's, allograft tissue was primarily used as a substitute for autografts in large defect sites. However in the years since then, allograft tissue use has expanded from approximately 5,000-10,000 cases in 1985 to almost 150,000 in 1996.[45] This increase was in part facilitated by the formation of tissue donation networks,

coordinating donor screening and tissue processing methodologies to reduce the risk of allograft tissue. With the increase in acceptance of allograft tissue, a number of products have emerged that are based on allograft tissue either alone or in combination with other materials. Later, the major problem became the disease transmission, namely HIV.[55]

Allograft is the most frequently chosen bone substitute and is regarded as the surgeon's second option.[66] The current increasing availability of allograft tissue has made it possible to manufacture customised types, such as dowels, strips, and chips.[58] Allograft bone has more limitations in the essential bone graft characteristics described earlier and yields more variable clinical results. In addition, allografts carry the risk of transferring viral diseases. The processing of allograft tissue lowers this risk but, that can significantly weaken the biologic and mechanical properties initially present in the bone tissue.[67-73] Allografts are prepared in fresh, frozen or freeze-dried forms, cortical or cancellous. Fresh allografts are rarely used as they might ignite an immune response or transmit diseases.[74] Frozen and freeze-dried allografts are more osteoconductive but are considered to have weak osteoinductive capabilities comparing to fresh allograft.[55]

Synthetic bone-graft substitutes

A large number of bone-graft alternatives are currently commercially available for orthopaedic use. They vary in composition, mechanism of action, and special characteristics. Among all of these bone graft alternatives, it is possible to find the synthetic bone substitutes, in which considerable advances over the past decade have been made.

A few years ago, synthetics bone substitutes were neglected in favour to autografts and allografts. Synthetic bone grafts at most possess only two of the four characteristics of an ideal bone graft material (osteointegration, osteoconduction). Ideally synthetic bone graft substitutes should be biocompatible, show minimal fibrotic reaction, undergo remodelling and support new bone formation. From a mechanical point of view synthetic bone substitutes should have similar strength to that of the cortical/cancellous bone being replaced. This needs to be matched with a similar modulus of elasticity to that of bone in an attempt to prevent stress shielding as well as maintaining adequate toughness to prevent fatigue fracture under cyclic loading. Synthetic materials that demonstrate some of these properties are composed of calcium, silicon or aluminium. The disadvantages encountered with such materials in clinical settings include: low or unpredictable resorption, difficulty in handling (coral derived hydroxyapatite), and poor

clinical results with occasional inflammatory foreign body reaction (degradable polymers).[75-77] Newer, modified materials, such as special ceramics would probably overcome these complications.

Ceramics

Among several synthetic bone substitutes options, there are the ceramics, glasses and glass ceramics that are synthetic scaffolds that have been used in dentistry and orthopaedics since the 1980s.[78,79]

In the clinical use of ceramics, commonly the surgeon requires different forms of the same material, such as in the form of dense blocks, porous solid pieces or in a granulated form. When using metallic implants, the ceramic coating is of utmost importance, since it will improve the attachment of the prosthesis to the host while stopping or at least reducing the release of metallic ions from the implant alloy to the living body, due to the barrier created by the ceramic layer. It is also possible to administrate ceramic materials in injectable form, in non invasive surgery applications.

Another important application of ceramic matrices could be the production of substrates for tissue engineering. Ceramics are clearly the most biocompatible functional materials and many of them are also very similar to the natural hard tissues.

Ceramic materials used in reconstructive surgery can be classified in three large groups: bioinert, resorbable and bioactive. Bioinert ceramics have almost no influence in the surrounding living tissue, and their finest example would be alumina. Resorbable ceramics, as the name implies, degrade upon implantation in the host. The resorbed material is replaced by endogenous tissues. The rate of degradation varies from material to material. Bioactive ceramics, by contrast, are capable of bonding with living osseous tissues; several calcium phosphates and certain compositions of glasses and ceramic glasses exhibit such feature. The chemical reactivity of ceramics can be attested by bioactivity tests, by pouring the ceramic under their environment: namely, an artificial solution chosen to perform the in vitro assays, or the physiological body fluids during *in vivo* assays.

From a structural point of view, ceramic materials can be classified as crystalline solids-ceramics, amorphous solids-glasses, or amorphous solids with crystallization nuclei-glass-ceramics, which can in turn be considered as inert, bioactive or resorbable. Therefore, it is important to analyse firstly the biological calcium phosphates as components of natural hard tissues, that is, bones and teeth.

Calcium phosphates for medical applications

In the last two decades, the biomedical applications of calcium phosphates have increased significantly due to their biological properties. Different types of calcium phosphates are used in the biomedical field, namely resorbable and non-resorbable ceramics, cements, prosthetic coatings, and composites. They are suited for several applications, including bone defect filling, bone reconstruction (especially in maxilla-facial applications), bone replacement (especially small bones and middle ear bones), drug carrier (antibiotics, anticancerous drugs, growth factors), coatings of metal prostheses (hip and knee joints), and even nerve guides.[80]

In the ternary system $Ca(OH)_2$-H_3PO_4-H_2O, there are several known calcium phosphates, with calcium-to-phosphate (Ca/P) molar ratios varying from 0.5 to 2.[81]

The most produced and less expensive industrial calcium phosphate biomaterial, remains hydroxyapatite (HA). Tricalcium phosphate is also available on an industrial scale and is probably the most used bioresorbable material.[80] It exists under two crystallographic forms: β-tricalcium phosphate (β-TCP) and α-tricalcium phosphate (α-TCP). The α-form is unstable at low temperature and is obtained by heating the β-form above approximately 1120ºC,[80,82,83] the precise transformation temperature remaining unclear. The β-form cannot be obtained by direct precipitation. It results from the calcining to 700-800ºC of Ca deficient apatite, with the loss of water, according to the equation:[82]

$$Ca_9(HPO_4)(PO_4)_5(OH) \rightarrow 3Ca_3(PO_4)_2 + H_2O$$

β-TCP is stabilised by the presence of small amounts of ionic impurities, such as Mg^{2+} ions, frequently associated with calcium salts.[80,84] It should not be confused with whitlockite, a natural iso-structural compound that contains Mg^{2+} ions substituted for Ca^{2+} and HPO_4^{2-} ions substituted for PO_4^{3-}.[80]

Hydroxyapatite

Preparation methods

Several methods of preparation of hydroxyapatite have been reported in the literature, including precipitation, conversion of other calcium salts, solid state reactions, and sol-gel crystallisation.[85-95] The two main ways of producing HA are however the wet

methods and solid state reactions. Depending upon the technique used, some variability may appear in the final product in terms of morphology, stoichiometry and crystallinity.[96] Apatites prepared from non aqueous systems are considerably larger in crystallite size than those prepared from aqueous systems. Solid state reactions usually give a stoichiometric and well-crystallised product but they require relatively high temperatures and long heat treatment times.[33] The crystallinity and Ca/P ratio of the product obtained depend strongly on the preparation conditions and are in many cases lower than for well-crystallised stoichiometric hydroxyapatite.

Chemically precipitated hydroxyapatites are often non-stoichiometric (usually calcium- and hydroxyl deficient). Generally, they have a high specific surface area (between 50 and 90 m^2/g) that may adsorb many ions or constituents, which can be incorporated into the lattice during growth or maturation of the crystals.[80] A general formula is suggested for non-stoichiometric (carbonate free) hydroxyapatites:[95]

$Ca_{10-x}(HPO_4)_x(PO_4)_{6-x}(OH)_{2-x}.nH2O$; $0 < x < 1$, $n = 0\text{-}2.5$

Calcium deficient hydroxyapatites are less thermally stable than stoichiometric hydroxyapatites and when heated to about 600ºC calcium pyrophosphate is formed.[97,98] Further heating until c.a. 800ºC, a temperature that does not affect stoichiometric hydroxyapatite, results in the Ca-deficient hydroxyapatite dehydration to form β-TCP plus some residual apatite.[97,98] Another aspect related to wet methods of preparation of HA is the incorporation of carbonate ions and/or other impurities, such as sodium or potassium in the lattice of the crystallised HA, since these cations are frequently introduced in the precipitation system with the reactants. Carbonate is so readily incorporated in HA that the preparation of a CO_3-free material requires the use of solutions free of carbonate and nitrogen purging during the experiment. In laboratory preparations with no precautions taken, one obtains a precipitated HA with about 1% CO_3 by weight.[98] Biological apatites precipitated from body fluids are about 4% in CO_3 content.[98]

Structure of HA

According to some authors,[99-101] the stoichiometric form of HA is monoclinic with space group P21/b, the structure being characterised by ordering within OH^- ion columns to form a sequence OH- OHOH- OH-, with an ordered arrangement of these

columns, so that the *b*-axis is doubled giving lattice parameters *a*=9.421(8), *b*=2*a*, *c*=6.8814(7) Å, γ=120º.[100] Although many preparations of HA have been described, only few studies have reported HA as monoclinic.[88,101] This can be justified by the practical difficulties in controlling its stoichiometry, because the simple precipitation route yields a basic calcium phosphate of variable composition. The calcium phosphates formed can have a Ca/P molar ratio in the range 1.50 to 1.67 (possibly beyond these limits) and contain variable amounts of water and hydrogen phosphate, while retaining the apatite structure.[101] Normally, only those preparations having a final high-temperature stage (e.g. hydrothermal or heating in steam at 900ºC) have the possibility of yielding monoclinic HA.[100] Other preparations are normally hexagonal, presumably because sufficient OH^- ions are missing, replaced by H_2O or impurity ions, so that the ordering is disturbed.[102] Slightly non-stoichiometric HA has a hexagonal space group P63/m with *a*=9.421 and *c*=6.884 Å.[99]

Substitutions in the HA lattice

There has been considerable interest in the ion-exchange properties of hydroxyapatites, in part as a consequence of their relevance in biological systems and as a result of potential applications for the removal of environmentally undesirable elements from both solids and liquids.[40,102-106]

The apatite structure is capable of accommodating various substituents (e.g. Sr^{2+} for Ca^{2+}, F^- for OH^-, CO_3^{2-} for PO_4^{3-}) and still maintains its structure. "Apatite" is a general term for crystalline minerals with a composition of $M_{10}(ZO_4)_6X_2$. The name was taken from the Greek word "apato" which means deceive, by Werner, a mineralogist in 1790[107,108] and its choice is justified because of the difficulties involved in the identification of apatites due to their non-stoichiometric existence.

All ionic sites of the apatitic structure accept substituents.[80,108-110] The substitutions in the HA are isoionic (ions from a solution phase exchange with identical ions of a solid phase in contact with it), or heteroionic (an ion of a solid phase is displaced by a different ion from a solution in contact with it, thereby altering the composition of both phases). The criteria for the substitution are the similarity of charge and proximity of sizes of the ions concerned.[108,110]

In what concerns HA applicability in the biomedical field, the capacity of its lattice to act as a host for different chemical species has been explored. The most common example is the preparation of carbonate-substituted HA[111,112] and fluoride-substituted

HA.[113,114] Another potential method for improving the biological activity of HA is the incorporation of silicon (or silicate groups) into its lattice.[115]

Effects on chemical and physical properties of apatites by the substitutions in the lattice

The HA properties that are affected by substitutions in the lattice are: lattice parameters (*a*- and *c*-axis dimensions), crystal size and shape, crystal strain, "crystallinity" from X-ray diffraction patterns, infrared absorption spectral properties, dissolution properties and thermal stability.[108] In some cases more than one substitution occurs simultaneously in the HA lattice and the presence of the substituents may have additive, synergistic or opposite effects on the properties of the apatite crystallites.[108] For instance, the combined effects of Mg^{2+} and CO_3^{2-} on reducing crystallinity are greater than the addition of their individual effects.[116] The simultaneous presence of CO_3^{2-} and F^- gives an additive effect on the contraction of the *a*-axis dimension.[112] As a consequence of the substitution, the lattice parameters can be expanded or contracted depending on the size and amount of the substituent.[95,110,117,118] Usually, if the substituent is larger than the ion substituted for (e.g. Sr^{2+} for Ca^{2+}; Cl^- for OH^-), the effect is to expand one or both of the lattice parameters. In some cases of substitutions, both *a* and *c* axes are affected either in the same or opposite directions. In other cases, only the *a*-axis dimensions are either increased or decreased, while the *c*-axis dimensions are not significantly different from the unsubstituted OH-apatite.[108,117] Some substitutions are coupled with others to maintain charge balance or neutrality in the apatite, e.g. CO_3^{2-} for PO_4^{3-} coupled with Na^+ for Ca^{2+}. The type of substituent also affects the crystallinity of the apatites. For instance, an increase in crystallinity is observed in apatite as a consequence of F^- incorporation, while a decrease is observed due to CO_3^{2-} incorporation. Moreover, the characteristics of the substituent influence the dissolution properties of apatite. Fluoride, carbonate and magnesium have specific effects on the solubility of HA. Fluoride decreases the solubility of HA[108,118,119] whether carbonate and magnesium increases it.[108,120,121]

Substituents for Ca^{2+}

The substitution of divalent ions for calcium in hydroxyapatite is well known for both aqueous and non-aqueous systems. Such substitutions are accompanied by changes in the apatite lattice parameters and these changes are generally related to the size of the

ionic radii of the cation compared to that of Ca^{2+} (0.99 Å).[108,117,118] For instance, the contraction in lattice parameters due to the partial substitution of Cd^{2+} (0.97 Å) or Mn^{2+} (0.80 Å) for Ca^{2+} is due to the fact that these cations have smaller ionic radii than Ca^{2+}. Contrarily, Sr^{2+} (1.12 Å), Ba^{2+} (1.34 Å), and Pb^{2+} (1.20 Å) are ions larger than Ca^{2+} and they cause expansion in both the *a*- and *c*-axis dimensions when they substitute in the apatite lattice. The incorporation of these ions also causes changes in the infrared absorption spectra[88,108,122] namely on the PO_4^{3-} absorption bands and the disappearance or masking of the OH^- absorption bands ascribed to its librational vibration mode.[108] Their effects on the crystallinity of apatites are not clear. Strontium-substituted apatites were reported to be more soluble than strontium-free apatites.[123] The unit cell lattice parameters were found to vary linearly with the Sr content in different Sr-HA solid solutions.[124] The substitution of Ca^{2+} by Sr^{2+} ions in the apatite lattice is a very important heteroionic substitution since it is known to interfere with the calcification mechanism.[125,126] There have been reports indicating that non-toxic amounts of Sr^{2+} may be beneficial in osteoporosis.[127,128] High Sr^{2+} intake seems however to result in poor bone formation and mineralisation, since the metabolism of Ca is depressed.[129]

Magnesium is a metal ion whose presence in the body has important biological implications. The incorporation of Mg^{2+} in the HA structure is very limited[100,108,130] with no perceptible effect on the lattice parameters in spite of the smaller atomic radius of Mg^{2+} compared to that of Ca^{2+}.[108] Several works described in the literature indicate that the presence of Mg^{2+} in the solution in which the apatite forms, causes a reduction in apatite crystallite size, favours the formation of Mg substituted-TCP, and promotes the formation and stabilisation of amorphous calcium phosphates (ACP) at 37ºC.[39,131-133] Posner *et al.* suggested that magnesium ions delay the ACP to HA conversion and the direct HA precipitation reactions by substituting for Ca^{2+} in forming embryonic clusters of HA.[134] This results in a distortion and subsequent destabilisation of these prenuclei due to the smaller size of magnesium relative to calcium ions, decreasing the probability of the initial formation of HA crystals.[135] Webster *et al.* prepared HA with 2 mol% substituted Mg^{2+} and found that osteoblasts adhesion was significantly greater on these substrates than on undoped HA.[136,137]

Other divalent cations which can also substitute Ca^{2+} in the HA lattice are Zn^{2+}, Cd^{2+} and Pb^{2+}. Zn^{2+} is reported to substitute Ca^{2+} up to 25 atom% when present in the supersaturated solution.[138] However, bone HA studies with labelled 65Zn have shown 100% substituted Ca^{2+} by Zn^{2+} ions.[139] The substitutions of Cd^{2+} and Pb^{2+} for Ca^{2+} are

associated with bone disorders. Cadmium ions interact directly with bone cells diminishing their ability to mineralise.[140] Moreover, their presence accelerates bone turnover, particularly bone resorption, a result of the induced calcium deficiency.[141] The interference of Cd^{2+} with mineralisation can certainly be explained by its inhibitory effect on HA nucleation and growth in addition to any cellular involvement.[142] Cd^{2+} incorporation into the HA lattice results in a decreasing of *c*-axis spacing and a corresponding crystal size decrease in that direction.[142] In what concerns Pb^{2+}, inorganic lead enters the body through inhalation, ingestion, or adsorbed through skin and is distributed in the organism in the blood, soft tissues and bone. The skeleton represents an accumulating reservoir containing approximately 95% of the body burden of lead in adults.[143] The mean residence time in cortical bone is 30 years.[144] Lead stored in bone may be released in states where demineralisation may occur, such as pregnancy, lactation, immobilisation, etc, resulting in endogenous exposure. The mechanism involved in lead fixation in bone is attributed to isomorphous substitution of Ca^{2+} by Pb^{2+}, resulting in the formation of solid solutions of HA and lead hydroxyapatite.[110]

The incorporation of monovalent ions in HA lattice such as Na^{+}, Li^{+} and K^{+} is also possible but it has to be coupled with another substitution to maintain charge neutrality.[108,145] The coupled substitution of Na^{+} for Ca^{2+} with CO_3^{2-} for PO_4^{3-} is an example.[146]

Trivalent ions are also known to substitute for Ca^{2+}. For instance Ergun *et al.* synthesised yttrium substituted HA and has shown that the doped ceramic had improved cytocompatibility properties for osteoblast adhesion.[136,137] In what concerns Al^{3+}, some authors indicate that it substitutes calcium in the HA structure[89,108,118] while others consider that the uptake of this metal ion is due to adsorption processes.[125] Apatites obtained from solutions containing Al^{3+} showed expanded *a*- and *c*- axis dimensions when compared to the lattice parameters of pure HA, supporting the possibility of substitution.[144] The adsorption theory is based on the fact that metal ions with ionic radii significantly different from the one of Ca^{2+} tend to adsorb rather than enter the HA lattice.[89] Aluminium is associated with several bone disorders. It accumulates in the skeleton, inhibits mineralisation and acts on bone cells.[91,123,129,135,147-152] Aluminium appears to enter skeletal tissue along with calcium, competing with it.[91] Although the mechanism by which aluminium disrupts bone calcification and leads to osteomalacia is not completely understood, it is suggested that aluminium ions block the calcification sites.[152]

The cationic sites of hydroxyapatite can also accept vacancies: up to a maximum of 2 sites out of the 10 existing in stoichiometric apatites.[80]

Substituents for OH

In calcium phosphate apatites the monovalent anionic site substitution of OH^- by F^-, Cl^-, or Br^- is possible to occur. Apatites without any ions in these lattice positions have never been described.[108] These sites may also be occupied by carbonate ions resulting in a type A carbonated HA.[91,111,112,153,154]

Substitution of CO_3^{2-} for OH^- has been observed in apatites from non-aqueous systems prepared at 1000ºC. The effect of such substitution on the lattice parameters is opposite to the CO_3^{2-} for PO_4^{3-} substitution, namely the former causes an expansion of the *a*- and a contraction of the *c*-axis.[111,112] The frequencies of the CO_3^{2-} infrared absorption bands are also different in these two types of carbonate substitution. The extent of CO_3^{2-} for OH^- substitution is 100 mol% ($Ca_{10}(PO_4)_6CO_3$).

In what concerns the substitution of Cl^- for OH^-, it differs in extent for apatites obtained from aqueous and those from non aqueous systems (40 and 100% respectively).[108] This substitution is accompanied by expansion in the *a*- with the contraction in the *c*-axis dimensions, changes in the characteristics of the absorption bands of the OH groups in the case of partially substituted $(Cl, OH)^-$ apatites and decrease in thermal stability.[113,155] However, it is predicted from the atomic arrangements of OH, F and Cl-apatites that structural stability is in the decreasing order: F-Apatite > OH-Apatite > Cl-Apatite.[100]

The substitution of F^- for OH^- predominates in mineral apatites. In both aqueous and non aqueous systems, F^- for OH^- substitution can be partial or full, $Ca_{10}(PO_4)_6(F,OH)_2$ or $Ca_{10}(PO_4)_6F_2$, respectively. The incorporation of F^- in the apatite is accompanied by a decrease in the *a*-axis without any significant change in the *c*-axis, an increase in crystallinity, and decreased dissolution rates and solubility in acid buffers.[100,113,114]

Biphasic calcium phosphates

Biphasic calcium phosphate ceramics (BCP) were developed to better control the process of biomaterials resorption and bone substitution. Daculsi found an optimum balance of the more stable phase of HA and more soluble TCP, enabling to gradually control the dissolution in the body, seeding new bone formation as it releases calcium ($Ca^{2+)}$ and phosphate (PO_4^{3-}) ions into the biological medium.[156,157]

Some authors have defended the superior properties of the BCP materials ‘‘directly’’ prepared over those obtained by mixing two single phases.[158] Despite this fact, there are several synthesis routes that can be employed in the preparation of BCPs. The most commonly used is precipitation[159,160,161,162] and the blending of different calcium phosphates.[163] Other techniques also employed are: solid state,[164] treatment of natural bone,[165] spray pyrolysis,[166] microwave,[167] combustion,[168] etc.

Some examples of commercial products based on these mixtures are: Triosite® (Zimmer, Rungis, France), MBCP® (Biomatlante, Nantes, France), Osteosynt® (Einco ltds, Belo-Horizonte, Brazil), etc.

Porous calcium phosphate ceramics

Calcium phosphate ceramics in porous form have been widely applied as bone substitutes, since they allow the growth of natural tissue inside the pores, providing a mechanical interlock leading to a firmer fixation of the materials.[33,107,169] However, for bone ingrowth, pores larger than 100 μm in diameter are required, which must be interconnected to guarantee the supply and the circulation of the necessary nutrients, through the ingrowth of fibrous tissue, vascular tissue and bone tissue.[107,170] Also necessary are smaller pores, which favour protein adsorption and adhesion of osteogenic cells. Thus, the pore size distribution in porous ceramics should be bimodal.[171]

The classical way to fabricate porous HA ceramics (pore size of 100–600 μm) is sintering the HA powder with appropriate pore-creating additives (for example paraffin, naphthalene, or hydrogen peroxide) which evolve gases at elevated temperatures.[172] The use of porogenic substances that leaves a pore after burning out is other possible way to create porosity.[173-175] Porous HA can also be cast into the $CaCO_3$ skeleton, which is then dissolved, leaving a porous network. Also worth mentioning is that the control of sinterability of the powders can lead to dense/ porous layered materials.[160]

Several low-temperature methods have been applied to fabricate porous HA. Natural porous materials, like coral skeletons made of $CaCO_3$ and cuttlefish bone, can be converted into HA under hydrothermal conditions with the microstructure undamaged.[164,165] Porous HA structure can also be obtained by hydrothermal hot pressing.[33]

It is generally agreed that it’s very difficult to produce porous HA with a structure similar to human bone, because the control of the porous structure is a critical point.

Consequently there is an increasing interest in the development of porous HA-based ceramic bodies with different but complementary purposes: restoration of vascularity and complete penetration of osseous tissue throughout the repaired site, applications such as scaffolds for tissue engineering, and systems for controlled delivery of drugs. The main shortcomings for spreading the use of these kinds of materials are the difficulty of tailoring the porous microstructures for the desired applications. Fabricating ceramic parts with precise sizes and shapes that match in the implant sites is another concern.

In order to obtain more complex shapes and to overcome these difficulties, the combination of well-known methods like slip casting, foaming, starch consolidation and others, enables to tailor the porous structures according to the requirements of the site of implantation.[107,170,176]

Calcium phosphate granules

Recently, porous granules have received much attention from the research field as well from the industry. They are commercially available and are widely used as fillers or packing materials. Depending of their size, microstructure, pores content and distribution, the granules find application in dental, periodontal, oral/maxillofacial surgical procedures and orthopaedics.

Granules behaviour in the body depends on its morphology and microstructure. Irregular morphology of the granules is known to cause inflammatory reactions, so the rounded forms with smooth geometry are preferable for defect filling.[177]

There are several reports of procedures for the development of granulates, namely hydrothermal reaction of corals, crushing of sintered blocks, vibration and rolling synthetic powders with water, dripping into liquid nitrogen and drip casting.[178] More recently, new methods were developed, one based on the liquids immiscibility effect,[179] and the other based on the ionotropic gelation.[180,181] Lemos *et al.* conclude that the method based in ionotropic gelation is suitable for the production of hydroxyapatite porous spherical granules with smooth surfaces.[181]

There are commercial granules, namely Interpore®, Pro Osteon® and Osteogen®, all with macroporosity and there is InBone G ®, with macro and microporosity.

Composite hybrid materials

Lactide-glycolide copolymers

To perform adequately during many years of service, implants in general must not cause abnormal responses in local tissue and should not produce toxic or carcinogenic effects, either locally or systemically.[182-187] Biodegradable implants in particular should serve their intended function while releasing products of degradation that are biocompatible and non-toxic, and without interfering with tissue healing.[188-192]

In general, polylactide/polyglycolide biomaterials have demonstrated satisfactory biocompatibility and absence of significant toxicity,[182,183,193] although some reduction in cell proliferation has been reported.

Glycolide (G) and lactide (L) monomers are cyclic monomers for use in medical applications can be assembled into a wide variety of polymers and copolymers. Polymer properties can be tailored from soft elastomerics to rigid engineering plastics. In addition to mechanical properties, other properties of polymers, including degradation rate, hydrophilicity and solubility can be customised for individual applications.[194] A detailed understanding of these properties is critical to designing a quality medical device or controlled-delivery system for use in humans.

Direct trials have demonstrated that the lactide/glycolide copolymer, produced by Ghimas S.p.A., is perfectly tolerated by the organism and it is absorbed in three to four months, with osteoexcitative properties, because it is penetrated and progressively and totally substituted by the bone.[193,195]

In the trabecula of the new-constituted bone, areas containing adipose and vascular cells are present, there are reports showing the formation of the bone marrow;[196,197] it has an excellent biocompatibility, also demonstrated in man by the absence of rejection and inflammation;[197,198,199] moreover it shows to be a carrier for bone growth factors, i.e. the morphogenetic protein BMP.[200-216]

A review of studies of toxicity, biocompatibility and clinical applications in the field of orthopaedics and surgery, using implants made of polylactic acid, polyglycolic acid and their copolymers, shows that the intrinsic nature of these biomaterials renders them suitable for applications where temporary slow release of bioactive agents *in situ* may be required; biocompatibility and toxicity studies suggest that, overall, these biomaterials may be suitable for orthopaedic application.[217]

In addition to biocompatibility,[25,189,191,192,195,199,218-221] the other properties of these polymers that make them uniquely suitable for these and other applications are:

thermoplasticity, high strength, controlled crystallinity, controlled degradation rates, controlled hydrophilicity and proven non toxicity.[222]

In the Unites States the FDA has approved many uses for these materials and continues to review and approve their use. Other potential medical uses include bone plates and other orthopaedic applications, ear vent tubes, nerve growth tubes and wound dressing.

Polylactide/polyglycolide copolymers have also been frequently used in bone repair applications and have been found to be biocompatible, non-toxic and non-inflammatory.[195,223-225] Implants made of these materials have shown to accelerate bone healing in the rat tibia[195] and induce higher bone formation than untreated controls in cranial defects.[223]

In recent years, the experimental and clinical uses of polylactide/polyglycolide polymers in the field of orthopaedics have seen enormous growth, especially as fracture fixation devices and scaffolds for tissue growth. The biodegradable and biocompatible nature of these polymers as well as their suitable mechanical properties have made them potential candidates for a variety of orthopaedic applications such as bone fixation repair of osteochondral defects, ligament and tendon reconstructions, and bone substitutes.

Because the mechanical properties of long bones usually exceed those of polylactide/polyglycolide materials, it is often necessary to reinforce these polymers with calcium phosphate powders or fibres which have higher stiffness and strength, such as carbon fibres or fibres of the copolymer itself. The use of self-reinforced polylactide/polyglycolide and polyglycolide rods has also been reported in other studies.[226-229]

The hydrolytic degradation of the aliphatic polyesters occurs by bulk erosion. The polylactide/polyglycolide polymer chains are cleaved by hydrolysis of ester bonds to form monomeric acids and are eliminated from the body through the Krebs cycle, primarily as carbon dioxide and water in urine. Because the rate of hydrolysis of the polymer chain is dependent only on significant changes in temperature and pH or presence of catalyst, a very little difference is observed in rate of degradation at different body sites.[230,231] Different factors affect the degradation kinetics, such as: chemical composition and configurational structure, processing history, molar mass, environmental conditions, stress and strain, crystallinity, device size, morphology (e.g. porosity) and chain orientation, distribution of chemically reactive compounds within the matrix, additives,[232,233] presence of original monomers and overall hydrophilicity.

The role of enzymatic involvement in the biodegradation of the polylactide/polyglycolide polymer has been somewhat controversial. Most early literature conclude that bioerosion of these materials occurred strictly through hydrolysis with no enzymatic involvement.[214] Other investigators suggest that enzymes do play a significant role in the breakdown of the lactide/glycolide materials.[234-237] Much of this speculation is based upon the differences observed between *in vivo* and *in vitro* degradation rates: it is supposed that a little enzyme involvement is expected in the early stages with polymers in the glassy state, whereas enzymes can play a significant role for polymers in the rubbery state.[238]

It can be summarized that the 50:50 lactide/glycolide copolymer has the fastest degradation rate of the D,L-lactide/glycolide materials, with that polymer degrading in about 50-60 days. The 65:35, 77:25 and 88:15 D,L-lactide/glycolides have progressively longer *in vivo* lifetimes, with the 88:15 lasting about 150 days *in vivo*, whereas poly(D,L-lactide) requires about 12-16 months to biodegrade completely, and poly(L-lactide), being more crystalline and less hydrophilic, can be found *in vivo* in about 1-½ to 2 years.[238-243]

Hybrid polymer/inorganic composite materials

Currently, composites of polymers and ceramics are being developed with the aim to increase the mechanical scaffold stability and to improve tissue interaction.[244-251] In addition, efforts have also been invested in developing scaffolds with a drug-delivery capacity. These scaffolds can locally release growth factors or antibiotics and enhance bone ingrowth to treat bone defects and even support wound healing.[2,252-254]

To fulfil as many requirements as possible, composite systems combining advantages of polymers and ceramics seem to be a promising choice, in particular for bone tissue engineering, as demonstrated by the increasing research efforts worldwide.[244-261]

To combine the advantages exhibited by calcium phosphates materials (CaP) and bioresorptive polymers (P), CaP/P composite biomaterials have been synthesized, and used for reconstruction and repair of bone defects. Various synthesis and designing routes to obtain CaP/P biomaterials have been developed by now.

Poly-lactide-glycolide acid (PLGA) has a wide range of degradation rates, the degradation kinetics being governed by both hydrophobic/hydrophilic balance and crystallinity. Composition of chains (i.e. contents in L-LA and D-LA and/or GA units)

determines the degradation rate of PLGA polymers. Blends containing the greatest amount of PGA have been shown to degrade faster.[232]

There are several reports on HA/PLGA hybrid composites materials, namely in dense, [200-263] and in porous form.[264,265] However, hybrid materials when exposed to an aqueous physiological environment can loose strength rapidly at the inorganic-organic interface if the two phases are not bound together.[266] The mechanical behaviour of hybrid structures describes the type of interaction between the two phases, and if there is no binding, either physical or chemical, there is a premature failure of the hybrid materials.[267] In order to enhance the hybrid materials integrity, studies have been done based on the modification of the surface of inorganic materials by adding a coupling agent, such as organofunctional silanes,[268-270] which showed to be effective in the improvement of the adhesion between mineral substrate and polymer matrix.[271-273]

Oliveira *et al.* reported the preparation route and physicochemical characterisation of Bonelike®/PLGA hybrid materials for bone regeneration, and concluded that silanization of HA and Bonelike® materials has been successfully obtained using γ - MPS as a coupling agent and that these novel Bonelike®/PLGA hybrid materials may find use for bone regeneration applications with simultaneous local delivery of therapeutic molecules.[262]

The present challenge in tissue engineering is to design and fabricate reproducible bioactive and bioresorbable 3D scaffolds of tailored porosity and pore structure, which are able to maintain their structure and integrity for predictable times, even under load-bearing conditions. The mechanical integrity of man-made composite scaffolds is still at least one order of magnitude lower than that of cancellous or cortical bone. Achieving the mechanical properties of bone might also allow replacing bigger parts of damaged bone tissue than what is possible today.

The incorporation of biomolecules such as growth factors with the aim to accelerate local bone healing is promising and currently under extensive research. However, incorporating biomolecules during scaffold processing is not simple as biomolecules are sensitive to elevated temperatures and extreme chemical conditions. A promising strategy is the immobilization of proteins and growth factors in the post-processing phase via surface functionalization of the scaffold.

References

1. Williams DF. The Williams Dictionary of Biomaterials. Liverpool, UK: Liverpool University Press, 1999.

2. Hench LL, Polak JM. Third-generation biomedical materials. Science 2002;295: 1014-7.

3. Hench LL. Biomaterials. Science 1980;208:826-831.

4. Williams DF. Titanium for medical applications. In: Brunette DM, Tengvall P, Textor M, Thomsen P, editors. Titanium in Medicine- Materials Science, Surface Science, Engineering, Biological Responses and Medical Applications. Berlin, Germany: Springer Verlag, 2001. p.14-23.

5. Bonfield W. Biomaterials Research and Development. In: European White Book on Fundamental Research in Materials Science, Max-Planck Institut Fur Metallforschung Stuttgart, 2001.

6. Hench LL, Wilson J. Surface-active biomaterials. Science 1984;226:630-636.

7. Bhaskar SN, Brady JM, Getter L, Growen MP & Driskell T. Biodegradable ceramic implants in bone. Oral Surg 1971;32:334-346.

8. Bonfield W, Grynpas MD, Tully AE, Bauman J & Abram J. Hydroxyapatite reinforced polyethylene - a mechanically compatible implant material for bone replacement. Biomaterials 1981;2:185-186.

9. Bonfield W, Behiri JC, Doyle C, Bowman S & Abram J. Hydroxyapatite reinforced polyethylene composites for bone replacement. In: Ducheyne P, van der Perre G, Aubert AE editors. Biomaterials and Biomechanics. Amsterdam, Holland: Elsevier Science, 1984. p.421-426.

10. Cameron HU, MacNeb I & Pilliar RM. Evaluation of a bidegradable ceramic. J Biomed Mater Res 1977;11:179-186.

11. Ducheyne P, van Raemdonck W, Heughebaert JC & Heughebaert M. Structural analysis of hydroxyapatite coatings on titanium. Biomaterials 1986;7:97-103.

12. Ferraro JW. Experimental evaluation of ceramic calcium-phosphate as a substitute for bone grafts. Plast Reconstruct Surg 1979;63:634-640.

13. Geesink RGT, de Groot K & Klein CPAT. Chemical implant fixation using hydroxylapatite coatings. Clin Orthop 1987;225:147-170.

14. Greenlee TK, Beckham CA, Crebo AR & Malmborg JC. Glass-ceramic bone implants. J Biomed Mater Res 1972;6:235-244.

15. de Groot K. Degradable ceramics. In: Williams DF, editor. Biocompatibility of Clinical Implant Materials, Vol I. Boca Raton, USA: CRC-Press, 1981. p.199-224.

16. de Groot K, Geesink RGT, Serekian P & Klein CPAT. Plasma sprayed coatings of hydroxylapatite. J Biomed Mater Res 1987;21:1375-1381.

17. Grote JJ, Kuypes W & de Groot K. Use of sintered hydroxylapatite in middle ear surgery. ORI 1981;43:248-254.

18. Hench LL, Splinter RJ, Allen WC & Greenlee TK. Bonding mechanism at the interface of ceramic prosthetic materials. J Biomed Mater Res 1971;2:117-141.

19. Hench LL. Ceramics, glasses and composites in medicine. Med Instrum 1973;7:136-144.

20. Jarcho M. Calcium phosphate ceramics as hard tissue prosthetics. Clin Orthop and Rel Res 1981;157:259-278.

21. Mors WA & Kaminsk EJ. Osteogenic replacement of tricalcium phosphate ceramic implants in the dog palate. Arch Oral Biol 1975;20:365-368.

22. Ogino M, Ochuchi F & Hench LL. Compositional dependence of the formation of calcium phosphate films on bioglass. J Biomed Mater Res 1980;14:55-59.

23. Rejda BV, Peelen JGJ & de Groot K. Tricalcium phosphate as a bone substitute. J Bioeng 1977;1:93-97.

24. Gilding DK & Reed AM. Biodegradable polymers for use in surgery: polyglycolic acid/ poly(lactic acid) homo- and copolymers. Polymer 1979;20:1459-1464.

25. Kulkarni RK, Pani KC, Neuman C & Leonard F. Polylactic acid for surgical implants. Arch Surg 1966;96:839.

26. Rhine W, Hsieh DS & Langer R. Polymers for sustained macromolecule release: procedures to fabricate reproducible delivery systems and control release kinetics. J Pharm Sc 1980;69:265-270.

27. Wahlig H & Dingeldein E. Antibiotics and bone cements. Experimental and clinical longterm observations. Act Orthop Scand 1980;51:49-56.

28. Wood DA. Biodegradable drug delivery systems. Int J Pharma 1980;7:1-18.

29. Ferber D. Tissue engineering: lab-grown organ began to take shape. Science 1999;284:422-425.

30. Lee KY & Mooney DJ. Hydrogels for Tissue Engineering. Chem Rev 2001;101:1869- 1879.

31. Lowenstam HA & Weiner S. On Biomineralization. Oxford University Press, New York, 1989.

32. Martin RB. Bone as a Ceramic Composite Material. Mater Sci Forum. 1999;7(1):5-16.

33. Suchanek W & Yoshimura M. Processing and Properties of HA-Based Biomaterials for Use as Hard Tissue Replacement Implants. J Mater Res Soc 1998;13(1):94-103.

34. Gunderson SL & Schiavone RC. International Encyclopedia of Composites. Lee SM. Ed., New York: VCH, vol. 5, 1991.

35. Bilezikian JP. Lawrence GR & Gideon AR. Principles of Bone Biology. Academic Press, USA, 1996.

36. Daculsi G, LeGeros RZ, Heughebaert M & Barbieux I. Formation of carbonate-apatite crystals after implantation of calcium phosphate ceramics. Calcif Tissue Int 1990;46:20-27.

37. Daculsi G, Bouler JM & LeGeros RZ. Adaptive crystal formation in normal and pathological calcifications in synthetic calcium phosphate and related biomatrials. Int Ver Cytol 1997;172:129-191.

38. Lakes R. Materials with structural hierarchy. Nature 1993;361:511-515.

39. LeGeros RZ. Phosphate minerals in human tissues. In: Nriagu JO, Moore PB, editors. Phosphate Minerals. Berlin, Germany: Springer Verlag, 1984. pp.351-385.

40. LeGeros RZ. Biological and synthetic apatites. In: Brown PW, Constanz B, editors Hydroxyapatites and Related Materials, Boca Raton, USA: CRC Press, 1994. pp.3-28.

41. Tracy BM & Doremus RH. Direct electron microscopy studies of the bone-hydroxyapatite interface. J Biomed Mater Res 1984;18:719-726.

42. Weiner S & Wagner HD. The Material Bone: Structure-Mechanical Function Relations. Annu Rev Mater Sci. 1998;28:271-298.

43. Sambrook P. Bone structure and function in normal and disease states. In:The Musculoskeletal System: Basic Science and Clinical Conditions, Philip Sambrook (ed), Churchill Livingstone, 2001.

44. Vallet-Regí M & González-Calbet JM. Calcium phosphates as substitution of bone tissues. Progress in Solid State Chemistry 2004;32:1-31.

45. Boyce T, Edwards J & Scarborough N. Allograft Bone: The Influence of Processing on Safety and Performance. Orthop Clin N Amer. 1999;30(4):571-581.

46. Van Heest A & Swiontowski M. Bone-graft substitutes. Lancet 1999;353 (suppl 1):28-9.

47. Lewandrowski K, Gresser JD, Wise DL & Trantolo DJ. Bioresorbable bone graft substitutes of different osteoconductivities: an histologic evaluation of osteointegration of poly (propyleneglycol-co-fumaric acid) based cement implants in rats. Biomaterials 2000;21(8):757-64.

48. Muschler GF, Negami S & Hyodo A. Evaluation of collagen ceramic composite graft materials in a spinal fusion model. Clin Orthop 1996;328:250-60.

49. Sauer HD & Schoettle H. The stability of osteosyntheses bridging defects. Arch Orthop Trauma Surg 1979;95:27-30.

50. Summers BN & Eisenstein SM. Donor Site pain from the ilium: a complication of lumbar spine fusion. J Bone Joint Surg Br 1989;71:677-80.

51. Younger EM & Chapman MW. Morbidity at bone graft donor sites. J Orthop Trauma 1989;3:192-5.

52. Banwart JC, Asher MA & Hassanein RS. Iliac crest bone graft harvest donor site morbidity: A statistical evaluation. Spine 1995;20:1055-60.

53. Cowley SP & Anderson LD. Hernias through donor sites for iliac-bone grafts. J Bone Joint Surg Am 1983;65:1023-5.

54. Freidlaender GE. Immune responses to osteochondral allografts: Current knowledge and future directions. Clin Orthop 1983;174:58-68.

55. William WT. Bone allografts: Past, present and future. Cell and Tissue Banking 2000;1:105-109.

56. Cypher TJ & Grossman JP. Biological principles of bone graft healing. J Foot Ankle Surg 1996;35:413-7.

57. Dodd CAF, Fergusson CM & Freedman L. Allograft versus autograft bone in scoliosis surgery. J Bone Joint Surg Br 1988;70:431-4.

58. Sandhu HS, Grewal HS & Parvataneni H. Bone grafting for spinal fusion. Orthop Clin North Am 1999;30:685-98.

59. Bridwell KH, O'Brien MF & Lenke LG. Posterior spinal fusion supplemented with only allograft bone in paralytic scoliosis. Does it work?. Spine 1994;19:2658-66.

60. Gau YL, Lonstein JE & Winter RB. Luque-Galveston procedure for correction and stabilization of neuromuscular scoliosis and pelvic obliquity: a review of 68 patients. J Spinal Disord 1991;4:399-410.

61. McCarthy RE, Peek RD, Morrissy RT & Hough Jr AJ. Allograft bone in spinal fusion for paralytic scoliosis. J Bone Joint Surg Am 1986;68:370-5.

62. Arrington ED, Smith WJ & Chambers HG. Complications of iliac crest bone graft harvesting. Clin Orthop 1996;329:300-9.

63. Ross N, Tacconi L & Miles JB. Heterotopic bone formation causing recurrent donor site pain following iliac crest bone harvesting. Br J Neurosurg 2000;14:476-9.

64. Seiler JG & Johnson J. Iliac crest autogenous bone grafting: donor site complications. J South Orthop Assoc 2000;9:91-7.

65. Skaggs DL, Samuelson MA & Hale JM. Complications of posterior iliac crest bone grafting in spine surgery in children. Spine 2000;25:2400-2.

66. Carter G. Harvesting and implanting allograft bone. AORN J 1999;70:660-70.

67. Bonfiglio M & Jeter WS. Immunological responses to bone. Clin Orthop 1972;18:19-27.

68. Bos GD, Goldberg VM & Zika JMc. Immune responses of rats to frozen bone allografts. J Bone Joint Surg Am 1983;65-A:239-46.

69. Damien CJ & Parsons JR. Bone graft and bone graft substitutes: a review of current technology and applications. J Appl Biomater 1991;2:187-208.

70. Henman P & Finlayson D. Ordering allograft by weight: suggestions for the efficient use of frozen bone-graft for impaction grafting. J Arthroplasty 2000;15:368-71.

71. Keating JF & McQueen MM. Substitutes for autologous bone graft in orthopaedic trauma. J Bone Joint Surg Br 2001;83(1):3-8.

72. Palmer SH, Gibbons CL & Athanasou NA. The pathology of bone allograft. J Bone Joint Surg Br 1999;81:333-5.

73. Pelker RR & Friedlaender GE. Biomechanical aspects of bone autografts and allografts. Orthop Clin North Am 1987;18:235-9.

74. Friedlaender GE, Strong DM, Tomford W & Mankin HJ. Longterm follow-up of patients with osteochondral allografts. A correlation between immunologic responses and clinical outcome. Orthop Clin North Am 1999;30:583-8.

75. Bostman O & Pihlajamaki H. Clinical biocompatibility of biodegradable orthopaedic implants for internal fixation: a review. Biomaterials 2000;21:2615-21.

76. Bucholz RW, Carlton A & Holmes R. Interporous hydroxyapatite as a bone graft substitute in tibial plateau fractures. Clin Orthop 1989;240:53-62.

77. Cornell CN. Osteoconductive materials and their role as substitutes for autogenous bone grafts. Orthop Clin North Am 1999;30:591-8.

78. Bohner M. Calcium orthophosphates in medicine: from ceramics to calcium phosphate cements. Injury 2000;31(Suppl. 4):SD 37-47.

79. Hollinger JO & Brekke J. Role of bone substitutes. Clin Orthop 1996;324:55-65.

80. Rey C. Calcium Phosphates for Medical Applications. In: Zahid Amjad, editor. Calcium Phosphates in Biological and Industrial Systems. Boston, USA: Kluwer Academic Publishers, 1998. pp. 217-251.

81. Tung SM. Calcium phosphates: structure, composition, solubility and stability. In: Zahid Amjad, editor. Calcium Phosphates in Biological and Industrial Systems. Boston, USA: Kluwer Academic Publishers; 1998. pp.1-19.

82. Gibson IR, Rehman I, Best SM & Bonfield W. Characterization of the transformation from calcium-deficient apatite to β-tricalcium phosphate. J Mater Sci Mater Med 2000;12:799-804.

83. Welcht JH & Gutt W. High temperature studies of the system calcium oxide-phosphorous pentoxide. J Chem Soc 1961;2:4442-4444.

84. Schroeder LW, Dickens B & Brown WE. Crystallographic studies of the role of Mg as a stabilizing impurity in β-$Ca_3(PO_4)_2$ - II. Refinement of Mg-containing β-$Ca_3(PO_4)_2$. J Sol State Chem 1977;22:253-262.

85. Bonel G, Heughebaert JC, Heughebaert M, Lacout JL & Lebugle A. Apatitic calcium orthophosphates and related compounds for biomaterials preparations. In: Ducheyne P, Lemons J, editors. Bioceramics: Material characteristics versus in vivo behaviour, Vol.253. New York, USA: Ann New York Acad Sci, 1988. pp.115-130

86. Brendel T, Engel A & Ruessel C. Hydroxyapatite coatings by a polimeric route. J Mater Sci: Mater in Med 1992;3:175-178.

87. Cheng PT. Formation of octacalcium phosphate and subsequent transformation to hydroxyapatite at low supersaturation: a model for cartilage calcification. Calcif Tissue Int 1987;40:339-343.

88. Fowler BO. Infrared studies of apatites. II Preparation of normal and isotopically substituted calcium, strontium, and barium hydroxyapatites and spectra-structure composition correlations. Inorg Chem 1974;13:207-214.

89. Koutsoukos PG. Influence of metal ions on the crystal growth of calcium phosphates. In: Zahid Amjad, editors. Calcium Phosphates in Biological and Industrial Systems. Boston, USA: Kluwer Academic Publishers, 1998. pp.143-171.

90. LeGeros RZ, Daculsi G, Orly I, Abergas T, Torres W. Solution mediated transformation of octacalcium phosphate (OCP) to apatite. Scann Microsc 1989;3:129-138.

91. Posner AS, Blumenthal N & Betts F. Chemistry and Structure of Precipitated Hydroxyapatites. In: Nriagu JO, Moore PB, editors. Phosphate Minerals. New York, USA: Springer Verlag, 1984. pp. 330-347.

92. Roy DM, Linnehan SA. Hydroxyapatite formed from coral skeleton carbonate by hydrothermic exchange. Nature 1974;247:220-227.

93. Tanahashi M, Kamiya K, Suzuki T & Nasu H. Fibrous hydroxyapatite grown in the gel system: effects of pH of the solution on the growth rate and morphology. J Mater Sci Mater Med 1992;3:48-53.

94. Takahashi H, Yashima M, Kakihana M & Yoshimura M. Synthesis of stoichiometric hydroxyapatite by a "gel" route from the aqueous solution of citric and phosphonoacetic acids. Eur J Solid State Inorg Chem 1995;32:829-835.

95. Yamashita K & Kanazawa T. Hydroxyapatite. In: Kanazawa T, editor. Inorganic Phosphate Materials. Tokyo, Japan: Kodansha, 1989. pp.15-54.

96. Young RA & Holcomb DW. Variability of hydroxyapatite preparations. Calcif Tissue Inter 1982;34:517-532.

97. Elliot JC. PhD Thesis 1964, University of London, London, England.

98. Posner AS. The mineral of bone. Clinical Orthopaedics 1985;200:87-99.

99. Elliot JC, Mackie PE & Young RA. Monoclinic hydroxyapatite. Science 1973;180:1055- 1057.

100. Elliot JC. In: Elliot JC, editor. Structure and chemistry of the apatites and other calcium orthophosphates. Amsterdam, Holland: Elsevier, 1994.

101. Morgan H, Wilson RM, Elliot JC, Dowker SEP & Anderson P. Preparation and characterisation of monoclinic hydroxyapatite and its precipitated carbonate apatite intermediate. Biomaterials 2000;21:617-627.

102. Watanabe T, Makitsuru K, Nakazawa H, Hara S, Suehiro T, Yamamoto A, Hiraide T & Ogawa T. Separation of double strand DNA fragments by high-performance liquid chromatography using a ceramic hydroxyapatite column. Anal Chim Acta, 1999;386:69-75.

103. Bett JAS, Christner LG & Hall WK. Studies of the hydrogen held by solids. XII. J Am Chem Soc 1967;89:5535-5541.

104. Matsumara Y, Kanai H & Moffat JB. Catalytic oxidation of carbon monoxide over stoichiometric and non-stoichiometric hydroxyapatites. J Chem Soc, Faraday Trans, 1997;93:4383-4387.

105. Suzuki T, Hastushika T & Miyake M. Synthetic. Hydroxyapatites as inorganic cation exchangers-Part 2. J Chem Soc, Faraday Trans I, 1981;78:3605-3611.

106. Takeuchi Y & Arai H. Removal of coexisting Pb2+, Cu2+ and Cd2+ ions from water by addition of hydroxyapatite powder. J Chem Eng of Japan 1990;23:75-80.

107. Aoki H. In: Aoki H, editor. Science and Medical Applications of Hydroxyapatite. Tokyo, Japan: Takayama Press System Center, 1991.

108. LeGeros RZ. Ultrastructural Properties of Human Enamel Apatite. In: Lazzari EP editor. Handbook of Experimental Aspects of Oral Biochemistry. Florida, USA: CRC Press, 1983. p.159-179.

109. Koutsopoulos S. Synthesis and characterization of hydroxyapatite crystals: a review study on the analytical methods. Biomaterials 2002;62:600-612.

110. Narasaraju TSB & Phebe DE. Review: Some physico-chemical aspects of hydroxyapatite. J Mat Sci 1996;31:1-21.

111. Bonel G & Montel G. Sur une nouvelle apatite carbonatée synthétique. Compt Rend 1964;258:923-926.

112. LeGeros RZ, Trautz OR., LeGeros JP & Klein E. Carbonate substitution in the apatite structure (1). Extrait du bulletin de la societé chimique de France 1968; special number:1712-1718.

113. Kreidler ER & Hummel FA. The crystal chemistry of apatite: structure fields of fluor and chloroapatite. The American Mineralogist 1970;55:171-184.

114. LeGeros RZ, Singer L, Ophaug RH, Quirolgico G, Thein A & LeGeros JP. The effect of fluoride on the stability of synthetic and biological (bone) mineral apatites. In: Menczel J, Robin GC, Makin M, Steinbeg R, editors. Osteoporosis. New York, USA: Wiley & Sons, 1982. pp. 327-341.

115. Gibson IR, Best SM & Bonfield W. Chemical characterisation of silicon-substituted hydroxyapatite. J Biomed Mater Res 1999;44:422-428.

116. LeGeros RZ, Shirra WP, Miravite M & LeGeros JP. Amorphous calcium phosphates: synthetic and biological. Physico-chimie et cristallographie des apatites d'interest biologique 1975;CNRS Nº230:105-115.

117. LeGeros RZ, Miravite MA, Quirolgico GB & Curzon MEJ. The effect of some trace elements on the lattice parameters of human and synthetic apatites. Calc Tiss Res 1977;22:362-367.

118. LeGeros RZ, Taheri MH, Quirolgico GB & LeGeros JP. Formation and stability of apatites: effects of some cationic substituents. In: Proceedings of 2nd International Congress on Phosphorous Compounds. Boston, USA, 1980. pp.89-103.

119. Sudarsanan K, Markie PE & Young RA. Comparison of synthetic and mineral fluorapatite Ca5(PO4)3F, in crystallographic detail. Mat Res Bull 1972;7:1331-1338.

120. Dickens B & Brown WE. The crystal structure of $Ca_7Mg_9(Ca,Mg)_2(PO_4)_{12}$. Tmpm 1971;16:79-104.

121. LeGeros RZ, Trautz OR, LeGeros JP & Shirra WP. Apatite crystallites: effects of carbonate on morphology. Science 1967;155:1409-1411.

122. Trombe JC & Montel G. Process for treating apatites applicable to other minerals. CR Acad Sci Ser C 1974;278:1227-1230.

123. Christoffersen MR, Thyregod HC & Christoffersen J. Effects of aluminum(III), chromium(III), and iron(III) on the rate of dissolution of calcium hydroxyapatite crystals in the absence and presence of chelating agent desferrixamine. Calcif Tissue Int 1987;41:27-30.

124. Koutsoukos PG & Nancollas GH. Influence of strontium ion on the crystallization of hydroxyapatite from aqueous solutions. J Phys Chem 1981;85:2403-2408.

125. Christoffersen J, Christoffersen MR, Kolthoff N & Barenholdt O. Effects of strontium ions on growth and dissolution of hydroxyapatite and on bone mineral detection. Bone 1997;20:47-54.

126. Neuman WF, Bjornerstedt B & Mulryan BJ. Synthetic hydroxyapatite crystals II. Aging and strontium incorporation. Arch Biochem Biophys 1963;101:215-224.

127. Brandi UL. New treatment strategies: Ipiflavone, strontium, vitamin D metabolites and analogs. Am J Med 1993;95:695-745.

128. Morohashi T, Sane T & Yamada S. Effects of strontium on calcium metabolism in rats. I. A distinction between the pharmacological and toxic doses. Japn J Pharmacol 1994;64:155-162.

129. Bronner F. Metals in bone: aluminium, boron, cadmium, chromium, lead, silicon, and strontium. In: Bilezikian JP, Lawrence GR, Gideon AR, editors. Principles of bone biology. San Diego, USA: Academic Press, 1996. pp. 295-303.

130. Abdelkader SB, Khattech I, Rey C & Jemal M. Synthése, caractérisation et thermochimie d'apatites calco magnésiennes hydroxylées et fluorées. Thermochimica Acta 2001;376:25-36.

131. Boskey AL & Posner AS. Mg stabilization of amorphous calcium phosphates: a kinetic study. Mater Res Bull 1974;9:907-916.

132. LeGeros RZ, Contiguglia SR & Alfrey AC. Pathological calcifications associated with uremia: two types of calcium phosphates deposits. Calcif Tissue Res 1973;13:173-179.

133. LeGeros RZ. The unit-cell dimensions of human enamel apatite: effect of chloride incorporation. Archs Oral Biol 1974;20:63-71.

134. Posner AS & Betts F. Molecular control of tissue mineralization. In: Veis A, editor. The chemistry and biology of mineralized connective tissue. New York, USA: Elsevier-zorth Holland, 1981. pp.257.

135. Posner AS, Blumenthal NC & Boskey AL. Model of aluminum-induced osteomalacia: inhibition of apatite formation and growth. Kidney Int 1986;29:17-19.

136. Ergun C, Webster TJ, Bizios R & Doremus RH. Hydroxylapatite with substituted magnesium, zinc, cadmium, and yttrium. I. Structure and microstructure. J Biomed Mater Res 2002;59:305-311.

137. Webster TJ, Ergun C, Doremus RH & Bizios R. Hydroxylapatite with substituted magnesium, zinc, cadmium, and yttrium. II. Mechanisms of osteoblast adhesion. J Biomed Mater Res 2002;59:312-317.

138. Bigi A, Foresti E, Gandolfi M, Gazzano M & Roveri N. Inhibiting effect of zinc on hydroxylapatite crystallisation. J Inorg Biochem 1995;58:49-58.

139. Samachon J, Dennis H, Fowler R & Schmitz A. The reaction of 65Zn with the surfaces of bone and bone mineral. Biochim Biophys Acta 1967;148:767-773.

140. Miyahara T, Yomada H, Takeuchi M, Kozuka H, Kato T & Sudo H. Inhibitory effects of cadmium on in vitro calcification of a clonal osteogenic cell, Mc3T3-E1. Toxicol Appl Pharmacol 1988;96:52-59.

141. Chang LW, Reuhl KR & Wade PR. Pathological effects of cadmium poisoning. In: Nriagu JO, editor. Cadmium in the environment, Part II: Health effects. New York, USA: Wiley, 1981. p.784-839.

142. Blumenthal NC, Cosma V, Skyler D, LeGeros J & Walters M. The effect of cadmium on the formation and properties of hydroxyapatite in vitro and its relation to cadmium toxicity in the skeletal system. Calcif Tissue Int 1995;56:316-322.

143. Barry PS. A comparison of concentrations of lead in human tissues. Br J Ind Med 1975;32:119-139.

144. Levin SM & Goldberg M. Clinical evaluation and management of lead-exposed construction workers. Am J Ind Med 2000;37:23-43.

145. Termine JD & Posner AS. Infrared analysis of rat bone: age dependency of amorphous and crystalline mineral fractions. Science 1966;153:1523-1525.

146. El Feki H, Savariault JM & Ben Salah A. Structure refinements by Rietveld method of partially substituted hydroxyapatite: $Ca_9Na_{0.5}(PO_4)_{4.5}(CO_3)_{1.5}(OH)_2$. J Alloys Compounds 1999;287:114-120.

147. Andress DL, Maloney NA, Endres DB & Sherrard DJ. Aluminum-associated bone disease in chronic renal failure: high prevalence in a long-term dialysis population. J Bone Min Res 1986;1:391-398.

148. Andress DL, Maloney NA, Coburn JW, Endres DB & Sherrard DJ. Osteomalacia and aplastic bone disease in aluminum-related osteodystrophy. J Clin End & Metab 1987;65:11-16.

149. Christoffersen MR & Christoffersen J. The effect of aluminium on the rate of dissolution of calcium hydroxyapatite: a contribution to the understanding of aluminium- induced bone diseases. Calcif Tissue Int 1985;37:673-676.

150. Goodman WG & Duarte MEL. Aluminum: effects on bone and role in the pathogenesis of renal osteodystrophy. Miner Electrolyte Met 1991;17:221-232.

151. O´Brien A, Moore DP & Keogh JAB. Aluminium osteomalacia in chronic renal failure patients neither on dialysis nor taking aluminium containing phosphate binders. Irish J Med Sci 1990;150:74-76.

152. Severson AR, Haut CF, Firling CE & Huntley TE. Influence of short-term aluminium exposure on demineralized bone matrix induced bone formation. Arch Toxicol 1992;66:706-712.

153. Rey C, Collins B, Goehl T, Dickson IR & Glimcher MJ. The carbonate environment in bone mineral: a resolution-enhanced Fourier transform infrared spectroscopy study. Calcif Tissue Int 1989;45:157-164.

154. Rey C, Renugopalakrishnan V, Collins B & Glimcher MJ. Fourier Transform infrared spectroscopic study of the carbonate ions in bone mineral during aging. Calcif Tissue Int 1991;49:251-258.

155. LeGeros RZ. Variations in the crystalline components of human dental calculus. I. Crystallographic and spectroscopic analysis. J Dent 1974;53:45-50.

156. Daculsi G. Biphasic calcium phosphate concept applied to artificial bone, implant coating and injectable bone substitute. Biomaterials 1998;19:1473-1478.

157. Heughebaert M, LeGeros RZ, Gineste M & Guilhem A. Hydroxyapatite (HA) ceramics implanted in non-bone forming site. Physico-chemical characterization. J Biomed Mat Res 1988;22:257-68.

158. Gauthier O, Bouler JM, Aguado E, LeGeros RZ, Pilet P & Daculsi G. Elaboration conditions influence physicochemical properties and in vivo bioactivity of macroporous biphasic calcium phosphate ceramics. J Mater Sci Mater Med 1999;10:199.

159. Kivrak N & Cuneyt Tas A. Synthesis of calcium hydroxyapatite-tricalcium phosphate (HA-TCP) composite bioceramic powders and their sintering behaviour. J Am Ceram Soc 1998;82:2245-2252.

160. Petrov OE, Dyulgerova E, Petrov L & Ropova R. Characterization of calcium phosphate phases obtained during the preparation of sintered biphase Ca-P ceramics. Mater Lett 2001;48:162-167.

161. Slosarczyk A & Piekarcyk. Ceramic materials on the basis of hydroxyapatite and tricalcium phosphate. Ceramics International. 1999;25[6]:561-565.

162. Tancred DC, McCormack BAO & Carr AJ. A synthetic bone implant macroscopically identical to cancellous bone. Biomaterials 1998;19:2303-2311.

163. Bouler JM, Trecant M, Delecrin J, Royer J, Passuti N & Daculsi GJ. Macroporous biphasic calcium phosphate ceramics: Influence of five synthesis parameters on compressive strength. J Biomed Mater Res 1996;32:603-609.

164. Yang X & Wang Z. Synthesis of biphasic ceramics of hydroxyapatite and β-tricalcium phosphate with controlled phase content and porosity. J Mater Chem 1998;8:2233-2237.

165. Lin FH, Liao CJ, Chen KS, Sun JS & Lin CY. Preparation of β-TCP/HAP biphasic ceramics with natural bone structure by heating bovine cancellous bone with the addition of $(NH_4)_2HPO_4$. J Biomed Mater Res 2000;51:157-163.

166. Itatani K, Nishioka T, Seike S, Howell FS, Kishiota A & Kinoshita M. Sinterability of β-Calcium Orthophosphate Powder Prepared by Spray-Pyrolysis. J Am Ceram Soc 1994;77:801-805.

167. Manjubala I & Sivakimar M. In situ synthesis of biphasic calcium phosphate ceramics using microwave irradiation. Mater Chem Phys 2001;71:272-278.

168. Cunneyt Tas A. Combustion synthesis of calcium phosphate bioceramic powders. J Eur Ceram Soc 2000;20:2389-2394.

169. Hench LL. Bioceramics: From Concept to Clinic. J Am Ceram Soc. 1991;75 (7),1487-1510.

170. Ohgushi H, Okumura M, Yoshikawa T, Inoue K, Senpuku N, Tamai S & Shors EC. Bone formation processin porous calcium carbonate and hydroxyapatite. J Biomed Mater Res 1992;26:885-895.

171. Oorlovskii, VP, Komlev VS & Barinov SM. Hydroxyapatite and Hydroxyapatite-Based Ceramics. Inorganic Materials 2002;38[10]:1159-1172.

172. Shors EC & Holmes RE. In: An Introduction to Bioceramics, edited by Hench LL, Wilson J. Adv. Ser. Ceram. 1 (World Scientific Publishing Co. Pte. Ltd., London, Hong Kong, Singapore, 1993), pp. 181.

173. Lemos IAF & Ferreira, JMF. Porous Bioactive Calcium Carbonate Implants Processed by Starch Consolidation. J Mat Sci & Engineering C 2000;C11:35-40.

174. Prado da Silva MH, Lemos AF, Ferreira JMF & Santos JD. Porous Glass Reinforced Hydroxyapatite Materials Produced With Different Organic Additives. Journal of Non-Crystalline Solids 2002;304[1-3]:284-292.

175. Prado da Silva MH, Lemos AF, Santos JD & Ferreira JMF. Production of Porous Biomaterials Based on Glass Reinforced Hydroxyapatite Composites. Key Engineering Materials. Advanced Materials Forum I 2002;230-232:483.

176. White E & Shors EC. Biomaterial aspects of Interpore-200 porous hydroxyapatite. Dent Clin North Am 1986;30:49-67.

177. Paul W & Sharma CP. Development of porous spherical hydroxyapatite granules: application towards protein delivery. J Mater Sci: Mater Med 1999;10:383-388.

178. Liu D. Fabrication and characterization of porous hydroxyapatite granules. Biomaterials 1996;17:1955-1957.

179. Komlev VS, Barinov SM & Koplik EV. A method to fabricate porous spherical hydroxyapatite granules intended for time-controlled drug release. Biomaterials 2002;23:3449-3454.

180. Lamprecht A, Shafer U & Lehr C. Structural analysis of microparticles by confocal laser scanning microscopy. AAPS PharmSciTech 2000;1[3]:article 17.

181. Lemos AF, Rocha JHG, Ventura JM & Ferreira JMF. Method for Tailoring and Control the Morphology, Size and Porosity of Calcium Phosphate Granules, Key Engineering Materials 2005;284-286:309-312.

182. Gourlay SJ, Rice RM, Hegyeli AF, Wade CWR, Dillon JG, Jaffe H & Kulkarni RK. Biocompatibility testing of polymers: in vivo implantation studies. J Biomed Mater Res 1978;12:219.

183. Kobayashi H, Shiraki K & Ikada Y. Toxicity test of biodegradable polymers by implantation in rabbit cornea. J Biomed Mater Res 1992;26:1476.

184. Lam KH, Schakenraad JM, Esselbrugge H, Feijen J & Nieuwenhuis P. The effect of phagocytosis of poly(L-lactic acid) fragments on cellular morphology and viability. J Biomed Mater Res 1993;27:1569.

185. Matlaga BF, Yasenchak LP & Salthuose TN. Tissue response to implanted polymers: the significance of sample shape. J Biomed Mater Res 1976;10:391.

186. Nakamura T, Shimizu Y, Okumura N, Matsui T, Hyon SH & Shimamoto T. Tumorigenicity of poly-Llactide (PLLA) plates compared with medical-grade polyethylene. J Biomed Mater Res 1994;28:17.

187. Vergara JA, Quinones CR, Nasjleti CE & Caffesse RG. Vascular response to guided tissue regeneration procedures using nonresorbable and bioabsorbable membranes in dogs. J Periodontol 1997;68[3]:217-24.

188. Athanasiou KA, Niederauer GG & Agrawal CM. Sterilization, toxicity, biocompatibility and clinical application of polylactic acid/polyglycolic acid copolymers. Biomaterials 1996;17:96.

189. Miller RA, Brady JM & Cutright DE. Degradation rates of oral resorbable implants (polylactates and polyglycolates): rate modification with changes in PLA/PGA copolymer ratios. J Biomed Mater Res 1977;11:711.

190. Verheyen C, Klein C, deBlieck-Hogervorst J, Wolke J, vanBlitterswijk C & deGroot K. Evaluation of hydroxylapatite/poly(L-lactide) composites: physico-chemical properties. J Mater Sci: Mater Med 1993;4:58-65.

191. Visscher GE, Robinson RL, Maulding HV, Fong JW, Pearson JE & Argentieri GJ. Biodegradation of and tissue reaction to 50:50 poly(DL-lactide-co-glycolide) microcapsules. J Biomed Mater Res 1985;19:349.

192. Visscher GE, Pearson JE, Fong JW, Argentieri GJ, Robinson RL & Maulding HV. Effect of particle size on the in vitro and in vivo degradation rates of poly(DL-lactide-co-glycolide) microcapsules. J Biomed Mater Res 1988;22:733.

193. Meikle MC, Papaioannou S, Ratledge TJ, Speight PM, Watt-Smith SR, Hill PA & Reynolds JJ. Effect of poly DL-lactide-co-glycolide implants and xenogeneic bone matrix-derived growth factors on calvarial bone repair in the rabbit. Biomaterials 1994;15[7];513.

194. Cutright DE & Hunsuck EE. The repair of fractures of the orbital floor using biodegradable polylactic acid. Oral Surg 1972;33[1]:28.

195. Hollinger JO. Preliminary report on the osteogenic potential of a biodegradable copolymer of polylactide (PLA) and polyglycolide (PGA). J Biomed Mater Res 1983;17:73.

196. Vert M, Li SM & Garreau H. Attempts to map the structure and degradation characteristics of aliphatic polyesters derivated from lactic and glycolic acids. J Biomater Sci Polym 1994;6:639.

197. Winet H & Hollinger JO. Incorporation of polylactide/polyglycolide in a cortical defect: neoosteogenesis in a bone chamber. J Biomed Mater Res 1993;27:667.

198. Saitoh H, Takata T, Nikau H, Shintani H, Hyon SH & Ikada Y. Tissue compatibility of polylactic acids in the skeletal site. J Mat Sci: Mat in Med 1994;5:194.

199. Schakenraad JM & Dijkstra PJ. Biocompatibility of poly(DL-lactic acid/glycine) copolymers. Clin Mater 1991;7:253.

200. Duggirala SS, Mehta RC & De Luca PP. Interaction of recombinant human bone morphogenetic protein-2 with poly(d,l lactide-co-glycolide) microspheres. Pharm Dev Technol 1996;1[1]:11-9.

201. Duggirala SS, Rodgers JB & De Luca PP. The evaluation of lyophilized polymer matrices for administering recombinant human bone morphogenetic protein-2. Pharm Dev Technol 1996;1[2]:165-74.

202. Hetherington HE, Hollinger JO, Morris MR & Panje WR. Onlay bone augmentation with an osteoinductive implant. Ann Otol Rhinol Laryngol 1996;105(7):568-73.

203. Isobe M. Characteristics and osteoinductive activity of bone morphogenetic protein (BMP) encapsulated with poly (DL-lactide-co-glycolide). Kokubyo Gakkai Zasshi 1995;62(4):506-12.

204. Isobe M, Yamazaki Y, Oida S, Ishihara K, Nakabayashi N & Amagasa T. Bone morphogenetic protein encapsulated with a biodegradable and biocompatible polymer. J Biomed Mater Res 1996;32(3):433-8.

205. Kenley R, Marden L, Turek T, Jin L, Ron E & Hollinger JO. Osseous regeneration in the rat calvarium using novel delivery systems for recombinant human bone morphogenetic protein-2 (rhBMP-2). J Biomed Mater Res 1994;28(10):1139-47.

206. Kirker-Head CA, Gerhart TN, Armstrong R, Schelling SH & Carmel LA. Healing bone using recombinant human bone morphogenetic protein 2 and copolymer. Clin Orthop 1998;349:205-17.

207. Laurencin CT, Attawia MA, Elgendy HE & Herbert KM. Tissue engineered bone-regeneration using degradable polymers: the formation of mineralized matrices. Bone 1996;19(1 Suppl):93S-99S.

208. Lee SC, Shea M, Battle MA, Kozitza K, Ron E, Turek T, Schaub RG & Hayes WC. Healing of large segmental defects in rat femurs is aided by RhBMP-2 in PLGA matrix. J Biomed Mater Res 1994;28(10):1149-56.

209. Mayer M, Hollinger J, Ron E & Wozney J. Maxillary alveolar cleft repair in dogs using recombinant human bone morphogenetic protein-2 and a polymer carrier. Plast Reconstr Surg 1996;98(2):247-59.

210. Meikle MC, Mak WY, Papaioannou S, Davies EH, Mordan N & Reynolds JJ. Bone-derived growth factor release from poly(alpha-hydroxy acid) implants in vitro. Biomaterials 1993;14(3):177-83.

211. Miyamoto S, Takaoka K, Okada T, Yoshikawa H, Hashimoto J, Suzuki S & Ono K. Evaluation of polylactic acid homopolymers as carriers for bone morphogenetic protein. Clin Orthop Rel Res 1992;278:274.

212. Miyamoto S, Takaoka K, Okada T & Yoshikawa H. Polylactic acid-polyethylene glycol block copolymer. A new biodegradable synthetic carrier for bone morphogenic protein (BMP). Clin Orthop 1993;294:333.

213. Miyamoto S & Takaoka K. Bone induction and bone repair by composites of bone morphogenetic protein and biodegradable synthetic polymers. Ann Chir Gynaecol Suppl 1993;207:69.

214. Puleo DA, Huh WW, Duggirala SS & De Luca PP. In vitro cellular responses to bioerodible particles loaded with recombinant human bone morphogenetic protein-2. J Biomed Mater Res 1998;41(1):104-10.

215. Rodgers JB, Vasconez HC, Wells MD, De Luca PP, Faugere MC, Fink BF & Hamilton D. Two lyophilized polymer matrix recombinant human bone morphogenetic protein-2 carriers in rabbit calvarial defects. J Craniofac Surg 1998;9(2):147-53.

216. Yamazaki Y, Oida S, Ishihara K & Nakabayashi N. Ectopic induction of cartilage and bone by bovine bone morphogenetic protein using a biodegradable polymeric reservoir. J Biomed Mater Res 1996;30(1):1-4.

217. Medical Division of Ghimas. Toxicological evaluation of the incorporation of polymers and copolymers based on L-, D- and D,L-lactide and glycolide. Internal Data Ghimas, 1997.

218. Chambers TJ. The response of the macrophage to foreign material. In: Fundamental aspects of biocompatibility. vol. I, Williams D.F. ed., CRC press, Inc., Boca Raton, Florida, 1981.

219. Menei P, Daniel V, Montero-Menei C, Brouillard M, Pouplard-Barthelaix A & Benoit JP. Biodegradation and brain tissue reaction to poly(D,L-lactide-co-glycolide) microspheres. Biomaterials 1993; 14(6): 470-8.

220. Pietrzak WS, Sarver DR, Bianchini SD, D'Alessio K. Effect of simulated intraoperative heating and shaping on mechanical properties of a bioabsorbable fracture plate material. J Biomed Mater Res 1997;38(1):17-24.

221. Stahelin AC, Weiler A, Rufenacht H, Hoffmann R, Geissmann A & Feinstein R. Clinical degradation and biocompatibility of different bioabsorbable interference screws: a report of six cases. Arthroscopy 1997;13(2):238-44.

222. Coombes AG & Heckman JD. Gel casting of resorbable polymers. 1. Processing and applications. Biomaterials 1992;13(4):217-24.

223. Kleinschmidt J, Marden L, Kent D, Quigley N & Hollinger J. A multiphase system bone implant for regenerating the calvaria. J Plast Reconstr Surg 1993;94:581.

224. Levy F, Hollinger J & Szachowicz E. Effect of a bioresorbable film on regeneration of cranial bone. J Plast Reconstr Surg 1994;96:307.

225. Nelson JF, Stanford HG & Cutright DE. Evaluation and comparisons of biodegradable substance as osteogenic agents. Oral Surg 1977;43(6):836.

226. Hirvensalo E. Fracture fixation with biodegradable rods. Acta Orthop Scand 1989;60:601.

227. Stolberg L, Rolfe R, Gitlin N, Merritt J, Mann L, Linder J & Finegolg S. D-lactic acidosis due to abnormal gut flora. New Engl J Med 1982;306:1344.

228. Tormala P, Vasenius J, Vainionpaa S, Pohjonen T, Rokkanen P & Laiho J. Ultra high strength absorbable self-reinforced polyglycolide (SR-PGA) composites rods

for internal fixation of bone fractures: in vitro and in vivo study. J Biomed Mater Res 1991;25:1.

229. Vainionpaa S, Kilpikari J, Laiho J, Helevirta P, Rokkanen P & Tormala P. Strength and strength retention in vitro, of absorbable, self-reinforced polyglycolide (PGA) rods for fracture fixation. Biomaterials 1992;13:1012.

230. Brandt RB, Waters MG, Rispler MJ & Kline ES. D- and L-lactate catabolism to CO2 in rat tissue. Proc Soc Exp Biol Med 1984;175:328.

231. Cutright DE & Hunsuck EE. Tissue reaction to the biodegradable polylactic acid sutures. Oral Surg 1971;31(1):134.

232. Andrew SD, Phil GC & Marra KG. The influence of polymer blend composition on the degradation of polymer/hydroxyapatite biomaterials. J Mater Sci: Mater Med 2001;12:673-7

233. Heidemann W, Jeschkeit S, Ruffieux K, Fischer JH, Wagner M & Kruger G. Degradation of poly(D,L)lactide implants with or without addition of calcium phosphates in vivo. Biomaterials 2001;22:2371-81.

234. Fukuzaki H, Yoshida M, Asano M & Kumakura M. In vivo characteristics of low molecular weight copolymers compared of L-lactic acid and various D,L-hydroxy acids as biodegradable carriers for drug delivery system. Biomaterials 1990;11:441.

235. Reed AM. In vivo and in vitro studies of biodegradable polymers for use in medicine and surgery. PH.D. Thesis, University of Liverpool, 1978.

236. Williams DF & Most E. Enzyme-accelerated hydrolysis of poly(glycolic acid). J Bio Eng 1977;1:231.

237. Williams DF. Enzyme hydrolysis of polylactic acid. Eng Med 1981;10:5.

238. Holland SJ, Tighe BJ & Gould PL. Polymers for biodegradable medical devices. 1. The potential of polyesters as controlled macromolecular release systems. J Controlled Rel 1986;4:155.

239. Cutright DE, Bienvenido P, Beasly JD & Larsen WJ. Degradation rates of polymers and copolymers of polylactic and polyglycolic acids. Oral Surg Oral Med Oral Pathol 1974;37:142.

240. Hausberger AG & De Luca PP. Estimation of poly(D,L-lactide-co-glycolide) 50:50 comonomer distribution by 13C-NMR and its effect on copolymer solubility. Pharmac Res 1993;10(10):PDD 7410.

241. Matsusue Y, Yamamuro T, Oka M, Shikinami Y, Hyon SH & Ikada Y. In vitro and in vivo studies on bioabsorbable ultra-high-strength poly(L-lactide) rods. J Biomed Mater Res 1992;26:1553.

242. Pistner H, Gutwald R, Ordung R, Reuther J & Muhling J. Poly(L-lactide): a long-term degradation study in vivo. Biomaterials 1993;14(9):671.

243. Yamaguchi K & Anderson JM. In vivo biocompatibility studies of Medisorb® 65/35 D,L-lactide/glycolide copolymer microspheres. J Controlled Rel 1993;24:83.

244. Boccaccini AR, Blaker JJ, Maquet V, Day RM & Jerome R. Preparation and characterisation of poly(lactide-co-glycolide) (PLGA) and PLGA/Bioglass(R) composite tubular foam scaffolds for tissue engineering applications. Mater Sci Eng C 2005;25:23-31.

245. Hedberg EL, Shih CK, Lemoine JJ, Timmer MD, Liebschner MAK & Jansen JA. In vitro degradation of porous poly(propylene fumarate)/ poly(DL-lactic-co-glycolic acid) composite scaffolds. Biomaterials 2005;26:3215-25.

246. Ignjatovic N, Tomic S, Dakic M, Miljkovic M, Plavsic M & Uskokovc D. Synthesis and properties of hydroxyapatite/poly-Llactide composite biomaterials. Biomaterials 1999;20:809-16.

247. Ignjatovic N, Plavsic M, Miljkovic M, Zivkovic Lj & Uskokovic D. Microstructural characteristic of Ca-hydroxyapatite/poly-L-lactide based composites. J Microsc 1999;196:243-8.

248. Kim HW, Knowles JC & Kim HE. Hydroxyapatite/poly([epsilon]- caprolactone) composite coatings on hydroxyapatite porous bone scaffold for drug delivery. Biomaterials 2004;25:1279-87.

249. Niiranen H, PyhaltoT, Rokkanen P, Kellomaki M & Tormala P. In vitro and in vivo behaviour of self-reinforced bioabsorbable polymer and self-reinforced bioabsorbable polymer/bioactive glass composites. J Biomed Mater Res A 2004;69A:699-708.

250. Yao J, Radin S, Leboy PS & Ducheyne P. The effect of bioactive glass content on synthesis and bioactivity of composite poly (lactic-coglycolic acid)/bioactive glass substrate for tissue engineering. Biomaterials 2005;26:1935-43.

251. Zhang K, Wang Y, Hillmayer MA & Francis LF. Processing and properties of porous poly(L-lactide)/bioactive glass composites. Biomaterials 2004;25:2489-500.

252. Di Silvio L & Bonfield W. Biodegradable drug delivery system for the treatment of bone infection and repair. J Mater Sci: Mater Med 1999;10:653-8.

253. Gittens SA & Uludag H. Growth factor delivery for bone tissue engineering. J Drug Target 2001;9:407-29.

254. Luginbuehl V, Meinel L, Merkle HP & Gander B. Localized delivery of growth factors for bone repair. Eur J Pharm Biopharm 2004;58:197-208.

255. Jiang G, Evans ME, Jones I, Rudd CD, Scotchford CA & Walker GS. Preparation of poly(e-caprolactone)/continuous bioglass fibre composite using monomer transfer moulding for bone implant. Biomaterials 2005;26:2281-8.

256. Khan YM, Dhirendra DS, Katti S & Laurencin CT. Novel polymersynthesized ceramic composite-based system for bone repair: an in vitro evaluation. J Biomed Mater Res A 2004;69A:728-37

257. Li H & Chang J. Preparation and characterisation of bioactive and biodegradable wollastonite/poly(D,L-lactic acid) composite scaffolds. J Mater Sci-Mater Med 2004;15:1089-95.

258. Lu HH, Tang A, Oh SC, Spalazzi JP & Dionisio K. Compositional effects on the formation of a calcium phosphate layer and the response of osteoblast-like cells on polymer-bioactive glass composites. Biomaterials 2005;26:6323-34

259. Maquet V, Boccaccini AR, Pravata L, Notingher I & Jerome R. Porous poly([alpha]-hydroxyacid)/Bioglass(R) composite scaffolds for bone tissue engineering. I: Preparation and in vitro characterisation. Biomaterials 2004;25:4185-94

260. Xu HHK, Quinn JB, Takagi S & Chow LC. Synergistic reinforcement of in situ hardening calcium phosphate composite scaffold for bone tissue engineering. Biomaterials 2004;25:1029-37.

261. Xu HHK & Simon JCG. Self-hardening calcium phosphate composite scaffold for bone tissue engineering. J Orthop Res 2004;22:535-43.

262. Oliveira JM, Miyazaki T, Lopes MA, Ohtsuki C & Santos JD. Bonelike®/PLGA hybrid materials for bone regeneration: Preparation route and physicochemical characterisation. J of Mater Sci: Mater in Med 2005;16:253- 259.

263. Petricca SE, Marra KG & Kumta PN. Chemical synthesis of poly(lactic-co-glycolic acid)/hydroxyapatite composites for orthopaedic applications. Acta Biomaterialia 2006;2:277-286.

264. Guan L & Davies JE. Preparation and characterisation of a highly macroporous biodegradable composite tissue engineering scaffold. J Biomed Mater Res 2004;71A:480-7.

265. Devin JE, Attawia MA & Laurencin CT. Three-dimensional degradable porous polymer-ceramic matrices for use in bone repair. J Biomater Sci Polym Ed 1996;7:661-9.

266. Dupraz AMP, De Wijn JR, Van De Meer SAT & de GrooT K. Characterization of silane-treated hydroxyapatite powders for use as filler in biodegradable composites. J Biomed Mater Res 1996;30(2):231-238.

267. Sheldon RP. Composite Polymeric Materials. Appl Sci Publ 1982;1:1.

268. Hooshmand T, Van Noort R & Keshvad A. Bond durability of the resin-bonded and silane treated ceramic surface. Dent Mater 2002;18:179-188.

269. Venhoven BAM, De Gee AJ, Werner A & Davidson CL. Silane treatment of filler and composite blending in a one-step procedure for dental restoratives. Biomaterials 1994;15(14):1152-1156.

270. Zhu PX, Ishikawa M, Seo WS, Hozumi A, Yokogawa Y & Koumoto K. Nucleation and growth of hydroxyapatite on an amino organosilane overlayer J Biomed Mater Res 2002;59(2):294-304.

271. Santos C, Luklinska ZB, Clarke RL & Davy KWM. Hydroxyapatite as a filler for dental composite materials: mechanical properties and in vitro bioactivity of composites. J Mater Sci: Mat Med 2001;12:565.

272. Wang M & Bonfield W. Chemically coupled hydroxyapatite-polyethylene composites: structure and properties. Biomaterials 2001;22(11):1311-1320.

273. Yerby SA, Paal AF, Young PM, Beaupr ´E GS, Ohashi KL & Goodman SB. The effect of a silane coupling agent on the bond strength of bone cement and cobalt-chrome alloy. J Biomed Mater Res 2000;49(1):127.

Chapter 2

Rietveld analysis and phase evolution with heat treatment temperature of calcium phosphates with different Ca/P ratios

A.F. Lemos,[a,b,c] D. Arcos,[d] M. Vallet-Regí,[d] and J.M.F. Ferreira[a]

[a] Dept. of Ceramics and Glass Engineering, University of Aveiro, CICECO, 3810-193 Aveiro, Portugal.

[b] Dept. of Metallurgic and Materials Engineering, Engineering Faculty of the University of Porto, Rua Dr. Roberto Frias, 4200-465 Porto, Portugal.

[c] Institute of Biomedical Engineering, University of Porto, Rua do Campo Alegre 823, 4150-180 Porto, Portugal.

[d] Dpto. Q. Inorganica y Bioinorganica, Ftad de Farmacia, UCM, Plaza Ramon y Cajal s/n, 28040 Madrid, Spain.

Abstract

A single phase stoichiometric hydroxyapatite (HA) and a calcium deficient hydroxyapatite (Ca-def-HA) were prepared by precipitation, adjusting the initial Ca/P ratios of the precursors under constant pH and temperature conditions. The as prepared powders were calcined at different temperatures to study the phase evolution and thermal stability. The powders were characterized by the following analytical techniques: thermo gravimetric and differential thermal analysis (TG–DTA), X-ray diffraction (XRD), X-ray fluorescence spectroscopy (XRF), Infrared Spectroscopy by Fourier Transformed (FT-IR), Raman, Scanning Electronic Microscopy (SEM) and Transmission Electronic Microscopy (TEM). The results have shown that Ca-def-HA resulted in the formation of biphasic (HA + β-TCP) or triphasic (HA+β-TCP+α-TCP) mixtures, upon heat treating above 700ºC or 1150ºC, respectively, while HA transforms into a biphasic mixture of (HA+α-TCP) above 1300ºC. Rietveld refinement was used to determine the phase analysis and the structural parameters of the phases formed. The information gathered is of high relevance for designing better calcium phosphate bioceramics.

Introduction

Hydroxyapatite [HA, $Ca_{10}(PO_4)_6(OH)_2$] and β-tricalciumphosphate [β-TCP, β-$Ca_3(PO_4)_2$] are potential bone substitutes for dental and orthopaedic applications due to their close chemical similarity with the inorganic component of vertebrate bone and tooth mineral[1-3] and their properties of biocompatibility and osteoconductivity.[4,5] Hydroxyapatite ceramics may be used in granular, dense or porous form, as a part of a composite or as a coating of a metal prosthesis,[6] and have been extensively used as an implant materials for non-load-bearing applications. In porous form, the surface area of HA bodies is greatly increased, which allows more cells or tissue to be carried into the implant, in comparison with dense HA. β-TCP is also currently used as bone graft replacement material due to its exceptional good tissue compatibility, direct bonding to regenerated bone without intermediate connective tissue, faster bone regeneration and resorbability.[7-10]

Presently, biphasic calcium phosphate (BCP) ceramics, an association of stable HA and resorbable β-TCP, have been recognized as most suitable bone substitutes having a better response to material resorption/bone substitution events than the single phase counterparts.[11-16] BCP mixtures of different HA/β-TCP ratios have also been proposed as delivery systems for drugs, antibiotics, hormones, carriers for growth factors and scaffolds for tissue engineering.[11] BCP are being used for repairing of periodontal and other orthopaedic related defects[14-15] and in oral and maxillofacial surgeries.[16] However, the preparation of BCP with the required phase compositions is not straightforward because several experimental factors can account for the final result. Up to the present, only some authors have reported on the synthesis of BCP from calcium deficient apatite (Ca-def-HA), ($Ca_{10-x}(PO4)_{6-x}(HPO_4)_x(OH)_{2-x}$), and on the effects of the heat treatment temperature on phase composition, including desirable (HA + TCP) and adverse (CaO) phases.[17-26] This is to say that more detailed studies are necessary to establish the relationships between the relevant process parameters and the final phase composition. In a previous work, Kannan *et al.*[27] have shown that different proportions of HA/β-TCP mixtures could be obtained by adjusting the Ca/P ratio of the precursors, but the effects of the sintering temperature were not studied.

The present work aims at detailing the influence of the sintering temperature on the phase transformation of a selected Ca-def-HA composition and of a single phase stoichiometric HA prepared under fixed pH and temperature conditions. The powders

properties were accessed by different characterisation techniques, including Rietveld refinement to determine the phase analysis and the structural parameters of the phases formed.

Experimental

Synthesis

The synthesis of stoichiometric hydroxyapatite (HA) and of a calcium deficient apatite (Ca-def-HA) was carried out with some minor modifications in the experimental procedure already reported.[27] Briefly, calcium nitrate tetrahydrate ($Ca(NO_3)_2.4H_2O$) (Ca) (Aldrich, Germany, purity > 99.5%) and diammonium hydrogen phosphate ($(NH_4)_2HPO_4$ (P) (Aldrich, Germany, purity > 99.5%) were used as starting chemical precursors for calcium and phosphorous, respectively. Two predetermined molar ratios of the precursor solutions were selected for the preparation of HA (Ca/P = 1.67) and Ca-def-HA (Ca/P = 1.62). The concentration of P precursor was kept constant (0.6 M) and the concentration of Ca precursor was conveniently adjusted. The precipitation was carried out in a fully automated apparatus that enables the control of pH, temperature and stirring conditions by slowly adding the $(NH_4)_2HPO_4$ solution to the continuously stirred (1000 rpm) solution of $Ca(NO_3)_2.4H_2O$. The pH of the mixed solution/suspension was maintained at 9 by adding the required amounts of a 8 M ammonium hydroxide (NH_4OH) solution. After the completion of the addition, the reaction was performed at 90ºC for 2 h under constant stirring conditions (1000 rpm). The precipitated suspension was poured out from the reactor, vacuum filtrated, and the as obtained cake was dried at 80°C overnight. The dried powders were ground and sieved through a mesh size of 200 μm, and then heat treated at different temperatures and fully characterised by different techniques described below.

Sample characterisation

The thermal behaviour of the dried powders was accessed by thermal analysis (TG–DTA), (Setaram Labsys TG–DTA/DSC, France), using a heating rate of $10ºC.min^{-1}$ between 30º and 1500ºC in air atmosphere. Based on the TG–DTA results, different temperatures in the range of 1100º to 1400ºC were selected to study the phase changes. The heat treatments were carried out in an electrical furnace equipped with a Pt30%Rh/Pt6%Rh-thermocouple (TERMOLAB, Fornos Eléctricos, Lda, Portugal) using a heating rate of 5ºC/min up to the required temperature, followed by a dwelling

time for 2 h and again cooled to room temperature at the rate of 5º/min. Particle size distributions were measured with a particle size analyser (COULTER LS230, UK), using the Fraunhofer optical model. The specific surface area and average pore diameter of the pores were assessed through the gas adsorption measurements in a Micromeritis Gemini 2370 V5.00 (Norcross, USA) after degassing the powders in a Micromeritis Flow prep 060 (Norcross, USA). The morphological features of the as prepared powders were observed by scanning electronic microscopy (SEM) (HITACHI, S-4100, Tokyo, Japan, 25 kV acceleration voltage, beam current 10 μA) and transmission electronic microscopy (TEM) (Hitachi-H-9000-NA, Japan) analysis.

Rietveld refinement

Refinement studies were performed for the powders heat treated at all temperatures indicated in Table 1. Collection of X-ray powder diffraction (XRPD) pattern data was performed with a high resolution Rigaku Geigerflex D/Mac, C Series diffractometer with Copper Kα radiation, λ = 1.540596 Å. For data collection, the following parameters were set; 2θ range of 5–110°; 2θ step width of 0.02°; time per step 6 s. The software FullProf.2k (Version 2.80 – Jul2004-LLB JRC) with the fundamental parameters approach was employed. Rietveld refinements were performed using the structural model of JCPDS card number # 70-2065 for β-TCP[28], # 29-0359 for α-TCP[29] and # 74-0565 for HA[30].

The size of individual crystallites was calculated from XRD data using the Scherrer approximation.[31] The values of full width at half maximum intensity ($\beta_{1/2}$) of the peak of (002) plane, representative of the crystallites along the *c*-axis, and of the peak of (300) plane, representative of the crystallites along the *a*-axis were used in the calculation according to equation (1)

$$D = \frac{k\lambda}{[\beta_{1/2}\cos\theta]} \qquad (1)$$

where D is the crystallite size, as calculated for the (hkl) reflection, λ is the wavelength of Cu Ka radiation (0.15406 nm), and k is the broadening constant varying with crystal habit and chosen as 0.85 for the elongated apatite crystallites.[32,33]

Results and Discussion

Characterisation of the as prepared powders

X-Ray diffraction

The XRD spectra of the as precipitated HA and Ca-def-HA powders shown in Fig. 1 reveal only small differences in peak width and absolute intensity of the diffraction patterns. Both show that poorly crystalline apatite characterized by broad diffraction bands has been obtained. The main characteristic peaks corresponding to hydroxyapatite (JCPDS # 74-0565) are assigned with the respective reflection planes. These results are according to other X-ray diffraction analysis of as-precipitated apatite powders that showed diffraction patterns similar to that of HA irrespective of the Ca/P ratio used.[34,35]

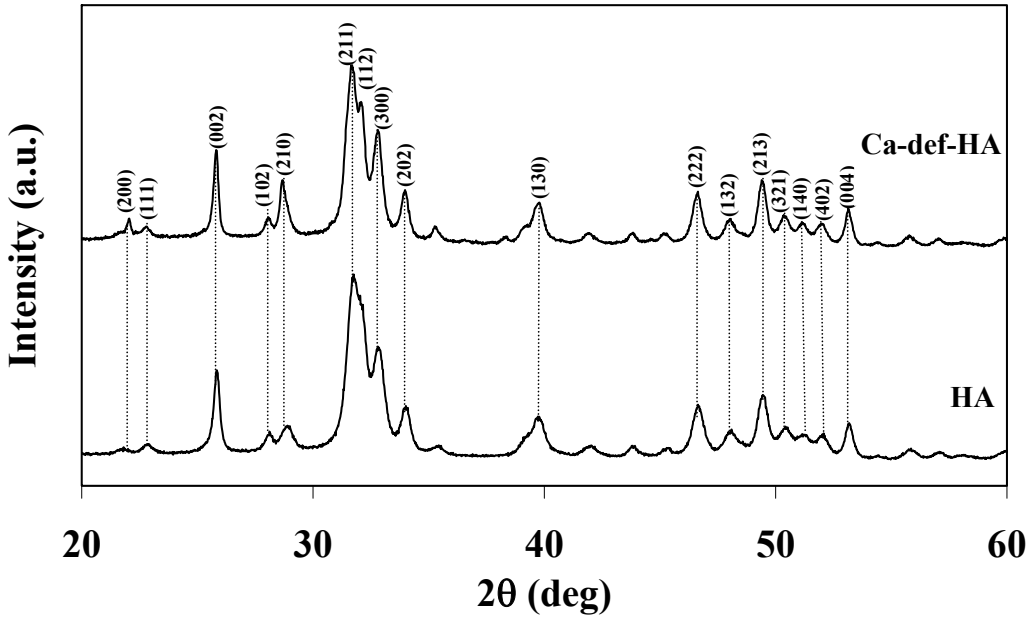

Figure 1. X-ray diffraction pattern for the as prepared powders, HA and Ca-def-HA.

FT-IR spectra

The FT-IR spectra of the as dried powders displayed in Fig. 2 also confirm the formation of apatite phase for both powders, with the observed fundamental vibrational modes of PO_4 group at 475, 574, 609, 966 e 1020-1120 cm^{-1}. The bands at 630 e 3570 cm^{-1} clearly notice the presence of OH group of apatite phase. Other relevant information from the FT-IR spectra is the presence of adsorbed water that could also be detected in the region around 3300-3600 cm^{-1}, and the presence of carbonate (CO_3) groups in both synthesized powders around the region at 1450 cm^{-1}, which might be due to the adsorbed species remaining from the aqueous precipitation.[33]

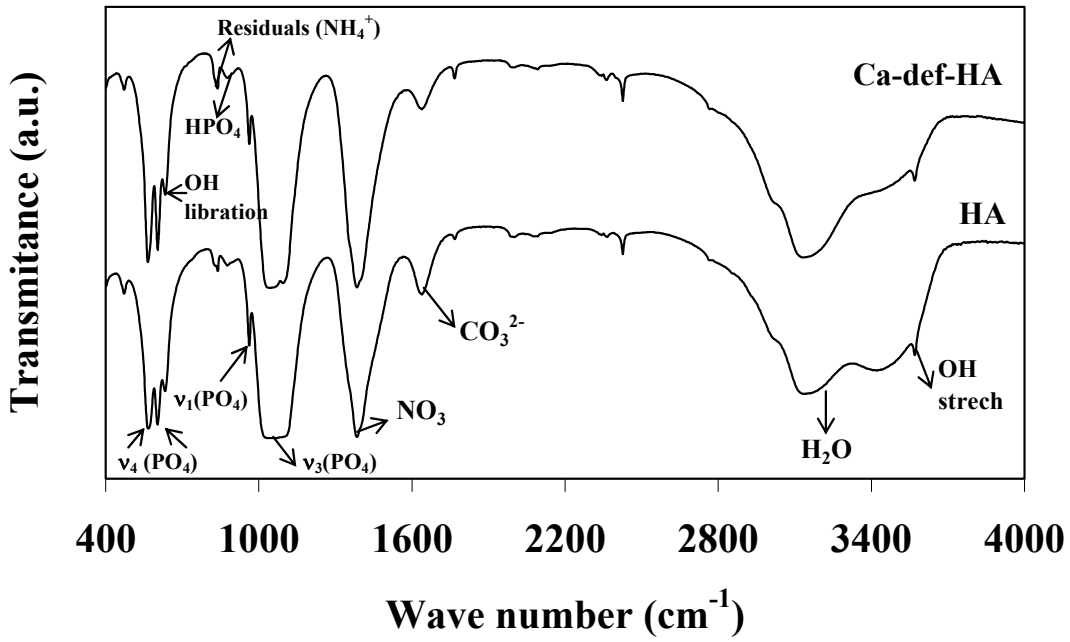

Figure 2. FT-IR spectra for as prepared powders, HA and Ca-def-HA**.**

The presence of nitrates (NO_3) is obvious from the peaks noticed in the FT-IR patterns in the region around 1320-1480 cm^{-1}. The presence of residual NH_4^+ ions at 875 cm^{-1} and nitrates is apparent in the two as prepared powders and tends to coincide with the observations made in a previous study.[36] Like with XRD results, no noticeable differences are apparent in the FT-IR spectra of the as prepared Ca-def-HA and HA powders. Therefore, hear treatments will be necessary to reveal the differences between the two compositions studied.

Physical characteristics

The particle/agglomerate size distributions of the powders right after precipitation are presented in Fig. 3. Ca-def-HA and HA powders present monomodal particle size distributions with average particle/agglomerate sizes, D_{50}, of approximately 9 μm, and 5 μm, respectively. Considering the relatively high specific surface areas of the as prepared powders, these size distribution curves support the hypothesis that the primary particles formed large agglomerates. This can be understood considering high ionic strength of the precipitation medium that compresses the electrical double layers around the colloidal particles leading to coagulation under the action of attractive Van der Waals forces.

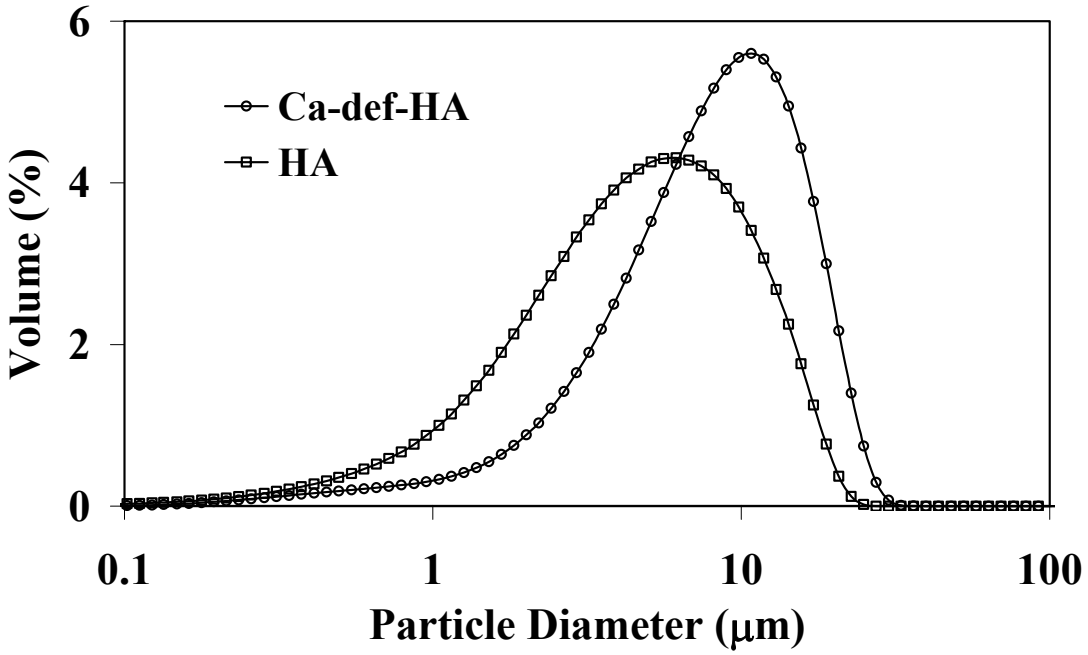

Figure 3. Particle size distribution of the as prepared powders, HA and Ca-def-HA.

The specific surface areas (SSA) and the average pore diameters (APD) of the powders HA and Ca-def-HA, as prepared and after calcinations at 1100ºC, are shown in Fig. 4. Values of 45.2 $m^2.g^{-1}$ and 31.8 $m^2.g^{-1}$ were measured for the as prepared HA and Ca-def-HA powders, respectively. This difference is consistent with an apparent higher

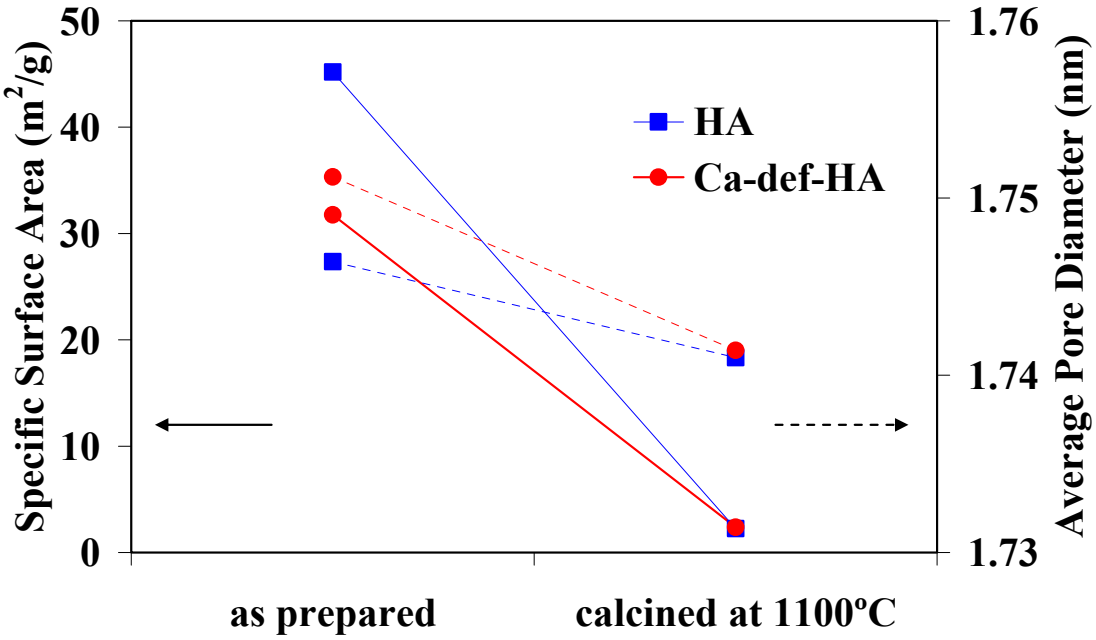

Figure 4. Specific surface area and average pore diameter of the as prepared and calcined at 1100ºC powders, HA and Ca-def-HA.

degree of particles agglomeration in the case of Ca-def-HA powder. This interpretation is also supported by the larger values of APD. After calcination at 1100ºC the values of SSA and APD of both powders decreased significantly to ~2.5 $m^2.g^{-1}$ and ~1.73 nm, respectively. Decreases of SSA and APD with the heat treatment temperature were more than expected due to the densification process,[37] with both samples reaching similar values after calcination.

Thermal analysis

The TG-DTA analysis for the as dried HA and Ca-def-HA samples presented in Fig. 5 show that mass loss has mostly occurred in three stages: (i) 30º-250ºC; (ii) 250º-700ºC; and (iii) 700º-800ºC. Along the first stage, both samples experienced similar weight losses of about 10%, thus accounting for the lattice bound water loss with no significant structural changes in this temperature range. Within the second temperature range, the samples HA and Ca-def HA show weight losses of about 10% and 20%, respectively.

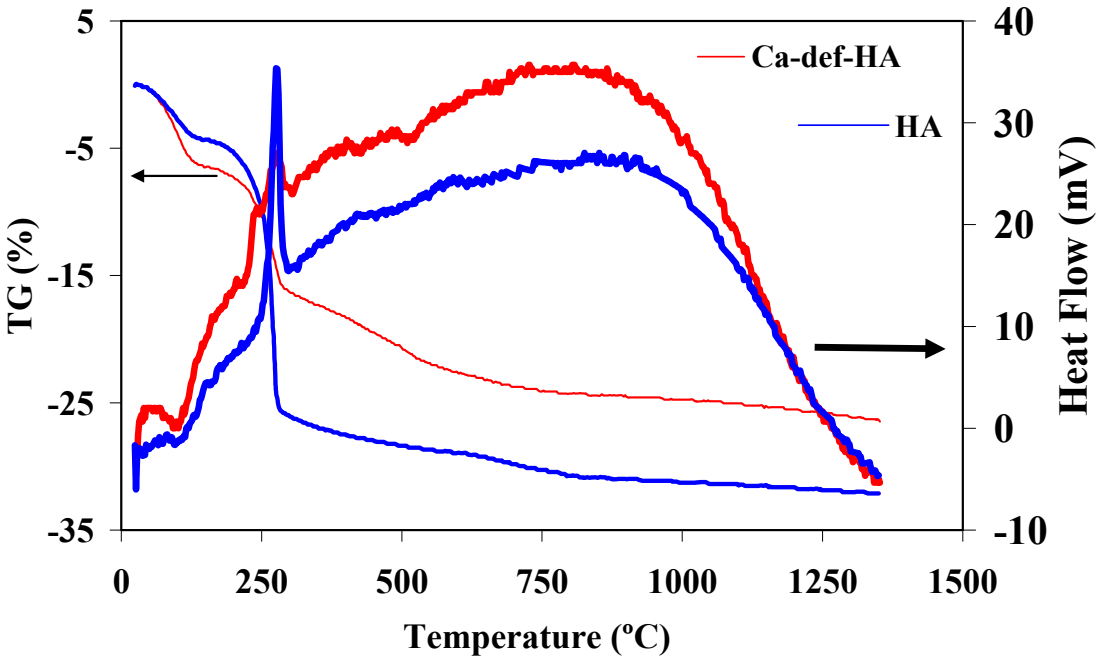

Figure 5. TG and DTA plots for the different Ca/P ratio powders, HA and Ca-def-HA.

The loss of residuals, chemisorbed water and carbonates are favoured in this temperature range.[37] The main differences in weight loss between the two powders are due to the different Ca/P ratios of the precursors. Since the starting phosphorous concentration was the same in both samples, the observed differences in loss could are

solely due to the different levels of added calcium. In this particular temperature range, some structural reorganization seems to occur as can be deduced from the exothermic peaks in the DTA curves at 280º-310ºC, the far most intense being observed for the Ca-def-HA powder. This exothermic effect can be attributed to the condensation of hydrogenophosphate ions (HPO_4^{2-}) to form pyrophosphates ($P_2O_7^{4-}$) as given below in equation 1:

$$2Ca^{2+} + 2HPO_4^{2-} \rightarrow Ca_2P_2O_7 + H_2O \qquad (1).$$

Along the temperature range of 700-800ºC the conversion of $Ca_2P_2O_7$ into β-$Ca_3(PO_4)_2$[38] occurred as described by equation 2, giving raise to a further weight loss of about 1.5% in the Ca-def-HA sample, being less evident in the case of HA.

$$Ca_2P_2O_7 + 2OH^- \rightarrow Ca_3(PO_4)_2 + H_2O \qquad (2).$$

These results show that calcium deficiency has a great impact on thermal behaviour of precipitated apatites.

Microstructural analysis

Fig. 6 shows the SEM microstructures of the as prepared powders: (a) HA; (b) Ca-def-HA. In both cases, it can be see that the primary particles are sub micrometer, but appear strongly agglomerated. The degree of agglomeration is apparently more severe in the case of Ca-def-HA, as inferred above from the SSA, APD data and by particle /agglomerate size distribution curves. Both powders consist of acicular shaped particles, with the aspect ratio being higher in the case of Ca-def-HA.

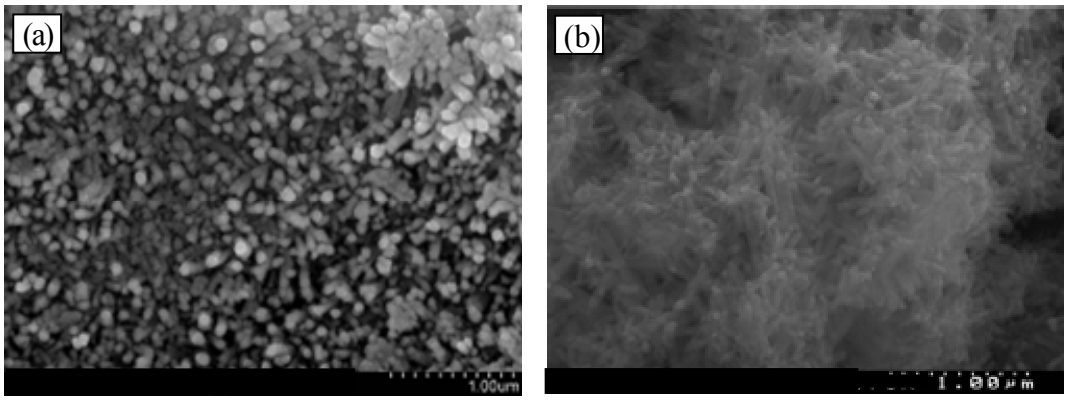

Figure 6. Microstructures of the samples HA (a) and Ca-def-HA (b) obtained by scanning electronic microscopy.

These microstructural differences were also confirmed by TEM observations. Fig. 7(a) is a HA diffraction pattern with a bright (211) peak and other typical rings like (002), (300), (222) and (213). The broad rings indicate the presence of amorphous material, being consistent with the observed broad XRD peaks (Fig. 1).

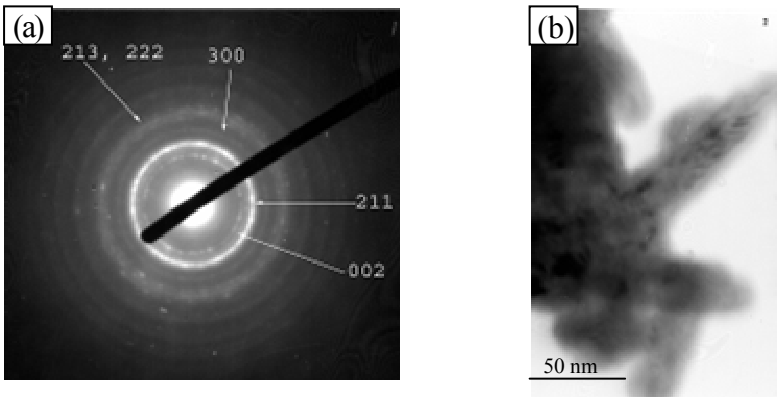

Figure 7. Transmission electronic microscopy results of the as prepared HA: (a) Powder diffraction cliché; (b) Particle size and morphology.

Fig. 7(b) confirms that the particles are needle like and form strong agglomerates. One sees an amorphous matrix in which are embedded needle like crystallites with a length of about 50 nm. From these observations it is possible to conclude that the as prepared HA consists of semi-crystalline and agglomerated particles.

Fig. 8 shows the TEM microstructural features of the Ca-def-HA powder. The particles are around 100 nm long and 20 nm wide and are made up of crystallites with sizes of ~ 20 nm. Fig. 8 (b) shows crystallites (bright) and amorphous part (greyish) indicating that each individual particle is semi-crystalline, with the crystalline part being surrounded by amorphous matter than bonds the crystallites, leading to the formation of agglomerates. The ED pattern (Fig. 8 (a)) shows that the (002) ring is not as prominent as in the case of HA powders and the thicker rings indicate the considerable amount of amorphous matter that the sample contains. These results enable to conclude that different starting Ca/P ratios affect the degree of crystallization of the apatite phase.

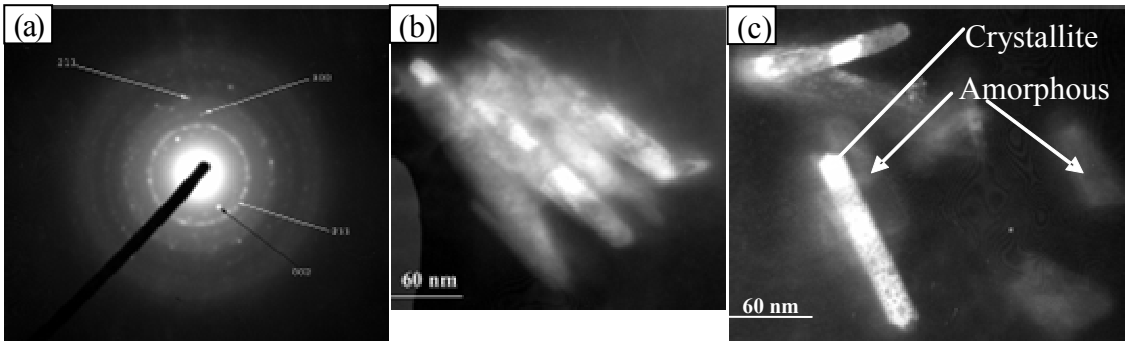

Figure 8. Transmission electronic microscopy results of the as prepared Ca-def-HA: (a) ED pattern; (b) Particle made up of crystallites and (c) Dark field image of single particles.

Characterisation of the calcined powders

Phase identification and determination of phase content by X-Ray diffraction

The evolution of crystalline phases with the heat treatment temperature for HA and Ca-def-HA powders, is shown in the XRD patterns of Fig. 9 and Fig. 10, respectively, within the 2θ range from 20º to 60º.

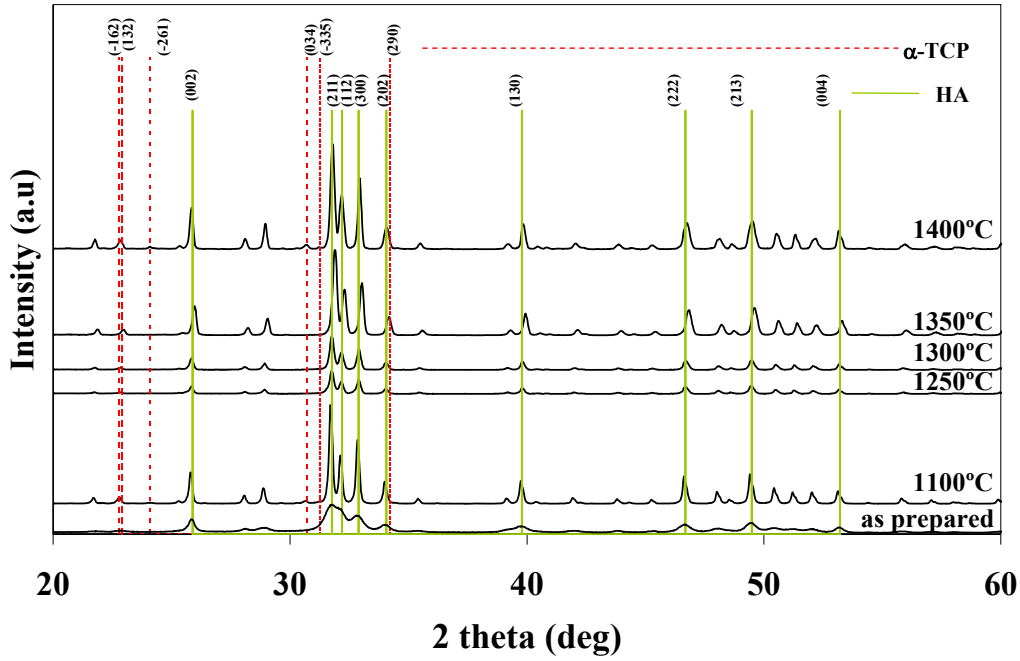

Figure 9. Crystalline phase evolution of HA powders with heat treatment temperatures.

The poor crystallinity of the as prepared powders, characterized by broad diffraction bands (Fig. 1), contrasts with the sharper spectral peaks exhibited after the different heat treatments. In the case of HA, highly crystalline hydroxyapatite (JCPDS # 74-565)[30] was obtained at 1100ºC, which then transformed into a biphasic mixture of HA+α-TCP for calcination temperatures ≥ 1350ºC. This is confirmed by the appearance of the characteristic reflection planes (-162) and (290) of α-TCP (JCPDS # 29-359).[29] This fact is corroborated by the results present in Table 1, where it is possible to observe that the formation of α-TCP could only be quantified at 1400ºC.

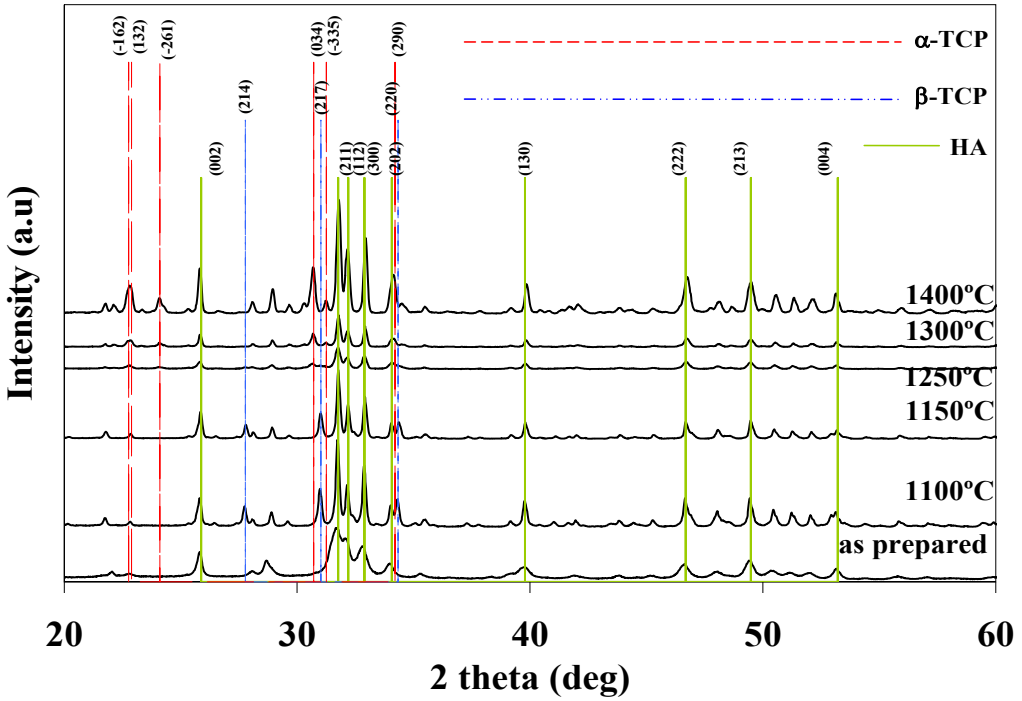

Figure 10. Crystalline phase evolution of Ca-def-HA powders with heat treatment temperatures.

Considering that the polymorph α-TCP usually derives from the transformation of β-TCP, as reported in literature,[39,40] these results suggest that the β-TCP formed from the partial decomposition of HA spontaneously transforms into α-TCP in the temperature range from 1350º-1400ºC.

The decrease of Ca/P ratio from 1.67 (HA) to 1.62 (Ca-def-HA) resulted in the formation of biphasic mixtures (HA+β-TCP) up to 1150ºC, as shown in Fig. 10 and Table 1. This temperature (1150ºC) seems to be the limit of the thermal stability of biphasic mixtures, since the component β-TCP starts to gradually transform into α-TCP at temperatures ≥ 1250ºC, disappearing completely at 1400ºC. The higher weight

fraction of HA was registered at 1250ºC and tended to slightly decrease with further increasing the temperature due to its direct transformation into α-TCP. The transformation of β-TCP into α-TCP was already reported[39,40] to occur at 1120ºC.

Table 1. Determined Rietveld quantification result of stoichiometric (HA) and calcium deficient apatite (Ca-def-HA).

Sample code	Sintering Temperature (ºC)	Wt. % of composition determined by Rietveld quantification			Ca/P ratio	
		HA	β-TCP	α-TCP	Experimental (in solution)	Calculated
HA	**1100**	100	-	-	1.67	1.67
	1250	100	-	-	1.67	1.67
	1300	100	-	-	1.67	1.67
	1350	100	-	-	1.67	1.67
	1400	94.38	-	5.62	1.67	1.66
Ca-def-HA	**1100**	64.3	35.7	-	1.62	1.60
	1150	68.6	31.4	-	1.62	1.61
	1250	69.7	9.5	20.7	1.62	1.61
	1300	64.7	2.4	32.9	1.62	1.60
	1400	66.4	-	33.6	1.62	1.61

In the case of Ca-def-HA, the phase composition was found to be strongly dependent on the heat treatment temperature. It was also attempted to determine the reliability of the resultant phase mixtures obtained through Rietveld refinement with those of experimental Ca/P ratios of the precursors by the following expression[41]:

$$Expected\ {}^{Ca}\!/_{P} = Wt.\%\ of\ HAP\,(Rietveld)\times 1.67 + Wt.\%\ of\ TCP\,(Rietveld)\times 1.5$$

From Table 1 it can be inferred that the experimental values used for the precursor solutions have shown good coincidence with the calculated Ca/P ratio determined from the phase content of the biphasic mixtures after refinement. As discussed before, HA only transforms into one of its polymorphs (α-TCP) at temperatures higher than 1350ºC, showing an excellent thermal stability. In the case of Ca-def-HA, a biphasic mixture seems to have been already formed in the as-precipitated powders. Upon heat treatment,

Ca-def-HA usually transforms into biphasic mixtures with the formation of β-TCP starting at about 750ºC and increasing at the expenses of HA as temperature increases up to ~1200ºC.[27] At 1250ºC, a third phase, α-TCP, could be identified and its content increases with sintering temperature, being the β-TCP phase completely transformed into α-TCP up to 1400ºC. These results are in good agreement with those reported by Kannan *et al.*[27], who have shown that the transformation of calcium deficient apatite into β-TCP strongly depends on the degree of calcium deficiency used in the precursor solutions.[39,40]

Refinement of lattice parameters

The unit cell and structural parameters determined by Dickens *et al.*[28] for β-TCP, Matthew *et al.* for α-TCP[29] and Sudarsanan *et al.*[30] for HA, were respectively used as starting values in the refinement of β-TCP, α-TCP and HA in biphasic and triphasic mixtures.

Tables 2, 3 and 4 collect the data of lattice parameters and the cell volumes calculated from the refined values for both powder mixtures. These values confirm the excellent similarities in the lattice data of HA, β-TCP and α-TCP phase of Ca-def-HA obtained after refinement which tends to follow well within the error limit.

Table 2. Refined lattice parameters and calculated cell volume of HA phase for HA and Ca-def-HA.

Sample code	Sintering Temperature (ºC)	Refined lattice data for HA phase			R-Bragg
		a-axis (Å)	*c*-axis (Å)	Cell volume (Å^3)	
HA	**1100**	9.41828 (4)	6.88089 (4)	1580.228	3.81
	1250	9.41309 (8)	6.88130 (8)	1578.581	3.71
	1300	9.41408 (8)	6.88198(7)	1579.069	3.33
	1350	9.41089 (9)	6.87995 (8)	1577.534	4.66
	1400	9.40231 (2)	6.87982 (7)	1574.629	4.85
Ca-def-HA	**1100**	9.42158 (6)	6.88401 (6)	1582.053	4.84
	1150	9.42049 (4)	6.88200 (5)	1581.225	4.65
	1250	9.40928 (0)	6.88029 (0)	1577.072	7.86
	1300	9.40928 (0)	6.88282 (0)	1577.652	5.67
	1400	9.40292 (0)	6.88459 (0)	1575.925	4.15

In the stoichiometric HA, although the lattice parameters are close to the reported ones, it is possible to note small distortions of the lattice with increasing temperatures (Table 2). At 1400ºC, the temperature at which α-TCP appears, there is a more pronounced decrease in cell volume, which can be attributed mainly to the decrease of the *a*-axis.

Table 3. Refined lattice parameters and calculated cell volume of β-TCP phase for Ca-def-HA.

Sample code	Sintering Temperature (ºC)	Refined lattice data for β-TCP phase			R-Bragg
		a-axis (Å)	*c*-axis (Å)	Cell volume (Å^3)	
Ca-def-HA	**1100**	10.43958 (13)	37.39925 (66)	3529.774	4.76
	1150	10.42575 (10)	37.44896 (61)	3525.107	4.63
	1250	10.40950 (0)	37.41093 (0)	3510.558	12.0
	1300	10.41991 (0)	37.56610 (0)	3532.173	10.6

In the case of Ca-def-HA, all the refined lattice data for HA phase confirmed its hexagonal structure (space group $P6_3/m$), the determined values being in close agreement with the crystal data for single phase HA ($a = b = 9.424$ Å, $c = 6.879$ Å, $\alpha = \beta = 90°$, and $\gamma = 120°$).[30] In case of β-TCP derived from Ca-def-HA, the refined lattice data also confirmed the typical rhombohedral structure (space group R3*c*) of this phase. The determined data are close to the values reported by Dickens *et al.*[28] for single phase crystalline β-TCP ($a = b = 10.439$ Å, $c = 37.375$ Å, $\alpha = \beta = 90°$, and $\gamma = 120°$). It is also clear from the data reported in Table 3 that the lattice parameters of the Ca-def-HA powder were not considerably affected by temperature within the temperature range there indicated.

The data reported in Table 4 shows excellent similarities with the lattice parameters values of α-TCP and of the Ca-def-HA powder after being heat treated in the at temperatures in the range of 1250º-1400ºC, confirming the conversion of Ca-def-HA powder into α-TCP phase.

Table 4. Refined lattice parameters and calculated cell volume of α-TCP phase for HA and Ca-def-HA.

Sample code	Sintering Temperature (ºC)	Refined lattice data for α-TCP phase				R-Bragg
		a-axis (Å)	*b*-axis (Å)	*c*-axis (Å)	Cell volume (Å^3)	
HA	**1400**	12.84371 (236)	27.27687 (339)	15.21204 (165)	5329.328	11.7
Ca-def-HA	**1250**	12.83815 (0)	27.29448 (0)	15.24982 (0)	5343.699	10.4
	1300	12.85953 (0)	27.30686 (0)	15.21533 (0)	5342.915	14.4
	1400	12.85596 (0)	27.28341 (0)	15.20737 (0)	5334.052	6.19

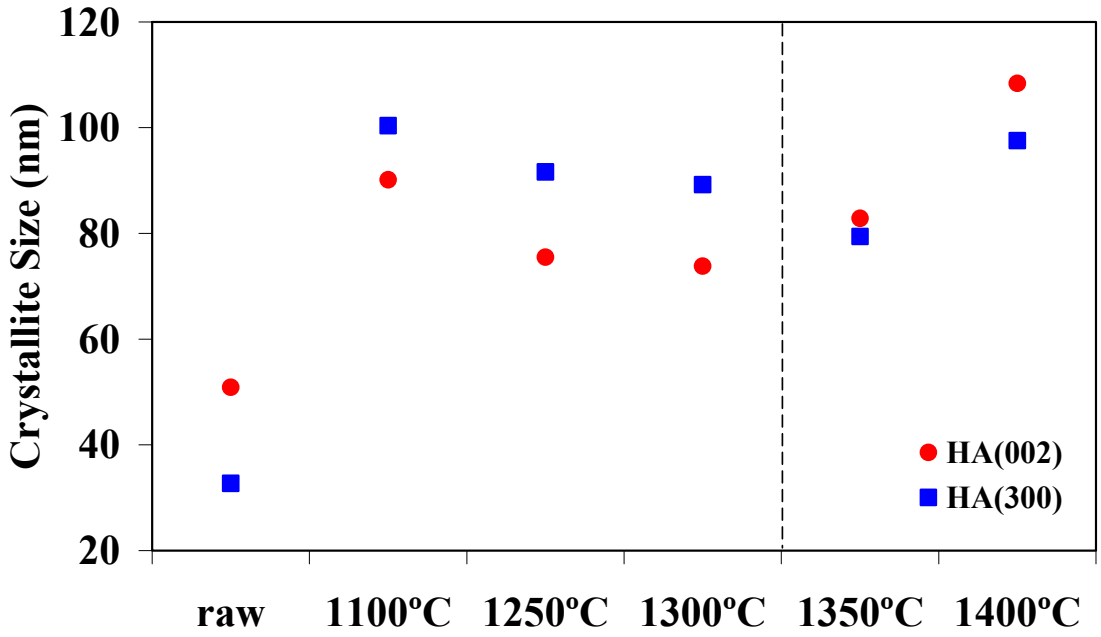

Figure 11. Crystallite size of the HA powders, as calculated for the (002) and (300) reflections. The dashed line represents the phase transformation.

The evolution of the crystallite size calculated along the directions *a* (300 plane) and *c* (002 plane), with increasing heat treatment temperatures for the HA and Ca-def-HA, are displayed in Figs. 11 and 12, respectively. The vertical dashed lines represent the

temperatures at which the main phase changes have been detected, namely the direct transformation of HA phase into α-TCP from HA, and the change from a biphasic to a

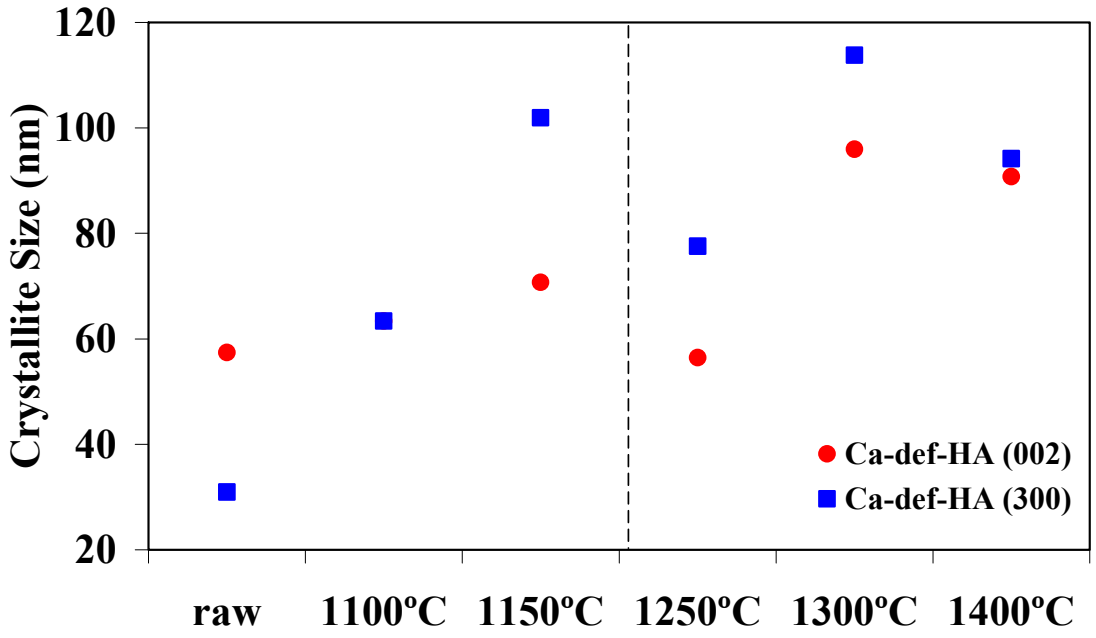

Figure 12. Crystallite size of the Ca-def-HA powders, as calculated for the (002) and (300) reflections. The dashed line represents the phase transformation.

triphasic mixture for the Ca-def-HA. As expected, the crystallite size of the HA powders (Fig. 11) increases with increasing calcination temperatures, but decreases when the phase transformation occurs, recovering again after that. The same trend is observed in the case of Ca-def-HA powders (Fig.12).

Conclusions

Both precipitated powders, HA and Ca-def-HA, consist of acicular shaped particles, with the aspect ratio being higher in the case of Ca-def-HA. The as prepared HA consists of semi-crystalline and agglomerated particles, with a length of about 50 nm. The Ca-def-HA particles are around 100 nm long and 20 nm wide and are made up of crystallites with sizes of ~ 20 nm. Different amounts of amorphous matter were found in both samples which enable to conclude that different starting Ca/P ratios affect the degree of crystallization of the apatite phase.

Ca-def-HA resulted in the formation of biphasic (HA + β-TCP) or triphasic (HA+β-TCP+α-TCP) mixtures, upon heat treating above 700ºC or 1150ºC, respectively, while HA transforms into a biphasic mixture of (HA+α-TCP) above 1300ºC.

The values of lattice parameters and cell volumes obtained after refinement have shown good coincidence with those of standard files of HA, β-TCP and α-TCP phases of Ca-def-HA. At low heat treatment temperatures the lattice parameters of stoichiometric HA were close to the reported ones for the standard, small lattice distortions were observed with the increase of heat treatment temperature.

The crystallite size of both powders tended to increase with increasing calcination temperatures, but decreased when phase transformations occur, recovering again after that.

References

1. Suchanek W & Yoshimura M. Processing and properties of hydroxyapatite-based biomaterials for use as hard tissue replacement implants. J Mater Res Soc 1998; 13[1]:94-117.

2. Enderle R, Goltz-Neunhoeffer F, Gobbels M, Muller FA. & Greil P. Influence of magnesium doping on the phase transformation temperature of β-TCP ceramics examined by Rietveld refinement. Biomaterials 2005; 26 [17]:3379-3384.

3. Kanazawa T. Inorganic Phosphate Materials. Materials Science Monographs, 52. Elsevier Science Publishers, Amsterdam 1989; pp. 15.

4. de Groot K. Bioceramics of Calcium Phosphates. CRC Press, Boca Raton, FL 1983.

5. Hench LL & Wilson J. An Introduction to Bioceramics. World Scientific. London 1993.

6. Elliot JC. Structure and chemistry of the apatites and other calcium orthophosphates. Studies in Organic Chemistry, 18. Elsevier Science, Netherlands 1994.

7. Klein CPAT. Interaction of biodegradable β-whitlockite ceramics with bone tissue: an in vivo study. J Biomed Mat Res 1984;18:845-859.

8. Kotani S, Fujita Y, Kitsugi T, Nakamura T, Yamamuro T, Ohtsuki C & Kokubo T. Bone bonding mechanism of β-tricalcium phosphate. J Biomed Mat Res 1991;25:1303-1315.

9. Jarcho M. Calcium phosphate ceramics as hard tissue prosthetics. Clin Orthop Rel Res 1981;157:259-278.

10. Feng-Huei L, Chun-Jen L, Ko-Shao C & Jui-Sheng S. Preparation of high-temperature stabilized β-tricalcium phosphate by heating deficient hydroxyapatite with $(Na_4P_2O_7)_{10}$.H2O addition. Biomaterials 1998;19[11-12]:1101-1107.

11. LeGeros R, Lin Z, Rohanizadeh S, Mijares RD & LeGeros JP. Biphasic calcium phosphate bioceramics: preparation, properties and applications. J Mater Sci Mater Med 2003;14[3]:201-209.

12. Yamada S, Heymann D, Bouler J-M & Daculsi G. Osteoclastic resorption of biphasic calcium phosphate ceramic in vitro. J Biomed Mater Res 1997;37[3]:346-352.

13. Ellinger RF, Nery EB & Lynch KL. Histological assessment of periodontal osseous defects following implantation of hydroxyapatite and biphasic calcium phosphate ceramics: a case report. Int J Periodont Restor Dent 1986;3:223-229.

14. Passuti N, Daculsi G, Rogez JM, Martin S & Bainvel JV. Macroporous Calcium Phosphate Ceramic Performance in Human Spine Fusion. Clin Orthop Rel Res 1989;248:169-178.

15. Daculsi G, Passuti N, Martin S, Deudon C, LeGeros RZ & Raher S. Macroporous calcium phosphate ceramic for long bone surgery in humans and dogs. Clinical and histological study. J Biomed Mater Res 1990;24:379-396.

16. Daculsi G, Bagot d'Arc M, Corlieu P & Gersdorff M. Macroporous biphasic calcium phosphate efficiency in mastoid cavity obliteration: experimental and clinical findings. Ann Otol Rhinol Laryngol 1992;101:669-674.

17. Asada M, Oukami K, Nakamura S & Takahashi K. Microstructure and mechanical properties of non-stoichiometric apatite ceramics and sinterability of raw powder. J Ceram Soc Jpn Int Ed 1988;96[1113]:595-598.

18. Osaka A, Miura Y, Takeuchi K, Asada M & Takahashi K. Calcium apatite prepared from calcium hydroxide and orthophosphoric acid. J Mater Sci: Mater Med 1991; 2[1]:51-55.

19. Royer A, Viguie JC, Heughebaert M & Heughebaert JC. Stoichiometry of hydroxyapatite: influence on the flexural strength. J Mater Sci: Mater Med 1993;4[1]: 76-82.

20. Slosarczyk A, Stobierska E, Paszkiewicz Z & Gawlicki M. Calcium phosphate materials prepared from precipitates with various calcium/phophorus molar ratios. J Am Ceram Soc 1996;79[10]:2539-2544.

21. Toriyama M, Ravaglioli A, Krajewski A, Celotti G & Piancastelli A. Synthesis of hydroxyapatite-based powders by mechanochemical method and their sintering. J Eur Ceram Soc 1996;16[4]:429-436.

22. Slosarczyk A, Paluszkiewicz C, Gawlicki M & Paszkiewicz Z. The FTIR spectroscopy and QXRD studies of calcium phosphate based materials produced from the powder precursors with different Ca/P ratios. Ceramics Int 1997;23[4]:297-304.

23. Vallet-Regi M, Rodriguez-Lorenzo LM & Salinas AJ. Synthesis and characterisation of calcium deficient apatite. Solid State Ionics 1997;101-103[2]: 1279-1285.

24. Tas AC, Korkusuz F, Timu-cin M & Akkas N. An investigation of the chemical synthesis and high-temperature sintering behaviour of calcium hydroxyapatite (HA) and tricalcium phosphate (TCP) bioceramics. J Mater Sci: Mater Med 1997;8[2]:91-96.

25. Slosarczyk A & Bialoskorski J. Hardness and fracture toughness of dense calcium-phosphate based ceramics. J Mater Sci: Mater Med 1998;9[2]:103-108.

26. Kivrak N & Tas AC. Synthesis of calcium hydroxyapatite-tricalcium phosphate (HA–TCP) composite bioceramic powders and their sintering behaviour. J Am Ceram Soc 1998;81:2245-2252.

27. Kannan S, Rocha JHG, Ventura JMG, Lemos AF & Ferreira JMF. Effect of Ca/P ratio of precursors on the formation of different calcium apatitic ceramics - An X-ray diffraction study. Scripta Materialia 2005;53:1259–1262.

28. Dickens B, Schroeder LW & Brown WEJ. Crystallographic studies of the role of Mg as a stabilizing impurity in β-$Ca_3(PO_4)_2$. The crystal structure of pure β-$Ca_3(PO_4)_2$. Solid State Chem 1974;10:232.

29. Mathew M, Schroeder LW, Dickens B & Brown WE. The crystal structure of α-$Ca_3(PO_4)_2$. Acta Crystallogr 1977;B33:1325-1333.

30. Sudarsanan K & Young RA. Significant precision in crystal structural details. Holly Springs hydroxyapatite. Acta Crystallogr 1969;B25:1534-1543.

31. Cullity BD. Elements of X-ray Diffraction. Addison Wesley, Reading, MA 1978.

32. Klug HP & Alexander LE. X-ray Diffraction Procedures. Wiley, New York 1959.

33. Mostafa NY. Characterization, thermal stability and sintering of hydroxyapatite powders prepared by different routes. Materials Chemistry and Physics 2005;94:333–341.

34. Kannan S, Lemos IAF, Rocha JHG & Ferreira JMF. Synthesis and mechanical behaviour of chlorapatite and chlorapatite-ß-TCP composites. J Solid State Chem 2005;178:3190-3196.

35. Gibson IR, Rehman I, Best SM & Bonfield W. Characterization of the transformation from calcium-deficient apatite to β-tricalcium phosphate. J Mater Sci: Mater Med 2000;11[9]:533-539.

36. Raynaud S, Champion E, Bernache-Assollant D & Thomas P. Calcium phosphate apatites with variable Ca/P atomic ratio I. Synthesis, characterisation and thermal stability of powders. Biomaterials 2002;23[4]:1065-1072.

37. Kannan S, Rebelo A, Lemos AF, Barba A & Ferreira JMF. Synthesis and mechanical behaviour of chlorapatite and chlorapatite/β-TCP composites. Journal of European Ceramic Society 2007;27:2287-2294.

38. Mortier A, Lemaitre J & Roushet PG. Temperature-programmed characterization of synthetic calcium-deficient phosphate apatites. Thermochim Acta 1989;143:265-282.

39. Hyun-Seung R, Hyuk-Joon Y, Sun HK, Bong-Sun C, Choon-Ki L & Sung-Soo C. An improvement in sintering property of β-tricalcium phosphate by addition of calcium pyrophosphate. Biomaterials 2002;23[3]:909-914.

40. Bouler JM, LeGeros RZ & Daculsi G. Biphasic calcium phosphates: Influence of three synthesis parameters on the HA/β-TCP ratio. Biomed Mater Res 2000;51[4]:680-684.

Rietveld analysis of magnesium substituted biphasic mixtures and influence of heat treatment temperature on phase evolution

A.F. Lemos,[a,b,c] D. Arcos,[d] M. Vallet-Regí,[d] and J.M.F. Ferreira[a]

[a] Dept. of Ceramics and Glass Engineering, University of Aveiro, CICECO, 3810-193 Aveiro, Portugal.

[b] Dept. of Metalurgic and Materials Engineering, Engineering Faculty of the University of Porto, Rua Dr. Roberto Frias, 4200-465 Porto, Portugal.

[c] Institute of Biomedical Engineering, University of Porto, Rua do Campo Alegre 823, 4150-180 Porto, Portugal.

[d] Dpto. Q. Inorganica y Bioinorganica, Ftad de Farmacia, UCM, Plaza Ramon y Cajal s/n, 28040 Madrid, Spain.

Abstract

Rietveld refinement technique was used to study the influence of Mg-substitution on the structural evolution of calcium deficient apatite powders (Ca-def-HA) upon heating. The resultant powders are biphasic (HA and β-TCP) or triphasic (HA, β-TCP and α-TCP), depending on the sintering temperature and on the presence or the absence of Mg^{2+}, respectively. The substituted Mg^{2+} was found in the β-TCP phase, and its addition has led to an increase of the HA content of Mg-containing biphasic mixture [Mg-(Ca-def-HA)]. The refined structural parameters of $Ca_{10}(PO_4)_6(OH)_2$, β-$Ca_3(PO_4)_2$ and α-$Ca_3(PO_4)_2$ confirmed that all the investigated compositions are crystalline with the corresponding hexagonal (space group $P6_3/m$), rhombohedral (space group $R3c$) and monoclinic (space group $P_{21/a}$) structures, respectively. The lattice parameters of the calcium deficient Ca-def-HA powders were almost unaffected by the sintering temperature, while increases in *a, b* and *c* lattice parameters were observed in the case of Mg-(Ca-def-HA) powders, indicating a structure volume expansion.

Introduction

Calcium phosphate-based powders, granules, dense or porous bodies, and coatings of metallic or polymeric implants are currently being used for a number of dental and skeletal prosthetic applications due to their excellent biocompatibility and osteointegration properties.[1–3]

Tricalcium phosphate $Ca_3(PO_4)_2$ (TCP), an osteoconductive as well as bioresorbable ceramic, has found applications as bone implant material and bone cement, respectively.

There are three polymorphs that TCP can form: β-TCP below 1180 ºC, α-TCP between 1180 and 1430 ºC, and α'- TCP above 1430 ºC.[4-8] Ceramics of the all polymorphs exhibit generally poor mechanical properties and mostly those based on β-TCP polymorph have reached acceptance in the biomedical field. Its brittleness and insufficient compaction after sintering below the β- to α- phase transformation temperature limits its use to non-load-bearing applications.

Previous studies reported that the phase transformation of β-TCP to α-TCP is closely related with the expansion of sample volume and declining in shrinkage rate,[8] preventing TCP from further densification.[6] Additionally, the expansion of TCP during sintering process causes micro-cracks in phase-transformed TCP,[5,8] which reduce the mechanical strength of TCP ceramics and turn β-phase-containing TCP ceramics useless for surgical implants that require high mechanical strength.

Magnesium is one of the most abundant trace ions present in biological hard tissues. In dental enamel the concentration of Mg is approximately 0.1-0.4%, in dentin it is higher with values up to 1.1%, and in bone Mg is found at around 0.6%.[9-12] The properties of biological apatites can be affected in several ways by the presence of Mg.[12] Bigi and co-workers[13] reported a quantitative relationship between the relative Mg content and the extent of apatite conversion into β-tricalcium phosphate by heat treatment, and they found indications that Mg is incorporated into the crystal lattice of the mineral. However, there has been controversy as to whether magnesium is incorporated into the apatite mineral of biological hard tissue, or whether it is simply adsorbed onto the surface.

Nonstoichiometric HA partially transforms to TCP at elevated temperatures.[14,15] Similar behaviour was found for Mg-containing synthetic apatites.[16,17] Mg usually stabilizes TCP and causes an increase of the TCP/HA ratio after heating to around 800°C.[18] Okazaki and Le Geros[19] synthesized Mg-containing hydroxyapatites, and reported changes in lattice dimensions related to Mg, as well as the formation of Mg-containing TCP at high Mg/Ca ratios. Mayer *et al.*[12] reported that Mg was incorporated into carbonated apatite during its formation and their results were consistent with the Rietveld structure refinements of hydroxyapatite,[20] reporting the possibility of Mg incorporation up to 10 atom % for Ca.

Other studies, like the one from Ando,[4] who selected magnesia (MgO) as a sintering additive due to its ability to stabilize the β-TCP phase, showed that the addition of MgO

to β-TCP increases the transformation temperature of β- to α-transformation up to temperatures as high as 1500ºC. This enabled using higher sintering temperatures for β-TCP than for Mg-free β-TCP without undergoing the phase transformation.[6,21] Ryu *et al.* [22] showed that MgO-doped hydroxyapatite/ TCP ceramics exhibited high density and significantly enhanced mechanical properties without any phase transformation of β-TCP to α-TCP up to 1300ºC. Moreover, the presence of magnesium in calcified living tissue suggests that Mg^{2+} may improve the biocompatibility of TCP ceramics.[23,24]

Gibson and Bonfield[25] have reported the formation of Mg substituted biphasic mixtures. According to their report, Mg^{2+} can stabilize either HA phase in the presence of carbonates (CO_3^{2-}) or β-TCP phase in the absence of CO_3^{2-}. However, the quantification in terms of Mg^{2+} influence in the biphasic mixtures and its position in the structure could not be explained from the so far reported studies.

Recently, the authors have reported that Mg-doped biphasic mixtures could be obtained by the wet precipitation route.[26] The present work aims at studying the influence of sintering temperature and the presence of Mg^{2+} in biphasic HA and β-TCP mixtures, or even triphasic (HA, β-TCP and α-TCP), through Rietveld refinement technique. It has to be mentioned that Rietveld method is a standard technique for the detailed analysis of crystallographic structures. To compare the results in an effective manner, a pure biphasic mixture without added Mg^{2+} was investigated in parallel.

Experimental

Synthesis

The synthesis of a calcium deficient apatite (Ca-def-HA) and of a Mg-containing biphasic mixture [Mg-(Ca-def-HA)] was carried out with some minor modifications, according to the experimental procedure previously reported.[4,27] Briefly, a predetermined concentration of diammonium hydrogen phosphate [$(NH_4)_2HPO_4$] solution was slowly added to the continuously stirred solution (1000 rpm) mixture containing calcium nitrate tetrahydrate [$Ca(NO_3)_2.4H_2O$] and magnesium nitrate hexahydrate [$Mg(NO_3)_2.6H_2O$] (concentrations of the precursors are described in Table 1). All the used reagents were from Aldrich (Germany), with a purity of at least 99.5%. After the completion of addition, the pH of the mixed solution / suspension was increased to 9 and maintained at this value by adding the required amounts of 8 M ammonium hydroxide (NH_4OH) solution. This was followed by performing the reaction at 90ºC for 2 hours under constant stirring conditions (1000 rpm). The precipitated

suspension was poured out from the reactor and precipitates were separated through vacuum filtration and dried at 80ºC overnight. The dried cakes were ground to fine powders and sieved through a mesh size of 200 μm. These powders were then calcined at different temperatures.

Sample characterisation

The as dried powders were subjected to thermal analysis using a heating rate of 10ºC.min^{-1} between 30 and 1500ºC in air atmosphere (Setaram Labsys TG–DTA/DSC, France) to analyse the thermal behaviour during heating. The prepared powders were calcined at different temperatures varying from 1100º to 1400ºC to study the phase changes.

Table 1. Molar concentrations of the precursors Ca and P used in the synthesis.

Sample code	Molar concentration of the precursors				
	Ca	**P**	**Mg**	**Ca/P ratio**	**(Ca+Mg)/P ratio**
Ca-def-HA	0.972	0.600	-	1.62	1.62
Mg-(Ca-def-HA)	0.972	0.600	0.06	1.62	1.72

The characteristics of the as prepared powders, Ca-def-HA and Mg-(Ca-def-HA), were evaluated by different techniques. The particle size distributions were analysed using a laser scattering instrument (COULTER LS230, UK) with Fraunhofer optical model. The specific surface area and average pore diameter of the pores were assessed in a Micromeritis Gemini 2370 V5.00 (Norcross, USA), through the gas adsorption measurements, after degassing the powders in a Micromeritis Flow prep 060 (Norcross, USA). The morphological study of the as prepared powders was accomplished by scanning electronic microscopy (SEM) (HITACHI, S-4100, Tokyo, Japan, 25 kV acceleration voltage, beam current 10 μA).

Rietveld refinement

For refinement studies, all the powders were heat treated at different temperatures in the range of 1100-1400ºC in a Termolab furnace (TERMOLAB, Fornos Eléctricos, Lda, Águeda, Portugal) equipped with a Pt30%Rh/Pt6%Rh-thermocouple with a heating rate of 5º/min up to the required temperature, followed by a dwelling time for 2 hours and again cooled to room temperature at the rate of 5º/min. Collection of X-ray powder diffraction (XRPD) data was performed with a high resolution Rigaku Geigerflex D/Mac, C Series diffractometer with Copper Kα radiation. The experimental details of the XRPD data collection are presented in Table 2. The software FullProf.2k (Version 2.80 – Jul2004-LLB JRC) with the fundamental parameters approach was employed for

Table 2. Experimental details of X-ray powder diffraction data collection.

Voltage (kV)	30		
Current (mA)	25		
Range (° 2θ)	5–110		
Step width(° 2θ)	0.02		
Time per step (s)	6		
Divergence slit (°)	0.5/0.5 fix		
Receiving slit (mm)	0.2		
Radiation	Wavelength (10^{-10} m)	Lorentz HW (10^{-13} m)	Intensity
Cu Kα	1.540596	0.5739404	0.5394935

Rietveld refinement was performed using the structural model of JCPDS card number # 70-2065 for β-TCP,[28] # 29-0359 for α-TCP[29] and # 74-0565 for HA.[30]

Results and Discussion

Structural characteristics of the as prepared powders

The XRD patterns for the as synthesized powders are presented in Fig. 1. Both powders have indicated the formation of HA phase, although with some differences in peak width and absolute intensity of the diffraction patterns.

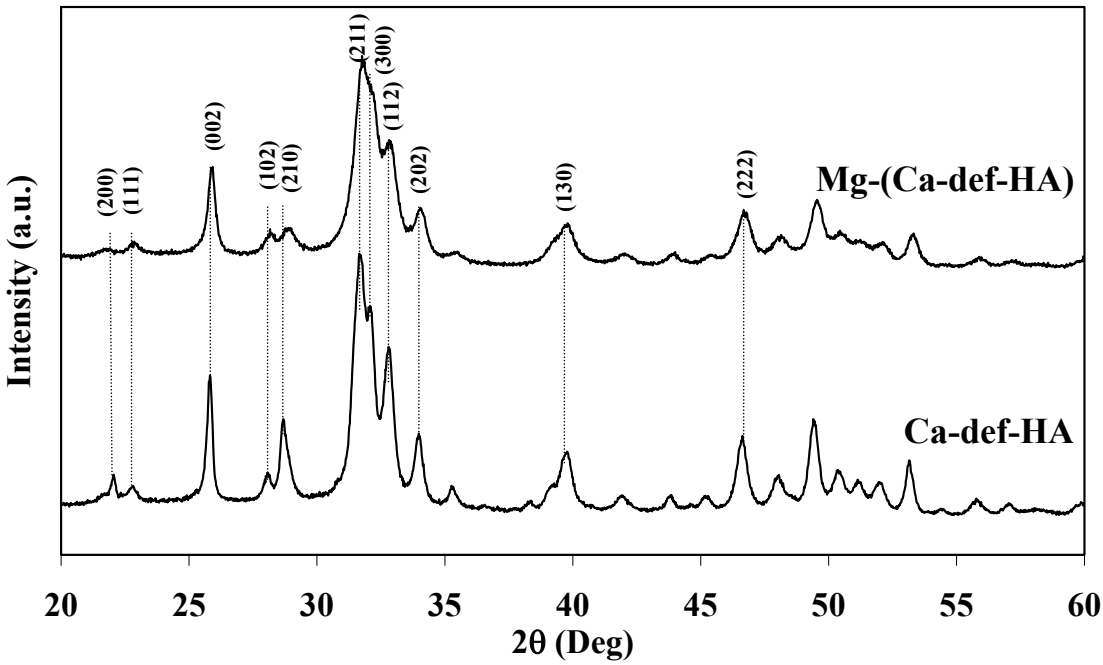

Figure 1. X-ray diffraction pattern for the as prepared powders, calcium deficient apatite (Ca-def-HA) and Mg doped calcium deficient apatite Mg-(Ca-def-HA).

The inhibiting effect of Mg^{2+} on the crystallization of hydroxyapatite precipitated from aqueous solutions is well documented in literature.[31,32] The introduction of magnesium is characterized by the broad diffraction patterns indicative of poor crystallinity of the as prepared powders. However Mg does not appear to affect the diffraction pattern of the apatite phase. These results are in agreement with those reported by Kim *et al.*[33] showing that XRD analysis of an as-precipitated apatite powder can result in diffraction patterns resembling that of HA even though the Ca/P is greater or less that the stoichiometric molar ratio of 1.67. Similar observations were made also for the apatites with elements substituted in trace levels.[34]

FT-IR spectra for the as dried powders presented in Fig. 2 have indicated the vibrational modes of PO_4 groups at 475, 574, 609, 966 and 1020–1120 cm^{-1} and OH groups (630 and 3570 cm^{-1}) of apatite phase for all the powders. FT-IR patterns also tend to coincide with the results from XRD by the way that the intensity of peak resolution of OH and PO_4 bands are viewed with less intensity with the introduction of Mg in the composition. The presence of adsorbed water could also be detected from FT-IR spectra in the region around 3300–3600 cm^{-1}. Other information from the FT-IR spectra of the

powders is the presence of carbonates (CO_3) groups at 1660 cm^{-1}, which are due to the adsorption of species remaining from the aqueous precipitation.[35]

The presence of nitrates (NO_3) in the as dried powders is clearly witnessed in the FT-IR patterns in the region around 1320–1480 cm^{-1}. The presence of nitrates and the band at 875 cm^{-1} resulting from the residual species (NO_3^-, NH_4^+) in the as synthesized powders tend to agree with the previous study.[36] Hence, a more precise and complete characterization of the precipitated powders requires thermal treatments. The bands at 1630 and 3540 cm^{-1} were assigned to OH^-. Additionally, a peak at 1424 cm^{-1} attributed to CO_3^{2-} groups, can also be observed for powders synthesized in air atmosphere.

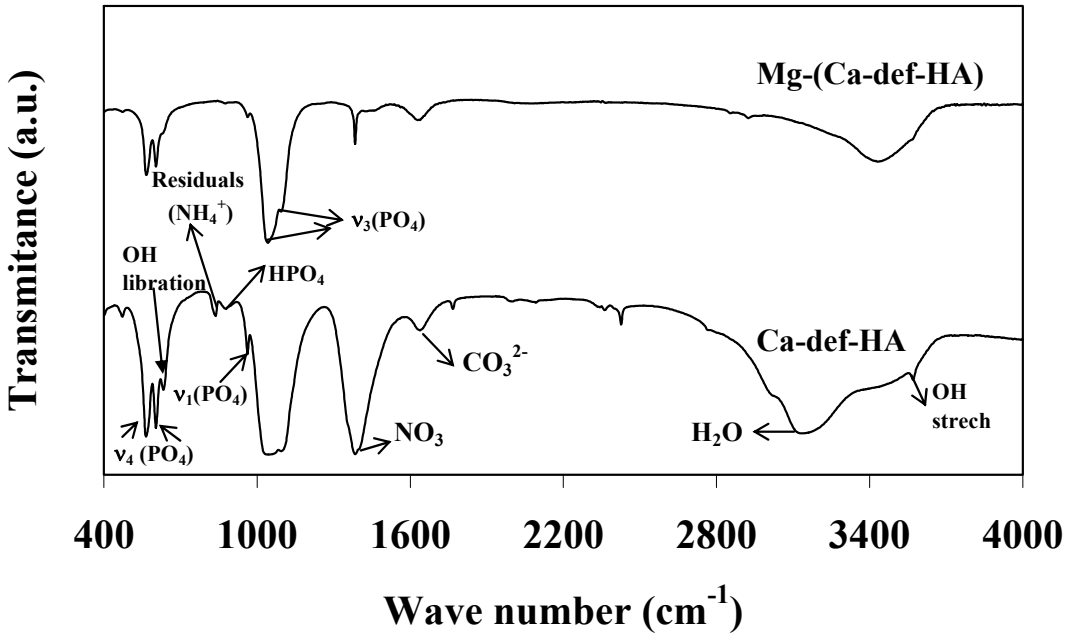

Figure 2. FT-IR spectra for as prepared powders, calcium deficient apatite (Ca-def-HA) and Mg doped calcium deficient apatite Mg-(Ca-def-HA).

According to LeGeros[3] the PO_4^{3-} group (B-type substitution) and the OH^- group (A-type substitution) of HA can be substituted by CO_3^{2-} groups. B-type CO_3^{2-} substitution, which is believed to occur mainly during wet chemical synthesis of calcium phosphates has a characteristic vibration band at 1428 cm^{-1} according to LeGeros *et al.*.[37] However, the FTIR band in the region of 1650 cm^{-1} might also correspond to water or some remaining nitrate, the bands of which tends to overlap with those of carbonate.

Thermal analysis and phase transformation

The TG and DTA plots illustrated in Fig. 3 report the weight loss and the thermal effects along the investigated temperature range for the precipitated powders with and without added Mg. The mass loss during heating could be classified into three different stages. The first stage occurs within the temperature range between 30º and 250ºC in which both samples have indicated a similar weight loss of about 5% thus accounting for the removal of physically adsorbed water. Differences in mass loss among the two samples could be witnessed in the second region (250º–800ºC) attributed to the structural changes associated with the incorporation of the Mg ion in the biphasic mixtures.

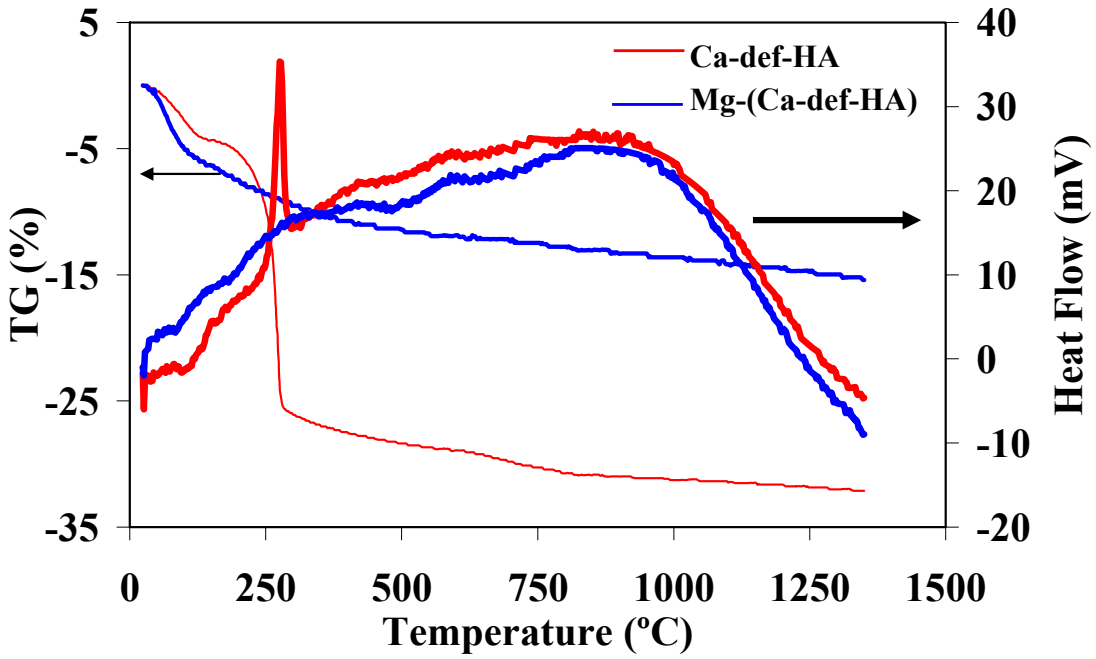

Figure 3. TG and DTA plots for the different Ca/P ratio powders, calcium deficient apatite (Ca-def-HA) and Mg doped calcium deficient apatite Mg-(Ca-def-HA).

It seems that the Ca/P ratio of 1.62 was not retained in the presence of Mg. According to Mortier *et al.*,[38] the presence of HPO_4^{2-} ions within the temperature range of 350º-720ºC gives rise to condensation phenomena to form pyrophosphates ($P_2O_7^{4-}$) according to equation (1):

$$2HPO_4^{2-} \rightarrow P_2O_7^{4-} + H_2O \qquad (1).$$

This explains the accentuated weight loss and the corresponding sharp exothermic peak presented by the (Ca-def-HA) at about 275ºC, as well as the smaller weight loss of

about 1.3% in the temperature range around 700º–850ºC due to the decomposition of pyrophosphates ($P_2O_7^{4-}$) and the formation of biphasic mixtures. However, neither an exothermic effect at about 275ºC nor a corresponding weight loss was observed for the Mg-containing calcium deficient apatite Mg-(Ca-def-HA). Instead, there was a much smaller and very gradual weight loss beyond 250ºC for this powder. This means that the effects of calcium deficiency were much less dramatic in the presence of some extra added Mg, which has apparently entered in the apatite structure although disturbing it in some extent, as deduced from Fig. 1 that reveals a bit less sharp apatite peaks, and from the higher thermal stability of the Mg-(Ca-def-HA) powder. Both powders show negligible weight losses due to gradual de-hydroxylation above 850ºC.

The XRD patterns for Ca-def-HA and Mg-(Ca-def-HA) powders calcined at temperatures equal or higher than 1100ºC, are presented in Figs. 4 and 5, respectively. In contrast to the observed from Fig. 1, where the patterns of both as precipitated powders reveal that poorly crystalline HA was the only phase detected, the heat treatment at 1100ºC led to the formation of β-TCP phase in addition to HA phase, thus confirming the formation of biphasic mixtures.

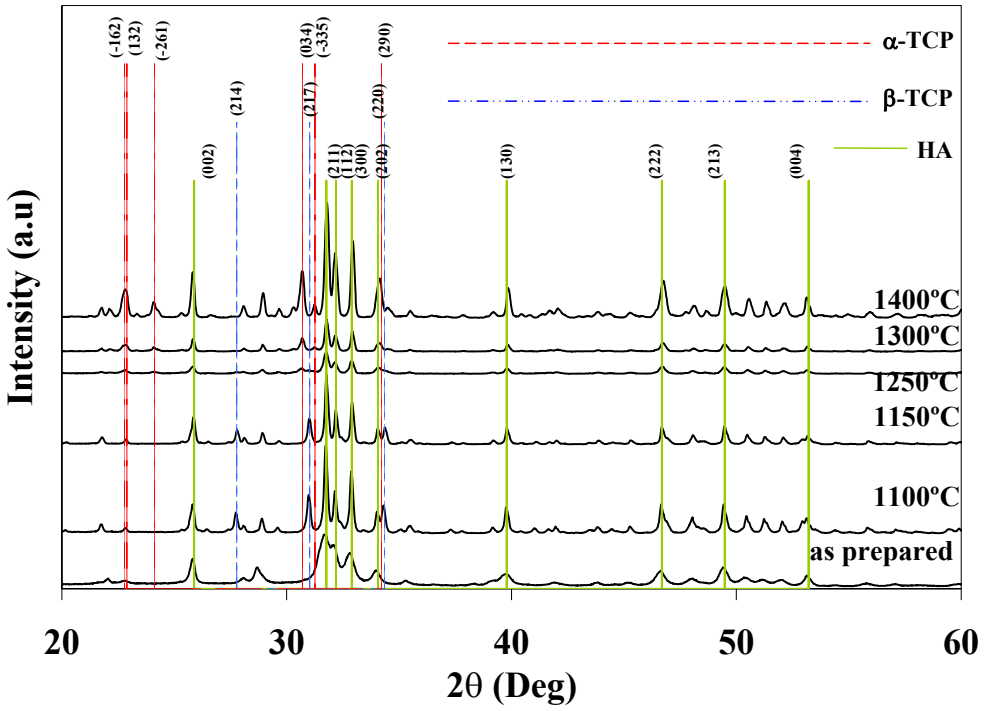

Figure 4. Crystalline phase evolution of Ca-def-HA powders with heat treatment temperatures.

Table 3. Comparison of diffraction angle (2θ) and *d*-spacing values of experimental X-ray patterns with respect to standard JCPDS values.

Sample	2 1 7 Plane	
	***d*-spacing**	**2θ**
JCPDS # 70-0265 (β-TCP)	2.8804	31.022
JCPDS # 70-0682 ($Ca_{2.81}Mg_{0.19}(PO_4)_2$)	2.8549	31.306
Ca-def-HA - 1150ºC	2.8825	30.999
Mg-(Ca-def-HA) – 1250ºC	2.8675	31.209

However, the peaks pertaining to this β-TCP have not shown exact matches with those of JCPDS # 70-2065, which in fact have indicated considerable shift in the 2θ and d-spacing values of maximum intensity plane (217), as represented in Table 3.

This observed shift is solely due to the incorporation of Mg into the β-TCP structure as reported elsewhere.[39,40] The 2θ and d-spacing values show considerable shift with respect to those of JCPDS # 70-2065 but tend to behave closer towards JCPDS # 70-0682 ($Ca_{2.81}Mg_{0.19}(PO_4)_2$) phase, thus confirming the stabilization effect of Mg on β-TCP phase. The observed small discrepancy in the values illustrated in Table 3 for the Mg-(Ca-def-HA) can thus be attributed to the incorporation of Mg into the β-TCP, which, in a simplified way, can be expressed as $(CaMg)_3(PO_4)_2$.

The discrepancies in the 2θ and d-spacing values given in Table 3 for the heat treated powders and the different thermal behaviour observed within the range of 250-800ºC (Fig. 3) are supporting evidences of the incorporation of Mg into the β-TCP structure. Considering the weight changes mentioned above, a qualitative expression of Mortier[38] could be used to explain the role of Mg in the formation of a mixture of stoichiometric HA and Mg stabilized β-TCP $(CaMg)_3(PO_4)_2$ for temperatures > 720ºC, equation (2).

$$Ca_{10-x}(Mg_2P_2O_7)_{x/2}(PO_4)_{6-x}(OH)_{2-x} + x/2H_2O \rightarrow$$
$$(1-x)Ca_{10}(PO_4)_6(OH)_2 + 3x(CaMg_{2x/9})_3(PO_4)_2 + xH_2O \qquad (2)$$

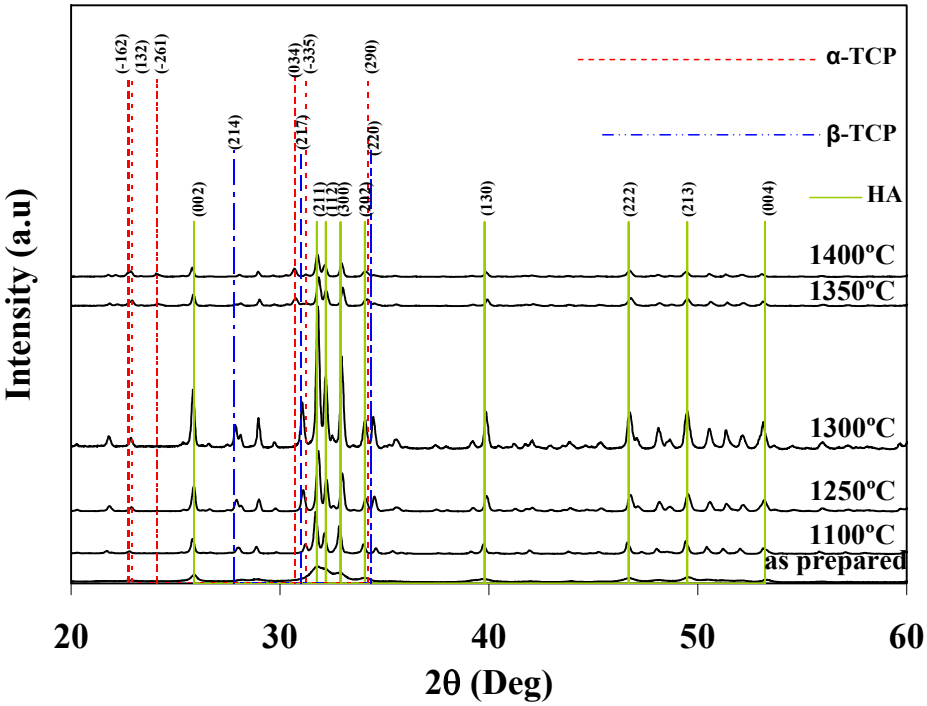

Figure 5. Crystalline phase evolution of Mg-(Ca-def-HA) powders with heat treatment temperatures.

Determination of phase content

The unit cell and structural parameters determined by Dickens *et al.*[28] for β-TCP, Matthew *et al.* for α-TCP[29] and Sudarsanan *et al.*[30] for HA, were respectively used as starting values in the refinement of β-TCP, α-TCP and HA in biphasic and triphasic mixtures. The XRD patterns for calcium deficient apatite (Ca-def-HA) and Mg-containing biphasic mixture [Mg-(Ca-def-HA)] powders at different temperatures are presented in Fig. 4 and Fig. 5, respectively.

All the XRD patterns have indicated the presence of more than one phase. Fig. 4 reveals that Ca-def-HA is a biphasic mixture of HA+β-TCP up to 1200ºC. Beyond this temperature, β-TCP starts to progressively transform into α-TCP, and at 1400ºC there is no more β-TCP in the composition. Fig. 5 shows that the incorporation of magnesium in the structure delays the β to α phase transformation, with the Mg-(Ca-def-HA) composition still remaining biphasic at 1300ºC. The β to α phase transformation only starts at 1350ºC and then completes up to 1400ºC. The quantitative phase composition determined through Rietveld analysis showed significant variations that were totally

dependent on the calcination temperature and on the presence or absence of magnesium. Table 4 indicates the wt.% of the phase composition for all the powders after refinement. It was also attempted to determine the reliability of the resultant phase mixtures obtained through refinement with those of experimental Ca/P ratio of the precursors by the following expression[41]:

$$Expected\ {}^{Ca}\!/_{P} = Wt.\%\ of\ HA\,(Rietveld)\times 1.67 + Wt.\%\ of\ TCP\,(Rietveld)\times 1.5$$

Table 4. Determined Rietveld quantification results of Ca-def-HA and Mg-(Ca-def-HA) biphasic mixtures.

Sample code	Sintering Temperature (ºC)	Wt. % of composition determined by Rietveld quantification			Ca/P ratio	
		HA	β-TCP	α-TCP	Experimental (in solution)	Calculated
Ca-def-HA	**1100**	64.3	35.7	-	1.62	1.60
	1150	68.6	31.4	-	1.62	1.61
	1250	69.7	9.5	20.7	1.62	1.61
	1300	64.7	2.4	32.9	1.62	1.60
	1400	66.4	-	33.6	1.62	1.61
Mg-(Ca-def-HA)	**1100**	84.15	15.85	-	1.62	1.61
	1250	72.83	27.17	-	1.62	1.62
	1300	76.59	23.41	-	1.62	1.63
	1350	73.61	5.95	20.44	1.62	1.61
	1400	70.82	-	29.28	1.62	1.61

From the values reported in Table 4, it can be inferred that the experimental concentrations used in the starting solutions have shown good coincidence with the calculated Ca/P ratios determined from the phase content of the biphasic mixtures after refinement. The added Mg^{2+} has been excluded from the calculation, since at this stage it is difficult to explain its role in the phase composition. This important aspect will be handled in the later part of discussion. However, it is worthy to note that Mg-substituted biphasic and triphasic mixtures derived from the powder Mg-(Ca-def-HA) have indicated higher HA contents in the respective phase mixtures in comparison with the HA contents determined derived from Ca-def-HA. Moreover, the HA phase derived

from the Mg-substituted powder is stable up to higher temperatures. These results show that the incorporation of Mg^{2+} enhances the thermal stability of the HA phase and delays its transformation into β-TCP with increasing temperatures. Moreover, the thermal stability of β-TCP was also significantly enhanced with α-TCP appearing only at 1350ºC, i.e., 100ºC above the onset of β to α phase transformation temperature observed for the undoped Ca-def-HA powder (1250ºC).

Refinement of lattice parameters

Tables 5, 6 and 7 collect the lattice parameters and the cell volumes calculated from the refined values for both powder mixtures. The values presented in Tables 5, 6 and 7 confirm the excellent similarities in the lattice data of HA, β-TCP and α-TCP phase of Ca-def-HA obtained after refinement, which tend to follow well within the error limits.

In fact, all the refined lattice data for HA phase in the Ca-def-HA confirmed its hexagonal structure (space group $P6_3/m$) and the values determined are in close agreement with the crystal data for single phase HA ($a = b = 9.424$ Å, $c = 6.879$ Å, $\alpha = \beta = 90°$, and $\gamma = 120°$).[30]

Table 5. Refined lattice parameters and calculated cell volume of HA phase for Ca-def-HA and Mg-(Ca-def-HA) biphasic mixtures.

Sample code	Sintering Temperature (ºC)	Refined lattice data for HA phase			R-Bragg
		a-axis (Å)	*c*-axis (Å)	Cell volume (Å^3)	
Ca-def-HA	**1100**	9.42158 (6)	6.88401 (6)	1582.053	4.84
	1200	9.42049 (4)	6.88200 (5)	1581.225	4.65
	1250	9.40928 (0)	6.88029 (0)	1577.072	7.86
	1300	9.40928 (0)	6.88282 (0)	1577.652	5.67
	1400	9.40292 (0)	6.88459 (0)	1575.925	4.15
Mg-(Ca-def-HA)	**1100**	9.41800 (6)	6.87922 (5)	1579.751	3.03
	1250	9.40687 (7)	6.88308 (6)	1576.904	3.00
	1300	9.40669 (10)	6.88852 (8)	1578.090	3.58
	1350	9.40206 (12)	6.89473 (10)	1577.958	3.38
	1400	9.40180 (13)	6.89463 (11)	1577.848	3.88

For the composition Mg-(Ca-def-HA), although the lattice parameters are close to the reported ones, small distortions of the lattice occurred with increasing temperatures (Table 5). There was a shrinkage trend along the *a-axis* and a first contraction at lower temperatures followed by an elongation trend along the *c-axis* with increasing temperatures. The refined lattice data of β-TCP phase in the Ca-def-HA composition confirmed its rhombohedral structure (space group R3*c*). The data are close to the values reported by Dickens *et al*.[28] for single phase crystalline β-TCP ($a = b = 10.439$ Å, $c = 37.375$ Å, $\alpha = \beta = 90°$, and $\gamma = 120°$).

Table 6. Refined lattice parameters and calculated cell volume of β-TCP phase for Ca-def-HA and Mg-(Ca-def-HA) biphasic mixtures.

Sample code	Sintering Temperature (°C)	Refined lattice data for β-TCP phase			R-Bragg
		a-axis (Å)	*c*-axis (Å)	Cell volume (Å^3)	
Ca-def-HA	**1100**	10.43958 (13)	37.39925 (66)	3529.774	4.76
	1200	10.42575 (10)	37.44896 (61)	3525.107	4.63
	1250	10.40950 (0)	37.41093 (0)	3510.558	12.0
	1300	10.41991 (0)	37.56610 (0)	3532.173	10.6
Mg-(Ca-def-HA)	**1100**	10.34309 (17)	37.09103 (88)	3436.271	7.03
	1250	10.38958 (13)	37.36847 (64)	3493.166	4.59
	1300	10.39763(17)	37.38681 (85)	3500.298	5.79
	1350	10.42790 (189)	37.44279 (821)	3525.980	4.56

However, comparing the refined lattice data obtained for β-TCP phase derived from Ca-def-HA and Mg-(Ca-def-HA) powders (Table 6), a decreasing trend in *a* and *c*-axis parameter values with the introduction of Mg^{2+} is observed. Therefore, a contraction of calculated cell volumes was found evident. From this decrease of lattice parameters, it could be confirmed that the added Mg^{2+} has entered the β-TCP structure. The reason for this contraction in refined cell parameters can be well understood by considering the substitution of lower ionic radii of sixfold-coordinated Mg^{2+} (0.72 Å) in comparison to that of Ca^{2+} ion (1.00 Å) at the Ca(5) site. Table 6 also clearly shows that the lattice parameters of β-TCP derived from Ca-def-HA did not appreciably change with the increase of sintering temperature. Contrarily, in the case of Mg-(Ca-def-HA), an increase in all lattice parameters (*a*, *b* and *c*) indicates that the structure is growing in all

directions with increasing calcination temperatures. This can be explained by the sample volume expansion associated with the phase transformation of β-TCP to α-TCP, and declining in shrinkage rate,[8] preventing TCP from further densification.[6] Table 7 confirms the excellent similarities in the lattice data of α-TCP phase of Ca-def-HA obtained after refinement and those reported by Matthew *et al.* for α-TCP.[29] Comparing the lattice parameters of the Ca-def-HA and Mg-(Ca-def-HA) compositions, it is possible to conclude that the Mg^{2+} practically does not interfere with this phase.

Table 7. Refined lattice parameters and calculated cell volume of α-TCP phase for Ca-def-HA and Mg-(Ca-def-HA) biphasic mixtures.

Sample code	Sintering Temperature (ºC)	Refined lattice data for α-TCP phase				R-Bragg
		a-axis (Å)	*b*-axis (Å)	*c*-axis (Å)	Cell volume (Å^3)	
Ca-def-HA	**1250**	12.83815(0)	27.29448(0)	15.24982(0)	5343.699	10.4
	1300	12.85953(0)	27.30686(0)	15.21533(0)	5342.915	14.4
	1400	12.85596(0)	27.28341(0)	15.20737(0)	5334.052	6.19
Mg-(Ca-def-HA)	**1350**	12.86221(96)	27.29521(115)	15.21369(64)	5341.172	8.16
	1400	12.86647(81)	27.29421(101)	15.20611(54)	5340.084	9.15

Conclusions

The structural refinement of Ca-def-HA and Mg-(Ca-def-HA) confirmed that all the powders consisted of biphasic (HA+β-TCP) and triphasic (HA+β-TCP+α-TCP) mixtures. The refined lattice parameters of HA, β-TCP and α-TCP confirmed that these crystalline phases belong to the hexagonal (space group $P6_3/m$), rhombohedral (space group *R3c*) and monoclinic (space group *P21/a*) structures, respectively. The determined weight percentage of HA, β-TCP and α-TCP content in the mixtures was found dependent on the presence or absence of Mg^{2+} and on the calcination temperature. Mg-substitution was found to occur in the β-TCP phase derived from Mg-(Ca-def-HA) and its influence on the composition has led to an increase of the HA content on Mg-

(Ca-def-HA) mixture when compared with the amount of HA detected in the Ca-def-HA mixture.

It is possible to conclude that increasing the calcination temperature did not considerably affect the lattice parameters for the HA and β-TCP phases derived from the Ca-def-HA powder, although in the case of Mg-(Ca-def-HA), an increase in all lattice parameters (*a*, *b* and *c*) of HA and β-TCP phases indicated a structure volume expansion, that could be explained by the phase transformation of β-TCP to α-TCP.

References

1. Hench LL. Bioceramics. J Am Ceram Soc 1998;81:1705–1728.

2. Hench LL. & Wilson AJ. editors. An introduction to bioceramics— advanced series in ceramics 1. World Scientific. Singapore 1993.

3. LeGeros RZ. Calcium phosphates in oral biology and medicine. Monogr Oral Sci 1991;15:1–201.

4. Jumpei A. Tricalcium phosphate and its variations. Bull Chem Soc Jpn 1958;31:196–201.

5. Itatani K, Nishioka T, Seike S, Howell FS, Kishioka A & Kinishita M. Sinterability of β-orthophosphate powder prepared by spray pyrolysis. J Am Ceram Soc 1994;77: 801–805.

6. Famery R & Richard PB. Preparation of α- and β-TCP ceramics, with and without magnesium addition. Ceram Int 1994;20:327–336.

7. Elliot JC. Structure and chemistry of the apatites and other calcium orthophosphates. Elsevier. Amsterdam 1994.

8. Hyun-Seung R, Hyuk-Joon Y, Sun HK, Bong-Sun C, Choon-Ki L & Sung-Soo C. An improvement in sintering property of β-tricalcium phosphate by addition of calcium pyrophosphate. Biomaterials 2002;23[3]:909-914.

9. Robinson IC, Weatherell JA & Hallsworth AS. Distribution of magnesium in mature human enamel. Caries Res 1981; 15:70.

10. Steinfort J, Driessens FCM, Heijligers HJM & Bertseen W. The distribution of magnesium in developing rat incisor dentin. J Dent Res 1991;70:187.

11. Tsuboi S, Nakagi H, Ishiguro K, Kondo K, Mukai M, Robinson C & Weatherell JA. Magnesium distribution in human bone. Calcif Tissue Int 1994; 54:34.

12. Mayer L, Scblam R & Featberstone JDB. Magnesium-Containing Carbonate Apatite. J Inorg Biochem 1997; 66:I-6.

13. Bigi A, Foresti E, Gregorini R, Ripamonfi A, Roveri N & Shah JS. The role of magnesium on the structure of biological apatites. Calcif Tissue Int 1992;50:439.

14. Apfelbaum F, Mayer I & Featherstone JDB. The Role of HPO_4^{2-} and CO_3^{2-} Ions in the Transformation of Synthetic Apatites to β-$Ca_3(PO_4)_2$. J Inorg Biochem 1991;38:I.

15. Zhou J, Zhang X, Chen J, Zeng S. & De Groot K. High temperature characteristics of synthetic hydroxyapatite. J Mater Sci: Mater Med 1993;4:83.

16. Featherstone JDB, Mayer I, Driessens FCM, Verbeeck RMH & Heijligers M. Synthetic apatites containing Na, Mg, and CO3 and their comparison with tooth enamel mineral. Calcif Tissue Int 1983; 35:169.

17. Mayer I, Featherstone JDB, Nagler R, Noejovich M, Deutsch D & Gedalia I. The thermal decomposition of Mg-containing carbonate apatites. J Solid State Chem 1985;56:230.

18. LeGeros R. in *Tooth Enamel I.,* Fearnhead RW & Suga X. Elsevier Eds. Amsterdam. 1984. pp. 32-36.

19. Okazaki M & LeGeros RZ. Crystallographic and chemical properties of Mg-containing apatites before and after suspension in solutions. Magnesium Res 1992;5: 103.

20. Bigi A, Falini G, Foresti E & Gazzano M. Rietveld structure refinements of calcium hydroxylapatite containing magnesium. Acta Cryst 1996;B52:87.

21. Jumpei A. Phase diagrams of $Ca_3(PO_4)_2$-$Mg_3(PO_4)_2$ and $Ca_3(PO_4)_2$-$CaNaPO_4$ systems. Bull Chem Soc Jpn 1958;31:201–205.

22. Hyun-Seung R, Kug-Sun H, Jung-Kun L, Joong KD, Hyup LJ, Bong-Soon C, Dong-Ho L, Choon-Ki L & Sung-Soo C. Magnesia-doped HA/beta-TCP ceramics and evaluation of their biocompatibility. Biomaterials 2004;25(3):393–401.

23. de Groot K. Bioceramics of calcium phosphate. Boca Raton, CRC Press. FL. 1983.

24. Enderle R, Gotz-Neunhoeffer F, Gobbels M, Muller FA & Greil P. Influence of magnesium doping on the phase transformation temperature of β-TCP ceramics examined by Rietveld refinement. Biomaterials 2005;26:3379–3384.

25. Gibson IR & Bonfield W. Preparation and characterization of magnesium/carbonate co-substituted hydroxyapatites. J Mater Sci: Mater Med 2002;13:685-693.

26. Kannan S, Lemos IAF, Rocha JHG & Ferreira JMF. Synthesis and characterization of magnesium substituted biphasic mixtures of controlled hydroxyapatite/β-tricalcium phosphate ratios. J Solid State Chem 2005;178:3190-3196.

27. Kannan S, Rocha JHG, Ventura JMG, Lemos AF & Ferreira JMF. Effect of precursors Ca/P ratio on the formation of different calcium apatitic ceramics - An X-ray diffraction study. Scripta Mater 2005;53:1259-1262.

28. Dickens B, Schroeder LW & Brown WEJ. Crystallographic studies of the role of Mg as a stabilizing impurity in β-$Ca_3(PO_4)_2$. The crystal structure of pure β-$Ca_3(PO_4)_2$. Solid State Chem 1974;10:232.

29. Mathew M, Schroeder LW, Dickens B & Brown WE. The crystal structure of α-$Ca_3(PO_4)_2$. Acta Crystallogr 1977;B33:1325-1333.

30. Sudarsanan K & Young RA. Significant precision in crystal structural details. Holly Springs hydroxyapatite. Acta Crystallogr 1969;B25:1534-1543.

31. Bertoni E, Bigi A, Cojazzi G & Gandolfi M. Nanocrystals of magnesium and fluoride substituted hydroxyapatite. J Inorg Biochem 1998;72:29-35.

32. Fadeev IV, Shvorneva LI, Barinov SM & Orlovskii VP. Synthesis and structure of magnesium-substituted hydroxyapatite. Inorganic materials 2003;39[9]:947-950.

33. Kim SR, Lee JH, Kim YT, Riu DH, Jung SJ, Lee YJ, Chung SC & Kim YH. Synthesis of Si, Mg substituted hydroxyapatites and their sintering behaviours. Biomaterials 2003;24:1389.

34. Gibson IR, Rehman I, Best SM & Bonfield W. Characterization of the transformation from calcium-deficient apatite to β-tricalcium phosphate. J Mater Sci: Mater Med 2000;12:799.

35. Gibson IR, Best SM & Bonfield W. Chemical characterization of silicon-substituted hydroxyapatite. J Biomed Mater Res 1999;44:422.

36. Raynaud S, Champion E, Bernache-Assollant D & Thomas P. Calcium phosphate apatites with variable Ca/P atomic ratio I. Synthesis, characterisation and thermal stability of powders. Biomaterials 2002;23:1065.

37. LeGeros RZ, Trautz OR, LeGeros JP & Klein E. Carbonate substitution in the apatite structure. Bull Soc Chim Fr 1968;special issue:1712-1718.

38. Mortier A, Lemaitre J & Rouxhet PG. Temperature-programmed characterization of synthetic calcium-deficient phosphate apatites. Thermochim Acta 1989;143-265.

49. Dickens B, Schroeder LW & Brown WE. Crystallographic studies of the role of Mg as a stabilizing impurity in β-$Ca_3(PO_4)_2$. II. Refinement of Mg-containing β-$Ca_3(PO_4)_2$. J Solid State Chem 1977;22:253.

40. Enderle R, Gotz-Neunhoefler F, Gobbels M, Muller FA & Greil P. Influence of magnesium doping on the phase transformation temperature of β-TCP ceramics examined by Rietveld refinement. Biomaterials 2005;26:3379.

41. Vallet-Regí M, Rodríguez-Lorenzo LM & Salinas AJ. Synthesis and Characterisation of Calcium Deficient Apatite. Solid State Ionics 1997;101-103, 1279-1285.

Biological-like calcium phosphates - Rietveld analysis and phase evolution with heat treatment temperature

A.F. Lemos,[a,b,c] M. Vallet-Regí,[d] and J.M.F. Ferreira[a]

[a] Dept. of Ceramics and Glass Engineering, University of Aveiro, CICECO, 3810-193 Aveiro, Portugal.

[b] Dept. of Metallurgic and Materials Engineering, Engineering Faculty of the University of Porto, Rua Dr. Roberto Frias, 4200-465 Porto, Portugal.

[c] Institute of Biomedical Engineering, University of Porto, Rua do Campo Alegre 823, 4150-180 Porto, Portugal.

[d] Dpto. Q. Inorganica y Bioinorganica, Ftad de Farmacia, UCM, Plaza Ramon y Cajal s/n, 28040 Madrid, Spain.

Abstract

Synthesis of hydroxyapatites (HA) with co-substituted essential trace elements (Na, Mg, K, Cl and F) of natural bone was performed through aqueous precipitation. The as prepared powders were calcined at different temperatures to study the phase evolution and thermal stability. The powders were characterized by the following analytical techniques: elemental analysis, thermo gravimetric and differential thermal analysis (TG–DTA), X-ray diffraction (XRD), Infrared Spectroscopy by Fourier Transformed (FT-IR), Scanning Electron Microscopy (SEM) and Transmission Electron Microscopy (TEM). Rietveld refinement was used to determine the phase analysis and the structural parameters of the phases formed. The information gathered is of high relevance for designing better calcium phosphate bioceramics. The results obtained proved that substituted elements play a crucial role in enhancing the thermal stability of the HA phase until 1400ºC. A noticeable amount of β-TCP along with the HA phase was detected in the samples heat treated at higher temperatures, which tended to increase with increasing the incorporation levels of trace elements.

Introduction

Synthetic hydroxyapatite (HA) is the most ubiquitous calcium phosphate used in biological applications. The close similarity of the crystallographic structure of synthetic HA and natural bone, enamel, and dentin, along with chemical analyses showing the presence of calcium and phosphate as principal constituent of these hard tissues, led to the belief that the inorganic component of bone and teeth is essentially

calcium HA represented by the chemical formula $Ca_{10}(PO_4)_6(OH)_2$.[1-4] In spite of the structural and crystallographic similarities with synthetic HA, the biological apatites are always nonstoichiometric with structural imperfections due to several incorporated elements on trace levels in its lattice.[5-7] Although present in such low amounts, several studies proved that these elements play a determining role on biological processes upon implantation.[8-18] For a thorough understanding, some of their salient features are described as follows: (a) sodium, a monovalent ion, available in abundance next to calcium and phosphorus, plays a significant role on bone metabolism and osteoporosis;[8,9](b) magnesium, undoubtedly one of the most important bivalent ions associated with the biological apatite, has its own significance in the calcification process, bone fragility, and a indirect influence on mineral metabolism;[10-12] (c) potassium is active in mineralization and biochemical processes;[13,14] (d) fluorine is well-recognized for its potential behaviour on the stability of apatite and on preventing dental caries;[15,16] and (e) chlorine, which enables an acidic environment to develop on the surface of bone that activates osteoclasts in the bone resorption process.[17,18] The recognition of the significant roles played by these trace elements in the biological process stimulated numerous recent studies aiming at the synthesis of ionic substituted HA either with single elements [19-27] or with coupled element substitutions.[28-33]

Because the hierarchical structure of apatite has the ability to accept a wide number of possible substitutions in its lattice,[34] the elemental substitutions were made in trace levels. It is expected that co-substituted apatites with a composition closer to that of the hard tissues will behave better in the biological environment in comparison to pure HA. However, the specific documentation on combined substitutions of several elements in the HA structure is very scarce.[35] The present work aims at (i), preparing synthetic HA with combined substitutions of biocompatible trace elements present in biological apatite and (ii), characterising the powders by Rietveld refinement to determine the phase analysis and the structural parameters of the phases formed.

Experimental

Synthesis

The synthesis of the calcium phosphate powders was carried out in a fully automated apparatus (capacity = 6 litres) with specific devices to control the stirring speed, the addition rate of reactants and the temperature of the system. Reagent grade calcium nitrate tetrahydrate [$Ca(NO_3)_2.4H_2O$, Aldrich-Germany], diammonium hydrogen

phosphate [$(NH_4)_2HPO_4$, Aldrich-Germany], sodium nitrate [$NaNO_3$, Aldrich-Germany], magnesium nitrate hexahydrate [$Mg(NO_3)_2.6H_2O$, Merck], potassium nitrate [KNO_3, Merck], ammonium chloride [NH_4Cl, Merck] and ammonium fluoride [NH_4F, Merck] were used as starting chemical precursors for the synthesis. Two different types of compositions were attempted to obtain biphasic calcium phosphates with co-substituted elements. The solution concentrations of precursors are detailed in Table I. A mixture of $(NH_4)_2HPO_4$, NH_4F and NH_4Cl solutions was added slowly at a rate of 50 mL/min to the solution mixture containing nitrates of Ca, Na, Mg and K stirred at a rate of 1000 rpm. After the addition of all the precursors, the pH value of the mixture was found to be around 4, being then increased to 9 by adding 8 M ammonium hydroxide (NH_4OH) solution. After the completion of addition, the reaction was performed at 90ºC for 2 h under a constant stirring rate of 1000 rpm. The precipitates were vacuum filtrated and washed repeatedly with de-ionized water and then dried at 80ºC overnight. The dried cakes were ground to fine powders, sieved through a mesh size of 200 μm and calcined at 1100ºC. These powders were then sintered at different temperatures and characterised.

Sample characterisation

Elemental analyses for the presence of all elements except fluorine were made using X-ray fluorescence spectroscopy (Philips PW2400 X-ray fluorescence spectrometer). The vacuum of the chamber was lower than 2 Pa. The error associated to each chemical element could be determined as ±1 of the last digit (Table 2) of the measured values. Fluorine was determined by the selective ion electrode method.

The thermal behaviour of as dried powders was analysed by thermal analysis (Setaram Labsys TG–DTA/DSC, France) using a heating rate of $10ºC.min^{-1}$ between 30ºC and 1500ºC in air atmosphere. The prepared powders were calcined at different temperatures varying from 1100ºC to 1400ºC to study the phase changes.

Table 1. Concentrations of the precursors used in the synthesis of the co-substituted calcium phosphates.

		BL-HA1	BL-HA2
Ca/P		1.67	1.67
Elements	**Reagent**	**Molarity**	
Ca	**$Ca(NO_3).4H_2O$**	2.00	2.00
P	**$(NH_4)_2HPO_4$**	1.20	1.20
Mg	**$Mg(NO_3)_2.6H_2O$**	0.04	0.08
Na	**$NaNO_3$**	0.05	0.10
K	**KNO_3**	0.03	0.06
Cl	**NH_4Cl**	0.05	0.10
F	**NH_4F**	0.05	0.10

The characteristics of the as prepared powders, BL-HA1 and BL-HA2 were evaluated by different techniques. Particle size distributions were measured in a particle size analyser (COULTER LS230, UK), with Fraunhofer optical model. The specific surface areas and average pore diameters were assessed in a Micromeritis Gemini 2370 V5.00 (Norcross, USA), through the gas adsorption measurements, after degassing the powders in a Micromeritis Flow prep 060 (Norcross, USA). The morphological study of the as prepared powders was accomplished by scanning electronic microscopy (SEM) (HITACHI, S-4100, Tokyo, Japan, 25 kV acceleration voltage, beam current 10 μA) and transmission electronic microscopy (TEM) (Hitachi-H-9000-NA, Japan) analysis.

Rietveld refinement

Rietveld refinement studies were performed in the powders heat treated in a Termolab furnace (TERMOLAB, Fornos Eléctricos, Lda equipped with a Pt30%Rh/Pt6%Rh-thermocouple) at different temperatures in the range of 1100ºC to 1400ºC, using a heating rate of $5º.min^{-1}$ up to the required temperature, followed by a dwelling time for 2 hours and cooling to room temperature at the rate of $5º.min^{-1}$. The X-ray powder diffraction (XRPD) data was collected with a high resolution Rigaku Geigerflex D/Mac, C Series diffractometer with Copper Kα radiation, λ = 1.540596 Å. The following parameters were set; 2θ range of 5–110°; 2θ step width of 0.02 °; time per step 6 s. The software FullProf.2k (Version 2.80 – Jul2004-LLB JRC) with the fundamental parameters approach was employed for Rietveld refinements, using the structural

models of JCPDS, card numbers # 70-2065 for β-TCP, [36]# 29-0359 for α-TCP [37] and # 74-0565 for HA.[38]

The size of individual HA crystallites was calculated from XRD data using the Scherrer approximation.[39] The values of full width at half maximum intensity ($\beta_{1/2}$) of the peak of (002) plane, representative of the crystallites along the *c*-axis, and of the peak of (300) plane, representative of the crystallites along the *a*-axis were used in the calculation according to equation (1)

$$D = \frac{k\lambda}{[\beta_{1/2}\cos\theta]} \qquad (1)$$

where D is the crystallite size, as calculated for the (hkl) reflection, λ is the wavelength of Cu Ka radiation (0.15406 nm), and k is the broadening constant varying with crystal habit and chosen as 0.85 for the elongated apatite crystallites. [40,41]

Results and Discussion

Characterisation of the as prepared powders

X-Ray diffraction

The XRD patterns for the as precipitated calcium phosphate powders with co-substituted elements (BL-HA1 and BL-HA2) are illustrated in Fig. 1. The patterns show that poorly crystalline hydroxyapatite, characterized by broad diffraction bands, was obtained in both compositions with only small differences in peak width and absolute intensity of the diffraction peaks. The main characteristic hydroxyapatite (JCPDS # 74-0565) peaks are assigned in Fig. 1 with the respective reflection planes.

The elemental co-substitutions did not appear to significantly affect the diffraction patterns of the as-prepared powders. These results are consistent with those found in earlier reports[1,42] showing that the as-precipitated apatite powders exhibit XRD diffraction patterns resembling HA, even though the Ca/P ratio was greater or less than the stoichiometric molar ratio of 1.67.

FT-IR spectra

FT-IR spectra of the as dried powders displayed in Fig. 2 also confirm the formation of apatite phase with the observed fundamental vibrational modes of PO_4 group at 475, 574, 609, 966 e 1020-1120 cm^{-1}. The absorption bands in the region around 3300-3600 cm^{-1}, corresponding to adsorbed water, and at around 1450 cm^{-1}, which might be due to

the presence of carbonate (CO_3) groups coming from the aqueous precipitation medium,[20] can also be observed in the FT-IR spectra of both synthesized powders.

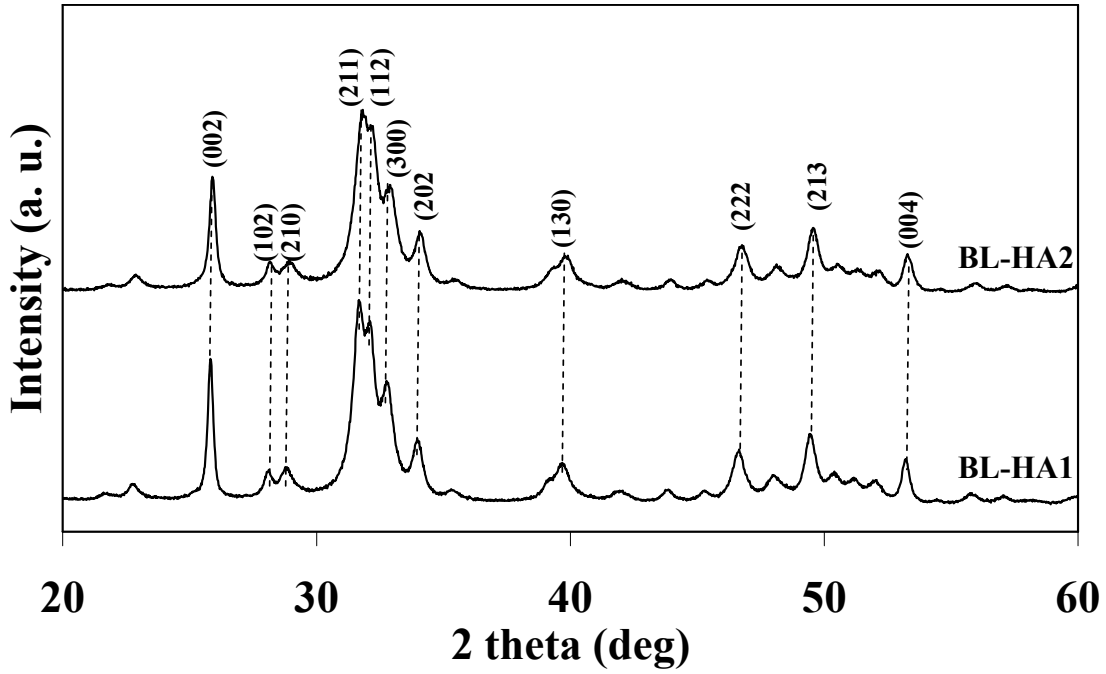

Figure 1. X-ray diffraction patterns for the as prepared powders, BL-HA1 and BL-HA2.

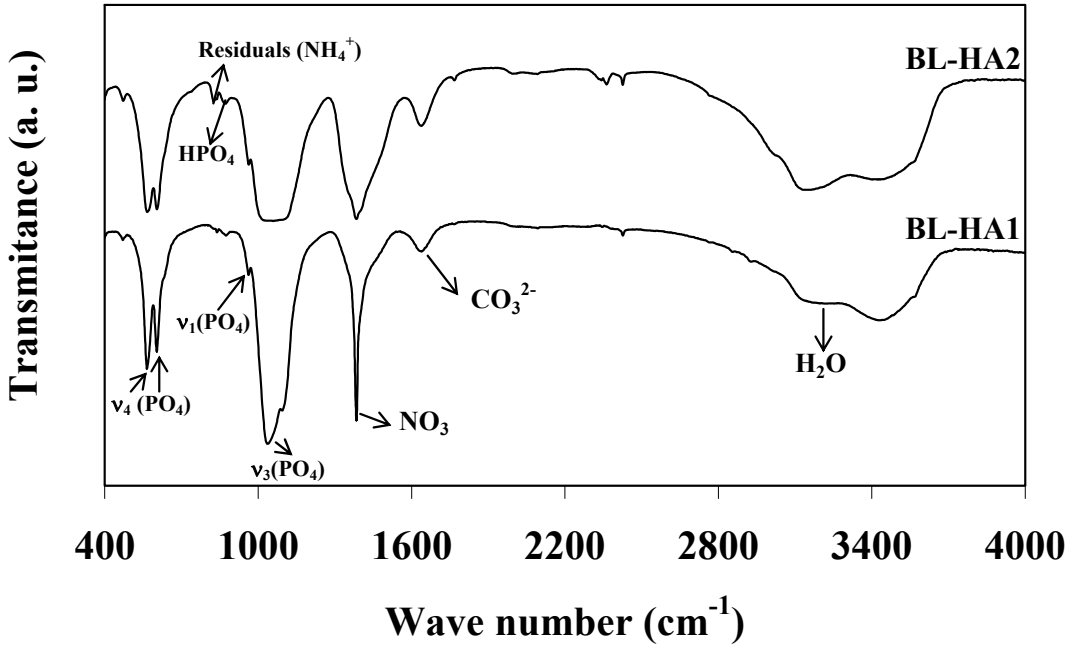

Figure 2. FT-IR spectra of the as prepared powders, BL-HA1 and BL-HA2.

The presence of residual NH_4^+ ions at 875 cm^{-1} and of nitrates in the region around 1320-1480 cm^{-1} is apparent in the FT-IR patterns of the two as prepared powders, in good agreement with observations made in a previous study.[43] The bands corresponding to OH group of the HA phase that should be witnessed at 630 and 3570 cm^{-1} are not clearly visible in the spectra of co-substituted powders BL-HA1 and BL-HA2. This is attributed to the replacement of OH group by the substituted anions of F and Cl.[44,45] Like with XRD results, no noticeable differences are apparent in the FT-IR spectra of the as prepared BL-HA1 and BL-HA2 powders. This means that the role of substituted elements in the structure of the as-prepared powders is difficult to explain due to the poor crystallinity of the phases formed, and that heat treatments will be required to improve the crystallinity for a more precise characterization.

Physical characteristics

The particle/agglomerate size analysis of the powders right after precipitation (Fig. 3) show that the BL-HA1 and BL-HA2 powders present monomodal size distributions with average particle/agglomerate sizes, D_{50}, of approximately 2 μm, and 1.5 μm, respectively. Their values of specific surface areas (SSA) were 36.0 $m^2.g^{-1}$ and 52.7 $m^2.g^{-1}$, respectively. These results of size distribution and specific surface area support the hypothesis that the primary particles formed large agglomerates. This can be understood considering high ionic strength of the precipitation medium that compresses the electrical double layers around the colloidal particles leading to coagulation under the action of attractive Van der Waals forces.

The SSA of the as prepared powders BL-HA1 and BL-HA2 decreased significantly to ~1.4 $m^2.g^{-1}$ after calcination even at the lowest heat treatment temperature (1100ºC), being also accompanied by less accentuated decreases in the average pore diameters (APD), as shown in Fig. 4. These changes are consistent with an apparent higher degree of particles agglomeration that has been promoted by calcinations, being more than expected due to the densification process,[46] with both samples reaching similar values after calcination.

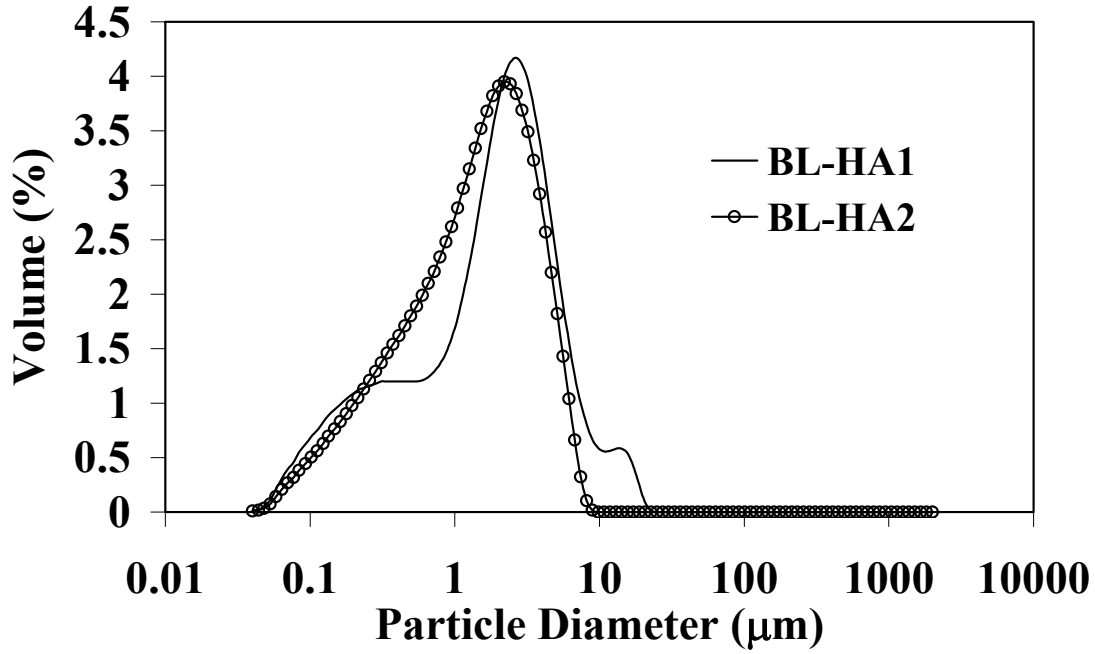

Figure 3. Particle size distribution of the as prepared powders, BL-HA1 and BL-HA2.

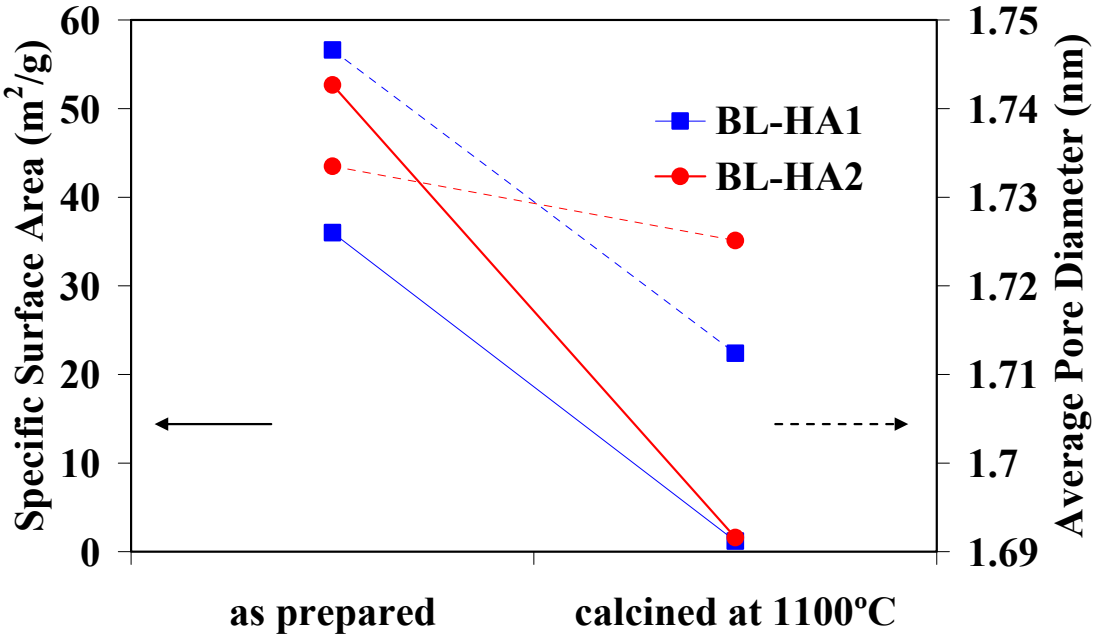

Figure 4. Specific surface area and average pore diameter of the as prepared and calcined at 1100ºC powders, BL-HA1 and BL-HA2.

Thermal analysis

The TG-DTA analysis for the as dried BL-HA1 and BL-HA2 samples presented in Fig. 5 show that their behaviour is very similar and that mass loss has mostly occurred in three stages: (i) 30º-250ºC; (ii) 250º-700ºC; and (iii) 700º-800ºC. Along the first stage, both samples experienced similar weight losses of about 5%, thus accounting for the

loss of lattice bound water with no significant structural changes in this temperature range. Within the second temperature range, the samples BL-HA1 and BL-HA2 show weight losses of about 5%. The loss of residuals, chemisorbed water and carbonates are favoured in this temperature range[42] in which some structural reorganization seems to occur as can be deduced from the exothermic peaks in the DTA curves at 280º-310ºC. This exothermic effect can be attributed to the condensation of hydrogenophosphate ions (HPO_4^{2-}) to form pyrophosphates ($P_2O_7^{4-}$) as given below in equation 1:

$$2Ca^{2+} + 2HPO_4^{2-} \rightarrow Ca_2P_2O_7 + H_2O \qquad (1).$$

Along the temperature range of 700-800ºC the conversion of $Ca_2P_2O_7$ into β-$Ca_3(PO_4)_2$ [41] occurred as described by equation 2, giving raise to a further weight loss of about 2.5% in both samples.

$$Ca_2P_2O_7 + 2OH^- \rightarrow Ca_3(PO_4)_2 + H_2O \qquad (2).$$

These results show that the amount of co-substituted elements had no impact on thermal behaviour of precipitated apatites.

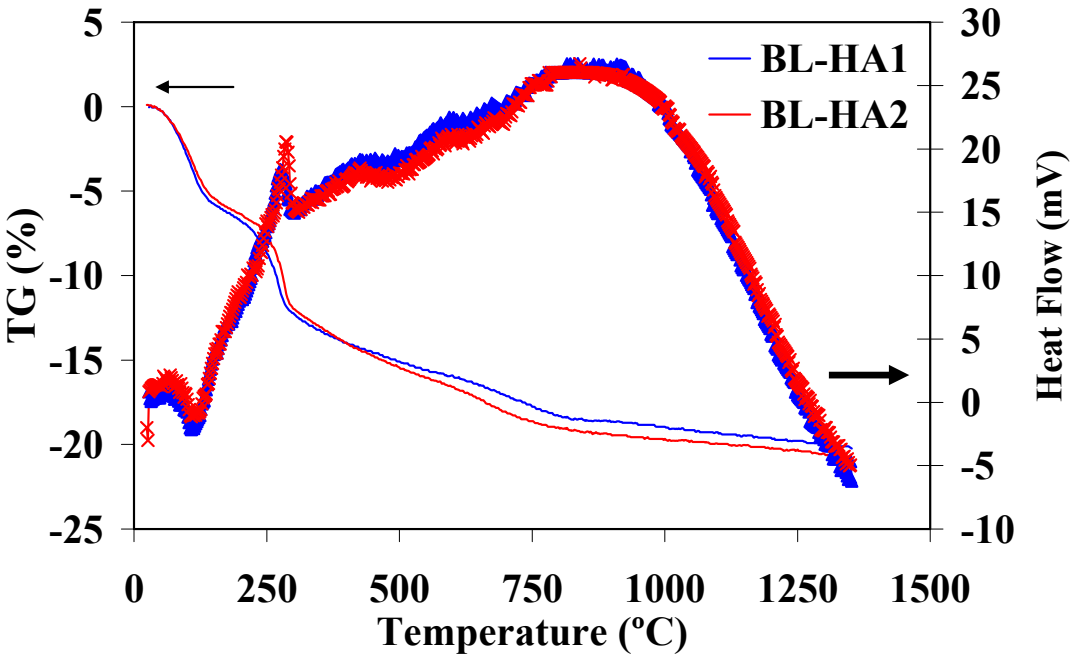

Figure 5. TG and DTA plots for the different Ca/P ratio powders, BL-HA1 and BL-HA2.

Microstructural analysis

Fig. 6 shows the SEM microstructures of the as prepared powders. In both cases, it can be see that the primary particles are sub micrometer, but appear strongly agglomerated. The degree of agglomeration is apparently more severe in the case of BL-HA1, as inferred above from the SSA, APD data and by particle/agglomerate size distribution curves. Both powders consist of acicular shaped particles, with the aspect ratio being higher in the case of BL-HA2.

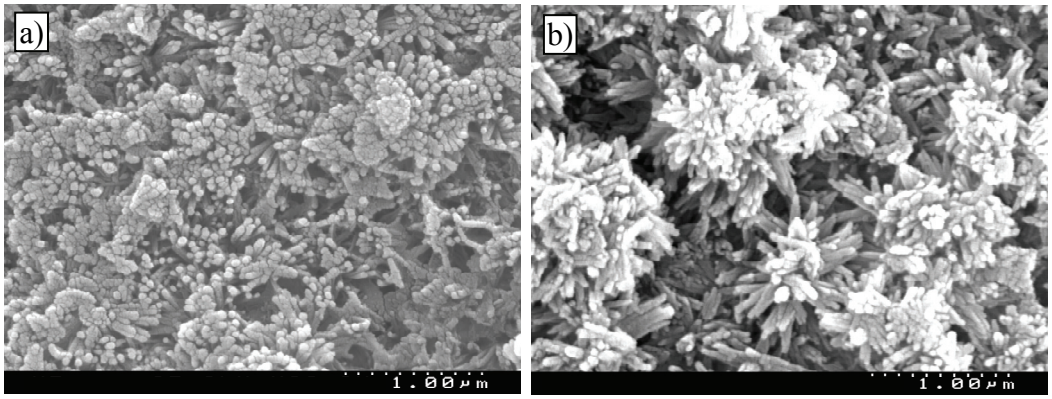

Figure 6. SEM microstructures of the samples BL-HA1 (a), and BL-HA2 (b).

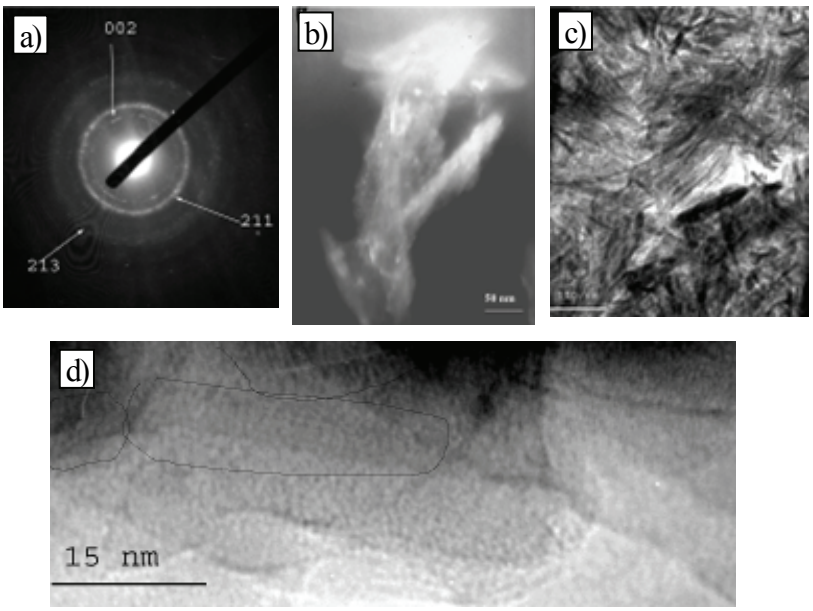

Figure 7. Transmission electron microscopy results of the as prepared BL-HA1: (a) Powder diffraction cliché; (b) Particle size and morphology; (c) Agglomeration and size of particles; (d) High resolution of one crystallite.

These microstructural differences were also confirmed by TEM observations. Fig. 7(a) is a HA diffraction pattern with a bright (211) peak and other typical rings like (002), (300) and (213). The broad rings indicate the presence of amorphous material, being consistent with the observed broad XRD peaks (Fig. 1).

The amorphous contribution is quite high as can be seen from Fig. 7(b). Fig. 7(c) illustrates the agglomeration of the particles. The high resolution image in Fig. 7(d) shows a crystallite that makes up a particle of BL-HA1 (size ~50 - 100 nm). Fig. 7(d) also shows other crystallites, the structure of which is not fully organized.

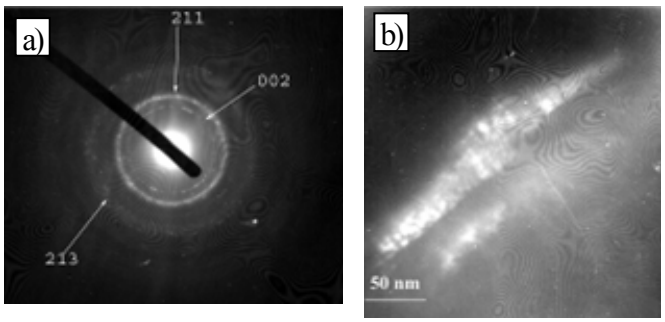

Figure 8. Transmission electron microscopy results of the as prepared BL-HA2: (a) Powder diffraction cliché; (b) Particle size and morphology.

Fig. 8 shows the TEM microstructural features of the BL-HA2 powder. This sample consists of particles that are around 150 nm in size and are less agglomerated compared to BL-HA1. The particle shape is better defined in this case, even though there is quite a large amount of amorphous phase. Morphology is similar to that of BL-HA1: amorphous matrix containing crystallites. However the density of crystallites is higher compared to BL-HA1.

Characterisation of the calcined powders

Elemental analysis

Table 2 compares the results of elemental analysis of the calcined powders with the compositions of hard tissues. From these data one can conclude that the measured Ca/P molar ratios for the BL-HA1 and BL-HA2 powders were Ca/P~1.66. A good correlation can be observed between the elemental analysis of calcined powders and the added elemental concentrations of each element upon synthesis. Accordingly, higher levels of incorporated elements are detected in BL-HA2 in comparison to the BL-HA2 that

shows more or less half the value of BL-HA1. It is also reasonable to mention that the natural bone and tooth mineral consists of all these elements, but the composition may vary depending upon the age, sex, and nature of the species.[46,47] Hence, it is obvious that this synthesis method can be effective in achieving the desired concentration of substituted elements by varying the concentration of the precursors added during the synthesis.

Table 2. Concentrations of the elements measured after heat treatment (HA-1200ºC; BL-HA1 and BL-HA2-1400ºC).

	Concentration of the element (wt.%)						
Sample	**Ca**	**P**	**Na**	**Mg**	**K**	**F**	**Cl**
Bone[2,4]	24.5	11.5	0.7	0.55	0.03	0.02	0.1
Enamel[2,4]	36.0	17.7	0.5	0.44	0.08	0.01	0.3
HA[48]	39.89	18.50	~0.02	~0.01			
BL-HA1	38.99	18.17	0.493	0.51	0.47	0.04	0.03
BL-HA2	39.31	18.32	1.11	0.94	1.09	0.09	0.06

Phase identification and determination of phase content by X-Ray diffraction

The evolution of crystalline phases with the heat treatment temperature for BL-HA1 and BL-HA2 powders, is shown in the XRD patterns of Fig. 9 and Fig. 10, respectively, within the 2θ range from 20º to 60º.

The poor crystallinity of the as prepared powders, characterized by broad diffraction bands (Fig. 1), contrasts with the sharper spectral peaks exhibited after different heat treatments.

All the XRD patterns have indicated the presence of more than one phase. It is apparent from the X-ray patterns (Fig. 9 and Fig. 10) that calcination at higher temperature has led to the formation of the β-TCP phase along with the HA for both powders. Fig. 9 shows that biphasic mixtures of HA+β-TCP were formed in the BL-HA1 sample heat treated up to 1300ºC. Beyond this temperature, β-TCP starts to progressively transform into α-TCP, and at 1400ºC there is no more β-TCP in the composition. Considering that the polymorph α-TCP usually derives from the transformation of β-TCP, as reported in literature,[49,50] these results suggest that the β-TCP formed from the partial decomposition of HA spontaneously transforms into α-TCP in the temperature range from 1350º-1400ºC.

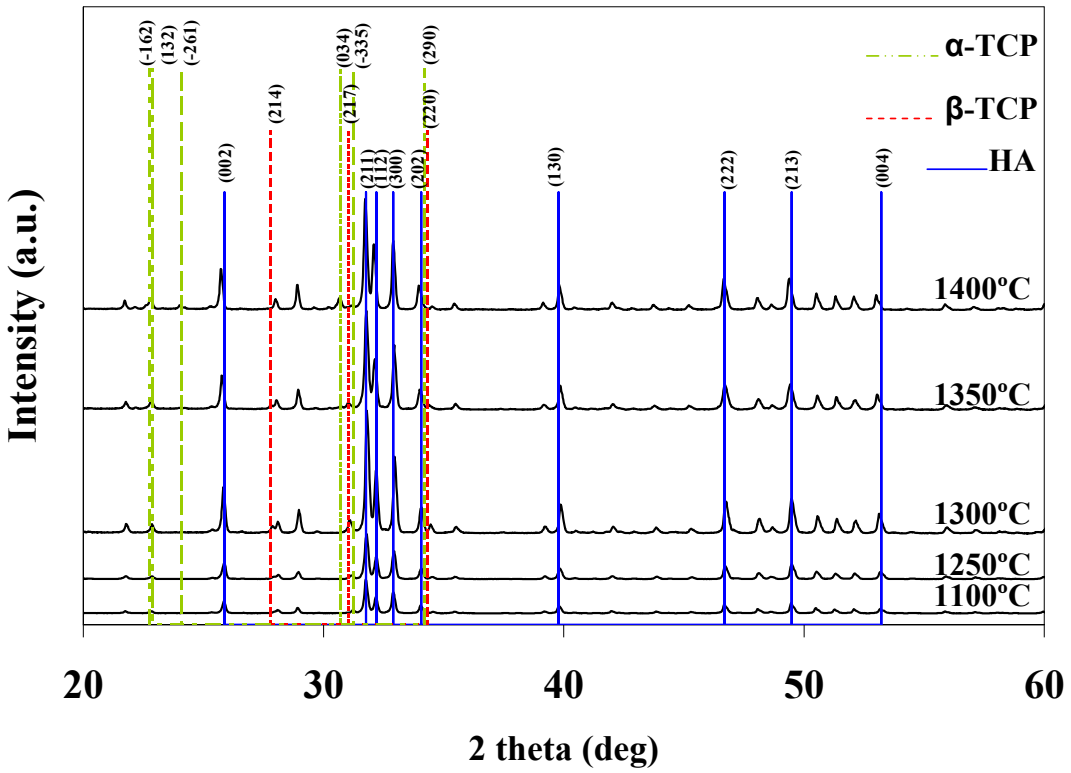

Figure 9. Crystalline phase evolution of BL-HA1 powders with heat treatment temperatures.

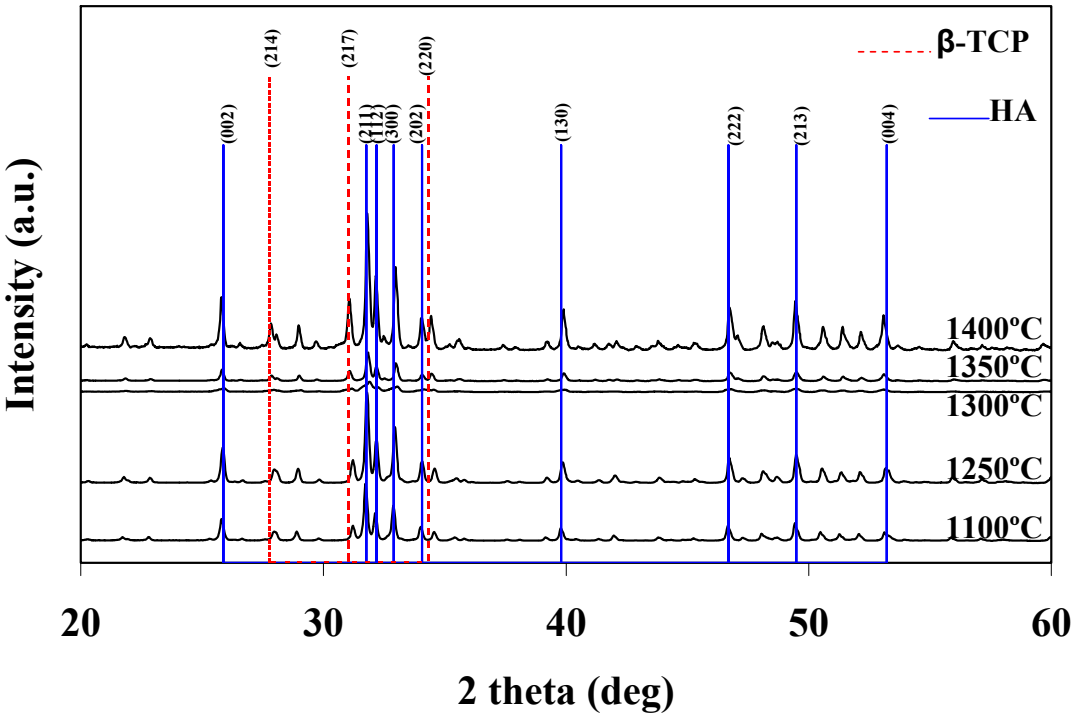

Figure 10. Crystalline phase evolution of BL-HA2 powders with heat treatment temperatures.

Fig. 10 shows that doubling the concentration of substituted elements resulted in improved thermal stability, delaying the β to α–TCP phase transformation, with the BL-HA2 powder still remaining biphasic at 1400ºC. The quantitative phase composition determined through Rietveld analysis showed significant variations that were totally dependent on the calcination temperature and on the amount of substituted elements. Table 3 indicates the wt.% of the phase composition for all the powders after refinement.

From Table 3 one can observe that the amount of β-TCP in BL-HA1 increases up to 1300ºC and then starts to transform into α-TCP. In the case of BL-HA2 powder with higher concentrations of substituted elements, the increase of the temperature of the heat treatment only give rise to an increase of the amount of β-TCP, reaching around 30 wt.% at 1400ºC. No transformation of α-TCP into β-TCP occurred within this temperature range (1100-1400ºC). This different behaviour between BL-HA1 and BL-HA2 can be attributed to the different incorporation levels of the substituted elements in the latice, with a special emphasis to Mg^{2+}. It has been reported[51] that magnesium plays an important role in stabilizing the β-TCP phase with α-TCP appearing only at 1350ºC, i.e., 100ºC above the onset of β to α phase transformation temperature observed for the undoped calcium deficient HA. Comparing the added amounts of magnesium in this work to the one already reported [51] it is possible to conclude that the amount of magnesium in BL-HA1 was not enough to completely stabilize the β-TCP phase, appearing the α-TCP phase at 1350ºC. In the case of BL-HA2, the higher amount of magnesium enabled a complete stabilization of β-TCP phase, hindering its transformation into α-TCP. In summary, at 1400ºC the BL-HA2 powder consists of about 70% HA + 30% β-TCP, while the BL-HA1 powder comprises about 87% HA + 13% α-TCP. This proves that the levels of elemental co-substitutions had a tremendous impact on the phase formation upon heat treatment. These results are in good accordance with the previous studies showing that even though the stoichiometric Ca/P molar ratio of 1.67 was used, essential for the formation of pure HA, the substituted elements in the apatite lattice can lead to formation of β-TCP upon calcination beyond 1000 °C.[52,53]

Table 3. Rietveld phase analysis quantification in the co-substituted calcium phosphates powders heat treated at different temperatures.

Sample code	Sintering Temperature (°C)	Wt. % of composition determined by Rietveld quantification		
		HA	β-TCP	α-TCP
BL-HA1	1100	91.94	8.06	-
	1250	91.83	8.17	-
	1300	89.77	10.23	-
	1350	88.94	6.36	4.70
	1400	87.14	-	12.86
BL-HA2	1100	77.87	22.13	-
	1250	77.67	22.33	-
	1300	76.09	23.91	-
	1350	70.51	29.49	-
	1400	70.54	29.46	-

Table 4. Refined lattice parameters and calculated cell volume of HA phase for BL-HA1 and BL-HA2.

Sample code	Sintering Temperature (°C)	Refined lattice data for HA phase			R-Bragg
		a-axis (Å)	*c*-axis (Å)	Cell volume (Å^3)	
JCPDS # 74-0565[37]	-	9.424	6.879	1581.714	-
BL-HA1	1100	9.41721 (5)	6.88173 (4)	1580.062	4.53
	1250	9.41304 (6)	6.88169 (5)	1578.654	3.98
	1300	9.40349 (6)	6.88803 (6)	1576.904	3.62
	1350	9.40148 (10)	6.89640 (9)	1578.145	5.24
	1400	9.39853 (12)	6.89442 (10)	1576.702	5.49
BL-HA2	1100	9.40906 (9)	6.88177 (7)	1577.338	4.01
	1250	9.40640 (9)	6.88291 (7)	1576.707	3.57
	1300	9.41576 (43)	6.89925 (36)	1583.597	10.9
	1350	9.39494 (18)	6.89065 (13)	1574.636	4.57
	1400	9.39434 (18)	6.89016 (13)	1574.323	5.40

The calculated lattice parameters for BL-HA1 and BL-HA2 (Table 4) samples also confirm the formation of a hexagonal apatite system with minor differences in comparison to the stoichiometric HA, which are solely due to the role of incorporated

elements in the apatite lattice. It can be observed that the lattice parameters of the samples are always smaller than the ones reported in the literature,[38] which is related to the co-substitution of elements in the hydroxyapatite structure. Moreover, increasing heat treatment temperatures leads to shrinkage along the *a*-axis and to an enlargement along the *c*-axis, fact that is related to the lattice distortions due to the incorporation of the co-substituted elements of different size in different lattice positions of HA.

The evolution of crystallite sizes with heat treatment temperature measured for BL-HA1 and BL-HA2 powders along the (002) and (300) planes, corresponding to *c* axis, and *a* axis, are plotted in Fig. 11 and Fig. 12, respectively. In both cases, there is an increasing trend of crystalline size as the heat treatment temperature increases, which is somewhat disturbed in the temperature range where phase transformations occur (Table 3). This deviation from the main trend is apparently more accentuated in the sample BL-HA2 in which higher amounts of β-TCP is formed (Table 3). Due to the relatively high calcination temperatures used, the calculated crystallite sizes tend to be above the values reported for bone mineral (~50 nm).[54,55]

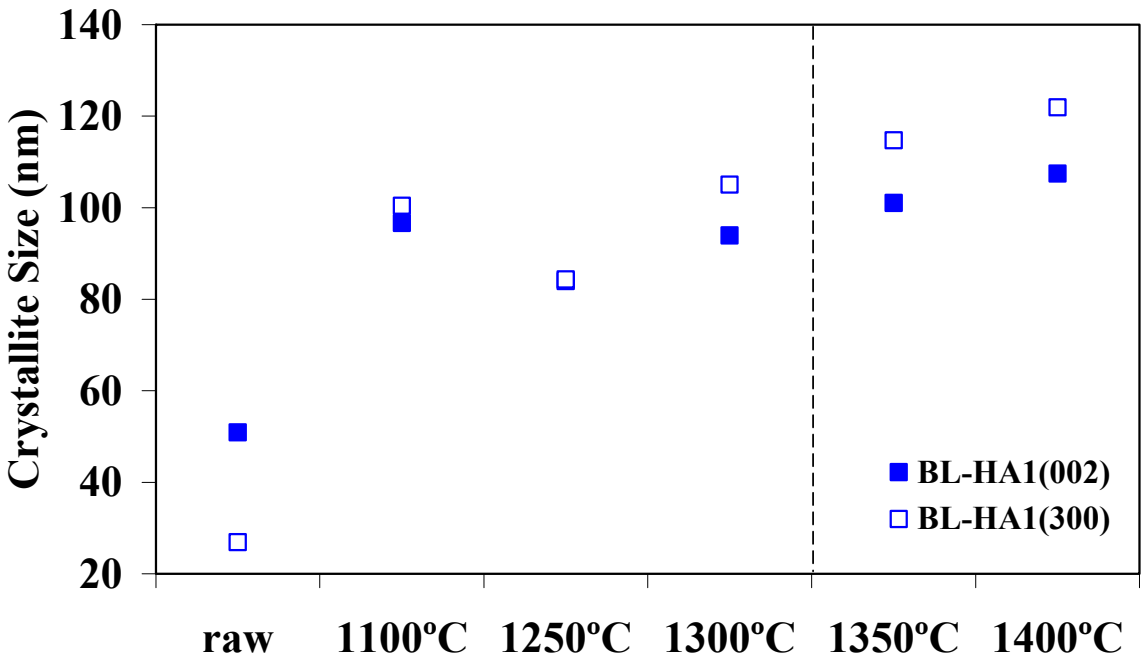

Figure 11. Evolution of crystallite sizes with heat treatment temperature of the BL-HA1 samples.

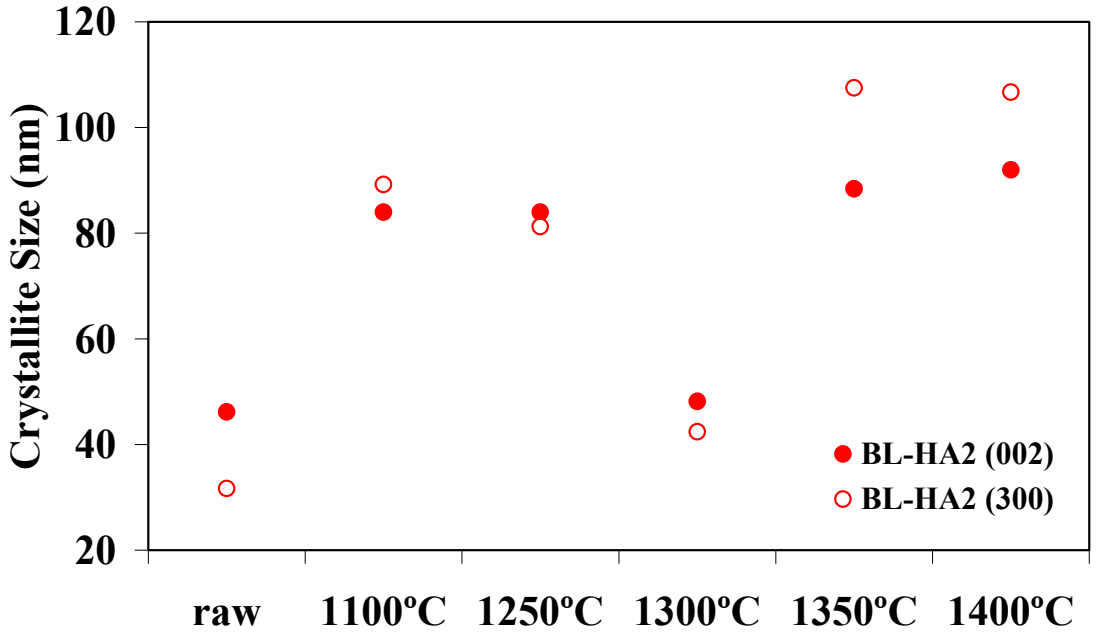

Figure 12. Evolution of crystallite sizes with heat treatment temperature of the BL-HA2 samples.

Role of substituted elements

The existing scientific reports on synthetic HA with substituted elements have well-documented the behaviour of single or coupled element substitution in the apatite lattice. The incorporation of foreign ions in the synthetic HA can induce subtle changes in the resultant crystallographic parameters depending upon its concentration and especially the size. The incorporation of Na (0.97 Å) seems to depend on the nature of the precursors. [26] With certain additives, it has been proved that Na incorporation favours the formation of pure HA whereas in certain cases trace levels of β-tricalcium phosphate (β-TCP) and calcium oxide (CaO) have been detected in the resultant powder after heat treatment. In the case of Mg, its stabilization role on the β-TCP phase upon heat treatment above 800ºC has been well-recognized.[20,21] There are reports on its significant influence on the lattice constant values due to size mismatch with Ca (Ca, 0.99 Å; Mg, 0.66 Å). Potassium (1.33 Å) has a bigger size than Ca and, hence its incorporation into the apatite structure can favour significant variations in the resultant lattice values. There is also evidence about the combined substitution of Mg and CO_3 as well as Na and CO_3 into the apatite structure that can result in the formation of pure HA phase while heating in careful consideration of preserving volatile CO_3 at high temperatures.[31,33] In the case of anionic substitutions of both Cl (1.81 Å) and F (1.36 Å),

the prevailing reports strongly suggest their replacement for OH groups while incorporation into the apatite structure, thus causing expansion or contraction of lattice constants. Some studies have indicated that partial replacement of F for the OH group can cause the formation of a trace level of the β-TCP phase upon heat treatment.[22] The effect of a single or a couple of substitutions on the apatite structure can be understood from the existing reports. However, the incorporation of all these elements in the apatite is more complex and has seldom been reported before.[35] The present results show that the structure of the apatite phase has been preserved except for some small observed discrepancies in the lattice values. Hence the statement that "hierarchical structure of apatite is ready to accept a wide variety of ionic substitutions (both cationic and anionic) with no significant changes in the hexagonal apatite structure"[34] is proved from the present results.

Conclusions

The results presented and discussed in this work enable the following conclusions to be drawn:

1. Synthetic HA powders with different levels of co-substituted essential trace elements found in the biological apatite could be prepared.
2. The co-substituted apatite BL-HA2 powder did not transform to the undesirable α-TCP until 1400ºC, giving rise to the formation of noticeable amounts of desirable β-TCP.
3. The amount of resorbable β-TCP formed, along with the nonresorbable HA, was shown dependent on the co-substitution levels, but both co-substituted BL-HA1 and BL-HA2 powders present compositions closer to the hard tissues when compared to pure, single or coupled element substituted HA, being therefore suitable for further experimentation in biomedical applications.
4. Although the exact position of the incorporated elements in the apatite structure cannot be determined from the present results, the method of synthesis proved that the essential biocompatible elements can be substituted in the synthetic apatite, without significant structural modifications.

References

1. Hench LL. Bioceramics: From Concept to Clinic. J Am Ceram Soc 1991;74:1487-1510.

2. Aoki H. Science and medical applications of hydroxyapatite. JAAS. Tokyo. 1991.

3. Jarcho M, Bolen CH, Thomas MB, Bobick J, Kay F & Doremus RH. Hydroxyapatite synthesis and characterization in dense polycrystalline form. J Mater Sci 1976;11:2027-2035.

4. Le Geros RZ & Le Geros JP. Dense hydroxyapatite. In: Hench LL & Wilson J Editors. Introduction to bioceramics. World Scientific. Singapore. 1993.

5. LeGeros RZ. Calcium phosphates in oral biology and medicine. Karger AG Publishers: Basel. Switzerland. 1991.

6. Rey C. Calcium phosphates for medical applications. In: Amjad Z Editor. Calcium Phosphates in Biological and Industrial Systems. Kluwer Academic Publishers. Boston. 1998. pp. 217–239.

7. Elliott JC. Structure and chemistry of the apatites and other calcium orthophosphates. Elsevier. Amsterdam. 1994.

8. Itoh R & Suyama Y. Sodium excretion in relation to calcium and hydroxyproline excretion in a healthy Japanese population. Am J Clin Nutr 1996;63:735-740.

9. Ginty F, Flynm A & Cashman KD. The effect of dietary sodium intake on biochemical markers of bone metabolism in young women. Br J Nutr 1998;79:343-350.

10. Bigi A, Foresti E, Gregoriani R, Ripamonti A, Roveri N & Shah JS. The role of magnesium on the structure of biological apatites. Calcif Tissue Int 1992;50:439-444.

11. Althoff J, Quint P, Krefting ER & Hohling HJ. Morphological studies on the epiphyseal growth plate combined with biochemical and X-ray microprobe analyses. Histochemistry 1982;74:541-552.

12. Martini LA. Magnesium supplementation and bone turnover. Nutr ReV 1999;57:227-229.

13. Wiesmann HP, Plate U, Zierold K & Hohling HJ. Potassium is involved in apatite biomineralization. J Dent Res 1998;77:1654-1657.

14. Krefting ER, Lissner L & Hohling HJ. Quantitative electronprobe microanalysis of the epiphyseal growth plate. J Phys 1984;45:465- 468.

15. Ten Cate JM & Featherstone JDB. Mechanistic Aspects of the Interactions Between Fluoride and Dental Enamel. Crit ReV Oral Biol Med 1991;2:283-296.

16. Caverzasio J, Palmer G & Bonjour JP. Fluoride: Mode of action.Bone 1998;22:585-589.

17. Schlesinger PH, Blair HC, Teitalbaum SL & Edwards JC. Characterization of the osteoclast ruffled border chloride channel and its role in bone resorption. J Biol Chem 1997;272:18636-18643.

18. Neuman WF & Neuman MW. The chemical dynamics of bone mineral. University of Chicago Press. Chicago. 1958.

19. Yang Z, Jiang Y, Yu L, Li F, Sun S & Hou T. Preparation and characterization of magnesium doped hydroxyapatite–gelatin nanocomposite. J Mater Chem 2005;15:1807-1811.

20. Kannan S, Lemos IAF, Rocha JHG & Ferreira JMF. Synthesis and characterization of magnesium substituted biphasic mixtures of controlled hydroxyapatite/β-tricalcium phosphate ratios. J Solid State Chem 2005;178:3190-3196.

21. Suchanek WL, Byrappa K, Shuk P, Riman RE, Janas VF & Ten Huisen KS. Preparation of magnesium-substituted hydroxyapatite powders by the mechanochemical–hydrothermal method. Biomaterials 2004;25:4647-4657.

22. Rodríguez-Lorenzo LM, Hart JN & Gross KA. Influence of fluorine in the synthesis of apatites. Synthesis of solid solutions of hydroxy-fluorapatite. Biomaterials 2003;24:3777-3785.

23. Kannan S, Ventura JM & Ferreira JMF. In Situ Formation and Characterization of Flourine-Substituted Biphasic Calcium Phosphate Ceramics of Varied F-HAP/*β*-TCP Ratios. Chem Mater 2005;17:3065-3068.

24. Gross KA & Rodríguez-Lorenzo LM. Sintered hydroxyfluorapatites. Part I: Sintering ability of precipitated solid solution powders. Biomaterials 2004;25:1375-1384.

25. Lin FH, Liao CJ, Chen KS & Sun JS. Preparation of high-temperature stabilized β-tricalcium phosphate by heating deficient hydroxyapatite with $Na_4P_2O_7 \cdot 10H_2O$ addition. Biomaterials 1998;18:1101-1107.

26. Suchanek W, Yashima M, Kakihana M & Yoshimura M. Hydroxyapatite ceramics with selected sintering additives. Biomaterials 1998;18:923-933.

27. Yanagisawa K, Rendon-Angeles JC, Ishizawa N & Oishi S. Topotaxial replacement of chlorapatite by hydroxyapatite during hydrothermal ion exchange. Am Mineral 1999;84:1861-1869.

28. Bertoni E, Bigi A, Cojazzi G, Gandolfi M, Panzavolta S & Roveri N. Nanocrystals of magnesium and fluoride substituted hydroxyapatite. J Inorg Biochem 1998;72:29-35.

29. Mayer I, Schlam R & Featherstone JDB. Magnesium-containing carbonate apatites. J Inorg Biochem 1997;66:1-6.

30. Feki HE, Amami M, Ben Salah A & Jemal M. Synthesis of potassium chloroapatites, IR, X-ray and Raman studies. Phys. Status Solidi 2004;1:1985-1988.

31. De Maeyer EAP, Verbeeck RMH & Naessens DE. Stoichiometry of sodium(+)- and carbonate-containing apatites obtained by hydrolysis of monetite. Inorg Chem 1993;32:5709-5714.

32. Yamasaki Y, Yoshida Y, Okazaki M, Shimazu A, Uchida T, Kubo T, Akagawa Y, Hamada Y, Takahashi J & Matsuura N. Synthesis of functionally graded MgCO3 apatite accelerating osteoblast adhesion. J Biomed Mater Res 2002;62:99-105.

33. Gibson IR & Bonfield W. Preparation and characterization of magnesium/carbonate co-substituted hydroxyapatites. J Mater Sci: Mater Med 2002;13:685-693.

34. Cazalbou S, Combes C, Eichert D & Rey C. Adaptative physico-chemistry of bio-related calcium phosphates. J Mater Chem 2004;14:2148-2153.

35. Kannan S, Neunhoefferb FG, Neubauerb J & Ferreira JMF. Ionic Substitutions in biphasic Hydroxyapatite and β-Tricalcium phosphate mixtures. Structural analysis by Rietveld Refinement. (Feature Article) J Am Ceram Soc 2008;91[1]:1–12.

36. Dickens B, Schroeder LW & Brown WEJ. Crystallographic studies of the role of Mg as a stabilizing impurity in β-$Ca_3(PO_4)_2$. The crystal structure of pure β-$Ca_3(PO_4)_2$. Solid State Chem 1974;10:232.

37. Mathew M, Schroeder LW, Dickens B & Brown WE. The crystal structure of α-$Ca_3(PO_4)_2$. Acta Crystallogr 1977;B33:1325-1333.

38. Sudarsanan K & Young RA. Significant precision in crystal structural details. Holly Springs hydroxyapatite. Acta Crystallogr 1969;B25:1534-1543.

39. Cullity BD. Elements of X-ray Diffraction. Addison Wesley. Reading. 1978.

40. Klug HP & Alexander LE. X-ray Diffraction Procedures.Wiley.New York.1959.

41. Mostafa NY. Characterization, thermal stability and sintering of hydroxyapatite powders prepared by different routes. Materials Chemistry and Physics 2005;94:333–341.

42. Kannan S, Rebelo A, Lemos AF, Barba A & Ferreira JMF. Synthesis and mechanical behaviour of chlorapatite and chlorapatite/b-TCP composites. Journal of European Ceramic Society 2007;27:2287-2294.

43. Mortier A, Lemaitre J & Roushet PG. Temperature-programmed characterization of synthetic calcium-deficient phosphate apatites. Thermochim Acta 1989;143:265-282.

44. Kannan S, Rocha JHG & Ferreira JMF. Synthesis of hydroxy-chlorapatites solid solutions. Materials Letters 2006;60**:**864–868.

45. Kannan S, Ventura JM & Ferreira JMF. *In situ* formation and characterization of Flourine substituted Biphasic calcium phosphate ceramics of varied F-HAP/Beta-TCP ratios. Chemistry of Materials 2005;17[12]:3065-3068.

46. Le Geros RZ, Balmain N & Bonel G. Age-related changes in mineral of rat and bovine cortical bone. Calcif Tissue Res 1987;41:137.

47. Handschin RG & Stern WB. Crystallographic and chemical. analysis of human bone apatite (Crista Iliaca). Clin. Rheumatol 1994;13:75.

48. Kannan S, Lemos AF & Ferreira JMF. Synthesis and Mechanical Performance of Biological-like Hydroxyapatites. Chem Mater. 2006;18:2181-2186.

49. Hyun-Seung R, Hyuk-Joon Y, Sun HK, Bong-Sun C, Choon-Ki L & Sung-Soo C. An improvement in sintering property of β-tricalcium phosphate by addition of calcium pyrophosphate. Biomaterials 2002;23[3]:909-914.

50. Bouler JM, LeGeros RZ & Daculsi G. Biphasic calcium phosphates: Influence of three synthesis parameters on the HA/β-TCP ratio. Biomed Mater Res 2000; 51 [4]:680-684.

51. Lemos AF, Arcos D, Vallet-Regí M & Ferreira JMF. Rietveld analysis of magnesium substituted biphasic mixtures and influence of heat treatment temperature on phase evolution. Submitted to J Eur Ceram Soc. 2008.

52. Kannan S, Rocha JHG & Ferreira JMF. Synthesis and thermal stability of Sodium, Magnesium co-substituted Hydroxyapatites. J Mater Chem 2006;3:286-291.

53. Kannan S & Ferreira JMF. Synthesis and thermal stability of hydroxyapatite-β-tricalcium phosphate composites with cosubstituted sodium, magnesium, and fluorine. Chem Mater 2006;18:198-203.

54. Danilchenko SN, Kukharenkoi OG, Moseke C, Protsenko IY, Sukhodubi LF & Sulkio-cleff B. Determination of the Bone Mineral Crystallite Size and Lattice Strain from Diffraction Line Broadening. Cryst Res Technol 2002;37:1234.

55. Kinney JH, Pople JA, Marshall GW & Marshall SJ. Collagen orientation and crystallite size in human dentin: A small angle x-ray scattering study. Calcif Tissue Int 2001;69.

Chapter 3

Colloidal Processing and Mechanical Performance of Biological-like Calcium Phosphate Ceramics

Alexandra F. Lemos [a,b,c,] and José M. F. Ferreira[a]

a Dept. of Ceramics and Glass Engineering, University of Aveiro, CICECO, 3810-193 Aveiro, Portugal.

b Dept. of Metallurgy and Materials Engineering, Engineering Faculty of the University of Porto, Rua Dr. Roberto Frias, 4200-465 Porto, Portugal.

c Institute of Biomedical Engineering, University of Porto, Rua do Campo Alegre 823, 4150-180 Porto, Portugal.

Abstract

The present work shows how a proper processing route can be used to develop strong calcium phosphate bioceramic materials for bone graft applications. The dispersion conditions of biphasic calcium phosphate powders were studied in aqueous media in the presence of two anionic dispersants. The properties of the suspensions investigated by rheological measurements indicated an ammonium polycarbonate as the most efficient dispersing agent and enabled to select optimal conditions to obtain very well dispersed slurries with solids content as high as 60 vol.%. Homogeneous freeze dried granules produced from these suspensions could be easily consolidated by dry pressing and sintered. The sintered biphasic calcium phosphate samples exhibited excellent mechanical properties, demonstrating that the colloidal processing route used is effective for preparing strong biphasic calcium phosphate materials for biological applications.

Introduction

The requirements for hard tissue replacements have been stimulating an increasing interest in calcium phosphates. Synthetic bone graft materials available as alternatives to autogenously bone for repair, substitution or augmentation, in particular synthetic biomaterials include, special glass ceramics described as bioactive glasses; calcium phosphates (hydroxyapatite, HA; tricalcium phosphate, TCP; and biphasic calcium phosphate, BCP mixtures). These materials differ in composition and physical properties from each other and from bone.[1-5] These biomaterials show excellent

biocompatibility with hard tissues and also with skin and muscles tissues, being the most appropriate ceramic materials for hard-tissue replacement.[2,6]

Unfortunately, due to low mechanical reliability,[7] the use of calcium phosphate (CaP) ceramics is still very limited.[6] In recent years, efforts were made towards preparing more reliable bioceramic bodies and colloidal processing is among the most promising routes for achieving this objective.[8] Colloidal approach has the potential for eliminating detrimental heterogeneities, avoiding their reintroduction during the successive processing steps and obtaining pieces with complex shapes similar to human bones.[9]

Colloidal processing of ceramic powders requires control of the homogeneity, rheology and dispersion of the suspensions. Particle dispersion is often the limiting factor, affecting both rheology and homogeneity of suspensions. The dispersion of calcium phosphate powders in aqueous media has been studied in literature.[10–16] It was reported that anionic polyelectrolytes were effective in obtaining homogeneous distribution of calcium phosphate powders.[12–16]

In spite of the structural and crystallographic similarities with synthetic HA, the biological apatites are always non-stoichiometric with structural imperfections due to several incorporated elements in the lattice.[17-20] Although these elements are embedded at trace levels in the composition of biological apatites, several studies proved their determining role on the biological process.[20-27] Some of the salient features of the trace elements have a thorough understanding as described below: (a) Sodium, a monovalent ion, available in abundance next to calcium and phosphorous, plays a significant role on bone metabolism and osteoporosis;[20,21] (b) Magnesium, undoubtedly one of the most important bivalent ions associated with the biological apatite, plays an important role in the calcification process and bone fragility and an indirect influence on mineral metabolism;[22] (c) Potassium plays an active role in mineralization and biochemical processes;[23] (d) Fluorine is well recognized for its potential behaviour on the stability of apatite and on preventing dental caries;[24,25] and (e) Chlorine – enables to develop an acidic environment on the surface of bone that activates osteoclasts in the bone resorption process.[26,27] As a result of the significant roles played by these trace elements in biological process, nowadays numerous studies have been undertaken aiming at the synthesis of ionic substituted hydroxyapatites either with single elements[28-36] or coupled element substitutions.[37-40]

Since the hierarchical structure of apatite has the ability to accept a wide number of possible substitutions in its lattice,[41] the significance of the job will be higher if the

substitution of the elements is made at levels similar to those found in bone. Kannan *et al.*[42] prepared synthetic calcium phosphates with combined substituted biocompatible trace elements of biological apatite to improve its biological response upon implantation.

The objective of the current work is to study the effects of the type and amount of deffocculant on the dispersing ability of CaP powders of different compositions in order to establish suitable colloidal processing conditions for preparing granules by freeze granulation that could be used to consolidated homogeneous green testing samples by uniaxial pressing and evaluate the influence of composition on the final mechanical properties.

Materials and Methods

Preparation

The synthesis of the calcium phosphate powders was carried out in a fully automated apparatus (capacity = 6 liters) with specific devices to control the stirring of suspensions, the addition rate of reactants and the temperature of the system. Reagent grade calcium nitrate tetrahydrate [$Ca(NO_3)_2.4H_2O$, Aldrich-Germany], diammonium hydrogen phosphate [$(NH_4)_2HPO_4$, Aldrich-Germany], sodium nitrate [$NaNO_3$, Aldrich-Germany], magnesium nitrate hexahydrate [$Mg(NO_3)_2.6H_2O$, Merck], potassium nitrate [KNO_3, Merck], ammonium chloride [NH_4Cl, Merck] and ammonium fluoride [NH_4F, Merck] were used as starting chemical precursors for the synthesis. Five different types of compositions were attempted to obtain pure HA materials, biphasic calcium phosphates and biphasic calcium phosphates with co-substituted elements. The solution concentrations of precursors are detailed in Table 1. In the case of biphasic calcium phosphates with co-substituted elements, a mixture of $(NH_4)_2HPO_4$, NH_4F and NH_4Cl solutions was added slowly at a rate of 50 mL/min to the solution mixture containing nitrates of Ca, Na, Mg and K stirred at a rate of 1000 rpm. After the addition of all the precursors, the pH value of the mixture was found to be around 4, being then increased to 9 by adding 8 M ammonium hydroxide (NH_4OH) solution. After the completion of addition, the reaction was performed at 90ºC for 2 h under a constant stirring rate of 1000 rpm. Pure stoichiometric HA with a Ca/P ratio of 1.67 and a deficient calcium

Table 1. Concentration of the precursors used in the synthesis of the calcium phosphate samples.

		HA	Ca-def-HA	Mg-(Ca-def-HA)	BL-HA1	BL-HA2
Ca/P		1.67	1.62	1.62	1.67	1.67
Elements	**Salt name**			**molarity**		
Ca	**$Ca(NO_3).4H_2O$**	2.00	1.94	1.94	2.00	2.00
P	**$(NH_4)_2HPO_4$**	1.20	1.20	1.20	1.20	1.20
Mg	**$Mg(NO_3)_2.6H_2O$**	-	-	0.06	0.04	0.08
Na	**$NaNO_3$**	-	-	-	0.05	0.10
K	**KNO_3**	-	-	-	0.03	0.06
Cl	**NH_4Cl**	-	-	-	0.05	0.10
F	**NH_4F**	-	-	-	0.05	0.10

phosphate with a Ca/P ratio of 1.62, without any additives were prepared under the same conditions to compare the results. The precipitates were vacuum filtrated and washed repeatedly with de-ionized water and then dried at 80ºC overnight. The dried cakes were ground to fine powders, sieved through a mesh size of 200 μm and calcined at 1100ºC. The calcined powders were then dry milled for 15 min in a high energetic ball milling to achieve mean particle sizes of around 1.5 μm.

X-Ray diffraction

X-ray diffraction analysis was performed on calcined calcium phosphate powders, using a high resolution Rigaku Geigerflex D/Mac, C Series diffractometer with Copper Kα radiation, λ = 1.540596 Å. For data collection, the following parameters were set; 2θ range of 20-60º; 2θ step width of 0.05º; time per step 2 s.

Zeta potential measurements

The electrophoresis method was used to measure the zeta potential of calcium phosphate powders using a Doppler Electrophoretic Light Scattering Analyser (DELSA 440SX - Coulter, UK) at several pH values. Zeta potential (ZP) values were calculated automatically by the instrument based on the Smoluchowski equation: $\zeta = 4\pi \mu\eta/E$, where ζ is the ZP (mV), μ the electrophoretic mobility (μm cm/V s), η the viscosity of the fluid, and E the dielectric constant of the fluid. The principle of electrophoresis is that a particle will move in a liquid under the influence of an applied electric field

provided that its ZP is different from zero. The electrophoretic mobility is proportional to the ZP as shown by the Smoluchowski equation.

The powders were firstly dispersed ultrasonically in 10 mM KCl, and allowed to stand for 1 h to let larger particles to settle. An aliquot taken from the supernatant was used to measure the zeta potentials. The average of 3 measurements was taken to represent the measured potential. The pH of the suspensions was adjusted with 0.1 M HCl and 0.1 M KOH.

Rheological characterization

Preliminary sedimentation tests were firstly used to evaluate the efficiency of two anionic polyelectrolytes, Targon 1128, an ammonium polycarbonate (Targon1128, BK Ladenburg, Germany) (T) and a polymethacrylic acid (Dolapix CE 64, PMAA) (Zschimmer & Schwarz, Germany) (D), in stabilizing the calcium phosphate powders in aqueous media. From these studies, the most promising dispersant for all the powders (Targon 1128), which has already proved to be effective in dispersing hydroxyapatite[43] could be selected and used throughout this work.

Aiming at selecting a suitable dose of dispersant, rheological analyses were firstly performed using aqueous slips with a fix solids loading of 40 vol.% and different added amounts of Targon 1128, ranging from 0.1 to 2 wt.%, based on the dry weight of solids. The rheological properties were evaluated using a C-VOR rheometer (Bohlin Instruments, USA) equipped with a cone and plate sensing system gradual incremental. From these studies, it was apparent that a maximum degree of dispersion was achieve for an added amount of 0.2 wt.% Targon 1128 for all the powders. This amount was then selected as a first approach to prepare more concentrated suspensions. However, the Ca-def-HA and Mg-(Ca-def-HA) powders required higher dispersant concentrations (0.4 wt.% and 1.5 wt.%, respectively) to achieve 60 vol.% solids loading, as will be discussed below.

In this stride for preparing high solid loaded suspensions, an energetic planetary ball milling process was adopted to investigate its effects on particles deagglomeration efficiency and on rheological behaviour of the suspensions. The solids, and the corresponding amount of dispersant, could then be gradually incremented followed by a new milling period up to achieving a total solids loading of 60 vol.%.

Samples preparation

The powders calcined at 1100ºC were then dry milled for 15 min in a high speed agata mill, resulting in mean particle sizes of around 1.5 μm for all the powders as measured in a particle size analyzer COULTER LS230, UK, with Fraunhofer optical model and dispersed in water. A stock suspension containing 60 vol.% solids loading could be prepared from each powder in the presence of the respective optimal amounts of Targon 1128. In order to obtain good compaction during dry pressing, 3 wt.% of Mowilith DM 2 HB (Clariant, Spain) and 1.5 wt.% of PEG200 (Aldrich, Germany) (based on the dry mass of solids) were added to suspensions, respectively as binder and plasticizer, and the mixtures let to homogenize for 1 h in a rolling system. The as-prepared suspensions were then granulated by freeze granulation (PowerPro freeze granulator LS-2, Sweden) and the granules dried in a freeze dry system (Labconco, LYPH Lock 4.5) for 72 h. After complete drying, the granules were pressed in rectangular bars with 4 mm x 5 mm x 50 mm by uniaxial pressing (80 MPa). After debinding at 550ºC for 2 h, the bars were sintered at different temperatures, according to the phase stability, for 2 h at a heating rate of 5ºC.min^{-1}.

Mechanical characterization of the samples

Flexural strength was measured in series of 20 specimens using a three-point bending device and a Shimadzu equipment (Shimadzu Autograph AG-IS – 10kN, Kyoto, Japan), at a strain rate of 0.5 mm.min^{-1}. For all the samples, the load-displacement curves presented an elastic region ending with brittle fracture. Weibull statistics was used to analyze the flexural strength data and to estimate the cumulative probability of failure under a given load, according to the distribution given in equation (1):

$$P = 1 - \exp\left[-\left(\frac{\sigma}{\sigma_0} \right)^m \right] \qquad (1),$$

where P is the probability of failure at a given applied stress, σ, σ0 is the stress at which 1/e (37%) of the samples survive, and m is a parameter called the Weibull modulus. The greater the value of m, the steeper the transition from survival to failure will be. For this analysis the mean ultimate flexural strength values were ranked in ascending order

and the failure probability was estimated as P=i/(N+1), where i was the rank order and N was the total number of teeth measured at each dentin site.

Vickers hardness tests were carried out using a Zwick/Roell hardness tester (Zwick/Roell ZHU, Ulm, Germany). Polished samples were indented with a Vickers diamond pyramidal indenter having a square base and 136º pyramidal angles. The load was 5 kg and 20 indentations were made and the averaged hardness values were taken for the analysis. Microstructural observations made at the fracture surfaces of the sintered bars were done by scanning electronic microscopy (SEM HITACHI, S-4100, Tokyo, Japan, 25 kV acceleration voltage, beam current 10 μA). The density of the sintered samples was determined by Archimedes method by immersion in mercury.

Results and Discussion

X-Ray diffraction

The XRD patterns of the HA, Mg-(Ca-def-HA), BL-HA1 and BL-HA2 powders after calcination at 1250ºC, and of the powder Ca-def-HA calcined at 1150ºC, are shown in Fig. 1. The HA pattern presents a single mineral phase, hydroxyapatite $Ca_{10}(PO_4)_6(OH)_2$, while the patterns of all other powders show hydroxyapatite and also peaks corresponding to beta-tricalcium phosphate (β-TCP), $Ca_3(PO_4)_2$.

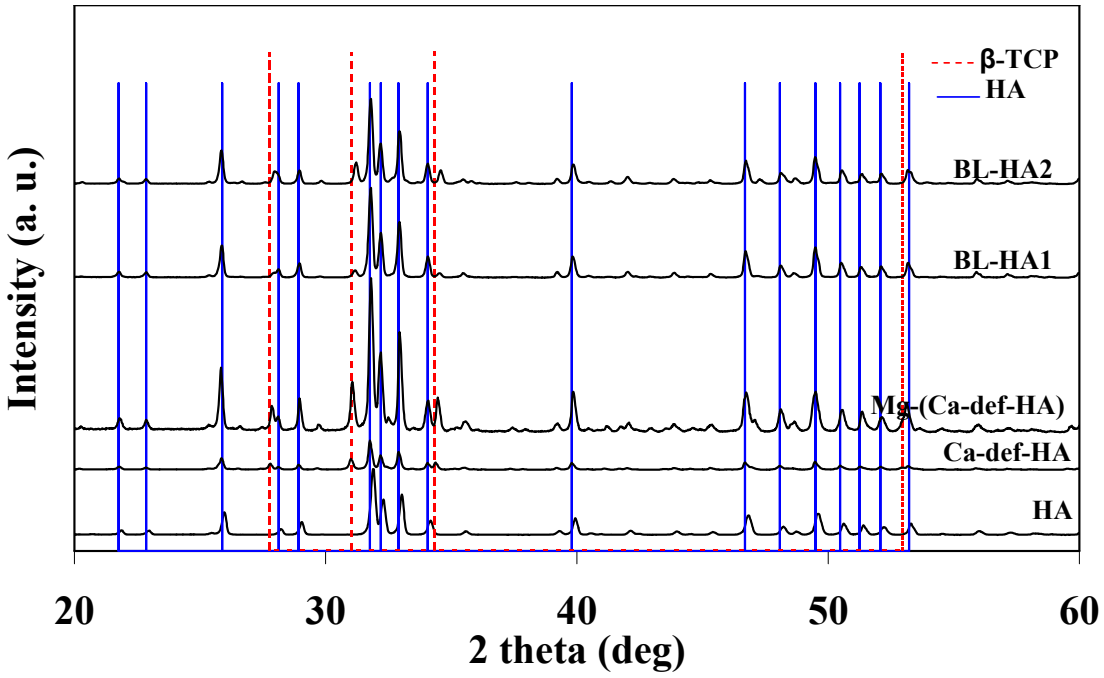

Figure 1. X-ray diffraction patterns for the powders calcined at 1150ºC (Ca-def-HA) and at 1250ºC (HA, Mg-(Ca-def-HA), BL-HA1 and BL-HA2).

The proportions of each phase as determined by Rietveld refinement are given in Table 2. The reason to limit the calcination temperature to 1150ºC for the Ca-def-HA was to avoid the phase transformation of β-TCP into α-TCP, which degrades the mechanical properties.[44-46] It has been shown that the incorporation of Mg into the lattice of β-TCP could significantly improve its thermal stability up to temperatures of about 1350ºC.[47]

Zeta potential

In order to obtain information about the effects of the dispersant on the solid/liquid interface potential of the powder particles, measurements of zeta potential (ZP) as a function of pH were performed for all the calcium phosphate powders in the presence and in the absence of Targon 1128.

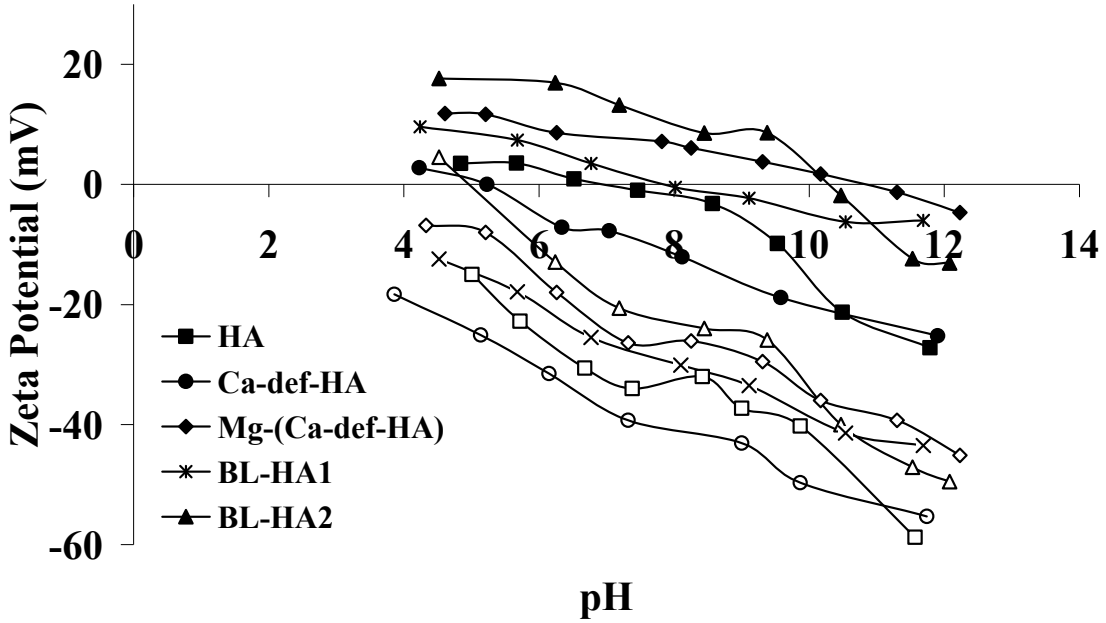

Figure 2. Zeta potential of the powders calcined at 1100ºC in absence (full bullets) and in the presence of Targon 1128 (open bullets).

Table 2. Rietveld quantification of phase compositions for HA, Ca-def-HA, Mg-(Ca-def-HA), BL-HA1 and BL-HA2 after calcination at different temperatures.

Sample code	Sintering Temperature (°C)	Wt. % of composition determined by Rietveld quantification		
		HA	β-TCP	α-TCP
HA	1100	100	-	-
	1250	100	-	-
	1300	100	-	-
	1350	100	-	-
	1400	94.38	-	5.62
Ca-def-HA	1100	64.3	35.7	-
	1150	68.6	31.4	-
	1250	69.7	9.5	20.7
	1300	64.7	2.4	32.9
Mg-(Ca-def-HA)	1100	84.15	15.85	-
	1250	72.83	27.17	-
	1300	76.59	23.41	-
	1350	73.61	5.95	20.44
	1400	70.82	-	29.28
BL-HA1	1100	91.94	8.06	-
	1250	91.83	8.17	-
	1300	89.77	10.23	-
	1350	88.94	6.36	4.70
	1400	87.14	-	12.86
BL-HA2	1100	77.87	22.13	-
	1250	77.67	22.33	-
	1300	76.09	23.91	-
	1350	70.51	29.49	-
	1400	70.54	29.46	-

The results presented in Fig. 2 show that in absence of dispersant the apparent isoelectric point (IEP) of the calcium phosphate particles is affected by the composition (Table 1), with the Ca/P ratio or the incorporated ions playing some roles. HA has an IEP at around 7, while the calcium deficient apatite, Ca-def-HA, presents a lower value of IEP (around 5). The incorporation of Mg into the lattice (Mg-(Ca-def-HA)) has caused a significant shifted of the IEP to pH 11, which can be attributed to the basic nature of Mg-containing oxide materials.[48] The biological–like hydroxyapatites, BL-HA1 and BL-HA2, exhibit values of IEP of about 8 and 10.5, respectively.

The addition of 0.5 wt.% of Targon 1128 as dispersing agent caused significant shifts of the entire electrophoresis curves towards the acidic region and more negative ZP values. The observed shifts attest the anionic nature of the polyelectrolyte ions, confirming the occurrence of their specific adsorption onto the surface of calcium phosphate particles. These data also shows that Targon 1128 has a strong ability to act as a surface charge modifier of the dispersed calcium phosphates powders.

Rheological characterization

The equilibrium shear stress *versus* shear rate curves for suspensions containing 40 vol.% solids, and different added amounts of dispersant, and 60 vol.% solids with the optimized doses of dispersant for each CaP powder studied are shown in Figs. 3 to 5.

The flow curves of suspensions containing 40 vol.% solids in the presence of 0.4 wt.% Dolapix CE 64 (D) confirmed the less suitability of this dispersant to stabilize the CaP suspensions. Deagglomeration was conducted up to achieving a suitable flowing behaviour. Different CaP powders required different milling periods for a good dispersion, with the Ca-def-HA being the easiest one to be deagglomerated and the Mg-(Ca-def-HA) powder the most difficult one (Fig. 5). It can be seen that all the suspensions present a shear-thickening behaviour, which becomes more pronounced with increasing solids loading (Fig. 4). The shear-thickening characteristics are attributed to agglomeration of the CaP particles upon calcination. The milling/deagglomeration procedure used enabled the preparation of suspensions with higher solids loading, but the shear-thickening behaviour of suspensions still remained, meaning that particle agglomerates have not been completely destroyed. From the figures presented, it is possible to infer that the amount of dispersant required for a good dispersion of the calcium phosphate powders strongly depends on the surface charge properties of the particles, especially when the solids loading increases from 40 to 60

vol.%. At a moderate solids loading (40 vol.%) the lowest shear stress values required for flowing are observed for 0.2 wt.% of Targon for all the powders, except for HA that showed a better dispersion for 0.1 wt.% dispersant (Figs. 3 and 4). However, the dispersing of powders becomes more and more critical with increasing solids volume fraction due to specific surface charge characteristics of the powder particles. The achievement of solids loading as high as 60 vol.% for CaP powders has never been reported so far unless by the present authors.[16] At this solids loading, some compositional differences between the powders have influenced their flowing properties, demanding higher optimal dispersant doses. These were the cases of Ca-def-HA and Mg-(Ca-def-HA) powders that required 0.4 wt.% and 1.5 wt.% of dispersant for an optimal dispersion (Fig. 5). The significantly higher amount of dispersant in the case of Mg-(Ca-def-HA) powder is in good agreement with the basic nature of Mg-containing oxide materials as shown by the electrophoretic results (Fig. 2). Concerning the biological-like hydroxyapatites, BL-HA1 and BL-HA2, their behaviour do not differ significantly (Figs. 4 and 5) despite their somewhat different surface charge characteristics. In both cases, a suitable dispersion was achieved for an added amount of 0.2 wt.% Targon 1128 after deagglomeration for 1 h.

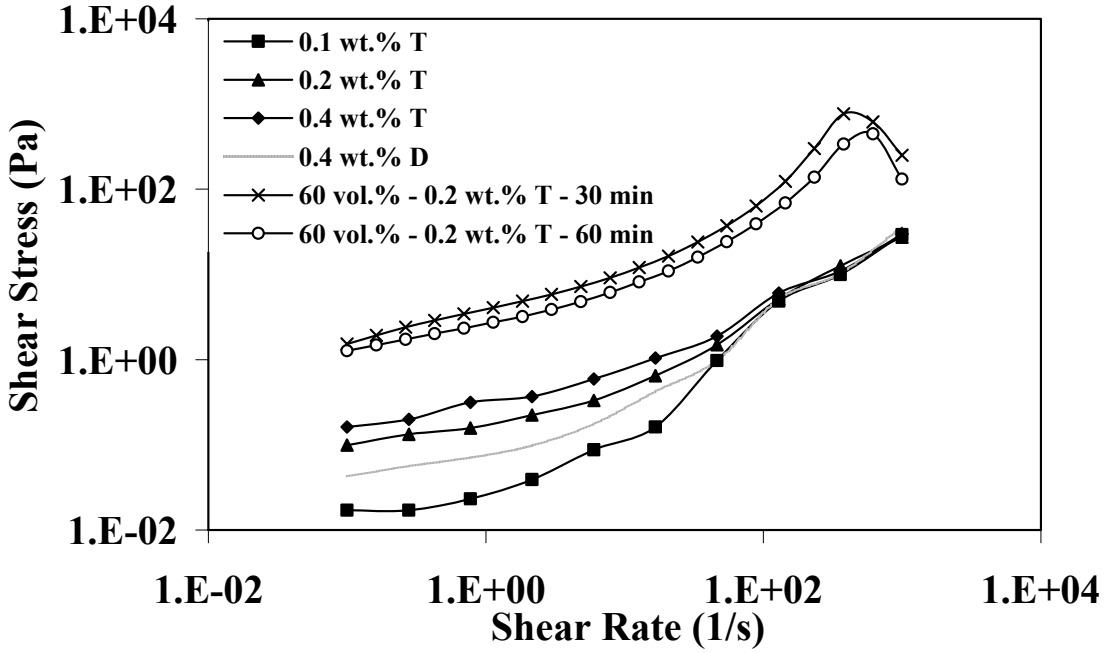

Figure 3. Equilibrium shear stress *versus* shear rate curves for the HA suspensions with 40 vol.% solids in the presence of different added amounts of dispersant and with 60 vol.% solids milled for different time periods.

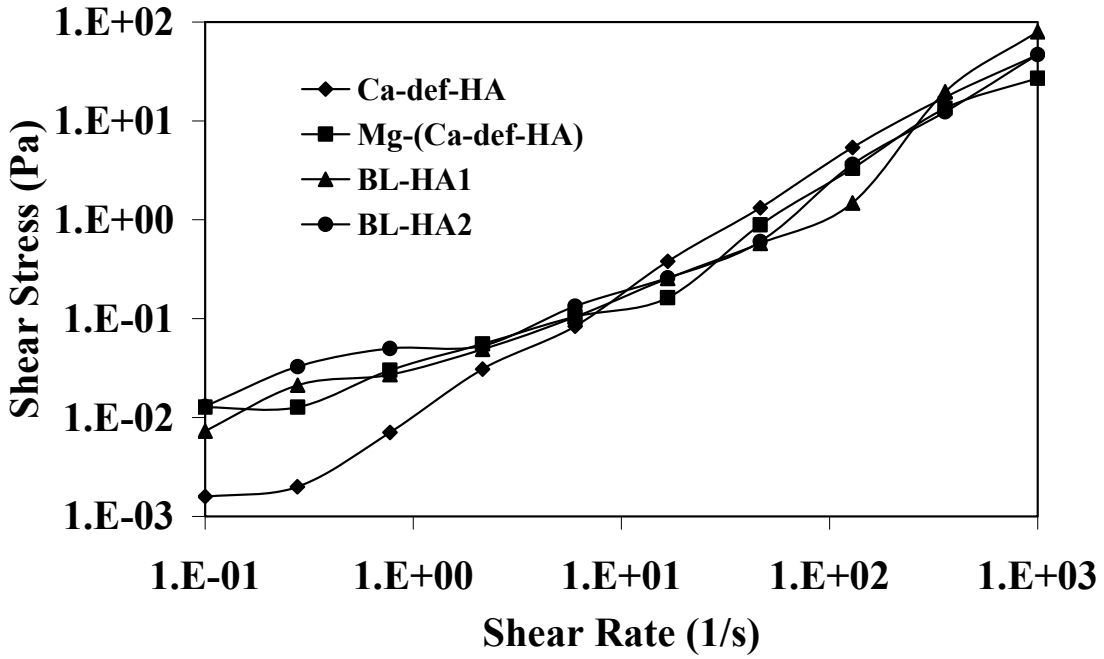

Figure 4. Equilibrium shear stress *versus* shear rate curves for the Ca-def-HA, Mg-(Ca-def-HA), BL-HA1 and BL-HA2 suspensions with 40 vol.% solids in the presence of 0.2 wt.% of dispersant, Targon 1128.

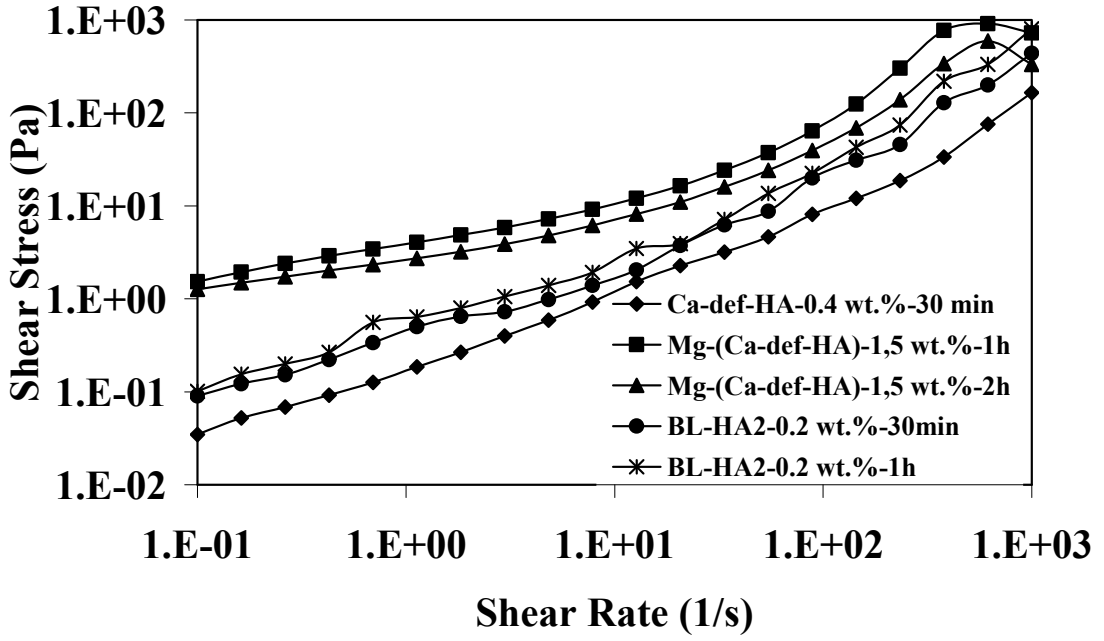

Figure 5. Equilibrium shear stress *versus* shear rate curves for the Ca-def-HA, Mg-(Ca-def-HA) and BL-HA2 suspensions with 60 vol.% solids in the presence of the optimal amounts of dispersant, after milling for different time periods.

Characterization of the sintered samples

The evolution of density, flexural strength and Vickers hardness with the sintering temperature for the different compositions studied is plotted in Fig. 6 and Fig. 7 and presented in Table 3, respectively. Fig. 8 shows the micrographs of the CaP samples sintered at 1150ºC, for the Ca-def-HA, and at 1250ºC for the other compositions. Fig. 9 shows the Weibull plot of cumulative failure probability *vs.* the logarithm of applied bending stress for samples sintered at different temperatures, at which the different compositions exhibited the maximum values of flexural strength, while Table 4 summarises. It can be seen that the noticeable increases in density and hardness of the Ca-def-HA with sintering temperature increasing from 1150º to 1250ºC were accompanied by a significant decrease of flexural strength and a concomitant decrease of porosity [Fig. 8 (a) and (b)]. These apparently contradictory results can be explained by the partial transformation of β-TCP to α-TCP,[45-47] as shown in Table 2. It has been shown that this phase transformation is accompanied by a declining shrinkage rate and an expansion of sample volume.[45-47] This expansion of TCP during sintering process causes micro-cracks in the phase-transformed TCP that reduce the mechanical strength of TCP ceramics and make β-phase-containing TCP ceramics unsuitable for surgical implant applications that require improved mechanical strength, explaining the results observed in Fig. 7. Densification of the Ca-def-HA samples did not progress beyond 1250ºC due to the hindering effect of the β-TCP to α-TCP phase transformation.

The density as well as the flexural strength of HA reached maximum values at 1250ºC, with the sintered microstructure showing only small pores [Fig. 8 (c)]. Beyond this temperature, the density is almost unchanged, but the mechanical properties tend to degrade due to a coarsening effect of the microstructure (not shown). These trends are different from those shown by the Mg-containing samples [Mg-(Ca-def-HA), BL-HA1 and BL-HA2] in which small increments of density with sintering temperature increasing have been accompanied by noticeable increases in flexural strength up to 1350ºC. Beyond this temperature, the mechanical properties of these samples tend to degrade again due to the partial transformation of β-TCP to α-TCP,[45-47] as shown in Table 2. Fig. 8 (d) to (f) confirms that all the Mg-(Ca-def-HA), BL-HA1 and BL-HA2 samples achieved a matrix with a high degree of densification, with some entrapped pores of regular size. The larger dimensions of these pores and of the grains in comparison to those observed for HA [Fig. 8 (b)] is the probable reason for the lower values of flexural strength presented by these samples, relative to HA.

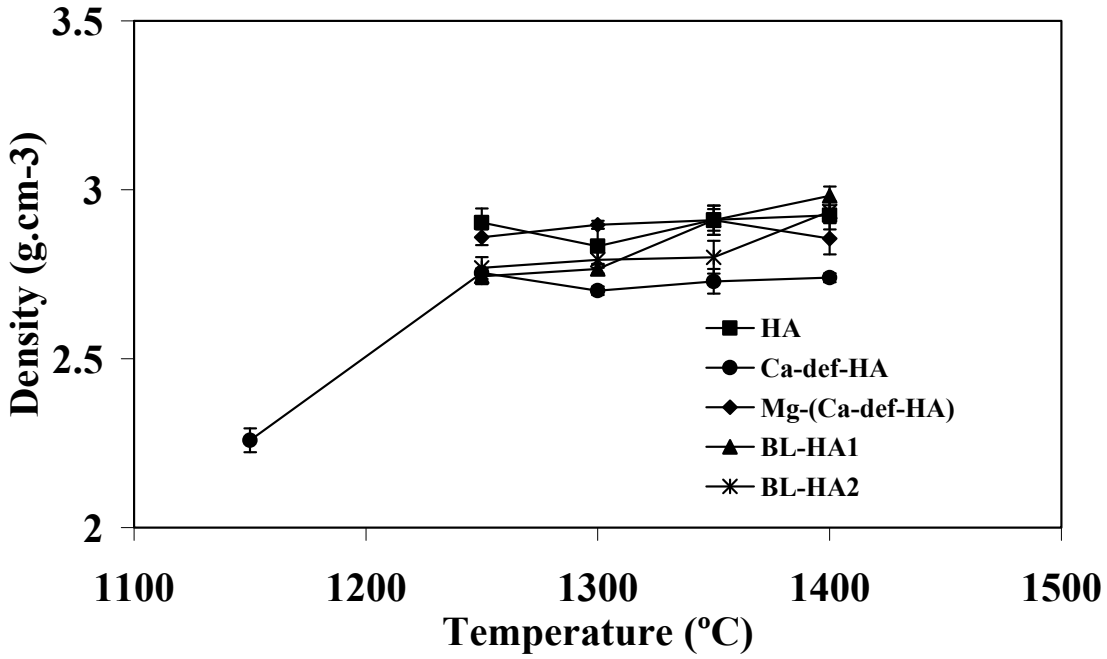

Figure 6. Evolution of density with the sintering temperature for the different compositions studied.

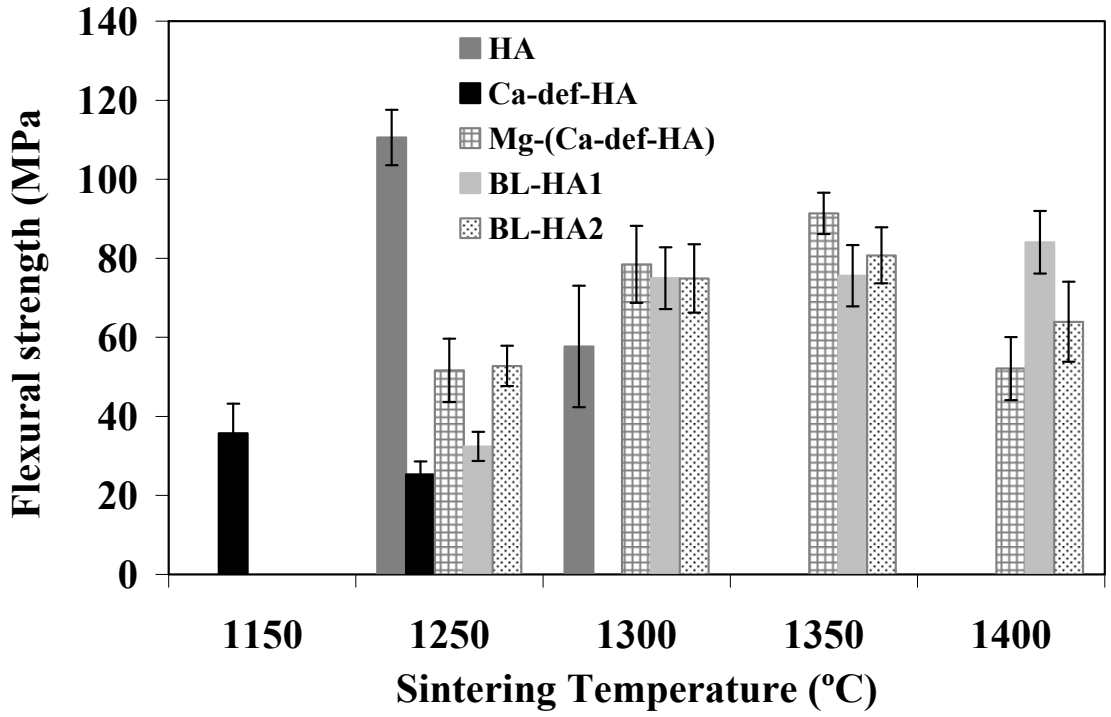

Figure 7. Evolution of flexural strength with the sintering temperature for the different compositions studied.

Table 3. Vickers hardness (HV5) of the sintered bars at different temperatures.

Temperature (ºC)	HA	Ca-def-HA	Mg-(Ca-def-HA)	BL-HA1	BL-HA2
1150	-	123.10 ± 4.99	-	-	-
1250	383.52 ± 10.48	223.43 ± 4.98	309.24 ± 6.26	224.20 ± 5.91	173.94 ± 7.09
1300	405.69 ± 5.93	259.68 ± 5.61	362.04 ± 8.55	337.89 ± 6.31	304.00 ± 7.21
1350	415.91 ± 7.59	290.93 ± 5.46	357.20 ± 10.15	388.39 ± 5.97	405.63 ± 7.02
1400	452.17 ± 6.08	298.45 ± 4.97	343.56 ± 7.74	414.65 ± 8.91	376.21 ± 8.18

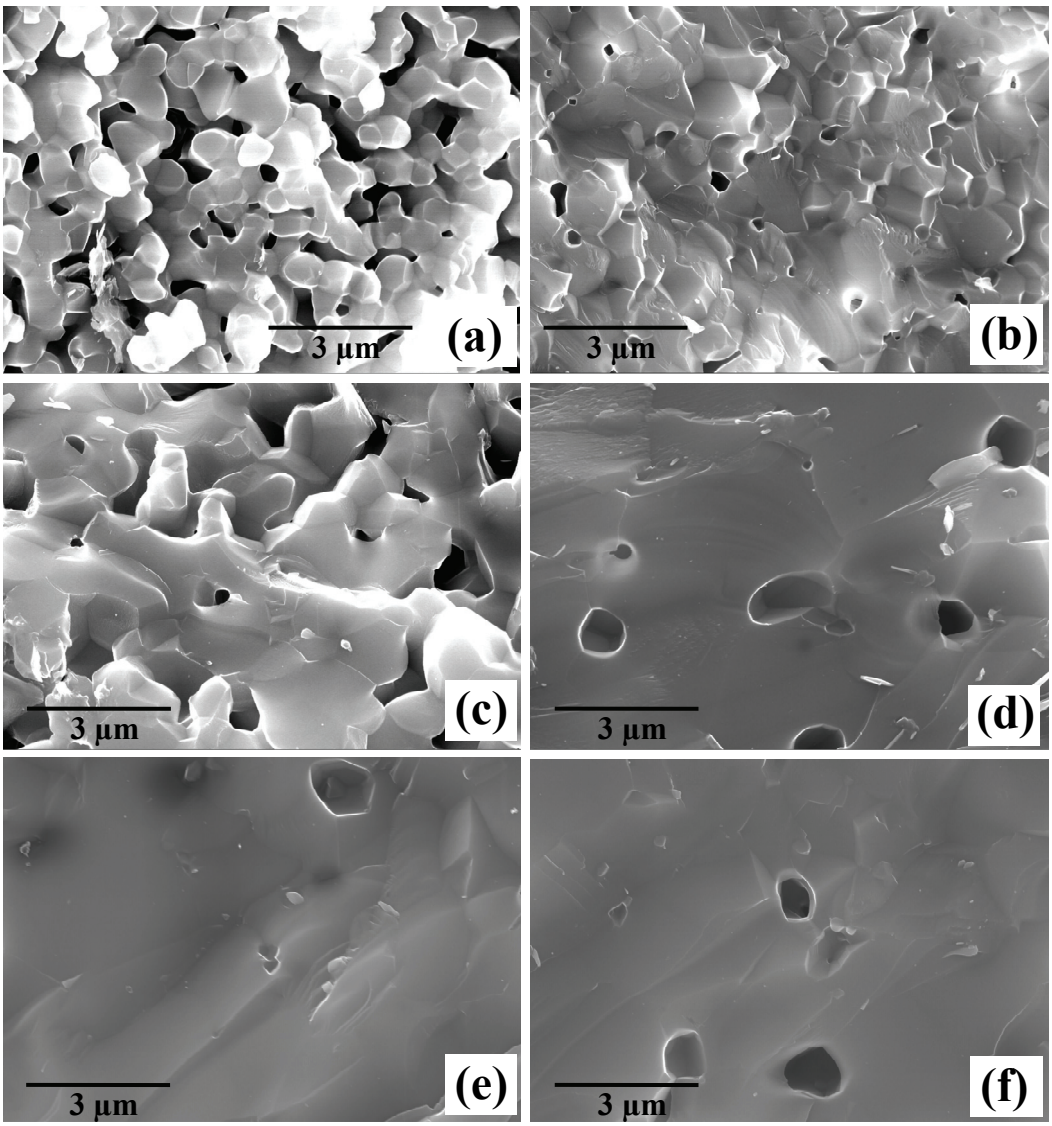

Figure 8. Micrographs of the calcium phosphate samples sintered at 1150ºC: (a) (Ca-def-HA) and at 1250ºC [(b) HA; (c) Ca-def-HA; (d) Mg-(Ca-def-HA); (e) BL-HA1; (f) BL-HA2].

Except for the Ca-def-HA composition, the data on flexural strength and hardness are consistent with the measured sintered density values and the microstructural features. It can be also concluded that the Mg-containing compositions exhibit an improved thermal stability, i.e., the formed β-TCP phase only transforms into the high temperature stable α-TCP polymorph at temperatures ≥ 1350ºC.[45-47,49] The improved thermal stability of Mg-containing compositions makes them attractive for coating implants by plasma spraying. The biological-like hydroxyapatites, BL-HA1 and BL-HA2, suggest that the incorporation of several ions in the structure has a beneficial effect on mechanical properties of the samples sintered at higher temperatures.[49]

The steeper the slopes of the curves of probability of failure *vs.* the logarithm of flexural strength are, the larger will be the *Weibull moduli* and, as a consequence, the higher will be mechanical reliability of the samples.

Fig. 9 and Table 4 shown that the specimens made of Ca-def-HA are the less reliable ones (m = 5.52), which are according to the highest porosity fraction and to the irregular pore sizes observed in Fig. 8 (a). Although the specimens of stoichiometric HA exhibit the highest average bending strength values (Fig. 7) due to the finest pores seen in the microstructure, they are not the most mechanically reliable ones (m = 20.71), probably because of a less regular pore size distribution [Fig. 8 (b)]. The specimens made of BL-HA2 showed a similar reliability as those of HA (m = 20.85), but the average bending strength is lower (Fig. 7).

Table 4. Weibull modulus of the samples sintered at different temperatures.

Sample	Sintering Temperature (ºC)	Weibull modulus
HA	1250ºC	20.71
Ca-def-HA	1150ºC	5.52
Mg-(Ca-def-HA)	1350ºC	27.98
BL-HA1	1350ºC	14.58
BL-HA2	1350ºC	20.85

The samples made of Mg-(Ca-def-HA) showed the lowest variability of bending strength values (m = 27.98), enabling a good predictability of the probability of failure/survival of the bioceramics. This finding may be due to the regular pore size and shape observed in the fracture surface of the specimens and to the high degree of densification of the matrix [Fig. 8 (d)] and to the improved thermal stability conferred by the Mg-doping. The beneficial effect of Mg-substitution in biological-like hydroxyapatites, BL-HA1 and BL-HA2, is also reflected in their relatively high values

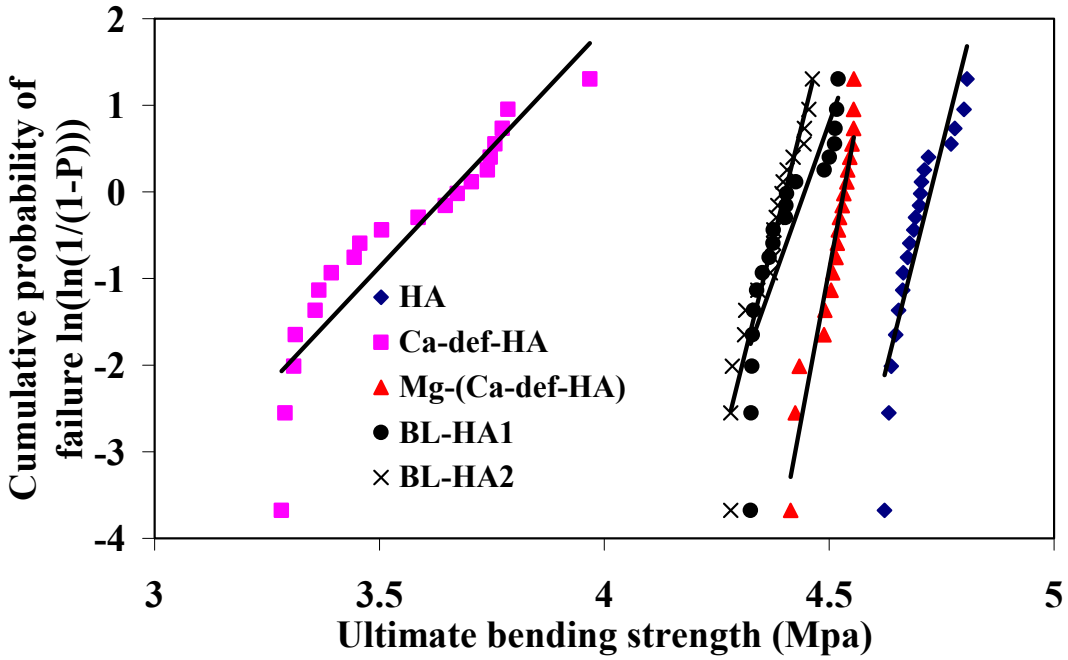

Figure 9. Curves of probability of failure *vs.* ultimate bending strength.

of *Weibull moduli* (Table 4). These results also suggests that very strong bioceramics could be prepared from stoichiometric HA or from Mg-doped calcium phosphates using a colloidal processing approach to obtain homogeneous green bodies followed by sintering at suitable temperatures. The reliability of the as obtained bioceramics is significantly higher in comparison to the values that have been reported for hydroxiapatite and hydroxyapatite-zirconia composites[49] or for dentine.[50]

Conclusions

The present work has shown that high concentrated (60 vol.% solids) suspensions of calcium phosphate powders could be prepared in the presence of a very efficient anionic

dispersant. The required amount of dispersant for an optimal dispersion was shown to be strongly dependent on the CaP composition, increasing from 0.2 wt.% for HA and for biological-like hydroxyapatites to 1.5 wt.% in the case of Mg-(Ca-def-HA) composition. Freeze-dried granules could easily be prepared from the suspensions with small added amounts of suitable processing additives (binder and plasticizer) and used to consolidate homogeneous green bodies by dry pressing. Upon sintering at 1250ºC (stoichiometric HA), or at 1350ºC (Mg-containing compositions), strong and high reliable monophasic (HA) and biphasic (HA + β-TCP) bioceramics could be obtained, attesting the benefits of colloidal processing for the ultimate material properties.

References

1. de Groot K. Ceramics of calcium phosphates: preparation and properties. In Bioceramics of calcium phosphate, Boca Raton: CRC Press 1983; pp100-14.
2. Hench LL. Bioceramics: from concept to clinic. J Am Ceram Soc 1991;74[7]:1487-510.
3. Jarcho M. Calcium phosphate ceramics as hard tissue prosthetics. Clin Orthop 1981;157:259-78.
4. Daculsi G, Bouler JM & Legeros RZ. Adaptive crystal formation: in normal and pathological calcifcation, in synthetic calcium phosphate and related biomaterials. Int Rev Cytology 1996;172:129-91.
5. Daculsi G. Biphasic calcium phosphate concept applied to artificial bone, implant coating and injectable bone substitute. Biomaterials 1998;19:1473-1478.
6. Suchanek W & Yoshimura M. Processing and properties of hydroxyapatite-based biomaterials for use as hard tissue replacement implants. J Mater Res 1998;13[1]:94-117.
7. de With G, van Dijk HJA, Hattu N & Prijs K. Preparation, microstructure and mechanical properties of dense polycrystalline hydroxy apatite. J Mater Sci 1981;16:1592-98.
8. Premechandran RS & Malghan SG. Dispersion characteristics of ceramic powders in the application of cationic and anionic polyelectrolytes. Powder Technol 1994;79[1]:53-60.

9. Alford NM, Birchall JD & Kendall K. High-strength ceramics through colloidal control to remove defects. Nature 1987;330:51-53.

10. Misra DN. Adsorption of potassium N-phenylglycinate on hydroxyapatite: role of solvents and ionic charge. Colloids Surf A: Physicochem Eng Aspects 1996;108: 277-85.

11. Kandori K, Saito M, Saito H, Yasukawa A & Ishikawa T. Adsorption of protein on non-stoichiometric calcium—strontium hydroxyapatite. Colloids Surf A: Physicochem Eng Aspects 1995;94[2-3]:225-230.

12. Shimabayashi S, Uno T & Nakagaki M. Formation of a surface complex between polymer and surfactant and its effect on the dispersion of solid particles. Colloids Surf A: Physicochem Eng Aspects 1997;123–124:283-295.

13. Rodríguez-Lorenzo LM, Vallet-Regí M & Ferreira JMF. Colloidal processing of hydroxyapatite. Biomaterials 2001;22[13]:1847-1852.

14. Padilla S, García-Carrodeguas R & Vallet-Regí M. Hydroxyapatite suspensions as precursors of pieces obtained by gelcasting method. J Eur Ceram Soc 2004;24 [8]:2223-2232.

15. Misra DN. Adsorption of Polyacrylic Acids and Their Sodium Salts on Hydroxyapatite: Effect of Relative Molar Mass. J Colloid Interface Sci 1996;181 [1]:289-296.

16. Lemos AF, Santos JD & Ferreira JMF. Influence of characteristics of the starting hydroxyapatite powders and of deagglomeration procedure, on rheological behaviour of HA suspensions. Materials Science Forum 2004;455-456:361-365.

17. LeGeros RZ. Calcium phosphates in oral biology and medicine. Karger AG Publishers, Switerland, Basel 1991.

18. Rey C. Calcium phosphates for medical applications. Kluwer Academic Publishers, Boston 1998; 217-239.

19. Elliott JC. Structure and chemistry of the apatites and other calcium orthophosphates. Elsevier, Amsterdam 1994.

20. Itoh R & Suyama Y. Sodium excretion in relation to calcium and hydroxyproline excretion in a healthy Japanese population. Am J Clin Nutr 1996;63[5]:735-740.

21. Ginty F, Flynm A & Cashman KD. The effect of dietary sodium intake on biochemical markers of bone metabolism in young women. Br J Nutr 1998;79[4]:343-350.

22. Bigi A, Foresti E, Gregoriani R, Ripamonti A, Roveri N, & Shah JS. The Role of Magnesium on the Structure of Biological Apatites. Calcif Tissue Int 1992;50:439-444.

23. Wiesmann HP, Plate U, Zierold K & Hohling HJ. Potassium is involved in apatite biomineralization. J Dent Res 1998;77[8]:1654-1657.

24. Cate JMT & Featherstone JDB. Mechanistic aspects of the interactions between fluoride and dental enamel. Crit Rev Oral Biol Med 1991;2[3]:283-296.

25. Caverzasio J, Palmer G & Bonjour JP. Fluoride: Mode of Action. Bone 1998;22[6]:585-589.

26. Schlesinger PH, Blair HC, Teitalbaum SL & Edwards JC. Characterization of the Osteoclast Ruffled Border Chloride Channel and Its Role in Bone Resorption. J Biol Chem 1997;272[30]:18636-18643.

27. Neuman WF & Neuman MW. The chemical dynamics of bone mineral, University of Chicago Press, Chicago 1958.

28. Yang, Z, Jiang Y, Yu L, Li F, Sun S & Hou T. Preparation and characterization of magnesium doped hydroxyapatite–gelatin nanocomposite. J Mater Chem 2005;15:1807-1811.

29. Kannan S, Lemos IAF, Rocha JHG & Ferreira JMF. Synthesis and characterization of magnesium substituted biphasic mixtures of controlled hydroxyapatite/β-tricalcium phosphate ratios. J Solid State Chem 2005;178[10]:3190-3196.

30. Suchanek WL, Byrappa K, Shuk P, Riman RE, Janas VF & TenHuisen KS- Preparation of magnesium-substituted hydroxyapatite powders by the mechanochemical–hydrothermal method. Biomaterials 2004;25[19]:4647-4657.

31. Rodriguez-Lorenzo LM, Hart JN & Gross KA. Influence of fluorine in the synthesis of apatites. Synthesis of solid solutions of hydroxy-fluorapatite. Biomaterials 2003;24[21]:3777-3785.

32. Kannan S, Ventura JM & Ferreira JMF. In Situ Formation and Characterization of Fluorine-Substituted Biphasic Calcium Phosphate Ceramics of Varied F-HAP/β-TCP Ratios. Chem Mater 2005;17[12];3065-3068.

33. Gross KA & Rodriguez-Lorenzo LM. Sintered hydroxyfluorapatites. Part I: Sintering ability of precipitated solid solution powders. Biomaterials 2004;25[7-8]:1375-1384.

34. Lin FH, Liao CJ, Chen KS & Sun JS. Preparation of high-temperature stabilized *β*-tricalcium phosphate by heating deficient hydroxyapatite with $Na_4P_2O_7 \cdot 10H_2O$ addition. Biomaterials 1998;18[11-12]:1101-1107.

35. Suchanek W, Yashima M, Kakihana M & Yoshimura M. Hydroxyapatite ceramics with selected sintering additives. Biomaterials 1997;18[13]:923-933.

36. Yanagisawa K, Rendon-Angeles JC, Ishizawa N & Oishi S. Topotaxial replacement of chlorapatite by hydroxyapatite during hydrothermal ion exchange. Amer Mineral 1999;84:1861-1869.

37. Bertoni E, Bigi A, Cojazzi G, Gandolfi M, Panzavolta S & Roveri N. Nanocrystals of magnesium and fluoride substituted hydroxyapatite. J Inorg Biochem 1998;72[1-2]:29-35.

38. Mayer I, Schlam R & Featherstone JDB. Magnesium-containing carbonate apatites. J Inorg Biochem 1997;66[1]:1-6.

39. De Maeyer EAP, Verbeeck RMH, Naessens DE. Stoichiometry of sodium(+)- and carbonate-containing apatites obtained by hydrolysis of monetite. Inorg Chem; 1993;32[25]:5709-5714.

40. Yamasaki Y, Yoshida Y, Okazaki M, Shimazu A, Uchida T, Kubo T, Akagawa Y, Hamada Y, Takahashi J & Matsuura N. Synthesis of functionally graded $MgCO_3$ apatite accelerating osteoblast adhesion. J Biomed Mater Res 2002;62[1]:99-105.

41. Cazalbou S, Combes C, Eichert D & Rey C. Adaptative physico-chemistry of bio-related calcium phosphates. J Mater Chem 2004;14[14]:2148-2153.

42. Kannan S, Lemos AF & Ferreira JMF. Synthesis and Mechanical Performance of Biological-like Hydroxyapatites. Chem Mater 2006;18[8]:2181-2186.

43. Lorenzo LMR. PhD Thesis. Síntesis, procesado y propriedades de cerámicas de fosfato de calcio con interés clínico. Madrid,1999.

44. Ryu H, Youn H, Hong KS, Chang B, Lee C & Chung S. An improvement in sintering property of β-tricalcium phosphate by addition of calcium pyrophosphate. Biomaterials 2002;23[3]:909.

45. Itatani K, Nishioka T, Seike S, Howell FS, Kishioka A & Kinishita M. Sinterability of β-Calcium Orthophosphate Powder Prepared by Spray-Pyrolysis. J Am Ceram Soc 1994;77[3]:801.

46. Famery R & Richard PB. Preparation of α- and β-tricalcium phosphate ceramics, with and without magnesium addition. Ceram Int 1994;20[5]:327.

47. Kannan S, Rocha JHG & Ferreira JMF. Synthesis and thermal stability of Sodium, Magnesium co-substituted Hydroxyapatites. J Mater Chem 2006;16[3]:286–291.

48. Parks GA. The Isoelectric Points of Solid Oxides, Solid Hydroxides, and Aqueous Hydroxo Complex Systems. Chem Rev 1965;65:177-98.

49. Bolboacă SD & Jäntschi L. Similarities Analysis on Hydroxyapatite-Zirconia Composites. Leonardo Journal of Sciences ISSN 2007;1583-0233[11]:153-164.

50. Staninec M, Marshall GW, Hilton JF, Pashley DH, Gansky SA, Marshall SJ & Kinney JH. Ultimate Tensile Strength of Dentin: Evidence for a Damage Mechanics Approach to Dentin Failure. J Biomed Mater Res (Appl Biomater) 2002;63:342–345.

Chapter 4

Design of porous calcium phosphate scaffolds for different orthopaedic applications

Alexandra F. Lemos[a,b,c] and José M. F. Ferreira[a]

[a] Department of Ceramics and Glass Engineering, CICECO, University of Aveiro, 3810-193 Aveiro, Portugal

[b] Faculdade de Engenharia da Universidade do Porto (FEUP), Rua Dr. Roberto Frias, 4200, Porto Codex, Portugal

[c] INEB–Lab. Biomateriais, R. do Campo Alegre, 823, 4150-180 Porto, Portugal.

Abstract

The most significant demand for biomaterials has emerged from the need to provide clinical solutions for a large number of patients in a great variety of situations. Calcium phosphates find various applications in the orthopedic field, namely, in replacing and regenerating damage parts of hard tissues, owing to their closest similarity to the mineral component of bone and their good biocompatibility and bone integration qualities.

This paper is inspired in the bone model and aims at designing porous calcium phosphate ceramics that can mimic the structure, the mineral composition and the properties of bone in order to develop reliable synthetic bone grafts for orthopedic applications. The paper makes a comprehensive review on the general aspects of bone model, biologically derived bone grafts, synthetic bone graft substitutes based especially on calcium phosphates, including powder synthesis methods and their composition *versus* properties. The state-of-the-art about the techniques used to produce porous materials, especially porous ceramic scaffolds is presented.

The present work takes advantage of the expertise of the research group developed in the fields of powder synthesis and on colloidal processing of ceramics, including new emerging consolidation techniques without liquid removal, to improve the performance of traditional consolidation methods and to explore the potentialities of the emerging techniques to design porous scaffolds and granular materials for orthopedic applications. The results obtained by exploring the complementarities of the old and the new consolidation methods are presented and discussed.

Introduction

Changing demographics, particularly a rapidly aging population, together with improved longevity, is having a direct impact on the number of musculoskeletal diseases. At the same time, changing lifestyle habits, such as smoking and poor nutrition with sports, are increasing the incidence of typically age-related diseases among the younger population. These trends are driving the demand for orthopedic biomaterials all over the world, being bone grafts often necessary to provide support, fill voids, and enhance biologic repair of skeletal defects. The ability to replace or augment diseased body parts totally or partially, has improved the quality and life span of millions of people over the quarter of a century.[1]

Designing synthetic materials to fulfill all the requirements in terms of composition, structure, mechanical properties, biological response, long-term function in the human physiological environment, etc., is a very challenging task. Hard tissue replacements with synthetic materials are better achieved by selecting the material with physical properties similar to those of natural tissue to be replaced.[2] Bioceramics based on CaP are often selected for applications in hard tissue regeneration, but the design of an interconnected porous structure with pore size and pore size distribution suitable to enable bone ingrowth and the circulation of blood and nutrients still remains a big challenge. To achieve this target, a good understanding of the bones structure that is intended to mimic is of paramount importance.

The bone model

General aspects

Bone is a composite material of organic and inorganic components. The mineral phase of bone comprises approximately 60 to 70% of the total dry bone weight while the remaining organic fraction is composed largely (85% to 90%) of the fibrous protein collagen.[3] It is the combination of mineral and protein fractions that yields the mechanical strength required for the skeletal support role which bone performs as a structural component of the body.[3] Bone mineral is involved in both biomechanical and metabolic functions of osseous tissue.[3,4] Besides giving structural stability to the skeleton, it provides the body fluids with inorganic ions to maintain the biologically required levels. It also acts as detoxifying depository to store ions unwanted in the organism (e.g. lead, strontium, etc.). Bone mineral compositions vary depending on

species, strain, type of bone, diet, etc.[5] However, according to Legros *et al.,*[6] its chemical composition can be represented approximately by a single chemical formula:

$$Ca_{8.3}\square_{.7}(PO_4)_{4.3}\ (HPO_4 \text{ and } CO_3)_{1.7}\ (2OH \text{ and } CO_3)_{0.15}\ \square_{1.7}$$

in which □ represents a vacancy. The amount of HPO_4^{2-} and CO_3^{2-} may vary considerably, however the sum of divalent ions is quite constant in most bone tissues.[5] Other ions are present in smaller quantities, such as Mg^{2+}, F^- and Cl^-. Due to cellular turnover, very small amounts of Na^+, K^+, ascorbic acid, citric acid, polysaccharides, among other substances, are also present.[7] Some specific heavy atoms may occasionally be found, such as Ba^{2+}, Sr^{2+}, Pb^{2+}, which show a preference for fixation precisely in bone tissues.

The amount of vacancies in cationic sites and in monovalent anionic sites is always very high and close to the maximum attainable for an apatitic structure. Although bone mineral is often described as an "hydroxyapatite" ($Ca_{10}(PO_4)_6OH_2$), it can be seen from the above formula that it contains very few OH^-.[5]

Bone seems lifeless but it is made up of a very alive, porous framework that is constantly being remodeled. The cells found in bone are of different types: osteoblasts, osteocytes, bone lining cells and osteoclasts, with the first three cell types being derived from mesenchymal-type cells called osteoprogenitor cells.[4] Bone tissue replaces itself through the action of osteoclasts that produce acids to dissolve (resorb) apatite and enzymes to break down collagen.[7] The resulting release of calcium and protein prompts other cells (osteoblasts), to lay down a new matrix that mineralizes, forming apatite and collagen.[7] In normal conditions bone density is maintained due to the dynamic equilibrium between the functions of osteoclasts and osteoblasts. If there is a change in this equilibrium, the resultant amount of bone formed might be reduced and bone disorders, such as osteoporosis, arise. In order to control bone remodeling, either increasing or decreasing it, bone cells produce growth factors such as morphogenetic proteins.

The initial stage of formation of bone mineral is extremely difficult to study, due to the tiny size of the crystals and their very high reactivity. The detailed chemical composition and microstructure of freshly deposited bone mineral, and how these properties change with bone maturation, have been studied intensively and still remain controversial. A key problem is whether the calcium phosphate phase, particularly in young bone, consists entirely of a poorly crystalline hydroxyapatite (HA), or contains

residual amounts of an initial precursor. Several hypotheses involving the existence of mineral precursors, such as amorphous calcium phosphate (ACP), dicalcium phosphate dihydrate or brushite (DCPD) and octacalcium phosphate (OCP) have been proposed, based on the study of calcium phosphate formation, *in vitro*.[8-12] However, despite isolated studies claiming the formation of one or the other of these phases, none of them has been reproducibly detected.[5] By the use of spectroscopic techniques, namely Fourier transform infrared (FT-IR) spectroscopy, and phosphorous-31 (31P) solid-state nuclear magnetic resonance (NMR) spectroscopy, it was possible to obtain information about the short-range order and crystal environment of specific ions in bone.[13-21] The existence of "non-apatitic" environments, different from those existing in pure well-crystallized apatites, which are specific to bone mineral crystals and freshly precipitated apatites in physiological conditions, were observed. Moreover, in early stages of bone formation, features such as a low carbonate and a high HPO_4^{2-} content are also characteristic.[6] During ageing, however, the amount of non-apatitic environments and of HPO_4^{2-} ions decrease, whereas the proportion of carbonate increases, and bone mineral evolves towards a regular carbonated apatite with a better crystallinity (maturation).[5]

Biologically Derived Bone Grafts

Bone graft is the second most common transplantation tissue, with blood being by far the commonest.[22,23] More than 500,000 bone grafting procedures are happening annually in the United States and 2.2 million worldwide in order to repair bone defects in orthopedics, neurosurgery and dentistry.[24,25] Additionally, the treatment of posttraumatic skeletal complications, such as delayed unions, nonunions, malunions, are challenging.[26] Bone grafting is usually required to stimulate bone-healing. Moreover, spinal fusions, filling defects following removal of bone tumors and several congenital diseases may require bone grafting. Several methods for reconstructing bone defects are available, namely, using autograft, allograft, dematerialized bone matrix, CaP, autologous bone marrow aspirates and bone morphogenetic proteins.

Osteogenesis, osteoinduction, and osteoconduction are the three essential elements of bone regeneration along with the final bonding between host bones and grafting material which is called osteointegration.

Osteoprogenitor cells living within the donor graft may survive during transplantation, having the potential to proliferate and differentiate to osteoblasts and eventually to osteocytes. These cells represent the ‘‘osteogenic’’ potential of the graft to provide

intercellular communication.[27] Although there are alternative views, the consensus of research indicates that the requisite pore size for bone ingrowth into porous implants is 100 to 500 μm, and the interconnections must be larger than 100 μm.[28]

Presently, the gold standard of bone grafting is harvesting autologous cortical and cancelous bone from iliac crest. All other forms of bone grafting have disadvantages compared to autograft and as such their use is suboptimal. However, technological evolution along with better understanding of bone-healing biology, have lead to the development of several bone graft substitutes that are currently available to the orthopedic surgeons.[29,30]

As mentioned before, autologous bone is the gold standard that all alternatives must meet or exceed. But autographs have significant limitations, including donor site morbidity, inadequate amount, and inappropriate form.[29,31,32] These limitations have prompted increasing interest in alternative bone grafts, designedly allografts. These may be cancellous, cortical, or a combination of both. Even if they are attractive sources, there are several problems encountered in using them, including the risk of disease transmission, immunogenicity,[33,34] loss of biologic and mechanical properties secondary to its processing, increased cost, and non-availability world-wide due to financial and religious concerns. Consequently, significant efforts are being made to develop ideal bone graft substitutes.

Synthetic Bone Graft Substitutes

Currently, a large number of bone-graft alternatives are commercially available for orthopedic use. They vary in composition, mechanism of action, and special characteristics. Although considerable advances have been made over the past decade towards developing synthetic bone substitutes to autografts and allografts, they only possess at most two of the four characteristics of an ideal bone graft material (osteointegration, osteoconduction). Ideally synthetic bone graft substitutes should be biocompatible, show minimal fibrotic reaction, undergo remodeling and support new bone formation. From a mechanical point of view, synthetic bone substitutes should have strength similar to that of the cortical/cancellous bone being replaced. This needs to be matched with a modulus of elasticity similar to that of bone in an attempt to prevent stress shielding, and adequate toughness to prevent fatigue fracture under cyclic loading. The disadvantages of synthetic materials in clinical settings include: low or unpredictable resorption, difficulty in handling (coral derived HA), and poor clinical

results with occasional inflammatory foreign body reaction (degradable polymers).[35-37] This means that materials with improved properties are required to overcome these complications.

Among several options for synthetic bone substitutes, scaffolds based on ceramics, glasses and glass ceramics have been used in dentistry and orthopedics since the 1980s.[38,39] Commonly the surgeon requires ceramic materials to be supplied in different forms such as dense blocks, porous solid pieces or granules. Ceramics are also of utmost importance when used as coatings of metallic implants to improve the attachment of the prosthesis to the host while stopping, or at least reducing, the release of metallic ions from the implant alloy to the living body due to the barrier created by the ceramic layer. Ceramic materials are often administrated in injectable forms in non invasive surgery applications. Calcium phosphate ceramics can also be used as substrates for tissue engineering because they are clearly the most biocompatible functional materials with a composition very similar to the natural hard tissues.

Ceramic materials used in reconstructive surgery can be classified in three large groups: bioinert, resorbable and bioactive. Bioinert ceramics have almost no influence in the surrounding living tissue, and their finest example is alumina. Resorbable ceramics, as the name implies, degrade upon implantation in the host. The resorbed material is replaced by endogenous tissues. The rate of degradation varies from material to material. Bioactive ceramics, by contrast, are capable of bonding with living osseous tissues; several CaP and certain compositions of glasses and ceramic glasses exhibit such feature. The chemical reactivity of ceramics can be attested by *in vitro* bioactivity tests in a simulated body fluid, or *in vivo* assays.

From a structural point of view, ceramic materials can be classified as crystalline solids, amorphous glasses, or amorphous solids with crystallization nuclei-glass-ceramics, which can in turn be considered as inert, bioactive or resorbable. This paper is focused on CaP bioceramics; therefore, it is important to firstly analyze the biological CaP as components of natural hard tissues (bones and teeth).

Calcium Phosphates

Calcium phosphate compounds are abundant in nature and in living systems. Different types of CaP phases play dominant and significant roles in biological systems, and find several clinical applications.[40-42] The chemical composition of the mineral constituents of bones is a very important starting point for synthesis of the HA-based biomaterials.

The inorganic phases present in the bones contain mostly Ca^{2+} and P, considerable amounts of Na^{+}, Mg^{2+}, K^{+}, also CO_3^{2-}, F^{-}, Cl^{-}, and H_2O. All these species, if applied in appropriate quantities, should be well tolerated as implants by the surrounding tissues. Hydroxyapatite, HA, is the calcium phosphate (CaP) phase mostly used for implantation purposes due to its similarity to the mineral component of bones. Its unit cell is arranged along the *c*-axis, justifying the preferred growth of crystals along the *c*-axis giving rise to needle-like morphology. HA is biocompatible, bioactive, osteoconductive, and directly bonds to bone tissues.

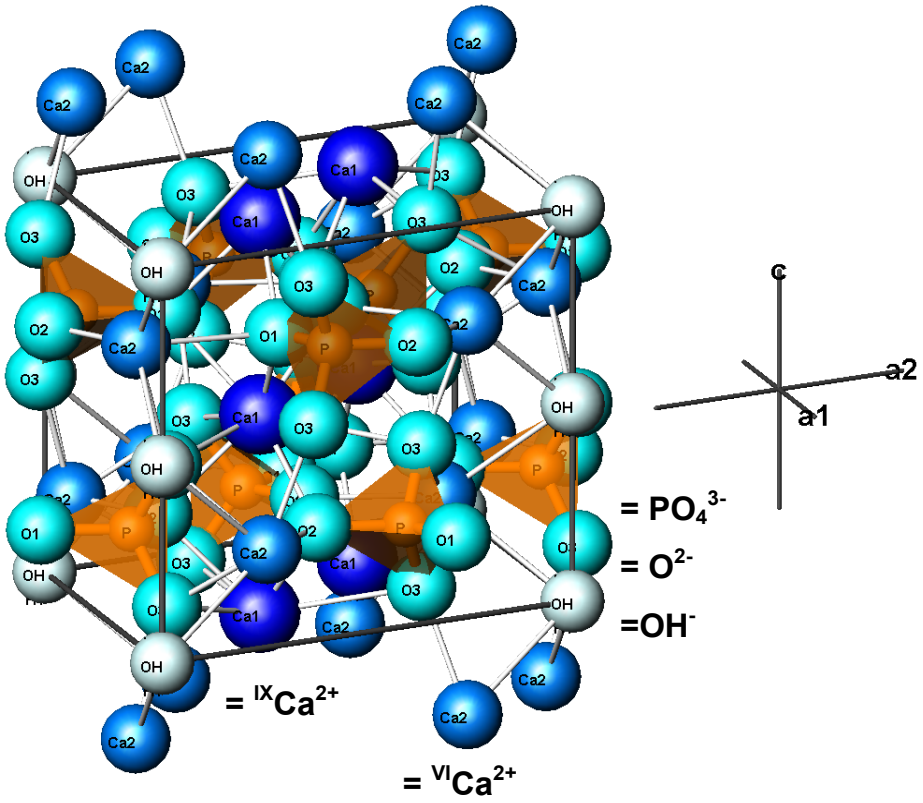

Figure 1a. Crystal structure of hydroxyapatite after Wilson *et al.*[43] projected perpendicular to *c*-axis.

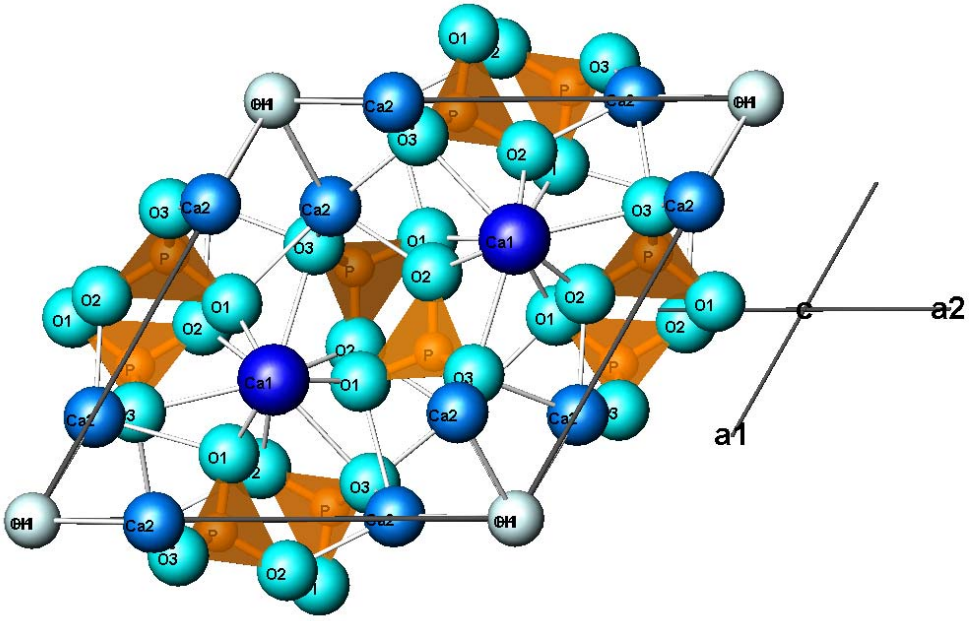

Figure 1b. Crystal structure of hydroxyapatite after Wilson *et al*.[43] projected on (001).

Among the wide range of available CaP, it is important to know the close relationship between the Ca/P ratio, acidity and solubility. For Ca/P < 1, both acidity and solubility are relatively high, and both parameters decrease substantially for Ca/P ratios close to 1.67, the stoichiometric ratio for HA.[44] Thus, the Ca/P ratio is a very useful parameter for scientists working in the field of CaP, since slight changes in Ca/P ratio can interfere in the calcium phosphate phase formed.

The lattice parameters of some of these CaP phases are quite similar, leading to overlapping of reflection maxima, which makes difficult, in some occasions, the adequate interpretation of the powder X-ray diffraction pattern. Therefore, a careful characterization by electron microdiffraction and high resolution electron transmission microscopy (HRTEM) is very useful to investigate small particles and mixtures of CaP. For instance, HA and β-tricalcium phosphate (β-TCP), often coexist in distinct proportions, depending on the synthesis conditions. Moreover, when HA is heated at 1050ºC it converts partially to β-TCP.[45]

Powder Synthesis Methods

The numerous potential applications of HA in biomedical fields stimulated the development of several synthesis techniques.[46,47] Wet methods involving aqueous solutions are among the most commonly used ones and can be accomplished by both by

simple precipitation[48,49] or hydrolysis of acidic calcium phosphate salts.[50-52] The synthesis of HA using wet methods requires special attention to control the crystallite size, morphology and structure through the Ca/P ratio and other experimental parameters. The substitution of phosphate ions PO_4^{3-} by hydrogen phosphate HPO_4^{2-} allows a continuous variation of the Ca/P atomic ratio between 1.5 and 1.67. This leads to calcium-deficient apatite, $Ca_{10-x}(PO_4)_{6-x}(HPO_4)_x(OH)_{2-x}$. Calcium-deficient apatite powders can be decomposed into mixtures of HA and β-TCP by thermal treatment above 700ºC. This allows a direct synthesis of biphasic calcium phosphate ceramics HA/TCP without the step of powder blending.[53]

Recently, emphasis has been put not only on the stoichiometry and crystal size and shape of synthetic HA, but also on controlling the state of agglomeration of the powder particles, since the synthetic powders will be further processed to produce ceramics or mixed polymers to produce biocomposites. Therefore, a number of novel processing routes have been developed for preparing fine HA powders, including sol–gel synthesis,[54,55] hydrothermal reactions,[56] emulsion and microemulsion synthesis,[57,58] coralline HA[59,60] and mechanochemical synthesis.[61-63] Other recent methods include hydrothermal or microwave conversion, and the Pechini method.

Composition versus Properties

Substituted Apatites

Biological apatites are non-stoichiometric, moving towards tissues formation, which is linked to an increase in crystallinity. These trends have a remarkable physiological meaning, since the younger, less crystalline tissue can develop and grow faster, while storing other elements that the body needs during its growth; this is due to the highly non-stoichiometric quality of HA, which caters for the substitutional inclusion of different amounts of several ions, such as Na^+, K^+, Mg^{2+}, Sr^{2+}, Cl^-, F, HPO_4^{2-}, etc.[59] Similarly, the synthetic HA has the ability to accept compositional variations incorporating a wide variety of ions in both cationic and anionic sublattices as schematized in Fig. 1 and Table 1, enhancing its bioactive behaviour.[59,64]

Table 1. Generic formulation of apatite minerals, and potential substitutions in the three sublattices.

$M_{10}(ZO_4)X_2$
M = Ca, Mg, Na, K, H, D, Sr, Ba, Cd, Pb, …
Z = P, CO_3, Si, V, As, S, Cr, B, …
X = OH, CO_3, BO_2, O, Cl, Br, F, …

Biphasic Calcium Phosphates

Biphasic calcium phosphate (BCP) ceramics have been developed to better control the processes of biomaterials resorption and bone substitution. HA is more stable than α- and β-TCP under physiological conditions, as it has a lower solubility and slower resorption kinetics. HA-based implants remain in the site of implantation for several years, but the same does not occurs with α- and β-TCP or with BCP.[41,65] Daculsi found an optimum balance of the more stable HA and more soluble TCP phases, enabling to gradually control the dissolution in the body, seeding new bone formation as it releases calcium (Ca^{2+}) and phosphate (PO_4^{3-}) ions into the biological medium.[66,67]

Some authors have defended the superior properties of the ‘‘directly’’ prepared BCP materials over those obtained by mixing two single phases.[68] Despite this fact, blending of different CaP is still often used,[69,70] although precipitation methods have been receiving preference for the synthesis of BCP,[71,72] as reviewed recently.[64]

Other synthesis routes include: solid state,[73] treatment of natural bone,[74] microwave,[75] combustion,[76] etc.

Implantable Products Based on Calcium Phosphate Ceramics

Several trade mark products based on BCP mixtures are commercially available: Triosite® (Zimmer, Rungis, France), MBCP® (Biomatlante, Nantes, France), Osteosynt® (Einco ltds, Belo-Horizonte, Brazil), etc. Calcium phosphates (HA, β-TCP, α-TCP or BCP), can be used for coating metallic implants, as bone cements, in the granular form for bone filling defects and bone augmentation, as dense implants or porous scaffolds, and integrated in biocomposites.[41,65,77]

Porous Scaffolds

The requirements for the porous scaffolds depend on the site of implantation, but generically include:

- Biodegradation rate comparable to the formation of new tissue;
- Sufficient mechanical stability;[41,65]
- Pore diameters larger than 100 μm to enable bone ingrowth.

Porous CaP ceramics have been widely applied as bone substitutes, since they allow the growth of natural tissue inside the pores, providing a mechanical interlock and leading to a firmer fixation of the implant materials.[78,79] Besides the requirement of pores larger than 100 μm in diameter, the pores must be interconnected to guarantee the supply and the circulation of the necessary nutrients through the ingrowth of fibrous tissue, vascular tissue and bone tissue.[78,80] Also necessary are smaller pores, which favor protein adsorption and adhesion of osteogenic cells. Thus, the pore size distribution of porous bioceramics should be bimodal.[81]

The classical way to fabricate porous HA ceramics (pore size of 100–600 μm) is sintering the HA powder with appropriate pore-creating additives (for example paraffin, naphthalene, or hydrogen peroxide) which evolve gases at elevated temperatures.[82] The use of substances that leave pores after burning out is other possible way to create porosity.[83-85] It is also worthy to mention that controlling the sinterability of the powders can give some room to obtain dense/ porous materials.[72]

Although controlling the porous structure of CaP scaffolds is a critical point, mimicking the structure of human bone is generally recognized as difficult, being the main shortcoming for spreading the use of this kind of synthetic bone grafts. Consequently, there is an increasing interest in developing porous HA-based ceramics with different but complementary purposes: restoration of vascularity and complete penetration of osseous tissue throughout the repaired site, or for applications such as scaffolds for tissue engineering, and systems for controlled delivery of drugs.

Building a foamy structure in a slurry has been proposed as a starting point to produce porous materials.[86,87] However, the consolidation of the foam and its transformation into a rigid network is the most critical step in the foaming methods, which cannot be achieved by using the traditional shaping techniques involving liquid removal. This transformation could be carried out by a new set of emerging "direct consolidation techniques", which are based on different setting mechanisms such as polymerisation reactions (*gel casting)*,[88] polycondensation reactions (*hydrolysis assisted solidification, HAS)*,[89] destabilisation of the suspension (*direct coagulation casting, DCC)*,[90] freezing (*quick set),*[91] or the gelling properties of starch,[83,92] methylcellulose[93] or proteins[94,95]

that occur on heating, or the gelation of other polysaccharides on cooling[96] to create a three-dimensional network. In these methods, the particulate structure of the ceramic slips is consolidated without powder compaction or liquid removal, thus preserving the homogeneity achieved in the slurry state.

Fabricating ceramic parts with precise sizes and shapes that match the implant sites is another concern. The combination of well-known methods like slip casting, foaming, starch consolidation and others, offer opportunities to tailor the porous structures according to the requirements of the site of implantation.[97] Following this approach, macroporous HA structures with pores larger than 100 μm were prepared by combining the foaming and starch consolidation methods.[83] The porous structure could be tailored according to the final application by varying the fraction of the foaming agents. Contrarily to the established knowledge, the structures obtained by the foaming method were open and the pores left by the burning out of starch granules or wax spheres offered further room to control the pore characteristics enhancing pore interconnectivity. Ceramic parts mimicking the complete bone structure were prepared by combining the foaming or the polymeric sponge methods for the trabecular part, with slip casting for cortical denser part wrapping the porous trabecular one.[83]

Several low-temperature methods have been used to fabricate HA-based porous scaffolds. Natural porous materials, like coral skeletons and cuttlefish bones made of $CaCO_3$, could be converted into HA under hydrothermal conditions with the microstructure undamaged,[73,74,98,99] or into fluorine substituted HA.[100]

One hour of hydrothermal treatment (HT) at 200ºC was enough to obtain predominantly HA. The monitoring of the crystallographic development of HA between 1 and 24 h of HT indicated that the transformation process was complete after 9 h.[98]

Fig. 2 shows the typically channelled microstructure of cuttlefish bone derived HA scaffolds. It was also shown that the channels follow winding pathways featuring interconnectivity.[98] Rocha *et al.* showed that this structure is preserved during sintering.[99]

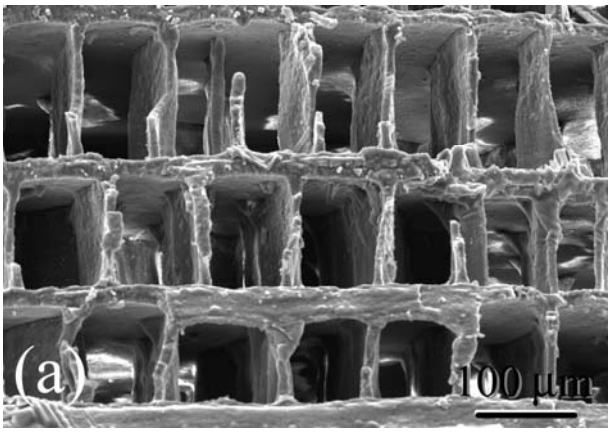

Figure 2. Typical porous microstructure of HA scaffolds obtained from hydrothermal transformation of cuttlefish bones.[98]

In orthopedic applications, porous CaP blocks that are usually cut by the surgeon to match the implant size. The cuttlefish bone derived HA scaffolds could be easily and rapidly machined into any shape as shown in Fig. 3.[99]

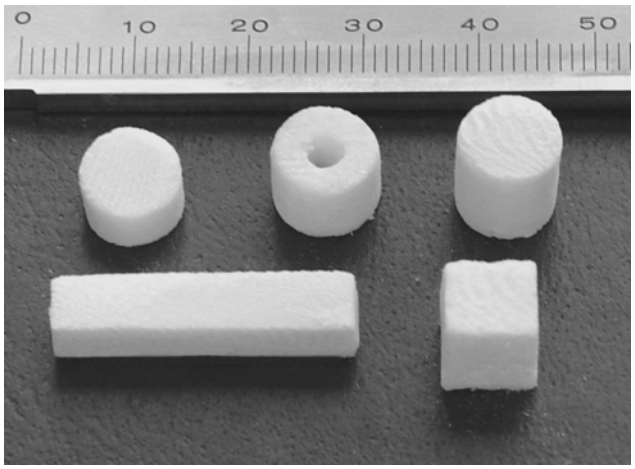

Figure 3. Machined cuttlefish bone derived porous HA scaffolds (scale in mm).[99]

Granular Materials

Industry offers several trade names for macroporous granular CaP materials, Interpore®, Pro Osteon® and Osteogen®, or for macro and microporosity, InBone G ®. Depending on microstructure, size distribution, and volume fraction of pores, granular materials find applications in dental, periodontal, oral/maxillofacial surgical procedures and orthopedics, including bone filling defects, alveolar ridge augmentation, maxillofacial reconstruction and drug delivery systems.[28,78,80] The morphology and microstructure of the granules dictate their behaviour in the body. Irregular morphology might cause

inflammatory reactions. So, rounded forms with smooth geometry are usually preferred for defect filling.[101]

Several procedures have been reported to prepare granulates, namely hydrothermal transformation of corals, crushing of sintered blocks, vibration and rolling synthetic powders with water, dripping into liquid nitrogen and drip casting.[102] More recently, new methods were developed, based on the liquids immiscibility effect,[103] and on the ionotropic gelation.[104,105] Lemos *et al.*[105] conclude that the method based in ionotropic gelation is suitable for the production of spherical porous HA granules with smooth surfaces.

Experimental Procedure

In the present work, synthetic calcium phosphate powders previously prepared and fully characterized were used.[106-109] After precipitation, the powders were heat treated at 1100ºC and milled to obtain an average particle size of about 1.5 μm. Well dispersed aqueous suspensions with solids loadings as high as 60-vol.% were prepared following a suitable deagglomeration procedure described elsewhere in the presence of a suitable amounts of an efficient dispersant, Targon 1128, for calcium phosphate powders.[108] The as prepared suspensions could then be used to consolidate simple or complex shaped ceramic products by slip casting and/or starch consolidation for obtaining microstructures resembling that of cortical bone. Designing of macroporous microstructures resembling that of trabecular bone was accomplished by suitably combining the microstructural capabilities of the foaming method or the polymeric sponge method, with the shaping capabilities of direct consolidation methods (starch consolidation, protein consolidation method and gel casting with polysaccharides).

Porous Scaffolds Prepared by the Polymeric Sponge Method

This method aims at replicating the structure of polymeric sponges and involves the impregnation of the sponges with a ceramic suspension with suitable rheological properties for preventing post-impregnation flow and the collapse of the structure during polymer removal. Three different sponges were used: (1) Flexipol 20D, density in the range of 18.5 – 21.5 $kg.m^{-3}$ and average pore diameter of 400 μm; (2) Recticel TM30, density in the range of 19.5 – 22.5 $kg.m^{-3}$ and average pore diameter of 600 μm; (3) Recticel TM40, density in the range of 17.5 – 20.5 $kg.m^{-3}$ and average pore diameter

of 1 mm. The sponge was firstly compressed to remove air, immersed in the suspension and then allowed to expand. This procedure was repeated until most air bubbles were eliminated. The excess ceramic suspension was then removed by passing it through preset rollers. The infiltrated sponge was then dried in an oven at 100ºC overnight. The dry sponge was slowly heated (0.5ºC·min^{-1}) in static air up to 500ºC to prevent collapse of the ceramic web, soaked for 2 h at this temperature, and then sintered at 1250ºC for 2 h.

The apparent density was calculated from the weight and dimensions of the samples.

For mechanical testing, rectangular blocks of dimensions 20x20x10 mm^3 were cut with a precision cutting machine (Secotom 10 – Struers, Germany). The crushing strength was measured on (approximately) using a standard mechanical testing machine (Model AG-IS – Shimadzu, Japan) fitted with a 10 kN load cell and flat steel plates closing with a cross head speed of 0.5 mm·min^{-1}. The cross-sectional area of the sample and the maximum failure load were used to calculate the fracture stress. A compliant polymeric layer (2 mm thickness PVC) was used between the loading rams and the samples to assist in uniformly loading the bulk foams.

Porous Scaffolds Prepared by the Foaming Method Using Egg White as Consolidator and Foaming Agent

Albumin (A) from chicken egg (dried egg white, grade II, Sigma Aldrich Chemie, Germany) was used in this method with a twofold role of foaming and consolidator agent. The foaming capability of albumin was firstly studied by preparing protein solutions of various concentrations (5 wt.% to 20-wt.% relative to mass of water) beaten for 5 minutes. The gelling behaviour of the as obtained foams with temperature increasing was accessed with rheological measurements using a C-VOR rheometer (Bohlin Instruments, USA). The evolution of viscoelastic parameters, such as storage modulus, loss modulus and phase angle were measured under oscillatory tests using an oscillating parallel plate sensor within the linear viscoelastic range.

Bodies with different porous microstructures were then prepared by adding suitable amounts of beaten albumin to aliquots of stock suspension of CaP powder to obtain different mass proportions of CaP powders and albumin. The rheological properties of the final mixtures were evaluated. Ceramic parts were consolidated by pouring the beaten mixtures into closed moulds followed by consolidation for 1 h at suitable temperatures in the range of 60-80ºC, according to the added amounts of egg white. The

samples were separated from the molds, dried and sintered according to the following heating schedule: 1ºC.min^{-1} from 20ºC up to 550ºC, a holding time of 2 h at this temperature, followed by a heating rate of 4ºC.min^{-1} up to 1250ºC, 2 h holding at the maximum temperature and free cooling down inside the furnace.

The apparent density was calculated from the weight and dimensions of the samples. Microstructural features of the porous structures were observed on fracture surfaces by using a SEM (S-4100, HITACHI, Japan). The crushing strength of the samples was also evaluated according to the procedure described for the polymeric derived foams. For mechanical testing, rectangular blocks of dimensions 20x20x10 mm^3 were cut with a precision cutting machine (Secotom 10 – Struers, Germany).

Combining Foaming and Starch Consolidation Methods to Produce Porous Scaffolds

In this part of the work an etherified potato starch modified by hydroxyl-propylation and cross-linking, TRECOMEX AET1 (Lyckeby Starkelsen AB, Sweden), was selected with a twofold role of consolidator and pore former agent. A foam-bath concentrate (FBC) (Dibel, S.A., Porto, Portugal) and Sodium Lauril Sulphate (SLS) (Texapon k 12, V. P., Lisbon, Portugal) were adopted as supplementary foaming agents.

The starch was added to the previously prepared stock suspension prior to the incorporation of the foaming agents in a proportion of 10 vol.% relative to calcium phosphate powder. Then, several mass proportions of FBC and SLS were added to aliquots of the stock suspensions to obtain bodies with different porous microstructures. The amounts of foaming agents, expressed as weight fractions relative to the mass of water present in the suspension, are presented in Table 2.

Table 2. Sample codes, total foaming agent (TFA) added and relative fractions of FBC and SLS.

Sample code	**I**	**II**	**III**	**IV**	**A82**	**A64**	**A55**	**B82**	**B64**	**B55**	**C82**	**C64**	**C55**
TFA [wt.%]	1.7	3.3	6.7	10	2.5	2.5	2.5	5	5	5	10	10	10
FBC [%]	100	100	100	100	80	60	50	80	60	50	80	60	50
SLS [%]	-	-	-	-	20	40	50	20	40	50	20	40	50

The final mixtures were poured into closed moulds and consolidated at 80ºC for 1 hour. The porous samples were taken from the moulds, dried at 60ºC for 24 h, and then at

110ºC for further 24 h. The dried samples were sintered according to the following heating schedule: 1ºC.min^{-1} from 100ºC up to 550ºC, a holding time of 2 h at this temperature, followed by a heating rate of 4ºC.min^{-1} up to 1250ºC, 2 h holding at the maximum temperature and free cooling down inside the furnace.

The microstructure and crashing strength of the sintered bodies were characterized following the procedures described above for the samples prepared by the other methods.

Complex Structures Produced by Miscelaneous Methods

Complex shapes and structures were prepared by making different combinations of the methods described above with slip casting,[110] starch consolidation,[92,111] among others. The starting suspension was always prepared with 60 vol.% of solids loading and dispersed with a previously determined amount of Targon 1128.[108] Some systems also included wax spheres as large dimension (~500μm) pore formers. The aim was to obtain ceramic parts mimicking closely the complete bone structure (cortical and trabecular).

Development of Porous Granules

In this process, stock suspensions of CaP powders were mixed with sodium alginate solution (3 wt./vol.%) at ratios of 0.4 and 0.2 (wt./wt.%), based on the weight of dried powder in the suspension. After complete homogenization of the mixtures, 50 vol.% of starch granules, based on the vol.% of calcium phosphate powder, was added to act as pore former. The flow properties of the final mixtures were characterized by rheological measurements in a C-VOR rheometer (Bohlin Instruments, USA) and suitably adjusted to spray them over the setting media through different diameter nozzles to prepare the granules. Several parameters of the process were varied in order to control the size of the granules, namely the nozzle diameter (0.5 and 1.5 mm); the suspension flow rate (0.6 and 3 mL.min^{-1}) and the distance between the nozzle and the setting media (10 and 50 mm). The sprayed granules were left to set for 10 min in the setting media and then removed and washed with distilled water. The drying step was performed at 40ºC overnight, and the granules were then sintered at 1250ºC for 2 h, with a heating rate of 4ºC.min^{-1}. Table 3 lists the sample codes and the values of process parameters used to prepare the granules.

Table 3. Sample codes (in capital bold) with respect to powder/setting agent ratio, nozzle diameter, flow rate and distance between the nozzle and the setting media.

Powder/Setting agent ratio		0.2			0.4	
Nozzle Diameter (mm)		0.5		1.5	0.5	1.5
Flow rate (mL.min^{-1})		0.6	3.0	3.0	0.6	3.0
Distance (mm)	**10**	**A**	**B**	**C**	**D**	**E**
	50	**F**	**-**	**G**	**-**	**-**

The apparent density was evaluated by the Archimedes method, which also allowed estimating the porosity values. Scanning electron microscopy analysis (S-4100, HITACHI, Tokyo, Japan) performed on polished surfaces of the granules was used to determine the overall size of the granules, characterize the microstructure and to qualitatively assess pore size and pore morphology.

Results and Discussion

Porous Scaffolds Produced by the Polymeric Sponge Method

The picture presented in Fig. 6 reflect the major advantage of the polymeric sponge method, namely the easy control of pores size and porosity fraction of the final structure.

The effectiveness of this method is strongly determined by the rheological properties of the suspension, particularly by the solids content and rheological behaviour. The viscosity should be low enough for an easy impregnation of the sponge, increasing after that by a structure build up mechanism to prevent post impregnation flow. Such suspension properties can be achieved by adding suitable setting agents (partially water soluble bioglass or agar). This will avoid drainage and the consequent density gradients due to accumulation of suspension in the bottom part. The result obtained after drying and burn-out of the sponge is a macroporous structure with a near total interconnection between pores. Sponge pieces of suitable sizes were cut from bigger blocks.

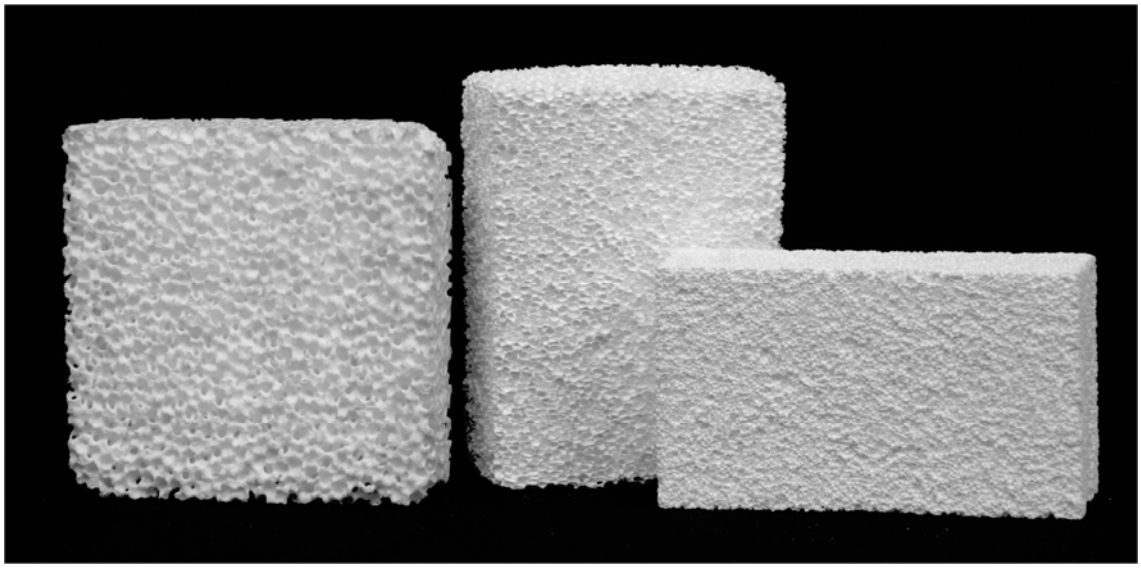

Figure 6. Macroporous HA structures obtained by the polymeric sponge method.

These foams were found to consist of a three-dimensional array of struts. Longitudinal strut cracks were observed at the relatively sharp edges of the hollow triangular cross-section struts of the poly-urethane substrate.

Table 4. Apparent density, estimated porosity and compressive strength of the porous samples obtained through the polymeric sponge method.

Sample	Apparent density ($g.cm^{-3}$)	Estimated Porosity (%)	Compressive Strength (MPa)
1	1.33	58	22.5 ± 4
2	1.00	68	17.6 ± 2
3	0.77	76	11.4 ± 3

In 1999, Milosevski *et al.*[112] developed macroporous structures based on the polymeric sponge method. They used a suspension with 45 vol.% of solids with added C-fibres to reinforce the foam structure. A high porous structure with integral porosity of 55±70% was created and compressive strength values of 11-22 MPa were reported. Tian *et al.*[113] also prepared macroporous HA structures through the polymeric sponge method and found an exponential decreasing trend of compressive strength with increasing porosity. Later, Ramay *et al.*[114] prepared porous hydroxyapatite scaffolds by combining gel-casting and polymeric sponge methods to produce open, uniform and interconnected

porous structures with pore sizes in the range of 200–400 μm. Although using the same polymeric sponge method as Milosevski *et al.*,[112] the porous structures prepared by Ramay *et al.*[114] were much weaker presenting a compressive strength of 5 MPa, probably due to the lack of C-fibres reinforcement. Using the same combination of gel casting and polymeric sponge methods, the same authors[115] prepared biphasic composite scaffolds reinforced with HA nanofibres. They claimed a significant enhancement of the compressive strength (9.8 MPa) by the inclusion of HA nanofibers, close to the upper limit for cancellous bone (2–10 MPa).[116]

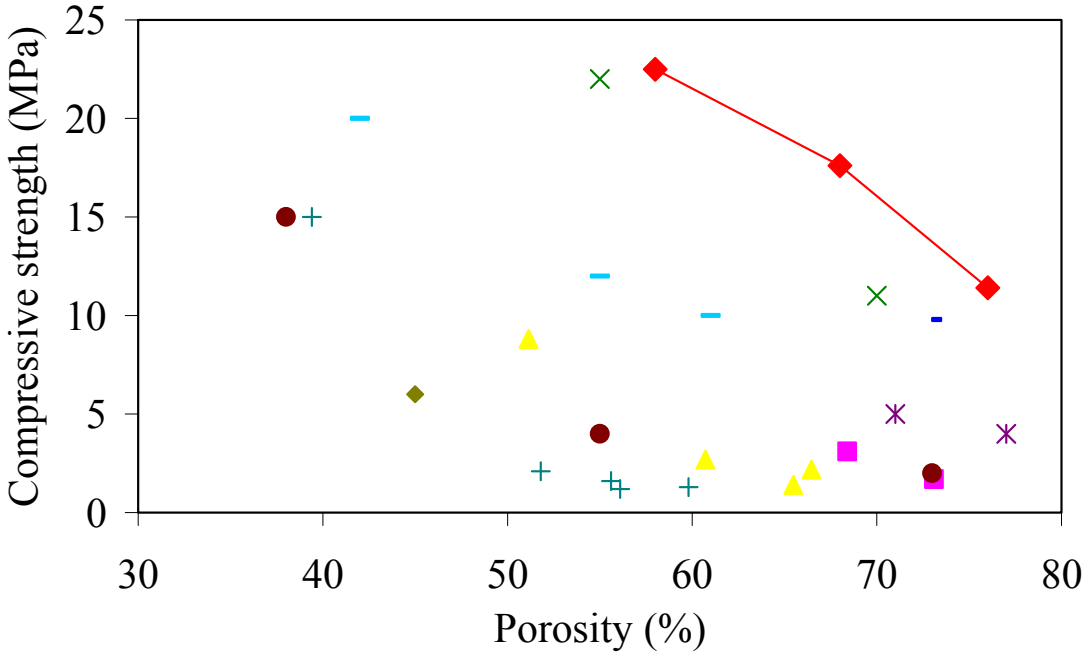

Figure 7. Comparison of compressive strength values vs. porosity of porous HA scaffolds for tissue engineering prepared by the polymeric sponge method achieved in the present work (◆) and reported in literature for the same preparation method, and for conventional and computer-assisted processing techniques. Each style of point corresponds to a different literature source.[112-115,117-127]

Three types of polymeric sponges corresponding to different pore size characteristics were employed in the present work to assess the influence of pore size on compressive strength. The results plotted in Fig. 7 confirm the expected decreasing trend of compressive strength with increasing porosity. However, for a given porosity fraction, the compressive strength values achieved in the present work are significantly higher than those reported in the earlier studies.[112-115,117-127] The improvement in this mechanical property can be attributed to the quality of the processing, namely, good

dispersion and deagglomeration degrees of the starting HA powder, a good impregnation of the polymeric sponges and suitable rheological properties of the suspensions (absence of drainage). The obtained mechanical properties are between the cortical[82] and cancellous bone.[116]

An increase in the macropore size of the sponges enabled to prepare macroporous samples with higher porosity and, consequently, lower compressive strength values. Liu[128] reported a pronounced porosity-strength dependence in the lower porosity range, while for relatively high porosity levels, e.g. > 70%, the compressive strength of the porous HA appeared to be less sensitive to the total pore volume.

Porous Scaffolds Produced by the Foaming Method Using Egg White as Consolidator and Foaming Agent

The gelling behaviour of the protein solutions beaten for 5 minutes was characterized under the oscillatory mode at a constant frequency (1 Hz) and strain (10^{-3}) during an increasing temperature sweep ($5^{\circ}C.min^{-1}$) from 25º to 90ºC. The results presented in Fig. 8 show that the gelling temperature did not change significantly with increasing amounts of protein from about 5-20 wt.%.

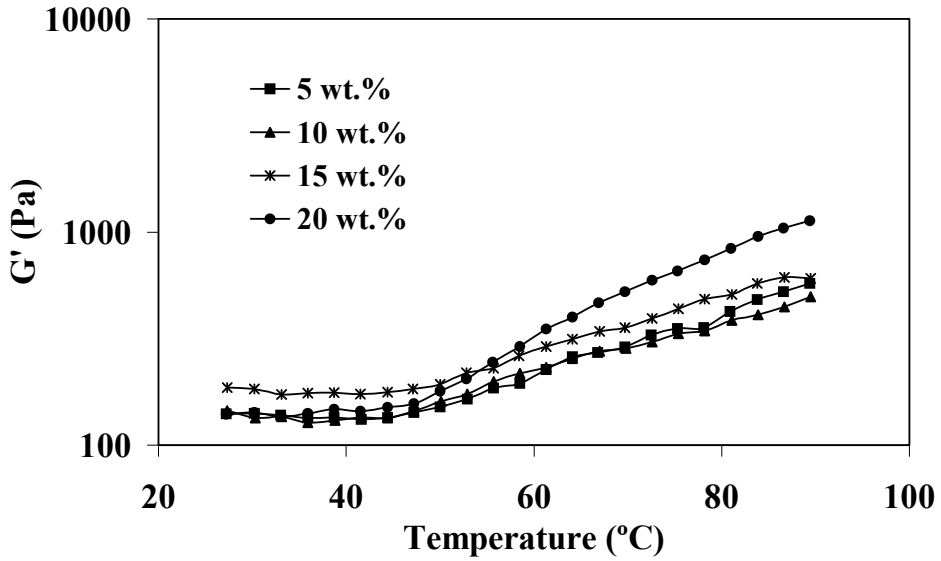

Figure 8. Elastic modulus (G') at a constant strain (10^{-3}) *versus* temperature for protein beaten solutions.

The gelatin process starts at around 50ºC for all the systems, as revealed by the increase of the elastic modulus (G') at this temperature. G´ tends to increase with increasing

amounts of added A, but the differences became more salient in the presence of 20 wt.% protein beaten solution.

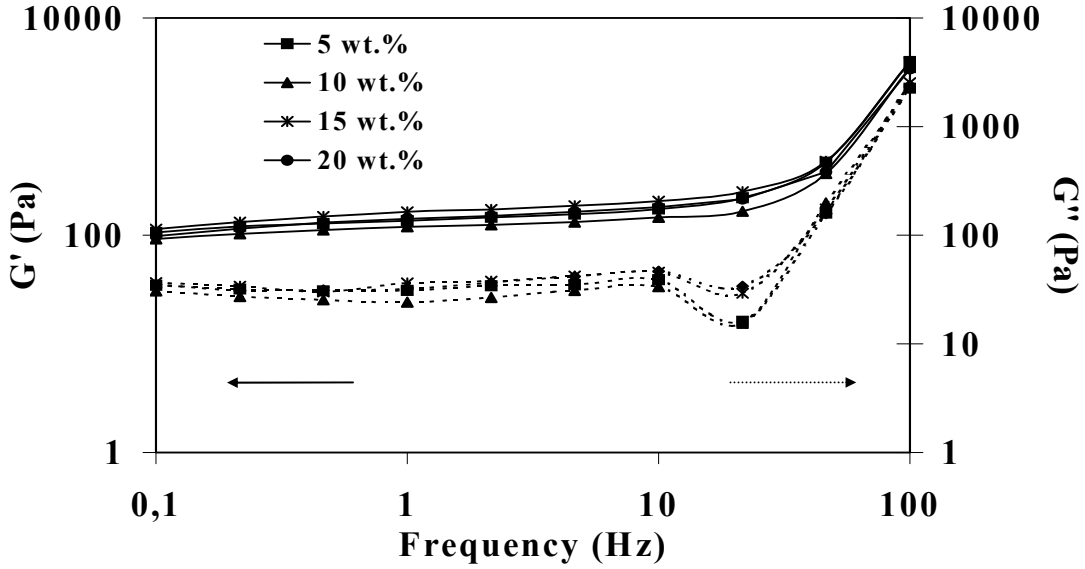

Figure 9. Elastic modulus (G') and viscous modulus (G'') of protein beaten solutions *versus* frequency at a constant temperature (25 ºC).

The stability of the foam during handling and stirring at room temperature is of paramount importance because it determines the mechanical conditions under which the foam can be used before collapsing. Fig. 9 shows the results of frequency sweeps performed at 25ºC. The unlinked albumin molecules are entangled with each other, i.e., only purely mechanical interactions such as friction forces occur between the molecule chains. The absence of a physical-chemical network enables the molecules to move slowly, glide along each other, and partly or completely disentangle, even under small shear forces. This explains the near plateau behaviour along the lower frequency range. However, with increasing frequency, the internal structure of the temporary network of entanglements becomes more inflexible and rigid. Therefore, more deformation energy is stored, increasing the storage modulus. It can be seen that G'>G'' along all the frequency range tested, indicating the predominance of solid-like characteristics of the foams over the viscous ones. The same increasing trend, as referred for Fig. 8 is also observed, although the changes with A concentration are less significant, since no gelation takes place at this temperature (25ºC). The incorporation of the beaten protein solutions into the HA suspensions confers to the mixed systems a dramatic increase of solid-like characteristics, as shown in Fig. 10. The gelation process occurs faster and at

a lower temperature. However, for all added amounts of beaten protein, G' reaches a plateau value of about 1 MPa at about 80ºC, which is about three orders of magnitude higher compared with the maximum valued (20 wt.% A) presented in Fig. 8.

The results presented in Fig. 11 reveal that the viscoelastic properties of the mixed systems are very sensitive to the concentration of beaten protein solutions. In fact the G' and G'' curves become more discrete when compared with Fig. 9. This confirms that the incorporation of the inorganic component enhances the consistency of the systems at room temperature, as expected, as well as the gel strength after heat treatment.

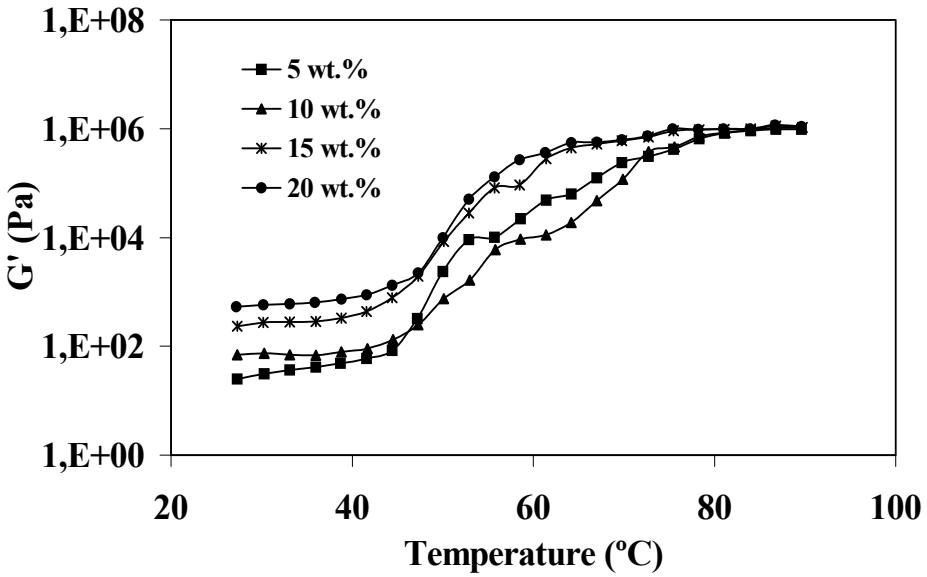

Figure 10. Elastic modulus (G'), at a constant strain (10^{-3}), versus temperature, of hydroxyapatite suspensions with different amounts of beaten protein solutions.

The average apparent density values evaluated from the weight and dimensions of the samples sintered at 1250ºC are reported in the Table 5. The estimated values of porosity are also presented as percentage relative to the true density of hydroxyapatite powder. The porous microstructures of the samples A5, A10, A15 and A20 presented in Fig. 12 show that the pore size ranges obtained are suitable for bone ingrowth.

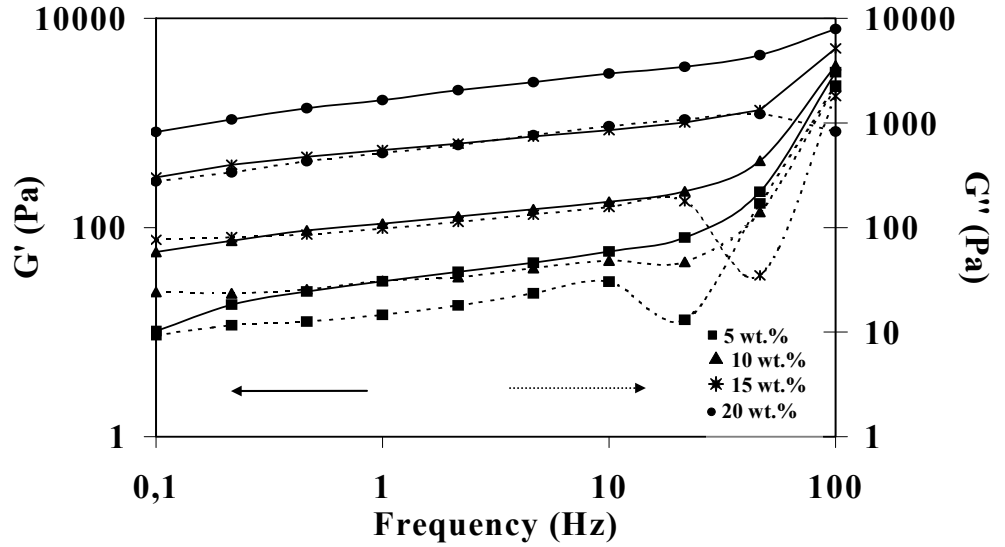

Figure 11. Elastic modulus (G') and viscous modulus (G''), at a constant temperature (25 ºC), versus frequency, of hydroxyapatite suspensions with different amounts of beaten protein solutions.

Table 5. Apparent density, porosity values and compressive strength of the porous samples prepared by the foaming method using egg white as consolidator and foaming agent.

Sample Code	Apparent Density [g.cm^{-3}]	Porosity [%]	Compressive strength [MPa]
A5	0.80	74.65	29.8 ± 2
A10	0.69	78.14	27.4 ± 5
A15	0.69	78.14	27.7 ± 3
A20	0.68	78.45	23.4 ± 4

Comparing the data from Table 5 and Fig. 12, it can be concluded that macroporous structures with pore volume fractions as high as ≈ 75-80% can be prepared by the present method.

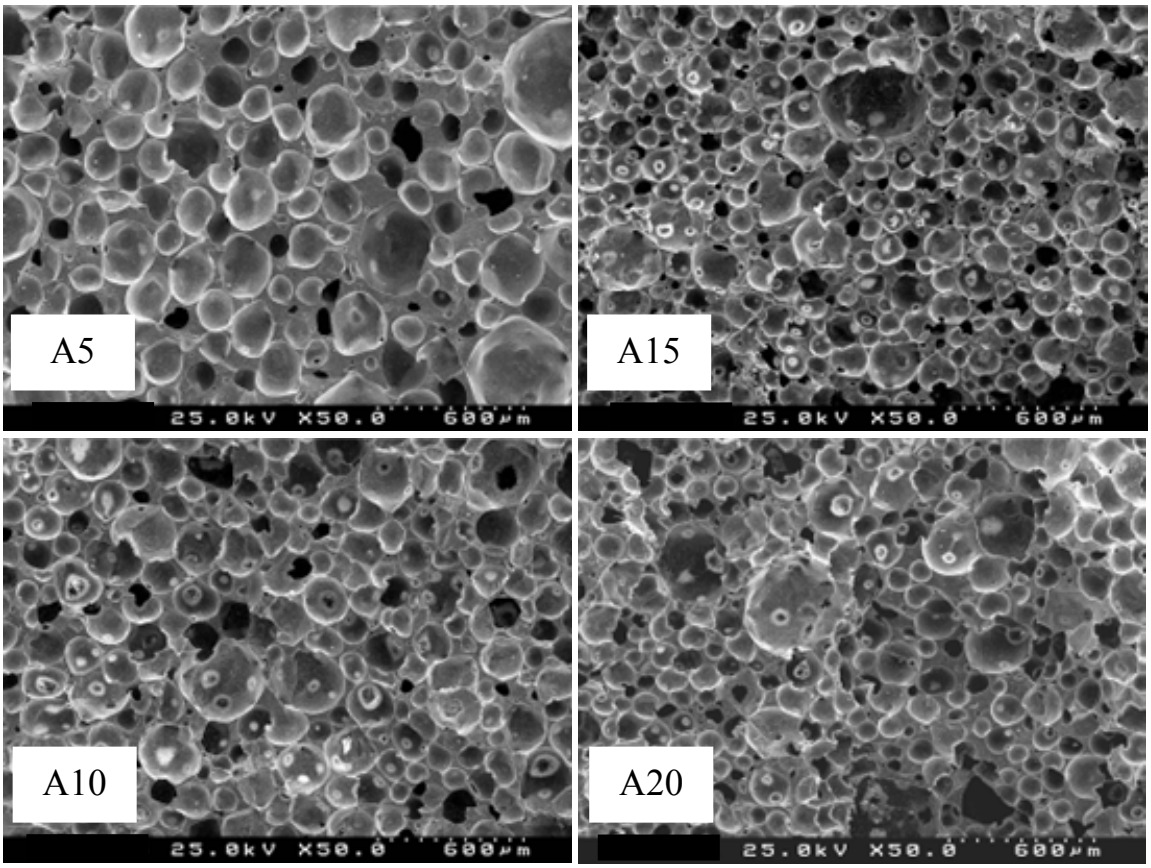

Figure 12. Microstructures of the samples A5, A10, A15 and A20 sintered at 1250ºC.

The average size of the pores tends to decrease and the degree of pore interconnectivity increases with increasing amounts of added protein. However, the degree of interconnectivity using albumin alone as foaming agent seems not to be completely satisfactory.

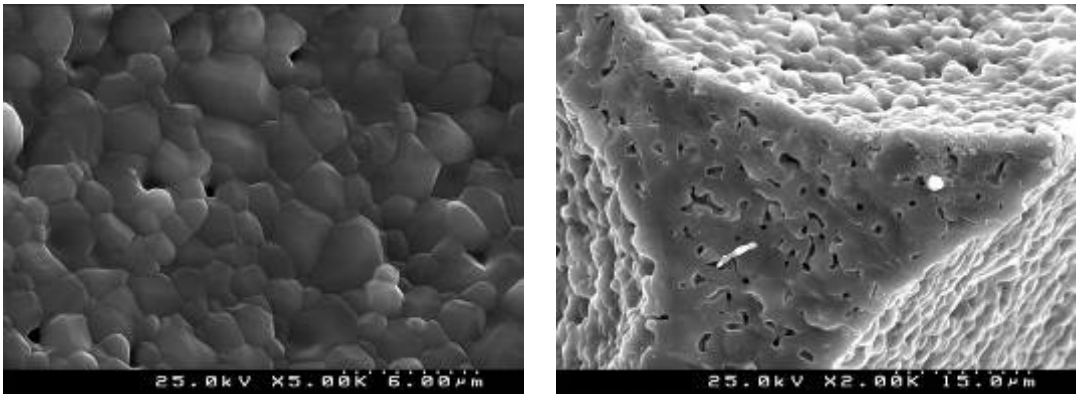

Figure 13. Microstructural details of sintered (1250ºC) porous samples prepared with egg-white as pore former and consolidator agent.

Liu[128] prepared porous hydroxyapatite ceramics with porosity volume fractions varying from 33% to 78% using poly-vinyl-butyral (PVB) as a pore-forming agent. The compressive strength behaviour of the porous HA was correlated exponentially with porosity volume with a correlation factor greater than 0.96. The achieved values of compressive strength were in the range of 10 to 20 MPa.

del Real *et al.*[129] used $NaHCO_3$ as blowing agent to produce macropores in calcium phosphate cements and achieved porosities of 40-60 % with much lower compressive strengths in the range of 1.2-2.1 MPa.

Almirall *et al.*[130] prepared porous materials by using H_2O_2 as porogenic agent and reached percentages of porosity in the range of 51 to 66 %, which combined an interconnected macroporosity with a high microporosity. The compressive strength values obtained were in the range from 8.81 and 2.18 MPa, which are in accordance to the values reported for the trabecular bone (2-10MPa).[116]

Table 5 reports the porosity and compressive strength values of the porous samples prepared by the foaming method using egg white as consolidator and foaming agent. The compressive values are relatively high when compared to the values for the cancelous bone[116] and to other reported values using porogenic agents to create porosity. Although the pore volume fractions are ≈ 75-80%, the pores are mainly closed, conferring high mechanical strength to the porous structure.

Combining Foaming and Starch Consolidation Methods to Produce Porous Scaffolds

The overall porosity of the samples, estimated from the apparent density data, is presented in Fig. 14. It is possible to observe that although FBC alone enables to obtain high porosity values, which increase with increasing added amounts of this foaming agent, its combination with SLS produces a synergetic effect, enhancing the total amount of porosity, even for lower total added amounts of foaming agents. Apparently, only small changes in the overall porosity seem to occur for TFA > 2.5 wt.% in the range of the FBC/SLS proportions tested.

Fig. 15 shows the microstructures of the sintered porous samples obtained by adding just FBC. It can be observed that porosity consists predominantly of open and interconnected pores. This means that the fraction of closed pores is relatively modest if one considers that foaming methods tend to form essentially closed porosity.[87]

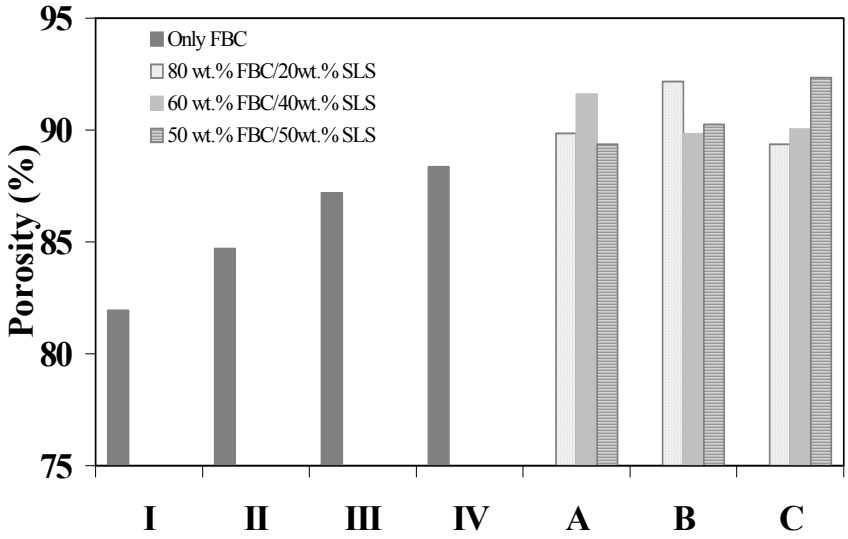

Figure 14. Estimated values of total porosity based on the measured apparent density.

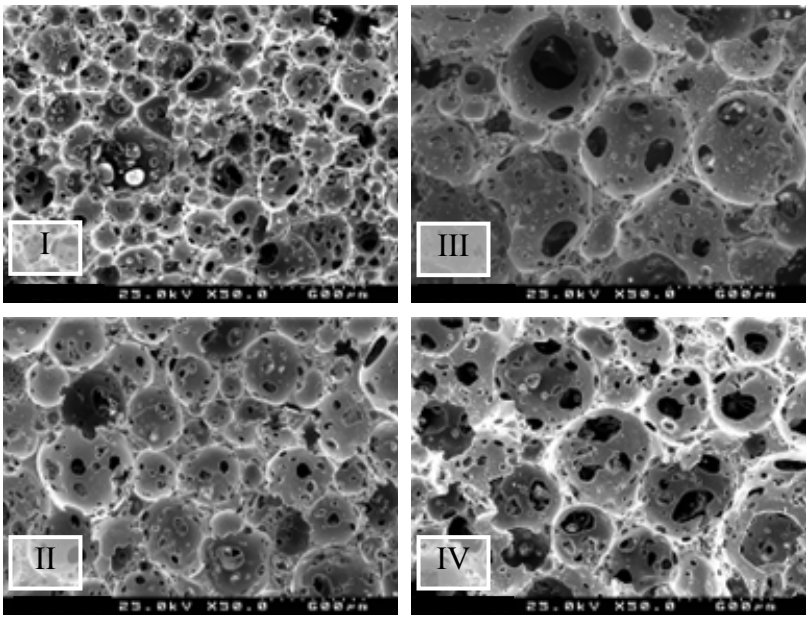

Figure 15. Microstructure of the samples I to IV, sintered at 1250ºC (see Table 2 for sample codes).

These results suggest that the pores left by the burning out of starch granules enhance pore interconnectivity. This also proves the suitability of combining the foaming method with the starch consolidation method to achieve the desired goals in terms of porous microstructure. However, pore size and pore interconnectivity also depends on the added amount of foaming agent. In fact, increasing the amount of FBC from 1.7

wt.% (sample I) to 10 wt.% (sample IV) tends to increase the size of pores and enhances pores interconnectivity.

Although the SLS tends to originate abundant foam, its use alone revealed to be unsuitable because of the very low stability of the foams formed, which quickly fade. Adding small amounts of SLS to the suspension with FBC greatly improved the foam stability and also contributed to significantly increase the size of air bubbles formed as well as the degree of their interconnections, as can be observed in Fig. 16. However, excess amounts of SLS imparted accentuated viscoelastic-type properties to the suspensions making handling and pouring very difficult.

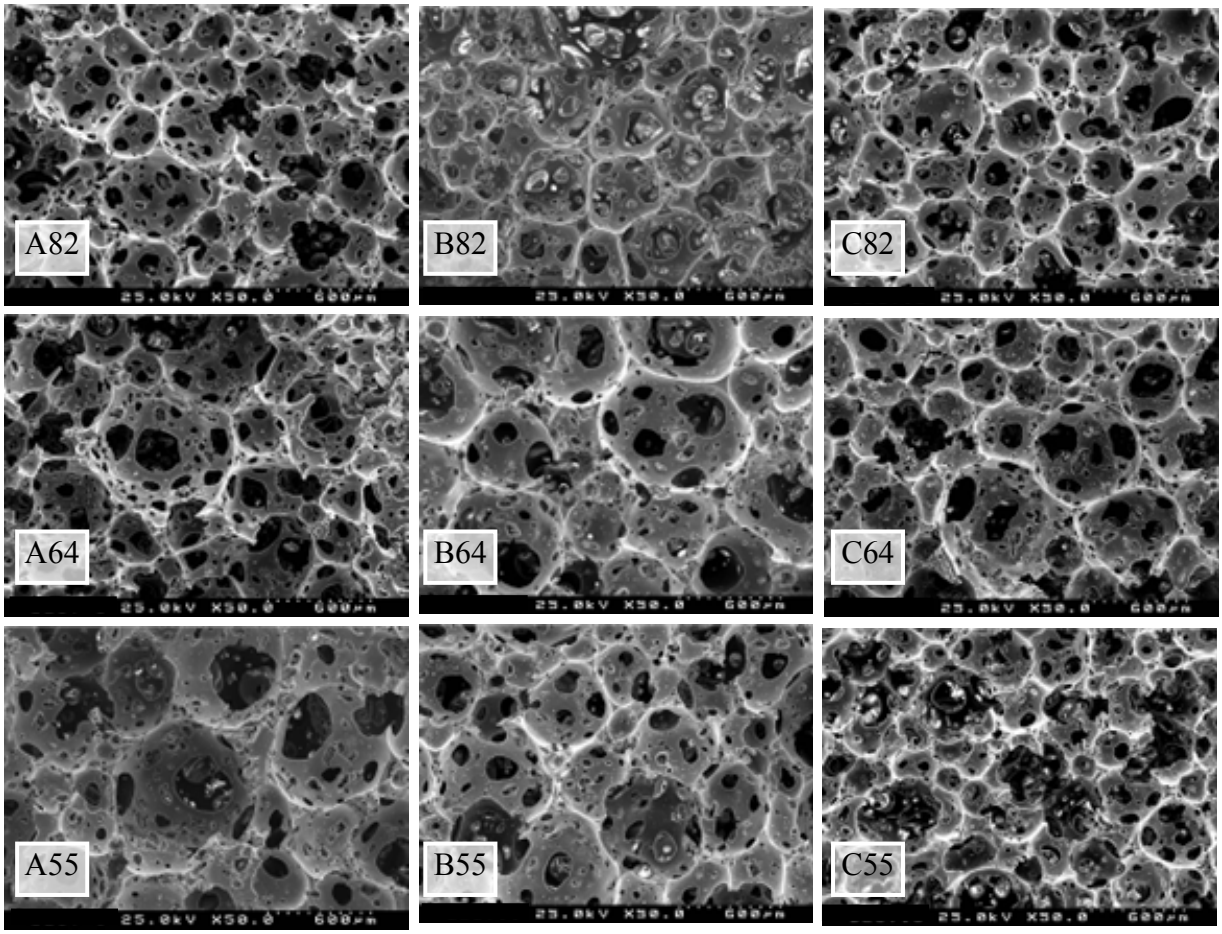

Figure 16. Microstructure of the samples A, B and C with different FBC/SLS proportions, sintered at 1250ºC.

The comparison between the samples A (TFA = 2.5 wt.%) and C (TFA = 10 wt.%), shows that increasing the total amount of foaming agents generates more pores, i.e., the average size of pores tends to decrease, but the size of the pore interconnections seems to be somewhat enhanced. The latter is mainly affected by the proportion of SLS, as can

be clearly seen by comparison of the two pairs of microstructures (top and bottom) in Figure 16. These results allow concluding that higher amounts of foaming agent produce more pores, and the addition of SLS promotes the increase of the number and the size of pore interconnections.

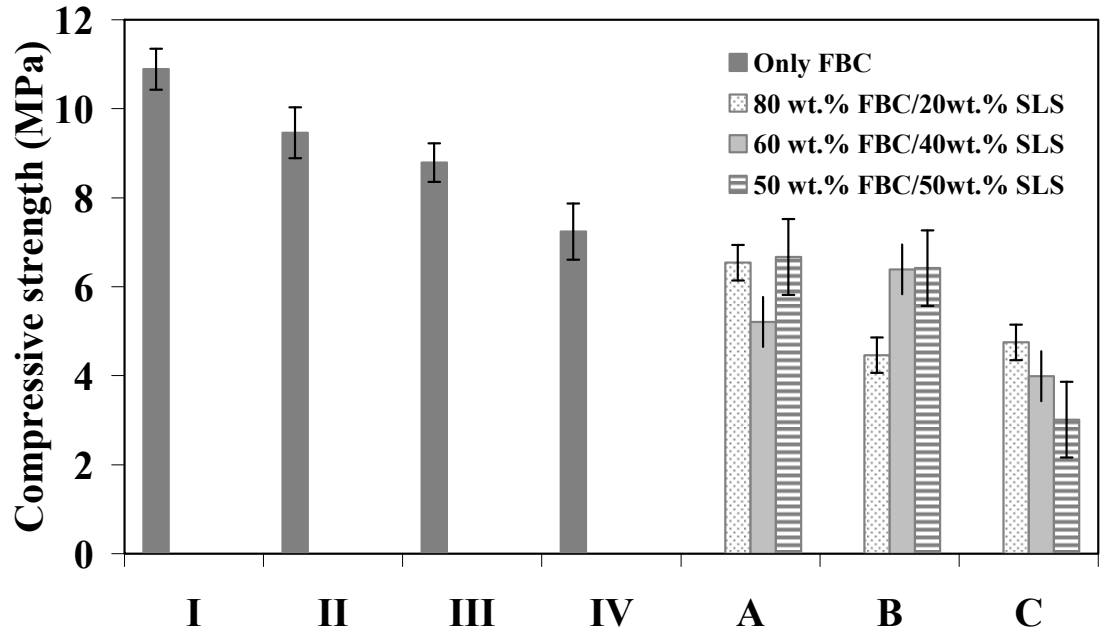

Figure 17. Compressive strength of the samples obtained by combining foaming and starch consolidation methods.

The values of compressive strength for the samples obtained by combining foaming and starch consolidation methods are presented in Fig. 16. When compared to the others results presented above, obtained for porous structures prepared by different methods, these values are relatively lower, being however in the range of values presented by the cancelous bone.[116] The expected decreasing trend of compressive strength with porosity increasing can be observed. The interconnectivity of the pores plays an important role in the mechanical behaviour of the samples. In fact, the introduction of a secondary foaming agent, SLS, increases the pore interconnectivity, weakening the pore walls and leading to a decrease of the compressive strength.

Complex Structures Produced by Miscelaneous Methods

Fig. 18 shows examples of some interesting techniques combinations in order to explore their capabilities to obtain complex shapes with controlled porosity characteristics. The combination of starch consolidation with wax spheres as large dimension pore formers (Fig. 18A), ensures a good control of pores size and porous fraction, but the degree of

pore interconnectivity (dependent on the total added amount of fugitive additives) is not satisfactory.

Combining the foaming and starch consolidation methods (Fig. 18B) enabled to prepare macroporous HA structures with pores larger than 100 μm, and presenting a high degree of pore interconnectivity, which are suitable for allowing bone ingrowth. This observation is contrary to the findings already reported for porous structures obtained by the foaming method, which has been associated with the formation of predominantly closed pores. The present results show that the used of suitable mixtures of foaming agents and of starch granules enhance pore interconnectivity and rehabilitate the foaming method for producing porous scaffolds for biomedical applications.

Ceramic parts mimicking the structure of trabecular bone [Fig. 18 (C-2) and (2C-4)] or the complete bone structure (cortical and trabecular), [Fig. 18 (C-1) and (2C-3)] were respectively obtained by the polymeric sponge method alone or by combining slip casting (for the cortical part) with the polymeric sponge method [Fig. 18 (C-1)] or with the foaming method [Fig. 18 (C-3)].

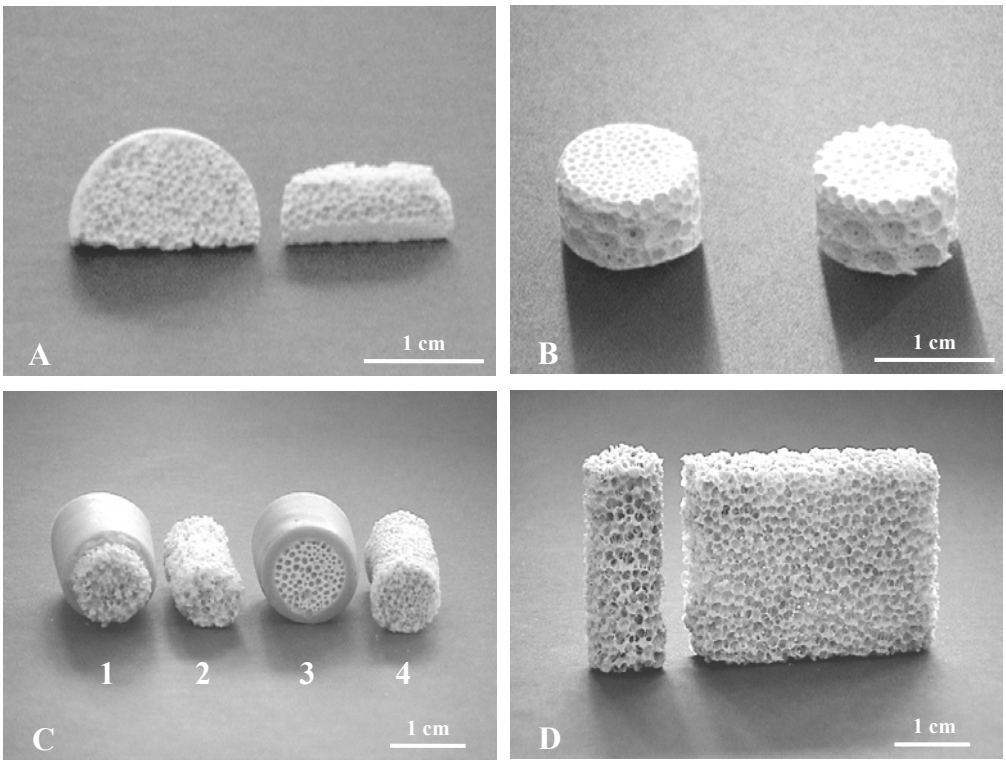

Figure 18. Macroporous HA structures of different shapes, obtained by different methods: (A) Starch consolidation with wax spheres; (B) Starch consolidation and foaming; (C) 1 - Slip casting and polymeric sponge; 2,4 - Polymeric sponge and 3 – Slip casting, starch consolidation and foaming; (D) Polymeric sponge using a partially

soluble bioglass (cylinder) and polysaccharide (block) as setting agents. Samples C1 and C3 present outer high density and inner macroporosity.

Porous Granules

Fig. 19 presents the rheological behaviour of the stock suspension with different HA/setting agent solution weight ratios of 0.2 and 0.4, represented with a solid and a dashed line, respectively. In both cases a shear-thinning behaviour is observed, which is more pronounced for the 0.4 ratio due to the higher solids loading. Although one could assume that both suspensions present a proper behaviour for spraying, it was verified that the increase of the viscosity was favorable for the production of larger size granules.

Table 6. Density and porosity of the sintered samples.

	Density (g/cm^3)	**Porosity (%)**
Sample Code	**Sintered Samples**	**Sintered Samples**
A	1.44	54.37
B	1.28	59.44
C	1.25	60.39
D	1.43	54.69
E	1.07	66.10

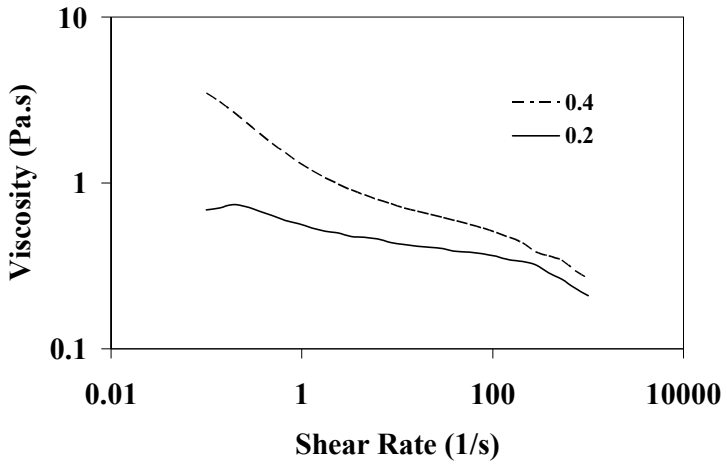

Figure 19. Rheological behaviour of HA suspensions mixed with different weight ratios of HA powder/setting agent solution of 0.2 (solid line) and 0.4 (dashed line).

The density and porosity of the sintered porous granules can be observed in Table 6. These values do not seem to be significantly affected by the powder/setting agent ratio. However, this variable strongly influenced the size of the granules as can be seen in Fig.

19 by comparing C and E pictures. As expected, more concentrated suspensions gives rise to larger granules.

The effects of nozzle diameter on the density and porosity are negligible, as expected, while the granules size is strongly affected by this parameter, with the larger diameter nozzle giving bigger granules as can be observed in Fig. 19 by comparing B and C pictures.

The trend for air bubbles entrapment with the increase of the flow rate due to the higher turbulence in the fluid during the dripping process explains the decrease of sintered density and the concomitant increase of porosity of samples A and B. The same trend can be found in the samples D and E. On the other hand, the increase of the flow rate produces smaller droplets.

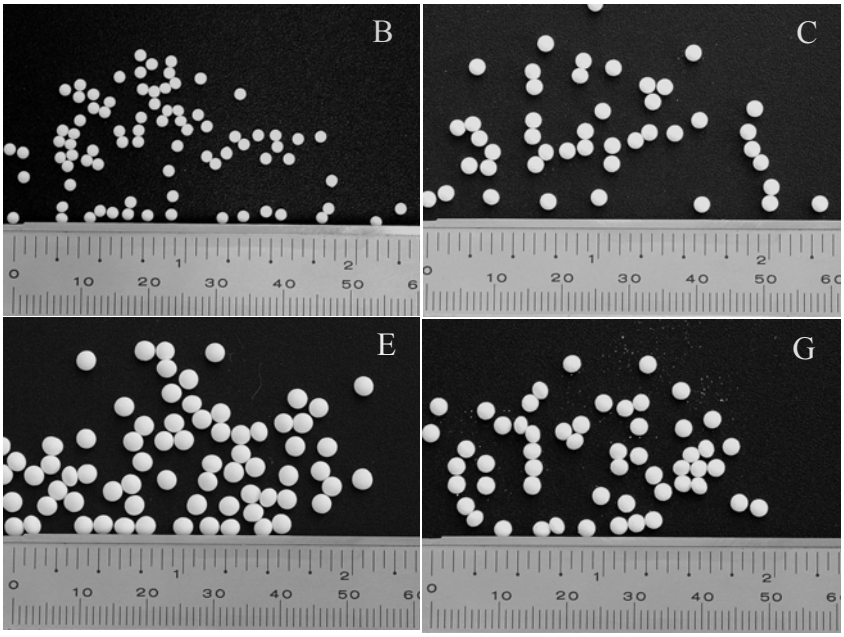

Figure 20. Digital pictures of some of the samples listed in Table 6 (B, C, E and G), showing the influence of the experimental parameters on the granule size and shape.

The morphology of the granules tends to change from rounded to oval as the distance of the nozzle from the setting media increases, as can be observed in Fig. 20 by comparing C and G. The measured porosity data presented in Table 5 is apparently not well supported by the microstructure of the sample D sintered at 1250ºC (porosity ~55%) shown in Fig. 20. This suggests that some pores derived from the burnout of starch granules appear as closed pores under this magnification. However, they are accessible to water as confirmed by water absorption measurements that tend to coincide with the measured porosity fraction. These features suggest that the porous granules might be

suitable as drug deliver systems. Moreover the mean pore size is about 50 μm, which is almost coincident with the mean particle size of the starch granules (55 μm).

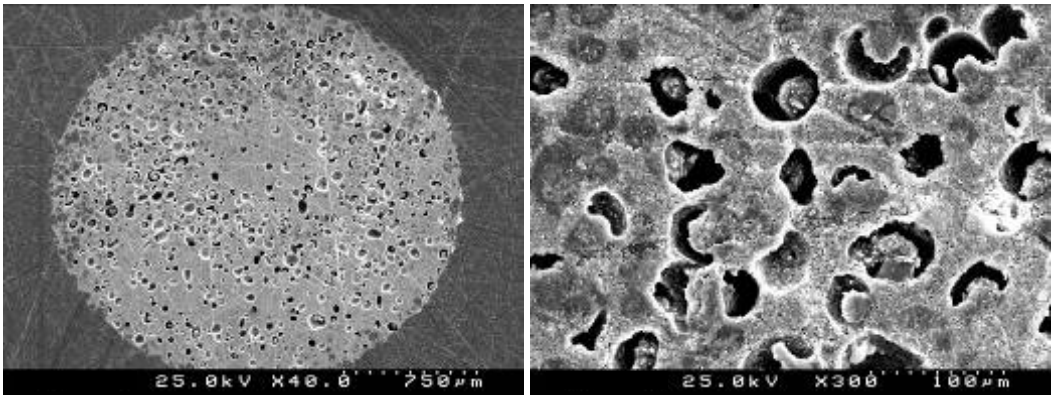

Figure 21. Microstructure of the sample D, sintered at 1250ºC.

Conclusions

The present work combined in suitable ways the knowledge coming from different but complementary areas of expertise to give new insights on designing porous scaffolds and granular calcium phosphate ceramics for orthopedic applications. The materials obtained were inspired in the bone model and attempt to mimic the structure, the mineral composition and the properties of bone in order to develop reliable synthetic bone grafts. The synergetic combinations of traditional new consolidation methods from well dispersed and high concentrated suspensions enable to draw the following conclusions:

1. Adding egg white to a concentrated ceramic suspension builds a foamy structure under stirring, which can be directly consolidated into rigid and highly porous green body by heat-treating it at moderate temperatures. The size of the pores in the range of a few hundred microns and the degree of interconnectivity could be modeled by the added amount of egg white.
2. Combining foaming and starch consolidation methods enables the preparation of macroporous HA structures with pores larger than 100 μm. The foam stability could be improved, and the porous structure, including pore size, porous fraction and pore interconnections could be tailored according to the requirements by varying the total amount and ration of supplementary foaming agents, SLS and FBC.

3. Ceramic parts mimicking the structure of trabecular bone or the complete bone structure were obtained by the polymeric sponge method alone or by combining slip casting (for the cortical part) with the polymeric sponge method or with the foaming method (for the trabecular part).
4. Porous spherical granules with smooth surfaces and tailor made size and porosity could be prepared by suitably setting the most relevant processing parameters (nozzle diameter, the total solids content, the distance between the nozzle and the setting media, and the flow rate of the suspension through the nozzle). The nozzle diameter is the parameter that most influences the size of the granules, while their morphology is mostly dictated by the distance between the nozzle and the setting media. The density and porosity are mainly affected by the solids content of the suspensions and by the HA/starch ratio, with the other processing parameters playing minor roles.

References

1. Hill D., Design Engineering of Biomaterials for Medical Devices, John Wiley and Sons, Chichester. 1998.
2. Hulbert SF, Bockros JC, Hench LL, Wilson J, Heimke G. Ceramics in clinical applications. High Tech Ceramics. Elsevier, Amsterdam. 1987;189-204.
3. Posner AS. The mineral of bone. Clinical Orthopaedics 1985; 200: 87-99.
4. Larsson C, Esposito M, Liao H & Thomsen P. The titanium-bone interface in vivo. In: Brunette DM, Tengvall P, Textor M, Thomsen P, editors. Titanium in Medicine-Materials Science, Surface Science, Engineering, Biological Responses and Medical Applications. Berlin, Germany: Springer Verlag, 2001. p.587-648.
5. Rey C. Calcium Phosphates for Medical Applications. In: Zahid Amjad, editor. Calcium Phosphates in Biological and Industrial Systems. Boston, USA: Kluwer Academic Publishers, 1998. p.217-251.
6. Legeros R, Balmain N & Bonel G. Age related changes in mineral of rat and bovine cortical bone. Calcif Tissue Int 1987;41:137-144.

7. Jain AK & Panchagnula R. Review- Skeletal drug delivery systems. Int J Pharm 2000;206:1-12.

8. Termine JD & Posner AS. Amorphous/crystalline interrelationships in bone mineral. Calcif Tissue Res 1967;1:8-23.

9. Eanes ED, Termine JD & Posner AS. Amorphous calcium phosphate in skeletal tissues. Clin Orthoped 1967;53:223-235.

10. Siew C, Gruninger SE, Chow LC & Brown WE. Procedure for the study of acidic calcium and phosphate precursor phases in enamel mineral formation. Calcif Tissue Int 1992;50:144-148.

11. Brown WE, Smith JP, Lehr JR & Frasier AW. Crystallographic and chemical relations between octacalcium phosphate and hydroxyapatite. Nature 1962;196:1050-1055.

12. Termine JD & Posner AS. Infrared analysis of rat bone: age dependency of amorphous and crystalline mineral fractions. Science 1966;153:1523-1525.

13. Boskey AL, Pleshko N, Doty SB & Mendelsohn R. Applications of Fourier transform infrared (FT-IR) microscopy to the study of the mineralization in bone and cartilage. Cells and Materials 1992;2:209-220.

14. Boskey AL, Camacho NP, Mendelsohn R, Doty SB & Binderman I. FT-IR microscopic mappings of early mineralization in chick limb bud mesenchymal cell cultures. Calcif Tissue Int 1992;51:443-448.

15. Rey C, Collins B, Goehl T, Dickson IR & Glimcher MJ. The carbonate environment in bone mineral: a resolution-enhanced Fourier transform infrared spectroscopy study. Calcif Tissue Int 1989;45:157-164.

16. Rey C, Renugopalakrishnan V, Collins B & Glimcher MJ. Fourier Transform infrared spectroscopic study of the carbonate ions in bone mineral during aging. Calcif Tissue Int 1991;49:251-258.

17. Rey C, Shimizu M, Collins B & Glimcher MJ. Resolution enhanced Fourier transform infrared spectroscopy study of the environment of phosphate ion in the early deposits of a solid phase calcium phosphate in bone and enamel and their evolution with age: investigations in the ν3 PO43- domain. Calcif Tissue Int 1991;49:383-388.

18. Rey C, Shimizu M, Collins B & Glimcher MJ. Resolution enhanced Fourier transform infrared spectroscopy study of the environment of phosphate ion in the early deposits of a solid phase calcium phosphate in bone and enamel and their evolution with age: investigations in the ν4 PO43- domain. Calcif Tissue Int 1990;46:384-394.

19. Herzfeld J & Berger SE. Sideband intensities in NMR spectra of samples spinning at the magic angle. J Chem Phys 1980;73:6021-6030.

20. Aue WP, Roufosse AH, Glimcher MJ & Griffin RG. Solid-state phosphorous-31 nuclear magnetic resonance studies of synthetic solid phases of calcium phosphate: potential models of bone mineral. Biochemistry 1984;23:6110-6114.

21. Wu Y, Glimcher MJ, Rey C & Ackerman JL. A Unique protonated phosphate group in bone mineral not present in synthetic calcium phosphates - Identification by phosphorous-31 solid state NMR spectroscopy. J Mol Biol 1994;244:423-435.

22. Boyce T, Edwards J, Scarborough N. Allograft Bone: The Influence of Processing on Safety and Performance. Orthop Clin N Amer 1999;30[4]:571-581.

23. Heest AV, Swiontowski M. Bone-graft substitutes. Lancet 1999;353(suppl 1):28-9.

24. Lewandrowski K, Gresser JD, Wise DL, Trantolo DJ. Bioresorbable bone graft substitutes of different osteoconductivities: an histologic evaluation of osteointegration of poly (propyleneglycol-co-fumaric acid) based cement implants in rats. Biomaterials 2000;21[8]:757-64.

25. Muschler GF, Negami S, Hyodo A. Evaluation of collagen ceramic composite graft materials in a spinal fusion model. Clin Orthop 1996;328:250-60.

26. Sauer HD, Schoettle H, The stability of osteosyntheses bridging defects. Arch Orthop Trauma Surg 1979;95:27-30.

27. Cypher TJ, Grossman JP. Biological principles of bone graft healing. J Foot Ankle Surg 1996;35:413-417.

28. White E, Shors EC. Biomaterial aspects of Interpore-200 porous hydroxyapatite. Dent Clin North Am 1986;30:49-67.

29. Summers BN, Eisenstein SM. Donor site pain from the ilium: a complication of lumbar spine fusion. J Bone Joint Surg Br 1989;71-B:677-80.

30. Younger EM, Chapman MW. Morbidity at bone graft donor sites. J Orthop Trauma, 1989;3:192-5.

31. Banwart JC, Asher MA, Hassanein RS. Iliac crest bone graft harvest donor site morbidity: a statistical evaluation. Spine 1995;20:1055-60.

32. Cowley SP, Anderson LD. Hernias through donor sites for iliac-bone grafts. J Bone Joint Surg Am 1983;65:1023-5.

33. Freidlaender GE. Immune responses to osteochondral allografts: Current knowledge and future directions. Clin Orthop 1983;174:58-68.

34. William WT. Bone allografts: Past, present and future. Cell and Tissue Banking, 2000;1:105–109.

35. Bostman O, Pihlajamaki H. Clinical biocompatibility of biodegradable orthopaedic implants for internal fixation: a review. Biomaterials 2000;21:2615-21.

36. Bucholz RW, Carlton A, Holmes R. Interporous hydroxyapatite as a bone graft substitute in tibial plateau fractures. Clin Orthop 1989;240:53-62.

37. Cornell CN. Osteoconductive materials and their role as substitutes for autogenous bone grafts. Orthop Clin North Am 1999;30:591-8.

38. Bohner M. Calcium orthophosphates in medicine: from ceramics to calcium phosphate cements. Injury, 2000;31(Suppl. 4): 37-47.

39. Hollinger JO, Brekke J. Role of bone substitutes. Clin Orthop 1996;324:55-65.

40. Black J, Hastings G, editors. Handbook of biomaterials properties. Chapman and Hall. 1998.

41. Legeros RZ. in Hydroxyapatite and Related Materials. Eds.:P. Brown W, Constantz B. CRC, Boca Raton, FL. 1994:3-28.

42. Vallet-Regí M. Introduction to the world of biomaterials. Ann Quim Int Ed 1997;93:S6–S14.

43. Wilson RM, Elliott JC, Dowker SEP. Rietveld refinement of the crystallographic structure of human dental enamel apatites Am Mineral 1999;84:406-14.

44. Aoki H. Medical applications of hydroxyapatite. Tokyo, St. Louis: Ishikayu Euro America Inc. 1994.

45. Vallet-Regí M, González-Calbet JM. Calcium phosphates as substitution of bone tissues Progress in Solid State Chemistry 2004;32:1-31.

46. Elliott JC. Structure chemistry of the apatites and other calcium orthophosphates. in Studies in Inorganic Chemistry, Elsevier, Amsterdam. 1994.

47. Papargyris AD, Botis AI, Papargyri SA. Synthetic Routes for Hydroxyapatite Powder Production. Key Eng Mater 2002;206–213:83.

48. Riman RE, Suchanek WL, Byrappa K, Chen C, Shuk P, Oakes CS. Solution synthesis of hydroxyapatite designer particulates. Solid State Ionics 2002;151[1-4]:393-402.

49. Yingkai L, Wang W, Zhan Y, Zheng C, Wang G. A simple route to hydroxyapatite nanofibers. Mater Lett 2002;56[4]:496-501.

50. Brown PW, Martin RI, TenHuisen KS. Factors influencing the formation of monolithic hydroxyapatite at physiological temperature. in: Biomedical and Biological Applications of Glass and Ceramics. Am Ceram Soc 1996;37:48.

51. Kevor ST, Brown PW. Formation of calcium-deficient hydroxyapatite from α-tricalcium phosphate. Biomaterials 1998;19[23]:2209-2217.

52. Martin RI, Brown PW. Aqueous formation of hydroxyapatite. J Biomed Mater Res 1997;35[3]:299-308.

53. Nasser YM. Characterization, thermal stability and sintering of hydroxyapatite powders prepared by different routes. Materials Chemistry and Physics 2005;94:333–341.

54. Ben-Nissan B, Green DD, Kannangara GSK, Chai CS and Milev A. 31P NMR Studies of Diethyl Phosphite Derived Nanocrystalline Hydroxyapatite. J Sol-Gel Scien Techn 2001;21[1-2]:27-37.

55. Kuriakose TA, Kalkura SN, Palanichamy M, Arivuoli D, Dierks K, Bocelli G, Betzel C. Synthesis of stoichiometric nano crystalline hydroxyapatite by ethanol-based sol–gel technique at low temperature. J Cryst Growth 2004;263[1-4]:517-523.

56. Yoshimura M, Suda H, Okamoto K, Ioku K. Hydrothermal synthesis of biocompatible whiskers. J Mater Sci 1994;29:3399-3402.

57. Lim GK, Wang J, Gan LM. Processing of fine hydroxyapatite powders via an inverse microemulsion route. Mater Lett 1996;30:431.

58. Murray MG, Wang J, Ponton CB, Marquis PM. An improvement in processing of hydroxyapatite. J Mater Sci 1995;30:3061.

59. Elsinger EC, Leal L. Coralline hydroxyapatite bone graft substitutes. J Foot Ankle Surg 1996;35:396—9.

60. Holmes RE. Bone regeneration within a coralline hydroxyapatite implant. Plast Reconstr Surg 1979;63:626-33.

61. Kim W, Zhang Q, Saito F. Mechanochemical synthesis of hydroxyapatite from Ca(OH)2-P2O5 and CaO-Ca(OH)2-P2O5 mixtures. J Mater Sci 2000;35:5401-5405.

62. Yeong BY, Junmin X, Wang J. Mechanochemical synthesis of hydroxyapatite from calcium oxide and brushite. J Am Ceram Soc 2001;84:465-467.

63. Yeong KCB, Wang J. Mechanochemical synthesis of nanocrystalline hydroxyapatite from CaO and CaHPO4. Biomaterials 2001;22:2705-2712.

64. Kannan S, Neunhoefferb FG, Neubauerb J, Ferreira JMF. Ionic Substitutions in biphasic Hydroxyapatite and β-Tricalcium phosphate mixtures. Structural analysis by Rietveld Refinement. (Feature Article) J Am Ceram Soc 2008;91[1]:1–12.

65. Legeros RZ. Calcium Phosphates in Oral Biology and Medicine. Monographs in oral science, vol. 15., Basel: Karger. 1991.

66. Daculsi G. Biphasic calcium phosphate concept applied to artificial bone, implant coating and injectable bone substitute. Biomaterials 1998;19:1473-1478.

67. Heughebaert M, LeGeros RZ, Gineste M, Guilhem A. Hydroxyapatite (HA) ceramics implanted in non-bone forming site. Physico-chemical characterization. J Biomed Mat Res 1988;22:257-68.

68. Gauthier O, Bouler JM, Aguado E, LeGeros RZ, Pilet P, Daculsi G. Elaboration conditions influence physicochemical properties and in vivo bioactivity of

macroporous biphasic calcium phosphate ceramics. J Mater Sci Mater Med 1999;10:199-204.

69. Bouler JM, Trecant M, Delecrin J, Royer J, Passuti N, Daculsi GJ. Macroporous biphasic calcium phosphate ceramics: Influence of five synthesis parameters on compressive strength.J Biomed Mater Res 1996;32:603-609.

70. Tancred DC, McCormack BAO, Carr AJ. A synthetic bone implant macroscopically identical to cancellous bone. Biomaterials 1998;19:2303-2311.

71. Kivrak N, Tas CA. Synthesis of calcium hydroxyapatite–tricalcium phosphate (HA–TCP) composite bioceramic powders and their sintering behaviour. J Am Ceram Soc 1998;82:2245-2252.

72. Petrov OE, Dyulgerova E, Petrov L, Ropova R. Characterization of calcium phosphate phases obtained during the preparation of sintered biphase Ca-P ceramics. Mater Lett 2001;48:162-167.

73. Yang X, Wang Z. Synthesis of biphasic ceramics of hydroxyapatite and beta-tricalcium phosphate with controlled phase content and porosity. J Mater Chem 1998;8:2233.

74. Lin FH, Liao CJ, Chen KS, Sun JS, Lin CY. Preparation of β-TCP/HAP biphasic ceramics with natural bone structure by heating bovine cancellous bone with the addition of (NH4)2HPO4. J Biomed Mater Res 2000;51:157-163.

75. Manjubala I, Sivakimar M. In situ synthesis of biphasic calcium phosphate ceramics using microwave irradiation. Mater Chem Phys 2001;71:272-278.

76. Tas CA. Combustion synthesis of calcium phosphate bioceramic powders. J Eur Ceram Soc 2000;20:2389-2394.

77. Zyman ZZ, Ivanov I, Rochmistrov D, Glushko V, Tkachenko N, Kijko S. J Biomed Mater Res 2001;54:256-263.

78. Aoki H. Science and Medical Applications of Hydroxyapatite. Tokyo: JAAS. 1991.

79. Hench LL. Bioceramics: From Concept to Clinic. J Am Ceram Soc 1991;75[7]:1487–1510.

80. Ohgushi H, Okumura M, Yoshikawa T, Inoue K, Senpuku N, Tamai S, Shors EC. Bone formation processing porous calcium carbonate and hydroxyapatite. J Biomed Mater Res 1992;26:885-895.

81. Oorlovskii VP, Komlev VS, Barinov SM. Hydroxyapatite and Hydroxyapatite-Based Ceramics, Inorganic Materials, 2002;38[10]:1159-1172.

82. Shors EC, Holmes RE. in An Introduction to Bioceramics. edited by Hench LL, Wilson J. Adv Ser Ceram 1. World Scientific Publishing Co. Pte. Ltd., London, Hong Kong, Singapore. 1993:181.

83. Lemos IAF, Ferreira JMF. Porous Bioactive Calcium Carbonate Implants Processed by Starch Consolidation. J Mat Sci & Engineering C. 2000;C11:35-40.

84. Prado da Silva MH, Lemos AF, Ferreira JMF, Santos JD. Porous Glass Reinforced Hydroxyapatite Materials Produced With Different Organic Additives. Journal of Non-Crystalline Solids 2002;304[1-3]:284-292.

85. Prado da Silva MH, Lemos AF, Santos JD, Ferreira JMF. Production of Porous Biomaterials Based on Glass Reinforced Hydroxyapatite Composites. Key Engineering Materials 2002;230-232:483.

86. Sepulveda P, Ortega FS, Murilo DM. Properties of Highly Porous Hydroxyapatite Obtained by the gelcasting of foams. J Am Ceram Soc 2000;3[12]:3201-3024.

87. Minnear WP. Processing of Foamed Ceramics. Ceramic Transactions, Forming Science and Technology for Ceramics Vol. 26. ed. M.J. Cima, The American Ceramic Society. USA 1992.

88. Omatete O, Janney MA, Strehlow RA. Gelcasting—A New Ceramic Forming Process. Am Ceram Soc Bull. 1991;70:1641.

89. Kosmac T, Novak S, Sajko M. Fourth Euro Ceramics Vol. 1, Basic Science: Developments. ed. C. Galassi. Gruppo Editoriale Faenza Editrice S.p.a., Italy. 1995.

90. Graule TJ, Baader FH, Gauckler LJ. Shaping of ceramic green compacts direct from suspensions by enzyme catalyzed reaction. cfi/Ber DKH 1994;71:317-323.

91. Novich BE, Sundback CA, Adams RW. Quickset Injection Molding of High-Performance Ceramics; pp. 157– 64 in Ceramic Transactions, Vol. 26, Forming Science and Technology for Ceramics, Edited by M. J. Cima. American Ceramic Society, Westerville, OH, 1992.

92. Lycfeldt O, Ferreira JMF. Processing of porous ceramics by 'starch consolidation'. J Eur Ceram Soc 1998;18:131-140.

93. Rives RD. Method of injection moulding powder metal parts. U.S. Patent 4113480, 1976.

94. Lemos AF, Ferreira JMF. The valences of egg white for designing smart porous bioceramics: as foaming and consolidation agent. Key Enginnering Materials 2004;254-256:1045-1048.

95. Lycfeldt O, Brandt J, Lesca S. Protein forming — a novel shaping technique for ceramics. J Eur Ceram Soc 2000;20[14-15]:2551-2559.

96. Olhero SM, Tarì G, Coimbra MA, Ferreira JMF. Synergy of polysaccharide mixtures in gelcasting of alumina. J Eur Ceram Soc 2000;20[4]:423-429.

97. Lemos AF, Ferreira JMF. Combining foaming and starch consolidation methods to develop macroporous HA implants. Key Enginnering Materials 2004;254-256:1041-1044.

98. Rocha JHG, Lemos AF, Agathopoulos S, Valério P, Kannan S, Oktar FN, Ferreira JMF. Scaffolds for Bone Restoration from Cuttlefish. Bone 2005;37:850–857.

99. Rocha JHG, Lemos AF, Agathopoulos S, Kannan S, Valerio P, Ferreira JMF. Hydrothermal grow of hydroxyapatite scaffolds from aragonitic cuttlefish bones J Biomed Mater Res-Part A 2006;77[1]:160-168.

100. Kannan S, Rocha JHG, Agathopoulos S, Ferreira JMF. Fluorine substituted hydroxyapatite scaffolds hydrothermally grown from aragonitic cuttlefish bones. Acta Biomaterialia 2007;3:243-249.

101. Paul W, Sharma CP. Development of porous spherical hydroxyapatite granules: application towards protein delivery. J Mater Sci: Mater Med 1999;10: 383.

102. Liu D. Fabrication and characterization of porous hydroxyapatite granules. Biomaterials 1996;17:1955-1957.

103. Komlev VS, Barinov SM, Koplik EV. A method to fabricate porous spherical hydroxyapatite granules intended for time-controlled drug release. Biomaterials 2002;23:3449-3454.

104. Lamprecht A, Shafer U, Lehr C. AAPS PharmSciTech 2000;3[1]:article 17.

105. Lemos AF, Rocha JHG, Ventura JM, Ferreira JMF. Method for Tailoring and Control the Morphology, Size and Porosity of Calcium Phosphate Granules. Key Engineering Materials 2005;284-286:309-312.

106. Lemos AF, Arcos D, Vallet-Regí M, Ferreira JMF. Rietveld analysis and phase evolution with heat treatment temperature of calcium phosphates with different Ca/P ratios. Submitted to J Eur Ceram Soc. 2008.

107. Lemos AF, Arcos D, Vallet-Regí M, Ferreira JMF. Rietveld analysis of magnesium substituted biphasic mixtures and influence of heat treatment temperature on phase evolution. Submitted to J Eur Ceram Soc. 2008a.

108. Lemos AF, Ferreira JMF. Colloidal Processing and Mechanical Performance of Biological-like Calcium Phosphates Ceramics. Submited to J Amer Ceram Soc. 2008c.

109. Lemos AF, Vallet-Regí M, Ferreira JMF. Biological-like calcium phosphates - Rietveld analysis and phase evolution with heat treatment temperature. Submitted to J Eur Ceram Soc. 2008b.

110. Rodríguez-Lorenzo LM, Vallet-Regí M, Ferreira JMF. Colloidal processing of hydroxyapatite. Biomaterials 2001;22:1847-1852.

111. Rodríguez-Lorenzo LM, Vallet-Regí M, Ferreira JMF. Fabrication of porous hydroxyapatite bodies by a new direct consolidation method: Starch consolidation. J Biomed Mater Res 2002;60:232-240.

112. Milosevski M, Bossert J, Milosevski D, Gruevska N. Preparation and properties of dense and porous calcium phosphate. Ceram Int 1999;25(8):693-696.

113. Tian J, Tian J. Preparation of porous hydroxyapatite. J Mater Sci 2001;36(12):3061- 3066.

114. Ramay HR, Zhang MQ. Preparation of porous hydroxyapatite scaffolds by combination of the gel-casting and polymer sponge methods. Biomaterials 2003;24(19):3293-3302.

115. Ramay HRR, Zhang M. Biphasic calcium phosphate nanocomposite porous scaffolds for load-bearing bone tissue engineering. Biomaterials 2004;25(21):5171-5180.

116. Gibson LJ. The mechanical behaviour of cancellous bone. J Biomech. 1985;18[5]:317-28.

117. Charriere E, Lemaitre J & Zysset P. Hydroxyapatite cement scaffolds with controlled macroporosity: fabrication protocol and mechanical properties. Biomaterials 2003;24[5]:809-817.

118. Kawata M, Uchida H, Itatani K, Okada I, Koda S, Aizawa M. Development of porous ceramics with well-controlled porosities and pore sizes from apatite fibers and their evaluations. J Mater Sci Mater Med 2004;15[7]:817-823.

119. Ioku K, Yanagisawa K, Yamasaki N, Kurosawa H, Shibuya K & Yokozeki H. Preparation and characterization of porous apatite ceramics coated with beta-tricalcium phosphate. Biomed Mater Eng 1993;3[3]:137-145.

120. Landi E, Celotti G, Logroscino G & Tampieri A. Carbonated hydroxyapatite as bone substitute. J Eur Ceram Soc 2003;23[15]:2931-2937.

121. Ota Y, Kasuga T & Abe Y. Preparation and compressive strength behaviour of porous ceramics with beta-Ca(PO3)(2) fiber skeletons. J Am Ceram Soc 1997;80[1]:225-231.

122. Sous M, Bareille R, Rouais F, Clement D, Amedee J & Dupuy B. Cellular biocompatibility and resistance to compression of macroporous beta-tricalcium phosphate ceramics. Biomaterials 1998;19(23):2147-2153.

123. Pilliar RM, Filiaggi MJ, Wells JD, Grynpas MD, Kandel RA. Porous calcium polyphosphate scaffolds for bone substitute applications - in vitro characterization. Biomaterials 2001;22[9]:963-972.

124. Barralet JE, Grover L, Gaunt T, Wright AJ & Gibson IR. Preparation of macroporouscalcium phosphate cement tissue engineering scaffold. Biomaterials 2002;23[15]:3063-3072.

125. Tancred DC, McCormack BAO, Carr AJ. A synthetic bone implant macroscopically identical to cancellous bone. Biomaterials 1998;19[24]:2303-2311.

126. Jian Dong HK, Toshimasa U, Masanori K, Tetsuya T & JunzoT. In vivo evaluation of a novel porous hydroxyapatite to sustain osteogenesis of transplanted bone marrow-derived osteoblastic cells. J Biomed Mater Res 2001;57[2]:208-216.

127. Chu T-MG, Orton DG, Hollister SJ, Feinberg SE & Halloran JW. Mechanical and in vivo performance of hydroxyapatite implants with controlled architectures. Biomaterials 2002;23[5]:1283-1293.

128. Liu D. Influence of Porosity and Pore Size on the Compressive Strength of Porous Hydroxyapatite Ceramic. Ceram Int 1997;23: 135-139

129. del Real RP, Wolke JGC, Vallet-Regi M, Jansen JA. A new method to produce macropores in calcium phosphate cements. Biomaterials 2002;23(17):3673-3680.

130. Almirall A, Larrecq G, Delgado JA, Martinez S, Planell JA, Ginebra MP. Fabrication of low temperature macroporous hydroxyapatite scaffolds by foaming and hydrolysis of an alpha-TCP paste. Biomaterials 2004;25(17):3671-3680.

Chapter 5

Preparation Route and Physicochemical Characterisation of Bone-Like Hydroxyapatite/PLGA Hybrid Materials for Bone Regeneration

Alexandra F. Lemos, [a,b,c] José D. Santos[b,c] and José M. F. Ferreira[a]

a Dept. of Ceramics and Glass Engineering, University of Aveiro, CICECO, 3810-193 Aveiro, Portugal.

b Dept. of Metalurgic and Materials Engineering, Engineering Faculty of the University of Porto, Rua Dr. Roberto Frias, 4200-465 Porto, Portugal.

c Institute of Biomedical Engineering, University of Porto, Rua do Campo Alegre 823, 4150-180 Porto, Portugal.

Abstract

Bone-like hydroxyapatite (BL-HA) / poly(D,L-lactide-*co*-glycolide) (PLGA) hybrid materials have been developed using γ -methacryloxypropyltrimethoxy- silane (γ –MPS) as silane-coupling agent between the inorganic and organic phases for controlled drug delivery applications.

Silanization showed to be more effective when a modified polar solvent method (mP method) was used, due to a chemical interaction between BL-HA and the silane film, while by using a non-polar solvent (nP method), a much thinner film was achieved.

Functional groups of PLGA, such as the carbonyl group (C=O), were identified using Raman and FTIR-ATR analysis and therefore these groups may be used to link therapeutic molecules. These novel hybrid materials prepared by combining silanization and *post*-hybridisation processes are expected to find use in medical applications of bone regeneration and as drug delivery carrier for therapeutic molecules.

Introduction

Materials that can be found in the nature are the consequence of millions of years of continuous evolution. These materials are morphologically very complex, being the bone tissue a perfect example, and poses huge technical challenges for those who try to replicate their unique behaviour. Unfortunately, bone, as many other tissues, may require temporary or permanent substitution in disease or traumatic situations. For such cases, synthetic bone-graft materials that reproduce, up to a certain extent, the whole

range of bone properties are of great medical interest. With the advances of tissue engineering, the scientific and technological basis for the substitution of damaged or deteriorated tissues by fully functional and compatible living equivalents are being launched. This will gradually reduce, in the coming years, the search for the new synthetic materials for pure tissue substitution. Until the proper development and clinical introduction of such technology and the lack of better alternatives, synthetic bone substitutes can play a major role as biocompatible materials to be used in prosthesis, fracture fixation devices or other bone replacement applications.

In order to do not compromise the bone growth or the tissue healing, it is crucial to replicate the mechanical behaviour in materials for bone replacement and fixation.

The biocompatibility of hydroxyapatite (HA) makes it very attractive for biomedical applications, including orthopedics,[1-4] dentistry,[5-6] and as a coating on metallic prostheses,[7,8] because it can develop a mechanically tight bond with bone.[9] Unfortunately, HA monoliths are brittle, have low tensile strengths, low resistance to impact loading, and tend to fail when subjected to repeated loading.[10,11] Thus, although the chemical composition of HA makes it osteoconductive, its mechanical properties make it less appropriate to serve in load-bearing applications.

Polylactic acid (PLA) and its copolymers with glycolic acid (PLGA) have received considerable attention because of their biocompatible[12,13] and resorbable character.[14-16] They degrade to nontoxic products in the physiological environment. They have been used as suture material, in the reconstruction of bone, and drug carrier systems.[17-19] However, they are too flexible and too weak to meet the mechanical demands in many weight-bearing applications.[20] Another disadvantage of these polymers is that they degrade to acidic products, which may accelerate degradation rates and induce a local inflammatory reaction at the implantation site.[21] There are incidences of these inflammatory reactions and bone resorption in some clinical applications of polyglycolic acid (PGA) or PLGA fracture fixation devices.[22,23] By changing the lactide/ glycolide ratio value, the polymer degradation may be controlled [24] and adjusted to new bone formation rate,[25] and the release of proteins and therapeutic molecules may also be controlled.[26]

Because of these limitations, there is growing interest in the development of ceramic-biodegradable polymer composites for use in bone repair.[27-31] A suitable synthetic composite implant may achieve properties, which cannot be attained in either of the component materials. Ideally, such a composite would combine the bone-bonding

potential of HA with the dynamic mechanical properties of the polymeric component. The selection of biodegradable polymer provides time-varying mechanical properties to avoid stress shielding and ensures dissolution of the implant. This eliminates long-term biocompatibility concerns and subsequent surgical intervention. Further, the presence of a biodegradable component provides a superior way to achieve complete bone reconstruction by progressive replacement of the prostheses by its biodegradation.

However, there is a problem with the hybrid materials, which can loose strength rapidly at the inorganic-organic interface if the two phases are not bound together when exposed to an aqueous physiological environment.[32] The mechanical behaviour of hybrid structures describes the type of interaction between the two phases, and if there is no binding, either physical or chemical, there is a premature failure of the hybrid materials.[33] In order to enhance the hybrid materials integrity, studies have been done based on the modification of the surface of inorganic materials by adding a coupling agent, such as organofunctional silanes,[34-36] which showed to be effective in the improvement of the adhesion between mineral substrate and polymer matrix.[37-39]

Surface modification of the calcium phosphates with a silane coupling agent has been considered as an important attempt to chemically link this inorganic phase and PLGA via the terminal reactive groups in the organofunctional silanes. These novel calcium phosphates/PLGA hybrid materials may be used as drug delivery systems with controlled degradation rate and therefore will greatly enlarge the fields of medical applications of calcium phosphates.

In this work, calcium phosphates/PLGA hybrid materials were prepared and physicochemical characterized using X-ray photoelectron spectroscopy (XPS), X-ray diffraction (XRD), Fourier transform infra-red attenuated total reflectance (FTIR-ATR), Raman spectroscopy and scanning electron microscopy (SEM- EDX).

Materials and methods

Preparation of inorganic materials

The synthesis of the calcium phosphate powders was carried out in a fully automated apparatus (capacity = 6 litres) with specific device to control the stirring of suspensions, the addition rate of reactants and the temperature of the system. Calcium nitrate tetrahydrate [$Ca(NO_3)_2.4H_2O$, Aldrich-Germany], diammonium hydrogen phosphate [$(NH_4)_2HPO_4$, Aldrich-Germany], sodium nitrate [$NaNO_3$, Aldrich-Germany], magnesium nitrate hexahydrate [$Mg(NO_3)_2.6H_2O$, Merck], potassium nitrate [KNO_3,

Merck], ammonium chloride [NH_4Cl, Merck] and ammonium fluoride [NH_4F, Merck] were used as starting chemical precursors for the synthesis. Two different types of compositions were attempted to form pure HA and a biphasic calcium phosphates with co-substituted elements. The solution concentrations of precursors are detailed in Table 1. In the case of biphasic calcium phosphates with co-substituted elements, BL-HA2, a mixture of $(NH_4)_2HPO_4$, NH_4F and NH_4Cl solutions was added slowly at a rate of 50 $ml.min^{-1}$ to the solution mixture containing nitrates of Ca, Na, Mg and K stirred at a rate of 1000 rpm. After the addition of all the precursors, the pH value of the mixture was found to be around 4. The pH of the mixed solution was then increased to 9 by the addition of 8 M ammonium hydroxide (NH_4OH) solution. After the completion of addition, the reaction was performed at 90°C for 2 hours under a constant stirring rate of 1000 rpm. The precipitated suspensions were separated through vacuum filtration and dried at 80°C overnight. The precipitates were washed and filtered repeatedly with de-ionized water. The dried cakes were ground to fine powders, sieved through a mesh size of 200 μm and calcined at 1100ºC. The calcined powders were then dry milled for 15 min in a high energetic ball milling to achieve a mean particle size of around 1.5 μm (measured in a particle size analyser COULTER LS230, UK, with Fraunhofer optical model). A stock suspension of each powder was prepared with 55-vol.% solids loading and stabilised using the previously determined amount of Targon 1128 (BK Ladenburg, Germany),[40] according to the procedure described. In order to obtain good compaction during pressing, 3 wt.% of Mowilith DM 2 HB (Clariant, Spain) and 1.5 wt.% of PEG200 (Aldrich, Germany) (based on the dry mass of solids) were added to suspensions, respectively binder and plasticizer, and the mixtures let to homogenize for 1 h in a rolling system. The as-prepared suspensions were then granulated by freeze granulation (PowerPro freeze granulator LS-2, Sweden) and the granules dried in a freeze dry system (Labconco, LYPH Lock 4.5) for 72 hours. After complete drying, the granules were pressed in cylinders with 10 mm of diameter by uniaxial pressing (80 MPa). After debinding at 550ºC for 2 hours, the cylinders were sintered at 1250ºC, for 2 hours at a heating rate of $5ºC.min^{-1}$.

Table 1. Concentration of the precursors used in the synthesis of the calcium phosphate samples.

		HA	BL-HA2
Ca/P		1.67	1.67
Elements	**Salt name**		
Ca	**$Ca(NO_3).4H_2O$**	2.00	2.00
P	**$(NH_4)_2HPO_4$**	1.20	1.20
Mg	**$Mg(NO_3)_2.6H_2O$**	-	0.08
Na	**$NaNO_3$**	-	0.10
K	**KNO_3**	-	0.06
Cl	**NH_4Cl**	-	0.10
F	**NH_4F**	-	0.10

Silanization procedure

The silanization solutions were prepared by two different methods, using a non-polar solvent (nP) and a modified polar solvent (mP). A 10 wt.% *γ*-methacryloxypropyltrimethoxy-silane (*γ*-MPS from SIGMA, USA) and 2 wt.% *n*-propylamine in cyclohexane solution was used for the nP method. For the mP method, 10 wt.% *γ*-MPS was dissolved in a 95/5 (V/V) methanol/water solution as previously reported by Davy *et al.*[39] and then the pH of silanization solution was adjusted to 3.5 using a 0.01 M chloridic acid solution. The sintered cylinders were immersed in the silanization solutions and ultrasonically treated for 45 min followed by increasing solution pH to 10.5 using a 25% ammonia solution.[32] The silane-treated specimens were firstly dried at room temperature to improve the stability of the coating, and then subsequently heated under vacuum at 120 ºC for 24 h to obtain the final condensed silane on the surface and washed gently with dichloromethane to remove weakly attached silane molecules.

Preparation of hydrid materials

Hybrid materials were prepared using poly(D,Llactide-*co*-glycolide) (PLGA) with ratio of D,L-lactide to glycolide of 85:15 (Aldrich, USA) and molecular weight ranging from 50,000 to 75,000. Silanized and non-silanized disc samples of calcium phospates were soaked in 1–20 wt.% of PLGA/ethyl lactate solution under ultrasonication, followed by solvent evaporation at room temperature and heat treated at 120 ºC in vacuum for about 8 h. To obtain a uniform coating, post-hybridisation was repeated three times for both dense and granular samples.

Materials characterization

X-ray diffraction analysis was performed on cylindrical samples of calcium phosphates before and after sintering, using a high resolution Rigaku Geigerflex D/Mac, C Series diffractometer with Copper Kα radiation, λ = 1.540596 Å. For data collection, the following parameters were set; 2θ range of 20-60°; 2θ step width of 0.05°; time per step 2s.

Thermogravimetric analysis were performed using a Labsys Setaram TG-DTA/DSC (Caluire, France) themogravimetric analyser on untreated and treated calcium phosphate powders at a heating rate of 10 ºC.min^{-1} between 30 ºC and 900 ºC, under air atmosphere.

Fourier Transformed Infra-Red (FTIR)-ATR analysis was performed using a Bruker IFS 55 spectrophotometer, with a Golden Gate accessory (ATR system of single reflection) (Karlsruhe, Germany). All spectra were recorded in the region of 4000-400 cm^{-1} using a 4 cm^{-1} resolution and 64 scans. The absorption bands in FTIR spectra were identified to confirm the presence of the silane coupling agent on the surface of the calcium phosphate samples.

Laser Raman spectroscopy (NRS-2100, Jasco Co., Tokyo, Japan) measurements were performed at 180º reflection configuration with 514.5 nm line of an Ar^+ laser at 200 mW. The relative atomic percentage of each element on the silane treated materials surface was estimated from the X-ray photoelectron spectra peak areas using a VG-SCIENTIFIC ESCALAB 200A spectrometer. An MgAl*α* radiation operating at 300 W and 15 keV was used. Survey spectra (2–1002 eV) were taken at pass energy of 50 eV. All spectra were referenced to C1s peak adventitious carbon fixed at 285.0 eV. High-resolution spectra of C1s peak, O1s peak, Si2p peak, Ca2p peak, P2p peak and N1s peak at pass energy of 20 eV were taken.

Results and Discussion

This work reports the preparation route of calcium phosphates combined with biodegradable PLGA polymer being these two phases grafted together by silane-coupling agent. Ray *et al.* reported that the biodegrability of the polymeric phase of calcium phosphate/PLGA may be controlled,[41] so this hybrid system has a great potential to be applied as a carrier for controlled drug delivery.

The XRD patterns of the HA and BL-HA2 powders are showed in the Fig.1. HA pattern presents only a mineral phase, hydroxyapatite $Ca_{10}(PO_4)_6(OH)_2$, while in the case of

BL-HA2 pattern, it is possible to assign the peaks correspondents to two different phases, hydroxyapatite and beta-tricalcium phosphate (β-TCP), $Ca_3(PO_4)_2$. Rietveld refinement was performed to determine the proportions of each phase and the contents of 77.67 % HA and 22.33 % β-TCP were found. Due to the presence of TCP phase BL-HA2 dissolves faster than sintered HA and therefore this novel biomaterial has the potential to degrade *in vivo* whilts encouraging simultaneous new bone formation.[42]

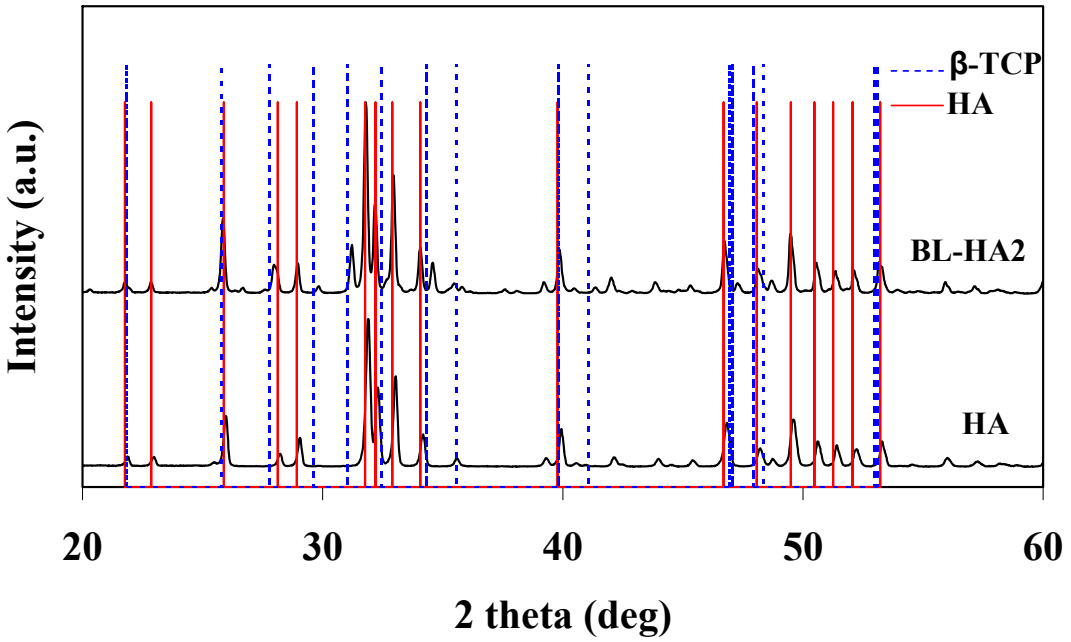

Figure 1. XRD patterns of the samples HA and BL-HA2 (straight line - HA phase, dashed line – β-TCP).

The thermogravimetric (TG) analysis for the samples HA and BL-HA2, silanized by different methods are presented in Fig. 2 and 3, respectively. During the course of heating of the samples, a mass loss could be observed. In both cases, attending to the mass loss, it is possible to conclude that a thinner layer of silane is achieved when using the nP method, and that higher concentration of silane in the starting solution enables the formation of a thicker layer. There was an effective coupling of the PLGA to silane treated surfaces of HA and BL-HA2, as can be observed by the higher mass loss during heating. Once again, and corroborating the results achieved by TG for the silanes, the mP method is more effective in coupling the two phases, inorganic and polymeric.

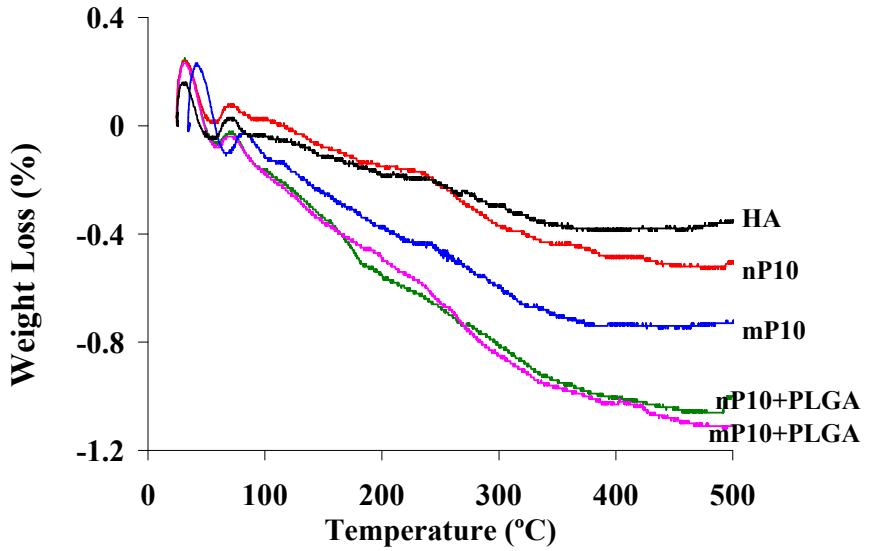

Figure 2. TG plots for HA samples, silanized and silanized and post-hybridized.

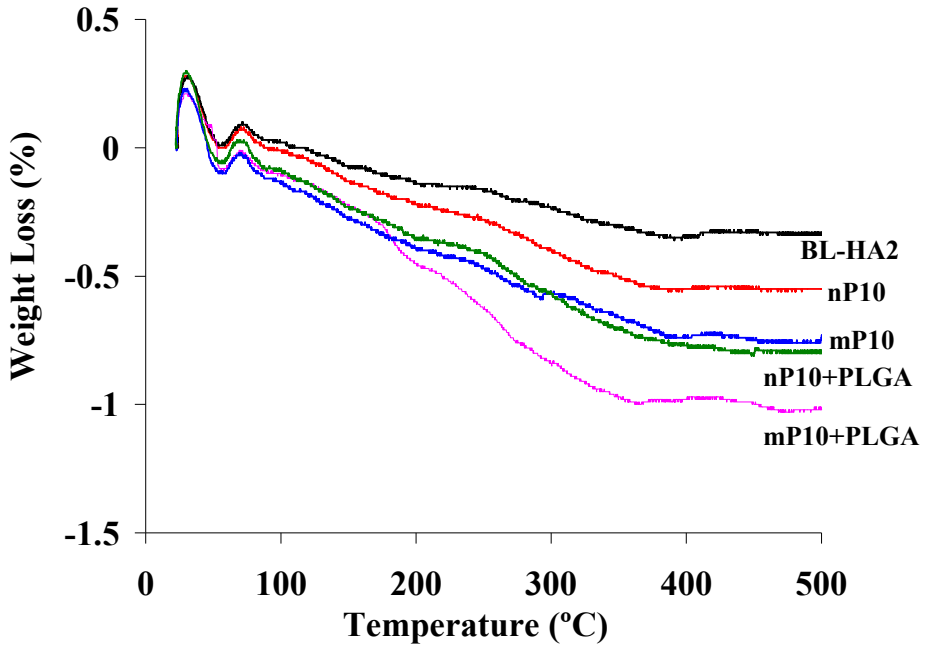

Figure 3. TG plots for BL-HA2 samples, silanized and silanized and post-hybridized.

The silane treatment was successfully performed on sintered HA samples, as it was clearly identified by silane-carbonyl (C=O groups) bands at 1726–1728 cm^{-1} for non-polar (nP) and modified polar (mP) methods presented on Fig. 4. The Si-O-Si stretching band at 1039 cm^{-1} and Si-OH band at 913 cm^{-1} also revealed the presence of the silane coating.[43] The Si-O-Si stretching was detected by the presence of a band at 1039 cm^{-1}, as confirmed by Fransen *et al.*,[44] and also one band at 913 cm^{-1} that indicates the

presence of silanols groups (Si-OH), as has been previously reported by Rider *et al.*.[45] The band at 1199 cm^{-1} is assigned to the silane Si-O-CH_3 group.

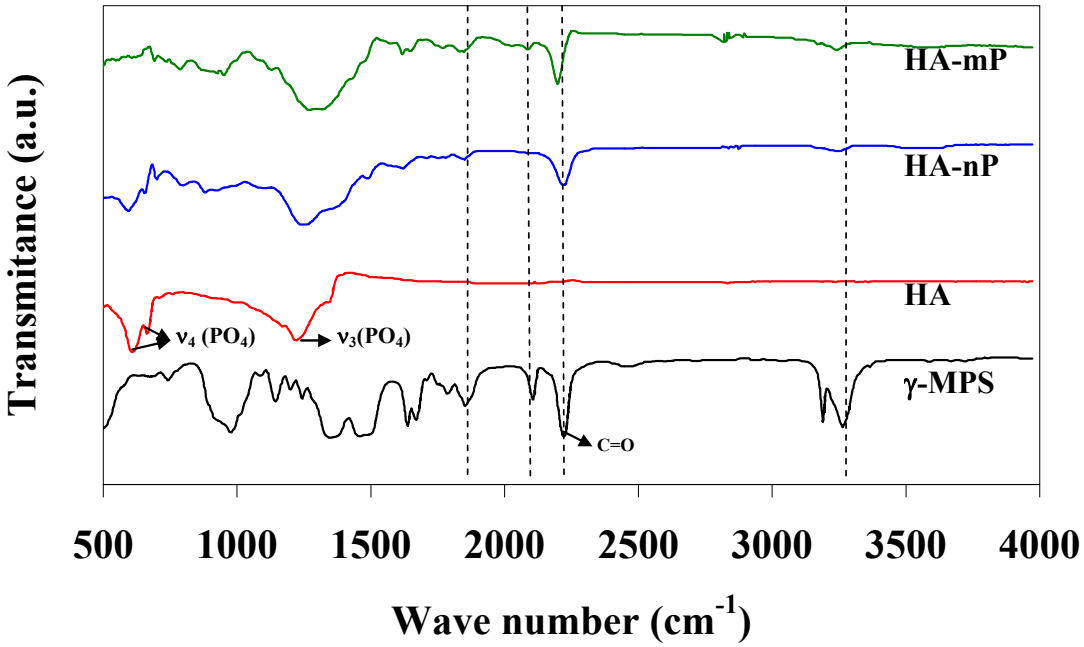

Figure 4. FT-IR spectra for HA samples silanized by different methods.

It is possible to observe an increase in the silane-carbonyl group at 1728 cm^{-1}, when the sintered HA samples were silanized using the mP method, indicating that the silane-film obtained for samples silanized by the mP method is thicker than that obtained by the nP method. The presence of PO_4^{3-} bands at 598 and 559 cm^{-1} can be observed in the HA sample, and that belongs to the HA substrate were detected when using the nP method. This observation is contradictory to previously reported results, which indicated that the silanization is more effective when non-polar solvents are used.[43,46] In the case reported here, the electrostacic interaction between the silane-coupling agent and calcium phosphate substrate is stronger than any other interaction, and that is the reason why mP method is more effective. The same results were obtained for the silane treated BL-HA2 surfaces (not presented here).

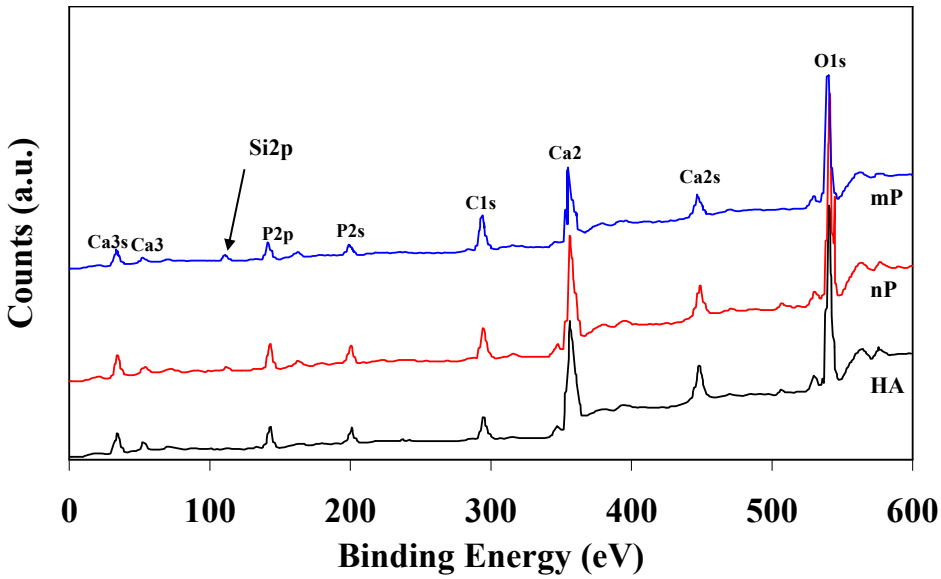

Figure 5. XPS spectra of HA silanized by solvent evaporation method using a 10 wt.% γ -MPS solution showing the appearance of most significant peaks Si2p, C1s, O1s, Ca2p (2p3 and 2p1), P2p.

The chemical composition and bonding state of the silane thin-film on HA and BL-HA2 treated with nP and mP methods were investigated by XPS. The XPS survey scan spectra revealed the presence of Si atoms on the HA and BL-HA2 surface both for nP and mP methods (Figs. 5 and 6) which were identified by Si2p band in all spectra with a binding energy of ~102 eV.

XPS quantification of the total relative atomic ratio of Si on the outermost layer was based on peak areas and results of 3.71% for nP method and 4.78% for mP method, for HA, and of 7.13% for nP method and 8.05% for mP method, for BL-HA2 were obtained. These clearly indicated that the mP method was more effective in grafting Si-based groups on the surface of calcium phosphates thus providing a method to prepare a more stable interface to link an organic phase or/and to control the degradation rate of the hydrid.

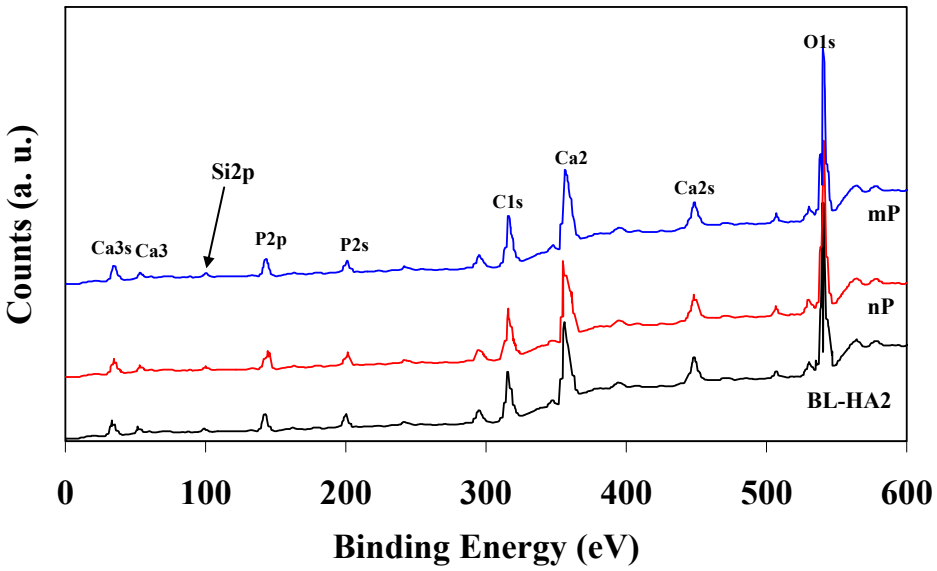

Figure 6. XPS spectra of BL-HA2 silanized by solvent evaporation method using a 10 wt.% γ -MPS solution showing the appearance of most significant peaks Si2p, C1s, O1s, Ca2p (2p3 and 2p1), P2p.

The aim of the present study was to use a silane-coupling agent to adhere a coating of PLGA to the surface of calcium phosphates. The modification proposed in silanization process consisted in controlling the rate of silane condensation by adjusting the pH of silanization solution and therefore eliminating the Si-O-CH3 groups.

PLGA coating was performed on BL-HA2 surface to develop the hybrid structures using *post*-hybridisation methods (Fig. 7). Raman analysis revealed the presence of one band at ~1740 cm^{-1} attributed to C=O stretching vibration of the carbonyl group and another at 1100 cm^{-1} due to C-O-C ether group, which clearly indicate that the PLGA coating was covering the BL-HA2 surface. A sharp and dominant band at 960 cm^{-1} was observed, which accounts for the presence of PO_4^{3-} groups of the BL-HA2 substrate. Additionally, PO_4^{3-} symmetric and antisymmetric stretching modes were also observed at 1080 and 1040 cm^{-1}.

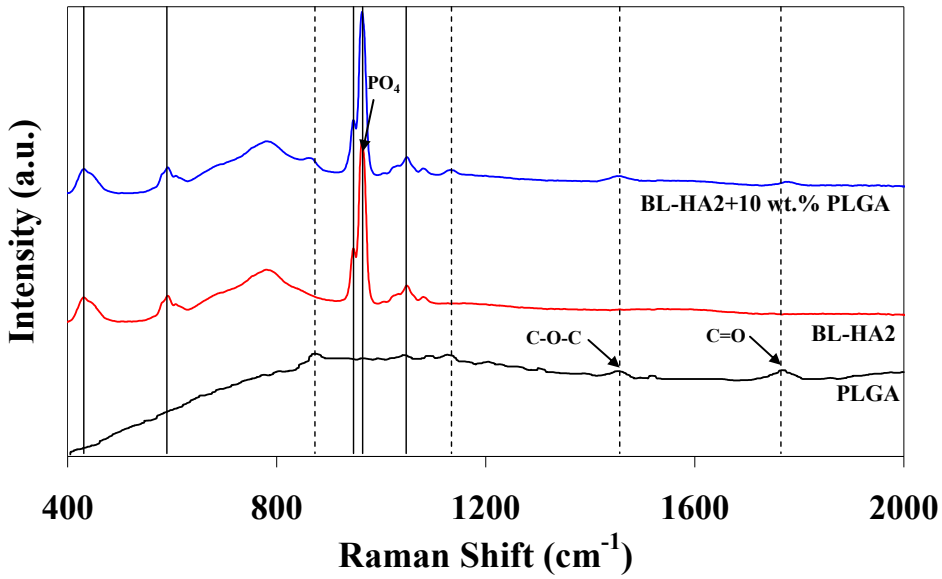

Figure 7. Raman spectra of BL-HA2 surface treated with 10 wt.% of PLGA/ethyl lactate solution using the solvent evaporation method.

FTIR-ATR studies (Fig. 8) corroborate the data presented in Fig. 7 which shows that the PLGA coating could be grafted to silanized BL-HA2 surface, as observed by the presence of bands at 1748 cm^{-1}, attributed to carbonyl group (C=O) stretching vibration, to ether (C-O-C) group at 1082 cm^{-1} and to the group C-H(CH_3) at ~1453 and 1348 cm^{-1}(Fig. 8).[47-50] The decrease in the intensity of PO_4^{3-} bands at 998, 599 and 551 cm^{-1} is also indicative of the availability of both the PLGA and the silane-coupling agent on BL-HA2 surface. For silanized BL-HA2 the decrease in the intensity of C=O band at 1748 cm^{-1} and the appearance of the PO_4^{3-} bands demonstrated that a thin PLGA coating was obtained. The observation of a band near 1603 cm^{-1} should reflect the linking between PLGA and the silane coating through the alcoholic oxygen atom of the ester group. [43]

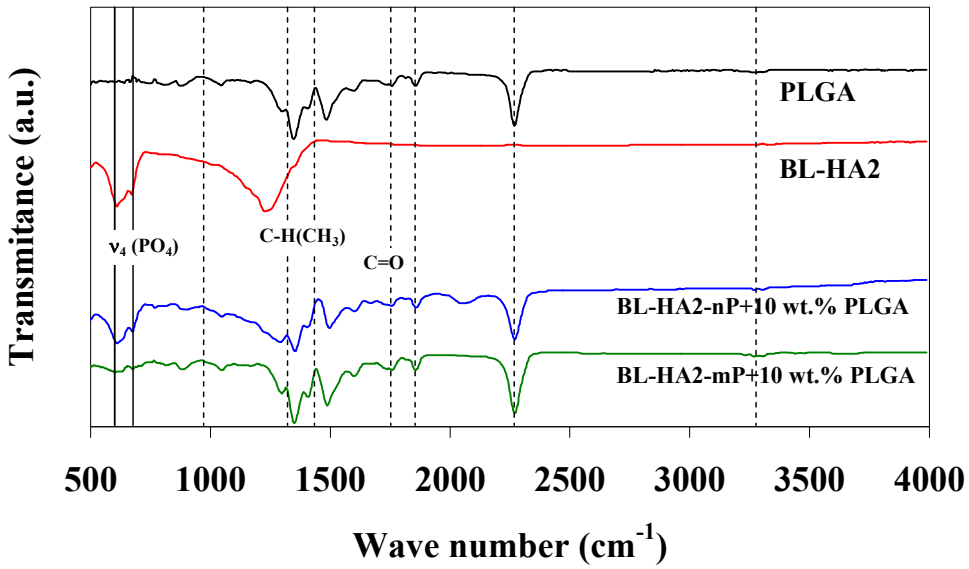

Figure 8. FTIR-ATR spectroscopic results of BL-HA2 surface treatment.

The work that has been performed clearly demonstrated that carbonyl functional groups from PLGA are present after the hybridisation of silanized BL-HA2, which indicates that these groups are available to link therapeutic molecules and therefore BL-HA2/PLGA hybrid materials have good potential to be used as drug delivery carrier.

Conclusions

Silanization of HA and BL-HA2 materials has been successfully obtained using γ -MPS as a coupling agent. In the present work, we concluded that an electrostatic/chemical interaction between the silane-coupling agent and BL-HA2 surface has been achieved more effectively by means of silanization using a modified polar method. Chemical interactions between the silane-coupling agent and PLGA phase seems to occur, as confirmed by the presence of C=C groups conjugated with C=C or in a C=O ambient detected by FTIR-ATR analysis.

These novel BL-HA2/PLGA hybrid materials may find use for bone regeneration applications with simultaneous local delivery of therapeutic molecules.

References

1. Jarcho M. Calcium phosphate ceramics as hard tissue prosthetics. Clin Orthop 1981;157:259–278.

2. Heimke G. Advanced ceramics for biomedical applications. Angew Chem 1989;28:111–116.

3. Wagner JR. Clinical and histological case study using resorbable hydroxyapatite for the repair of osseous defects prior to endosseous implant surgery. J Oral Implantol 1989;15:186–192.

4. LeGeros RZ & Daculsi G. *In vivo* transformation of biphasic calcium phosphate ceramics: Ultrastructural and physicochemical characterizations. In: Yamamura N, Hench L, Wilson–Hench J, editors. Handbook of bioactive ceramics. Vol. II: Calcium phosphate ceramics. Boca Raton, FL: CRC Press; 1990. p 17–28.

5. Aoki H, Kato K, Ogiso M & Tabata T. Studies on the application of apatite to dental materials. J Dent Eng 1977;18:86–89.

6. Hosaka N & Nagata T. Evaluation of a new dense-porous hydroxylapatite endosteal dental implant. J Oral Maxillofac Surg 1987;45:583–593.

7. de Groot K. Hydroxylapatite coatings for implants in surgery. In: Vincenzini P, editor. High tech ceramics. Amsterdam: Elsevier Science Publishers; 1987. p 381–386.

8. Ducheyne P, Radin S, Heughebaert M & Heughebaert JC. Calcium phosphate ceramics coatings on porous titanium: Effect of structure and composition on electrophoretic deposition, vacuum sintering and *in vitro* dissolution. Biomaterials 1990;11:244–253.

9. Jarcho M, Kay JF, Gumaer KI, Doremus RH & Drobeck HP. Tissue, cellular and subcellular events at a bone ceramic hydroxylapatite interface. J Bioeng 1977;1:79–92.

10. Jarcho M, Bolen CH, Thomas MB, Bobick J, Kay JF & Doremus RH. Hydroxylapatite synthesis and characterization in dense polycrystalline form. J Mater Sci 1976;11:2027–2035.

11. Akao M, Aoki H & Kato K. Mechanical properties of sintered hydroxyapatite for prosthetic applications. J Mater Sci 1981;16:809–812.

12. Nelson JF, Stanford HG & Cutright DE. Evaluation and comparisons of biodegradable substances as osteogenic agents. Oral Surg 1977;43:836–844.

13. Hollinger JO. Preliminary report on the osteogenic potential of biodegradable copolymer of polylactide (PLA) and polyglycolide (PGA). J Biomed Mater Res 1983;17:71–82.

14. Cutright DE, Perez B, Beasley JD, Larson WJ & Posey WR. Degradation rates of polymers and copolymers of polylactic and polyglycolic acids. Oral Surg Oral Med Oral Pathol 1974;37:142–152.

15. Miller RA, Brady JM & Cutright DE. Degradation rates of oral resorbable implants (polylactates and polyglycolates): Rate modification with changes in PLA/PGA copolymer ratios. J Biomed Mater Res 1977;11:711–719.

16. Vert M, Christel P, Chobat F & Leray J. Bioresorbable plastic materials for bone surgery. In: Hastings GW, Ducheyne P, editors. Macromolecular biomaterials. Boca Raton, FL: CRC Press; 1984. p 120–142.

17. Kulkarni RK, Pani KC, Neuman C & Leonard F. Polylactic acid for surgical implants. Arch Surg 1966;93:839–843.

18. Cutright DE, Hunsuck EE & Beasley JD. Fracture reduction using a biodegradable material, polylactic acid. J Oral Surg 1971; 29:393–397.

19. Gombotz WR & Pettit DK. Biodegradable polymers for protein and peptide drug delivery. Bioconjug Chem 1995;6:332–351.

20. Daniels AU, Chang MK & Andrianoa K. Mechanical properties of biodegradable polymers and composites proposed for internal fixation of bone. J Appl Biomater 1990;1:57–78.

21. Vert M, Mauduit J & Li S. Biodegradation of PLA/GA polymers: Increasing complexity. Biomaterials 1994;15:1209–1213.

22. Bostman O, Hirvensalo E, Makinen J & Rokkanen P. Foreignbody reactions to fracture fixation implants of biodegradable synthetic polymers. J Bone Joint Surg 1990;72B:592–596.

23. Bostman O, Hirvensalo E, Vainionpaa S, Makela A, Vihtonen K, Tormala P & Rokkanen P. Ankle fractures treated using biodegradable internal fixation. Clin Orthop 1989;238:195–203.

24. Mikos AG & Temenof JS. Formation of highly porous biodegradable scaffolds for tissue engineering. Electr J Biotechn 2000;3[2]:114-119.

25. Laurencin CT, Attawia MA, Lu LQ, Borden D, Lu HH, Gorum WJ & Ieberman JR. Poly(lactide-co-glycolide)/hydroxyapatite delivery of BMP-2-producing cells: a regional gene therapy approach to bone regeneration. Biomaterials 2001;22:1271-1277.

26. Takenaga M, Yamaguchi Y, Kitagawa A, Gawa Y, Mizushima Y & Igarashi R. A novel sustained-release formulation of insulin with dramatic reduction in initial rapid release. J Contr Rel 2002;79[1-3]:81-91.

27. Higashi S, Yamamuro T, Nakamura T, Ikada Y, Hyon SH & Jamshidi K. Polymer-hydroxyapatite composites for biodegradable bone fillers. Biomaterials 1986;7:183–187.

28. Verheyen CC, de Wijn JR, van Blitterswijk CA & de Groot K. Evaluation of hydroxylapatite/poly(L-lactide) composites: Mechanical behaviour. J Biomed Mater Res 1992;26:1277–1296.

29. Kikuchi M, Suetsugu Y, Tanaka J & Akao M. Preparation and mechanical properties of calcium phosphate/copoly-L-lactide composites. J Mater Sci Mater Med 1997;8:361–364.

30. Devin JE, Attawia MA & Laurencin CT. Three-dimensional degradable porous polymer-ceramic matrices for use in bone repair. J Biomater Sci Polym Ed 1996;7:661–699.

31. Thomson RC, Yaszemski MJ, Powers JM & Mikos AG. Hydroxyapatite fiber reinforced poly a-hydroxy ester foams for bone regeneration. Biomaterials 1998;19:1935–1943.

32. Dupraz AMP, De Wijn JR, Van De Meer SAT & de Groot K. Characterization of silane-treated hydroxyapatite powders for use as filler in biodegradable composites. J Biomed Mater Res 1996;30[2]:231-238.

33. Sheldon RP. Composite Polymeric Materials. Appl Sci Publ 1982; 1**:** 1.

34. Zhu PX, Ishikawa M, Seo WS, Hozumi A, Yokogawa Y & Koumoto K. Nucleation and growth of hydroxyapatite on an amino organosilane overlayer. J Biomed Mater Res 2002;59[2]:294-304.

35. Hooshmand T, Van Noort R & Keshvad A. Bond durability of the resin-bonded and silane treated ceramic surface. Dent Mater 2002;18[2]:179.

36. Venhoven BAM, De Gee AJ, Werner A & Davidson CL. Silane treatment of filler and composite blending in a one-step procedure for dental restoratives. Biomaterials 1994;15;1152-1156.

37. Yerby SA, Paal AF, Young PM, Beaupré GS, Ohashi KL & Goodman SB. The effect of a silane coupling agent on the bond strength of bone cement and cobalt-chrome alloy. J Biomed Mater Res 2000;49[1]:127-133.

38. Wang M & Bonfield W. Chemically coupled hydroxyapatite–polyethylene composites: structure and properties. Biomaterials 2001;22:1311-1320.

39. Santos C, Luklinska ZB, Clarke RL & Davy KWM. Hydroxyapatite as a filler for dental composite materials: mechanical properties and in vitro bioactivity of composites. J Mater Sci: Mat Med 2001;12:565.

40. Lemos AF & Ferreira JMF. Colloidal Processing and Mechanical Performance of Biological-like Calcium Phosphates Ceramics. Submitted to J Am Ceram Soc 2008.

41. Agrawal CM & Ray RB. Biodegradable polymeric scaffolds for musculoskeletal tissue engineering. J Biomed Mater Res 2001;55:141-150.

42. Afonso A, Santos JD, Vasconcelos M, Branco R & Cavalheiro J. Granules of osteopatite and glass-reinforced hydroxyapatite implanted in rabbit tibiae J Mater Sci: Mater. Med 1996;7[8]:507-510.

43. Oliveira JM, Miyazaki T, Lopes MA, Ohtsuki C & Santos JD. Bonelike®/PLGA hybrid materials for bone regeneration: Preparation route and physicochemical characterisation. J of Mater Sci: Mater in Med 2005;16**:**253– 259.

44. Hoffman R, Westheim JGF, Pouwel I, Fransen T & Gellings PJ. FTIR and XPS Studies on Corrosion-resistant SiO2 Coatings as a Function of the Humidity during Deposition. Surf Interf Anal 1996;24**:**1-6.

45. Rider AN & Arnott DR. Durability of Bonds Formed Between Epoxy Adhesive and Aluminium Alloy Treated with Phosphonate Inhibitors. Surf Interf Anal 1996;24**:**583-590.

46. Santos C, Luklinska ZB, Clarke RL & Davy KWM. Hydroxyapatite as a filler for dental composite materials: mechanical properties and in vitro bioactivity of composites J Mater Sci: Mat Med 2001;12[7]:565-573.

47. Fowler BO, Moreno EC & Brown WE. Infrared spectra of hydroxyapatite octacalcium phosphate and pyrolyzed octacalcium phosphate Arch Oral Biol 1966;11:477–492.

48. Kister G, Cassanas G, Vert M, Pauvert B & Terol A. Vibrational analysis of poly(L-lactic acid). J Raman Spectrosc 1995;26:307– 311.

49. LeGeros RZ, Daculsi G, Orly I, Abergas T & Torres W. Solution-mediated transformation of OCP to apatite. Scan Microsc 1989; 3:129–138.

50. Durucan C, Brown PW. Low temperature formation of calcium-deficient hydroxyapatite-PLA/PLGA composites. J Biomed Mater Res 2000:51;717–725.

Chapter 6

Osteoblast Response to Macroporous Biological-Like Apatites and Biological-Like Apatites/PLGA Hybrid Composites

Alexandra F. Lemos,[a,b,c] Carolina B. Machado,[d] Patrícia Valério,[d] Alfredo M. Goes[d] and José M. F. Ferreira[a]

a Dept. of Ceramics and Glass Engineering, University of Aveiro, CICECO, 3810-193 Aveiro, Portugal.

b Dept. of Metalurgic and Materials Engineering, Engineering Faculty of the University of Porto, Rua Dr. Roberto Frias, 4200-465 Porto, Portugal.

c Institute of Biomedical Engineering, University of Porto, Rua do Campo Alegre 823, 4150-180 Porto, Portugal.

d Department of Physiology and Biophysics, Federal University of Minas Gerais, Av. Antonio Carlos 6627 Belo Horizonte, 31270–901 Minas Gerais, Brazil.

Abstract

Macroporous structures were developed in this work to be used as scaffolds for bone tissue engineering applications. These macroporous scaffolds were prepared trough a method that combines in a suitable way the foaming and the starch consolidation methods. The hybrid materials were obtained by post-hybridization with poly(D,Llactide-*co*-glycolide) (PLGA) of silanized macroporous samples.

The macroporous structures were tested in osteoblast cultures to evaluate proliferation, collagen and alkaline phosphatase production. Osteoblast proliferation was higher in the presence of all tested samples when compared to pure hydroxyapatite. Collagen secretion and alkaline phosphatase production also showed an increase tendency. Under optical microscopy, viable osteoblasts could be seen on the culture and attached to the samples, showing that the produced structures are promising materials for bone repair, providing a good environment for proliferation of osteoblasts, without impairment of their secretion capabilities.

Introduction

Bioactive ceramics have been developed over the last decades and the accomplishments in the field of biomaterial applications have attracted wide attention. The development of bioceramics has provided promising alternatives to healing, replacing or augmenting parts of the skeletal system. There are many principles that may be observed when testing a specific bioceramic. It may not be toxic or immunogenic, may allow or induce neoformation of the surrounding tissues and it should not inhibit the re-establishment of the normal function.[1] Bioceramics have been used experimentally and clinically for filling bone defects, and they have been shown to bond within days to bone and to stimulate osteogenesis.[2,3] Their composition, crystallinity, particle size and porosity are characteristics that influence their dissolution rate and affect their material–tissue interaction.[4] However, the mechanisms whereby this interaction occurs still need more investigation.

Calcium phosphate materials have been widely used as bone substitutes in dentistry as well as orthopaedic and reconstructive surgery.[5-10] This group of materials exhibits a high level of biocompatibility and osteoconductivity, and binds directly to bone tissues. Of the various calcium phosphates, hydroxyapatite (HA) has received considerable attention because its mineral composition is close to that of natural bone. However, HA is less soluble than other calcium phosphates such as tricalcium phosphate (TCP), and consequently remains in the body longer and impedes new bone replacement.[11,12]

Because of these limitations, there is growing interest in the development of ceramic-biodegradable polymer composites for use in bone repair.[13-17] A suitable synthetic composite implant may achieve properties, which cannot be attained in either of the component materials. Ideally, such a hybrid would combine the bone-bonding potential of HA with the dynamic mechanical properties of the polymeric component.

Considering that osteoblasts are the cells that support the formation, secretion and mineralization of extracellular bone matrix, in this work we investigate the behaviour of these cells in the presence of biological-like hydroxyapatites and biological-like hydroxyapatites/PLGA hybrid composite materials. It was analyzed the effect of calcium phosphates on cellular viability, collagen secretion, alkaline phosphatase activity and cell morphology.

Materials and characterization techniques

Materials

In this study three different types of calcium phosphates were used, namely, pure HA, a Mg-substituted biphasic calcium phosphate, Mg-(Ca-def-HA), and a biological-like apatite, BL-HA2, with several co-substituted elements (Na, K, Mg, Cl and F). The synthesis of the calcium phosphate powders was carried out in a fully automated apparatus (capacity = 6 litres) with specific devices to control the stirring of the solution/suspensions, the addition rate of reactants and the temperature of the system. Reagent grade chemical precursors were used for the synthesis, namely, calcium nitrate tetrahydrate [$Ca(NO_3)_2.4H_2O$, Aldrich-Germany], diammonium hydrogen phosphate [$(NH_4)_2HPO_4$, Aldrich-Germany], sodium nitrate [$NaNO_3$, Aldrich-Germany], magnesium nitrate hexahydrate [$Mg(NO_3)_2.6H_2O$, Merck], potassium nitrate [KNO_3, Merck], ammonium chloride [NH_4Cl, Merck] and ammonium fluoride [NH_4F, Merck]. The solution concentrations of precursors are detailed in Table 1.

Table 1. Concentration of the precursors used in the synthesis of the calcium phosphate samples.

		HA	**Mg-(Ca-def-HA)**	**BL-HA2**
Ca/P		1.67	1.62	1.67
Elements	**Salt name**		**molarity**	
Ca	**$Ca(NO_3).4H_2O$**	2.00	1.94	2.00
P	**$(NH_4)_2HPO_4$**	1.20	1.20	1.20
Mg	**$Mg(NO_3)_2.6H_2O$**	-	0.06	0.08
Na	**$NaNO_3$**	-	-	0.10
K	**KNO_3**	-	-	0.06
Cl	**NH_4Cl**	-	-	0.10
F	**NH_4F**	-	-	0.10

In the case of biological-like apatite with several co-substituted elements, a mixture of $(NH_4)_2HPO_4$, NH_4F and NH_4Cl solutions was added slowly at a rate of 50 $ml.min^{-1}$ to the solution mixture containing nitrates of Ca, Na, Mg and K stirred at a rate of 1000 rpm. After the addition of all the precursors, the pH value of the mixture was found to be around 4. The pH of the mixed solution was then increased to 9 by the addition of 8 M ammonium hydroxide (NH_4OH) solution. After the completion of addition, the reaction was performed at 90°C for 2 hours under a constant stirring rate of 1000 rpm. The precipitated suspensions were separated through vacuum filtration and dried at

80°C overnight. The precipitates were washed and filtered repeatedly with de-ionized water. The dried cakes were ground to fine powders, sieved through a mesh size of 200 μm and calcined at 1100ºC. The calcined powders were then dry milled for 15 min in a high energetic ball milling to achieve mean particle sizes of around 1.5 μm.

The as obtained powders were well dispersed in water in the presence of a suitable dispersing agent (Targon 1128, BK Ladenburg, Germany) and the suspension was then used to produce macroporous samples according to a methodology already reported by Lemos *et al*.[18] that combines in a suitable way the foaming and the starch consolidation methods. The all porous structures so obtained were then sintered at 1250ºC for 2 h. In the case of the BL-HA2 sample a higher sintering temperature (1400ºC) was also selected to evaluate the effect of the heat treatment temperature on phase composition and its influence on the osteoblastic response.

Preparation of the composite hybrid materials

The silanization solution was prepared using a modified polar solvent (mP). The mP solvent was prepared by dissolving 10 wt.% *γ*-MPS in a 95/5 (V/V) methanol/water solution as previously reported by Davy *et al.*[19] and then the pH of silanization solution was adjusted to 3.5 using a 0.01 M chloridic acid solution. The macroporous samples were immersed in the silanization solutions and ultrasonically treated for 45 min followed by increasing solution pH to 10.5 using a 25% ammonia solution.[20] The silane-treated specimens were firstly dried at room temperature to improve the stability of the coating, and then subsequently heated under vacuum at 120ºC for 24 h to obtain the final condensed silane on the surface and washed gently with dichloromethane to remove weakly attached silane molecules.

Hybrid materials were prepared using poly(D,Llactide-*co*-glycolide) (PLGA) with ratio of D,L-lactide to glycolide of 85:15 (Aldrich, USA) and molecular weight ranging from 50,000 to 75,000. Silanized macroporous samples of calcium phosphates were soaked in 10 wt.% of PLGA/ethyl lactate solution under ultrasonication, followed by solvent evaporation at room temperature and heat treated at 120ºC in vacuum for about 8 h. To obtain a uniform coating, post-hybridisation was repeated three times.

Characterization techniques

X-ray diffraction analysis was performed on macroporous samples of calcium phosphates after sintering, using a high resolution Rigaku Geigerflex D/Mac, C Series

diffractometer with Copper Kα radiation, λ = 1.540596 Å. For data collection, the following parameters were set; 2θ range of 20-60°; 2θ step width of 0.05°; time per step 2 s.

Infrared spectra were obtained using an infrared Fourier spectrometer (FT-IR, model Mattson Galaxy S-7000, USA). The porous sintered samples were powdered and tested before and after immersion in simulated body fluid (SBF). For this purpose each powder was mixed with KBr in the proportion of 1/150 (by weight) for 15 min and pressed into a pellet using a hand press.

A scanning electron microscope (HITACHI, S-4100, Tokyo, Japan, 25 kV acceleration voltage, beam current 10 μA) was used to analyse the microstructure of the prepared materials surfaces. Specimens were coated with gold using a Quick Coater (UPS-020) before examination. The current was set at 5mA with a coating time of 180 s.

Dissolution tests

The dissolution rates and the possible bioactivity of the calcium phosphates were investigated by immersion of either powders (pulverized from sintered bulk samples) or bulk materials in simulated body fluid (SBF), at 37ºC. In this study a novel SBF formulation was used. This new formulation developed by Cuneyt Tas has an ionic concentration that closely matches more the human plasma than the Kokubo's formulation.[21,22] The ionic concentrations of the SBF solutions and of the human plasma are compared in Table 2.

The most significant differences between this new formulation and the Kokubo's formulation may be summarized as follows:

(a) The nominal, initial HCO_3^- ion concentration of SBF was increased from 4.2 mM[21-28] to 27.0 mM which is exactly the same concentration as that of human plasma;

(b) The Cl^- ion concentration was decreased from 147.8 mM[21-28] to 125.0 mM, approaching more the Cl^- ion concentration of human plasma [103.0 mM].

Table 2. Ionic concentrations of the SBF solutions and of the human plasma (adapted from[19]).

Ion	Kokubo *et al.* (mM)	Cuneyt Tas (mM)	Human Plasma (mM)
Na^+	142.0	142.0	142.0
Cl^-	147.8	125.0	103.0
HCO_3^-	4.2	27.0	27.0
K^+	5.0	5.0	5.0
Mg^{2+}	1.5	1.5	1.5
Ca^{2+}	2.5	2.5	2.5
HPO_4^{2-}	1.0	1.0	1.0
SO_4^{2-}	0.5	0.5	0.5

These significant improvements in Cl^- and HCO_3^- concentrations of SBF are shown to be achievable just by changing the starting chemical $K_2HPO_4.3H_2O$[23-30] to $Na_2HPO_4.2H_2O$ during solution preparation, while keeping all remaining chemicals the same.

Sampling took place at 1 h, 6 h, 12 h, 1 d, 3 d, 7 d, 14 d, and 30 d (h: hours; d: days). The obtained results were independent, which means that each sample was individually treated without interfering with others. An amount of calcium phosphate powder corresponding to 1 m^2 surface area was immersed in 10 ml of filtered (through sterilized filters, cameo 25 AS-MSI, pore size 0.22 μm) SBF solution and immediately sealed into sterilized plastic flasks, which were stored afterwards at 37ºC (±0.1º). After each experiment, the powder was separated from the liquids by filtering. Similar procedure was followed for the bulk materials. In this case, the response of material to the *in vitro* tests in SBF was observed at the surfaces of the pores. The analysis of the liquids comprised the determination of the concentration of Ca^{2+}, Mg^{2+}, B^{3+}, P^{5+}, Si^{4+}, Na^+, and Al^{3+} by inductively coupled plasma-optical emission spectroscopy (ICPOES, Jobin Yvon, JY 70 plus, France). The dried samples were examined by SEM/EDS.

In vitro tests with osteoblasts

For the *in vitro* tests with osteoblasts the following materials were used: Penicillin, streptomycin, fetal bovine serum, Dulbecco's phosphate buffered saline, trypsin-EDTA, [3(4,5 dimethylthiazol-2yl) 2,5 diphenyltetrazoliumbromide] MTT, BCIP-NBT kit: Gibco (Burlington, Ont., Canada). Crude bacterial collagenase: Boehringer (Biberach, Germany). RPMI Cell culture medium: Sigma (St. Louis, USA), SIRCOL kit: Biocolor

(Newtonabbey, N. Ireland) T25 culture flasks and 24 well plates: Nunc products (Naperville, USA).

Osteoblasts were isolated from the calvaria of 1-5 days old neonatal Wistar rats. The calvaria were dissected and freed from soft tissue, cut into small pieces and rinsed in sterile phosphate-buffered saline without calcium and magnesium. The calvaria pieces were incubated with 1% trypsin-EDTA for 5 min, followed by four sequential digestions with 2% collagenase at 37 $^{\circ}$C for 45 minutes each. The supernatant of the first collagenase incubation, which contained a high proportion of periosteal fibroblasts, was discarded. The other digestions produced a suspension of cells with high proportion of preosteoblasts and osteoblasts. After centrifugation at 1000g for 5 min, each pellet were resuspended in 5 ml of RPMI medium supplemented with 10% FBS, 1% antibiotic-antimycotic. The cells were seeded into 25 ml tissue culture flasks, and allowed to grow in a controlled 5% CO_2 95% humidified incubator at 37 ºC. For experiments, only confluent cells from the 2nd passage were used.

Stimulation of osteoblasts with macroporous bodies

In this case there would be osteoblasts were plated at 5 X 10^4 cells.ml^{-1} cell density, and after adhesion, the macroporous samples HA, Mg-(Ca-def-HA), BL-HA2 (previously immersed on culture medium) were gently deposited over the cells. This procedure avoids the hypothesis of cells being carried into the pores due to capillarity action. After 72 hours of incubation, osteoblast morphology, viability and secretion capability were tested. As control, we used cultures without samples and pure hydroxyapatite sample.

Cellular viability

The cellular proliferation and viability in the presence of each macroporous sample was evaluated by MTT assay, based on the reduction of tetrazolium salt to formazan crystals by dehydrogenase present in living cells mitochondria. The formazan salt formation is directly related to the amount of dehydrogenase, providing an indirect measurement of cell proliferation.[32] In total, 60 mL of MTT (5 mg.ml^{-1}) were added to each well. Two hours later, the cell morphology was analysed by inverted optical microscopy and formazan salts were solubilized with SDS 10% HCl. After incubation for 18 h, optical density was measured at 595 nm.[33]

Alkaline phosphatase activity

The alkaline phosphatase production was evaluated by BCIP-NBT assay. This assay is based on a chromagenic reaction initiated by the cleavage of the phosphate group of BCIP by alkaline phosphatase present in the cells. This reaction produces a proton, which reduces NBT to an insoluble purple precipitate. In brief, the supernatant of each well was removed and the cell layer was rinsed twice with PBS. Then, a volume of 200 mL of BCIP-NBT solution, prepared according to manufacturer protocol, was added to each well. After 2 h of incubation, the cells were observed by optical microscopy and the insoluble purple precipitates were solubilized with 210 ml of SDS 10% HCl and incubated for 18 h. The optical density was measured at 595 nm.[34]

Collagen production

The osteoblast collagen production was analysed by SIRCOL assay in the culture's supernatant, following the manufacturer instructions. This method is based on the selective binding property of the syrius-red dye to the [Gly–X–Y] tri-peptide end sequence of mammalian collagen.[35] The collagen present in the supernatant, precipitated by syrius-red, was solubilized and measured by an optical density analysis at 595 nm. The collagen concentration was calculated basing on a linear regression from previously known concentrations of type I collagen and their optical density measurement.

The results are presented as Means±SD (the numbers of the experiments are mentioned in the legend of the figure). The statistical significance was measured by ANOVA and Bonferroni's post-test.

Results and Discussion

The XRD patterns of the powdered samples HA, Mg-(Ca-def-HA) and BL-HA2 sintered at 1250ºC and of the BL-HA2 sintered at 1400ºC, are showed in the Fig. 1.

HA pattern presents a single mineral phase, hydroxyapatite $Ca_{10}(PO_4)_6(OH)_2$, while in the patterns of Mg-(Ca-def-HA) and BL-HA2 sintered at 1250ºC, it is possible to assign peaks of two different phases, hydroxyapatite and beta-tricalcium phosphate (β-TCP), $Ca_3(PO_4)_2$. Increasing the sintering temperature to 1400ºC in the case of BL-HA2 induced the formation of more β-TCP. Rietveld refinement was performed to determine the proportions of each phase and the results are presented in Table 3. Due to the presence of β-TCP phase,

the biphasic macroporous materials dissolve faster than sintered HA and therefore these novel biomaterials have the potential to degrade *in vivo* whilst encouraging simultaneous new bone formation.

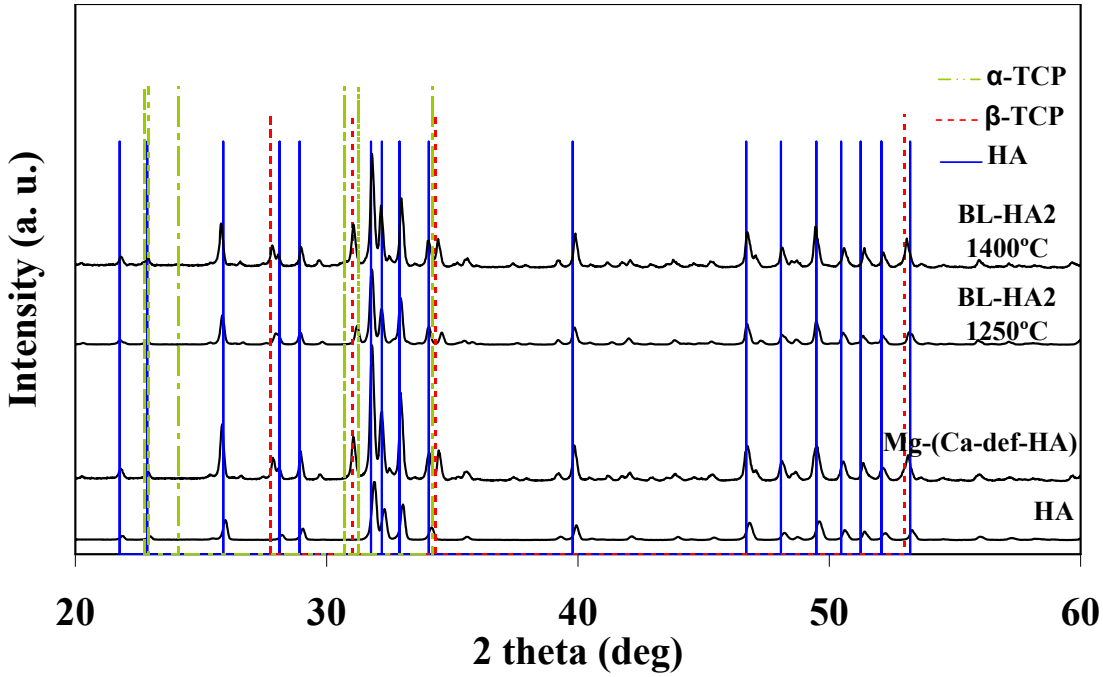

Figure 1. XRD patterns of the samples HA, Mg-(Ca-def-HA), BL-HA2-1 and BL-HA2-1 (straight line - HA phase, dashed line – β-TCP).

Table 3. Rietveld quantification of phase compositions for samples HA, Mg-(Ca-def-HA) and BL-HA2 sintered at 1250ºC and of the BL-HA2 sintered at 1400ºC.

Sample code	Sintering Temperature (ºC)	Wt. % of composition determined by Rietveld quantification	
		HA	β-TCP
HA	1250	100	-
Mg-(Ca-def-HA)	1250	72.83	27.17
BL-HA2	1250	77.67	22.33
	1400	70.54	29.46

The microstructures of the different porous samples after sintering at 1250ºC are presented in Fig. 2. Independently of the composition of the sample, it is possible to observe an interconnected porous structure with pore sizes in the range of 50 to 500 μm.

The surfaces of the pores appear completely dense suggesting that a high degree of densification has been achieved.

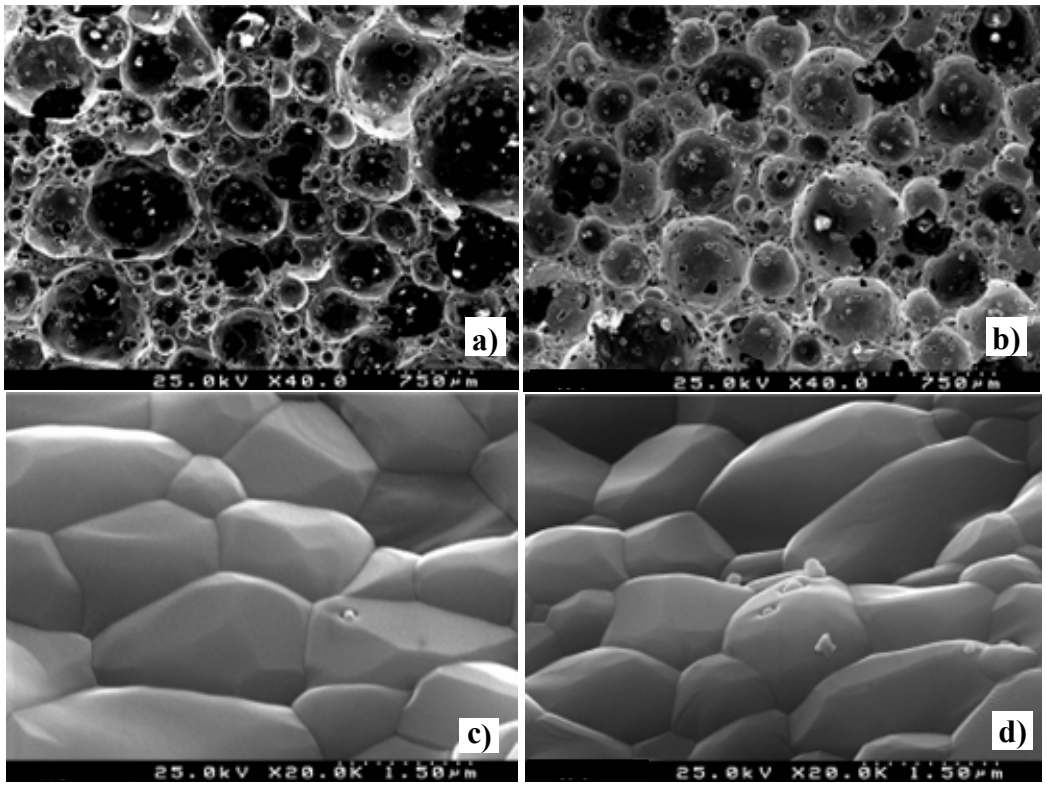

Figure 2. Microstructure of the different samples after sintering at 1250ºC: (a) Mg-(Ca-def-HA); (b) BL-HA2; (c) magnification of a pore surface of Mg-(Ca-def-HA); (d) magnification of a pore surface of BL-HA2.

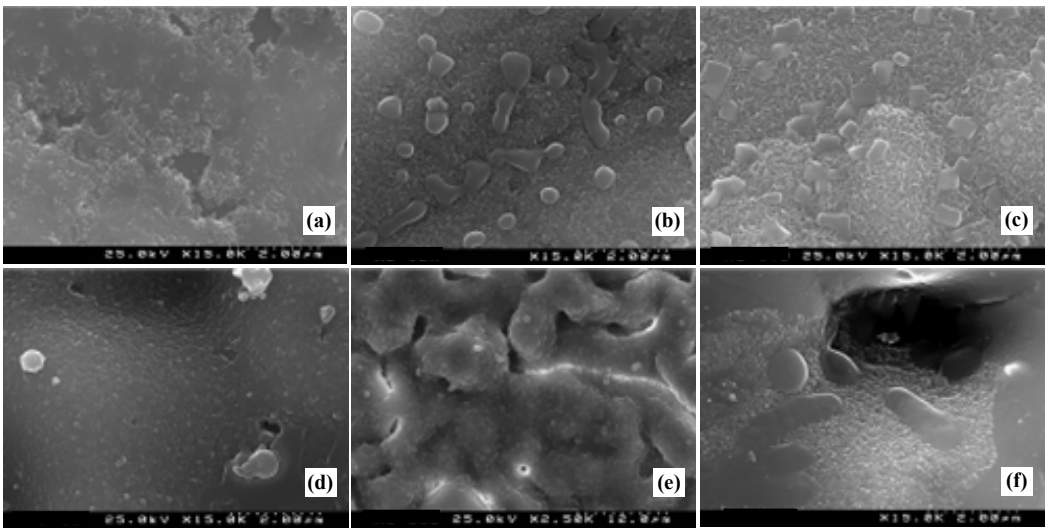

Figure 3. Microstructures of the samples sintered at 1250ºC (a-e) and at 1400ºC (f) after immersion in SBF for different time periods: (a) HA, 3 days; (b) Ca-def-HA, 12

hours; (c) Ca-def-HA, 14 days; (d) Mg-(Ca-def-HA), 3 days; (e) BL-HA2, 30 days and (f) BL-HA2, 1 day.

The morphology observed in Fig. 2 was altered after immersion of the samples in SBF due to the deposition on the surface of the porous samples of an apatitic layer. The micrographs shown in Fig. 3 reveal that this apatitic layer could be observed even after a short period of 1 day, Fig. 3 (f). The BL-HA2 sample sintered at 1250ºC appears completely covered by an amorphous apatitic layer after 30 days of immersion in SBF, Fig. 3 (e), as can be confirmed by XRD pattern (Fig. 4) and FTIR spectrum (Fig. 5).

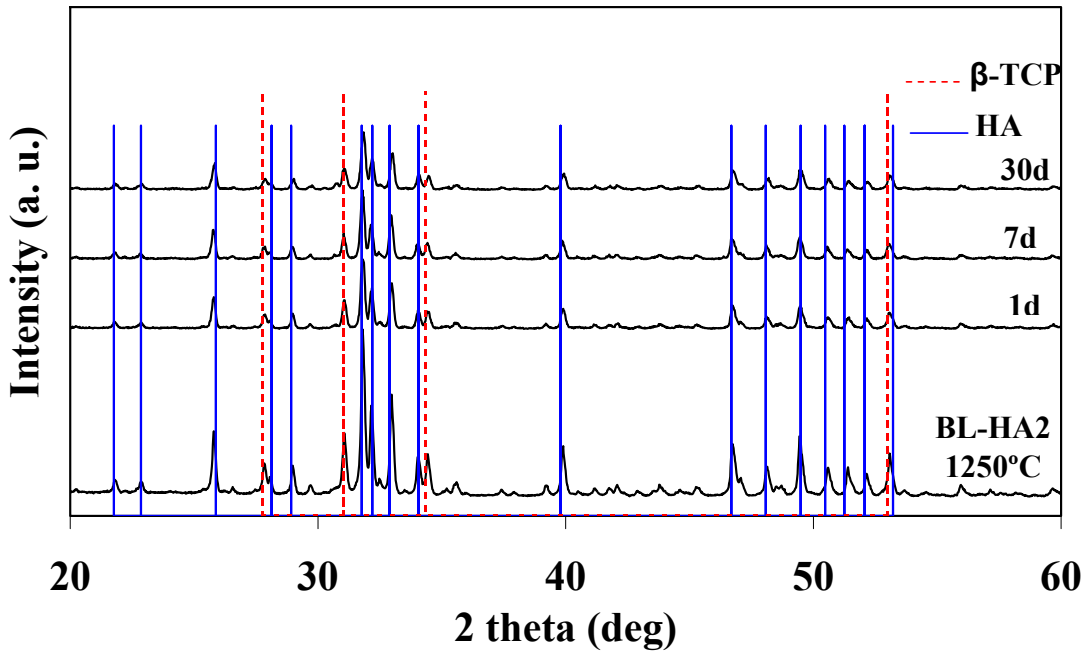

Figure 4. XRD patterns of the sample Mg-(Ca-def-HA) sintered at 1250ºC before and after and immersed in SBF for different time periods (straight line - HA phase, dashed line – β-TCP).

In Fig. 4 it is worth to note that the layer that has been formed is mostly amorphous, as can be deduced from the observed decrease in intensity of the crystalline peaks. The same trend is observed in Fig. 5, where the bands became smoother after immersion in SBF. Similar results have been observed for all the studied compositions. The comparison of the surface morphology of the samples before and after immersion in SBF (Figures 2 and 3), and the XRD and FT-IR results shown in Figures 4 and 5,

respectively, confirm that all the compositions tested in the present work exhibit a good bioactivity *in vitro*.

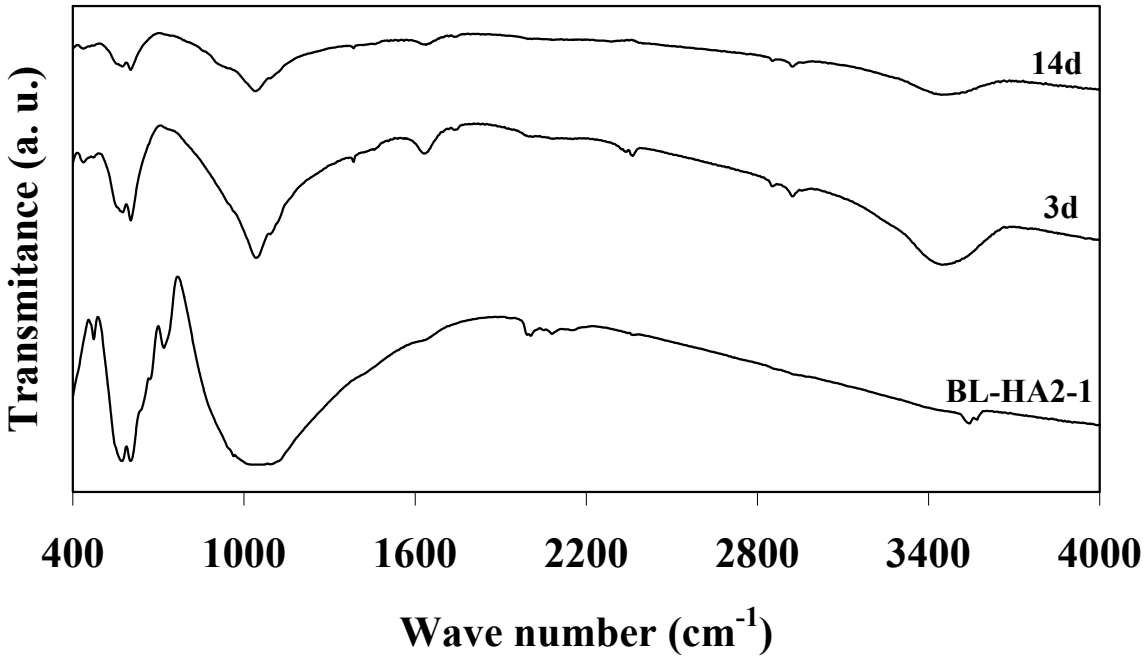

Figure 5. FT-IR spectra for BL-HA2 sintered at 1250ºC before and after immersion in SBF for different time periods.

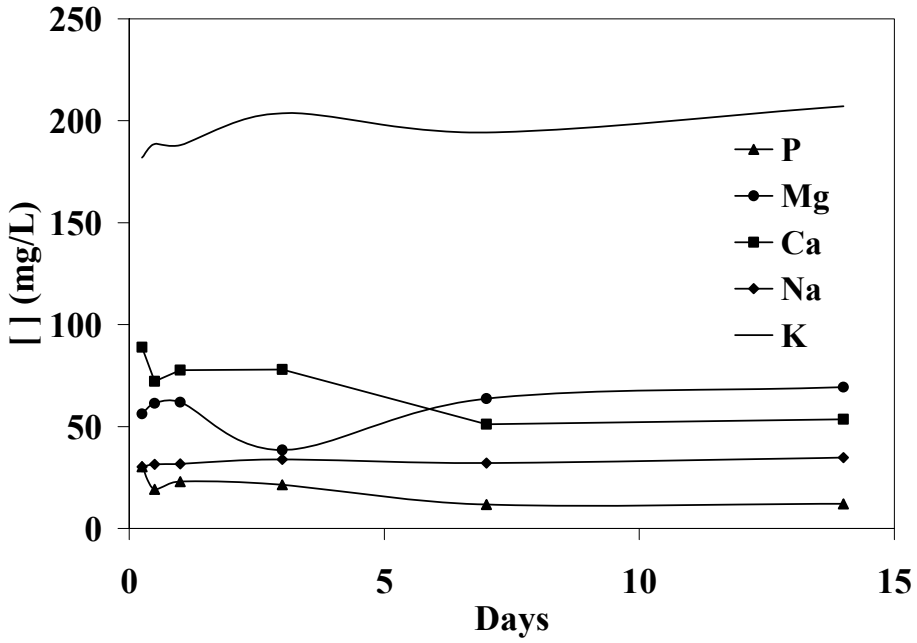

Figure 6. Evolution of the ionic concentrations with the time of immersion in SBF the BL-HA2 sample sintered at 1250ºC.

The evolution of the ionic concentrations in the SBF solutions along the time of immersion of the samples was also monitored in this study. Fig. 6 reports the data for the BL-HA2 sample sintered at 1250ºC, as an example.

It can be seen that the concentrations of both P and Ca firstly decrease and then tend to achieve constant values after 7 days of immersion. This decrease is consistent with the observed deposition of an apatite layer onto the surface of the porous samples and with the establishment of an apparent equilibrium situation, with the rate of depositions being roughly balanced by the rate of dissolution of the solid. The Na concentration remains unchanged along the whole testing period, while a slight increase of [K] is apparent. On the other hand, the Mg concentration seems to first decrease up to the end of the 3rd day, probably due to adsorption effects on the surface of the solid phase, recovering after that, or even overcoming the initial concentration at the end of 7 and 14 days. This last increase might be due to some preferential dissolution of the incorporated Mg in comparison to Ca ions.

It is also well known that the mineral component of bone is similar to hydroxyapatite but contains other ions as impurities.[36-38] Na has been detected in natural bone and tooth mineral as an abundant trace element next to the presence of calcium and phosphorous, playing potential roles in cell adhesion and in bone metabolism and resorption processes.[39,40]

Mg has been attributed a significant impact on the mineralization process and some influence in the HA crystal formation and growth.[41,42] Additionally, the deficiency of Mg in bone has been suggested as a possible risk factor for osteoporosis in humans.[43]

The significance of potassium in the bone composition comes from its great influence on the biomineralization process[44] and in the regulation of biochemical and apatite mineral nucleation processes.[45-46] Therefore, the data shown in Fig. 6 suggest that the tested material is able to release most of the essential elements in the physiological fluids. This, together with the ability to direct bond to the hard tissues makes the material very promising for biomedical applications.

The osteoblast responses to macroporous biological-like apatites and to biological-like apatites/PLGA hybrid materials were accessed by different techniques. The cellular viability/ proliferation studies (Fig. 7A) showed that osteoblasts were viable in the cultures. Concerning the viability/proliferation there was a statistic difference on the metabolization of tetrazolium salt by osteoblasts incubated in the presence of the HA sample, when compared to control ($p<0.05$) osteoblasts. The optical density

(A)

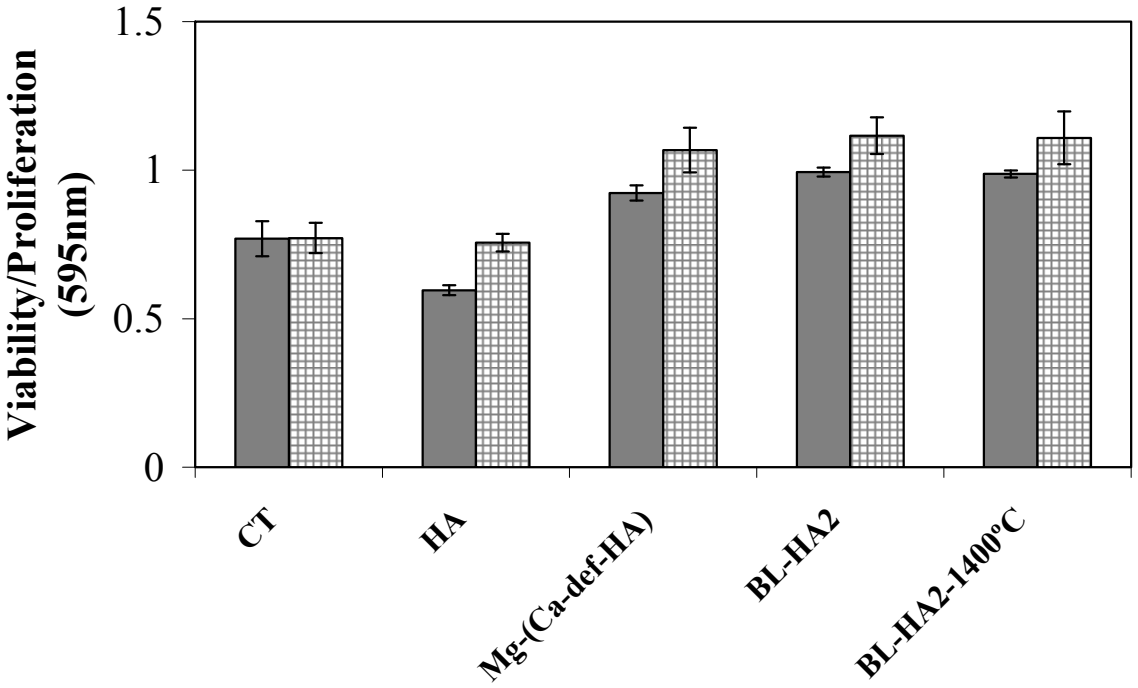
Viability/Proliferation (595nm)
1.5
1
0.5
0
CT
HA
Mg-(Ca-def-HA)
BL-HA2
BL-HA2-1400°C

(B)

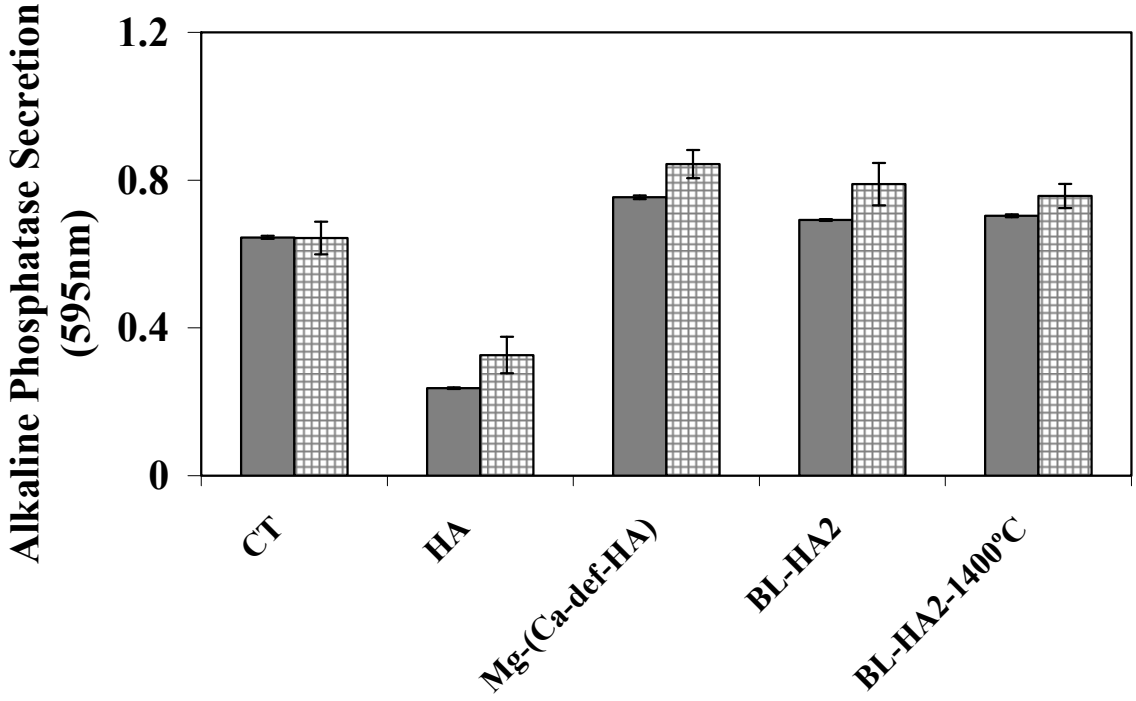
Alkaline Phosphatase Secretion (595nm)
1.2
0.8
0.4
0
CT
HA
Mg-(Ca-def-HA)
BL-HA2
BL-HA2-1400°C

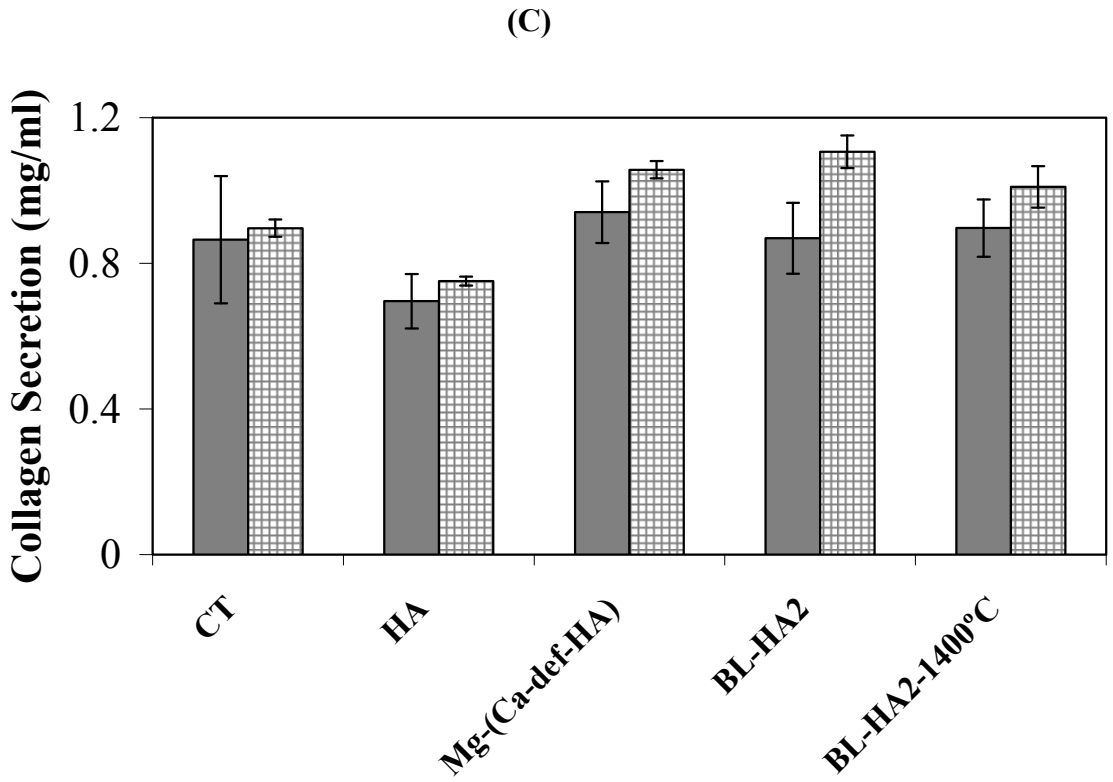

Figure 7. (A) Viability/proliferation. (B) Alkaline phosphatase production. (C) Collagen secretion. $1x10^5$ osteoblasts were plated in the presence of HA, Mg-(Ca-def-HA) and BL-HA2 powders. After 72 h of incubation, viability and proliferation were evaluated by MTT assay (A), alkaline phosphatase production by NBT-BCIP assay (B), and the collagen present in the supernatant was measured by SIRCOL method (C). In (A), (B) and (C) results represent Mean±SD of triplicates from three separate experiments ($P<0.05$). Smooth columns-samples without surface treatment; squared columns-hybrid samples.

measurement of the solubilized formazan crystals showed that osteoblast viability/proliferation slightly increased in the presence of the tested samples, compared to control and particularly compared to pure hydroxyapatite. The collagen secretion and the alkaline phosphatase production showed a tendency to be enhanced in the presence of the tested samples. The measurement of the alkaline phosphatase present in the supernatant of the cultures showed that osteoblasts incubated in the presence of HA decreased significantly ALP production compared to control and to the other samples ($p<0.001$). Relatively to the collagen production, considering a p value <0.05, there was only a tendency of increased collagen production in the presence of the samples. Development of porous bioresorbable materials of high bioactivity, for tissue

engineering, has been the focus of many researchers. The bone formation supporting capacity of any biomaterial is determined by its physico-chemical as well as surface geometrical properties.[47] However, the dissolution rate of the material may interfere, positively or negatively, with the bone tissue response. It has been demonstrated that the active ions released by the dissolution of biomaterials and their exchange with the medium provide alteration in cell proliferation and tissue repair.[48,49] Our results indicated that the dissolution of the tested samples positively stimulate the osteoblasts. Another important characteristic is the osteoblast shape. It is known that cells in a rounded configuration divide at a lower rate than those flattened. Cells that attach themselves to the material but spread little will show lower proliferative rates than those with greater spreading.[50] Under optical microscopy (Fig. 8) it can be observed that the samples allowed flattening and spreading of the osteoblasts, showing adequate cell shape for proliferation and secretion functions.

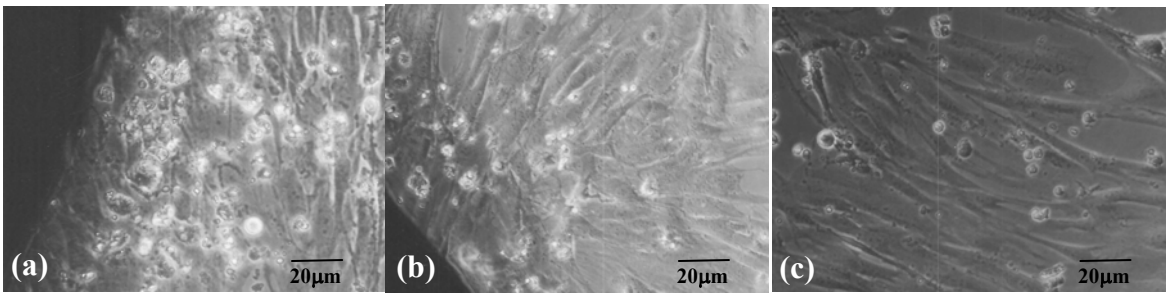

Figure 8. Photomicrographs (400x) of (a) control; (b) Mg-(Ca-def-HA) and (c) BL-HA2 at 1400ºC.

Conclusions

It is possible to conclude that for both the samples, untreated and hybrid materials, an apatitic layer is formed onto their surface even after a short period of 1 day. After 30 days of immersion in SBF the surface of the porous samples appears completely covered by an amorphous apatitic layer.

Together our findings lead to the conclusion that the produced samples are promising materials for bone repair, providing a good environment for osteoblasts.

References

1. Brekke JH, Toth JM, Vogelin E & Jones NF. Principles of tissue engineering governing osteogenic devices. Bioceramics 1998;11:57–62.

2. Ducheyne P & Qiu Q. Bioactive ceramics: the effect of surface reactivity on bone formation and bone cell function. Biomaterials 1999;20:2287–303.

3. Hench L. Bioceramics. J Am Ceram Soc 1998;81:1705–28.

4. Langer R. Tissue Engineering. Mol Ther 2000;1:12–5.

5. de Groot K. Bioceramics consisting of calcium phosphate salts. Biomaterials 1980;1:47–50.

6. Jarcho M. Calcium phosphate ceramics as hard tissue prosthetics. Clin Orthop 1981;157:259 –278.

7. Kent JN, Quinn JH, Zide MF, Guerra LR & Boyne PJ. Alveolar ridge augmentation using nonresorbable hydroxylapatite with or without autogenous cancellous bone. J Oral Maxillofac Surg 1983;41:629–642.

8. Bagambisa FB & Joos U. Preliminary studies on the phenomenological behaviour of osteoblasts cultured on hydroxyapatite ceramics. Biomaterials 1990;11:50–56.

9. Kitsugi T, Yamamuro T, Nakamura T & Oka M. Transmission electron microscopy observations at the interface of bone and four types of calcium phosphate ceramics with different calcium/ phosphorous molar ratios. Biomaterials 1995;16:1101–1107.

10. Bohner M. Calcium orthophosphates in medicine: from ceramics to calcium phosphate cements. Injury 2000;31(Suppl 4):37–47.

11. Klein CP, Driessen AA, de Groot K & van den Hooff A. Biodegradation behaviour of various calcium phosphate materials in bone tissue. J Biomed Mater Res 1983;17:769–784.

12. Klein CP, de Blieck-Hogervorst JM, Wolke JG & de Groot K. Studies of the solubility of different calcium phosphate ceramic particles *in vitro*. Biomaterials 1990;11:509–512.

13. Higashi S, Yamamuro T, Nakamura T, Ikada Y, Hyon SH & Jamshidi K. Polymer-hydroxyapatite composites for biodegradable bone fillers. Biomaterials 1986;7:183–187.

14. Verheyen CC, de Wijn JR, van Blitterswijk CA & de Groot K. Evaluation of hydroxylapatite/poly(L-lactide) composites: Mechanical behaviour. J Biomed Mater Res 1992;26:1277–1296.

15. Kikuchi M, Suetsugu Y, Tanaka J & Akao M. Preparation and mechanical properties of calcium phosphate/copoly-L-lactide composites. J Mater Sci Mater Med 1997;8:361–364.

16. Devin JE, Attawia MA & Laurencin CT. Three-dimensional degradable porous polymer-ceramic matrices for use in bone repair. J Biomater Sci Polym Ed 1996;7:661–699.

17. Thomson RC, Yaszemski MJ, Powers JM & Mikos AG. Hydroxyapatite fiber reinforced poly α-hydroxy ester foams for bone regeneration. Biomaterials 1998;19:1935–1943.

18. Lemos AF & Ferreira JMF. Colloidal Processing and Mechanical Performance of Biological-like Calcium Phosphates Ceramics. Submitted for publication on Journal of American Ceramic Society.

19. Santos C, Luklinska ZB, Clarke RL & Davy KWM. Hydroxyapatite as a filler for dental composite materials: mechanical properties and in vitro bioactivity of composites. J Mater Sci: Mat Med 2001;12:565.

20. Dupraz AMP, De Wijn JR, Van De Meer SAT & de Groot K. Characterization of silane-treated hydroxyapatite powders for use as filler in biodegradable composites. J Biomed Mater Res 1996;30(2):231-238.

21. Tas AC. Synthesis of biomimetic Ca-hydroxyapatite powders at 37ºC in synthetic body fluids, Biomaterials 2000;21:1429-1438.

22. Tas AC. Combustion synthesis of calcium phosphate bioceramic powders, Journal of the European Ceramic Society 2000;20:2389-2394.

23. Kokubo T. Surface chemistry of bioactive glass ceramics. J Non- Cryst Solids 1990;120:138-51.

24. Ohtsuki C, Kokubo T & Yamamuro T. Mechanism of HA formation of CaO-SiO2-P2O5 glasses in simulated body fluid. J Non- Cryst Solids 1992;143:84-92.

25. Li P, Ohtsuki C, Kokubo T, Nakanishi K & Soga N. Apatite formation induced by silica gel in simulated body fluid. J Am Ceram Soc 1992;75:2094-7.

26. Li P, Kangasniemi I, de Groot K & Kokubo T. Bone-like hydroxyapatite induction by a gel-derived titania on a titanium substrate. J Am Ceram Soc 1994;77:1307-12.

27. Li P, Nakanishi K, Kokubo T & de Groot K. Induction and morphology of HA precipitated from metastable simulated body fluids on sol-gel prepared silica. Biomaterials 1993;14:963-8.

28. Li P, Kangasniemi I, de Groot K, Kokubo T & Yli-Urpo AU. Apatite crystallization from metastable calcium phosphate solution on sol-gel prepared silica. J Non-Cryst Solids 1994;168:281-6.

29. Cho SO, Nakanishi K, Kokubo T, Soga N, Ohtsuki C, Nakamura T, Kitsugi T & Yamamuro T. Dependence of apatite formation on silica gel on its structure: effect of heat treatment. J Am Ceram Soc 1995;78:1769-74.

30. Kokubo T, Miyaji F, Kim HM & Nakamura T. Spontaneous formation of bonelike apatite layer on chemically treated titanium metals. J Am Ceram Soc 1996;79:1127-9.

31. Silver IA, Deas J & Erecinska M. Interactions of bioactive glasses with osteoblasts in vitro. Biomaterials 2001;22:175–85.

32. Amaral M, Costa MA, Lopes MA, Silva RF & Santos JD. Si_3N_4- bioglass composites stimulate the MG63 osteoblast-like cells. Biomaterials 2002;23:4897–906.

33. Meleti Z, Shapiro IM & Adams CS. Inorganic phosphate induces apoptosis of osteoblastic-like cells in culture. Bone 2000;27:359–66.

34. Klein B, Bem-Bassat H & Solomon V. Structurally different bisphosphonates exert oposite effects in Alp. J Cell Biochem 1998;68:186–94.

35. Tullberg-Reinert H & Jundt G. In situ measurement of collagen synthesis by human bone cells with Sirius-Red based colorimetric microassay. Histochem Cell Biol 1999;112:271–6.

36. Legeros RZ. Calcium phosphates in oral biology and medicine. Karger, Basel 1991.

37. Daculsi G, Bouler J-M & Legeros RZ. Adaptive crystal formation in normal and pathological calcifications in synthetic calcium phosphate and related biomaterials. Int Rev Cytology 1997;172:129-91.

38. Dorozhkin SV. Calcium orthophosphates. J Mater Sci 2007;42:1061–95.

39. Itoh R & Suyama Y. Sodium excretion in relation to calcium and hydroxyproline excretion in a healthy Japanese population. Am J Clin Nutr 1996;63:735-40.

40. Ginty F, Flynm A & Cashman KD. The effect of dietary sodium intake on biochemical markers of bone metabolism in young women. Br J Nutr 1998;79:343-50.

41. Ergun C, Webster TJ, Bizios R & Doremus RH. Hydroxylapatite with substituted magnesium, zinc, cadmium, and yttrium. I. Structure and microstructure. J Biomed Mater Res 2002;59(2):305-11.

42. Creedon A, Flynm A & Cashman A. The effect of moderately and severely restricted dietary magnesium intakes on bone composition and bone metabolism. Br J Nutr 1999;82:63-9.

43. Rude RK. Magnesium Deficiency: A Cause of Heterogenous Disease in Humans. J Bone Miner Res 1998;13(4):749-58.

44. Wiesmann HP, Plate U, Zierold K & Hohling HJ. Potassium is involved in apatite biomineralization. J Dent Res 1998;77(8);654-57.

45. Suelter CH. Enzymes activated by monovalent cations. Science 1970;168:789-95.

46. Hohling HJ, Mishima H, Kozawa Y, Daimon T, Barckhaus RH & Richter KD. Microprobe analyses of the potassium calcium distribution relationship in predentin. Scan Microsc Int 1991;5:247-53.

47. Roether JA, Boccaccini AR, Hench LL, Maquet V, Gautier S & Jerôme R. Development and in vitro characterisation of novel bioresorbable and bioactive composite materials based on polylactide foams and Bioglass® for tissue engineering applications. Biomaterials 2002;23[18]:3871-3878.

48. Sepulveda P, Jones JR & Hench LL. In vitro dissolution of melt-derived 45S5 and sol-gel derived 58S bioactive glasses. J Biomed Mat Res 2002;61:301-311.

49. Xynos ID, Edgard AJ, Buttery LDK & Hench LL. Gene-expression profiling of human osteoblasts following treatment with the ionic products of Bioglass® 45S5 dissolution. J Biomed Mat Res 2001;55:151-157.

50. Verne E, Bosetti M, Brovarone CV, Moisescu C, Lupo F, Sapriano S & Cannas M. Fluoroapatite glass-ceramic coatings on alumina: structural, mechanical and biological characterisation. Biomaterials 2002;23[16]:3395-3403.

Chapter 7

Conclusions

In the present work five different calcium phosphate compositions, including pure HA, biphasic mixtures of HA+β-TCP, undoped and co-substituted with essential elements found in mineral bone composition were prepared. The pure stoichiometric HA with a Ca/P ratio of 1.67 has shown thermal stability up to 1300ºC, tending to partially transform into α-TCP above this temperature. Undoped calcium deficient apatites (Ca-def-HA) with Ca/P ratio = 1.62 resulted in the formation of biphasic (HA + β-TCP), or triphasic (HA+β-TCP+α-TCP) mixtures, upon heat treating above 700ºC or 1150ºC, respectively. Mg-substituted calcium deficient apatites (Mg-(Ca-def-HA)) with a Ca/P ratio = 1.62 has led also to the formation of biphasic (HA + β-TCP) or triphasic (HA+β-TCP+α-TCP) mixtures with enhanced thermal stability, because magnesium stabilized the β-TCP phase and the occurrence of triphasic mixtures (formation of α-TCP) was delayed to 1350ºC. The co-substitution of different levels of essential trace elements to obtain biological like apatites (BL-HA1 and BL-HA2) further enhanced their thermal stability. These co-substituted apatite powders did not transform into undesirable α-TCP phase until 1400ºC, leading to the formation of noticeable amounts of desirable β-TCP.

The prepared powder compositions have shown to be suitable for colloidal processing enabling to prepare suspensions with a concentration of solids as high as 60 vol%. Strong and high reliable monophasic (HA) and biphasic (HA + β-TCP) bioceramics could be obtained, upon sintering stoichiometric HA (1250ºC), or Mg-containing compositions (1350ºC), attesting the benefits of colloidal processing for the ultimate material properties.

The synergetic combinations of traditional new consolidation methods from well dispersed and high concentrated suspensions enable to obtain biomaterials inspired in the bone model and attempting to mimic the structure, the mineral composition and the properties of bone in order to develop reliable synthetic bone grafts. Combining foaming and starch consolidation methods enables the preparation of macroporous HA structures with pores larger than 100 μm. Egg white enables to directly consolidate foamed suspensions into rigid and highly porous materials, with pores size in the range of a few hundred microns and the degree of interconnectivity could be modelled by the added amount of egg white. The trabecular and the complete bone structure could be mimicked by using the polymeric sponge method alone or by combining slip casting

(for the cortical part) with the polymeric sponge method or with the foaming method (for the trabecular part).

Bone like hydroxyapatite (BL-HA) / poly(D,L-lactide-*co*-glycolide) (PLGA) hybrid materials have been developed using γ -methacryloxypropyltrimethoxy- silane (γ –MPS) as silane-coupling agent between the inorganic and organic phases. An electrostatic/chemical interaction between the silane-coupling agent and BL-HA surface has been achieved more effectively by means of silanization using a modified polar method. These novel BL-HA/PLGA hybrid materials may find use for bone regeneration applications with simultaneous local delivery of therapeutic molecules.

BL-HA/PLGA hybrid materials induce the formation of an apatitic carbonate layer on its surface when immersed in SBF, are cytocompatible and promote proliferation of osteoblastic cells. The results obtained showed that this material can be envisaged as an alternative to traditional calcium phosphates.

In conclusion, this work opens good perspectives for the application of BL-HA/PLGA hybrid materials in the field of bone regeneration, both as bone graft substitutes and drug delivery matrixes.

Chapter 8

Prospects for future work

The present work has contributed to the advancement of the state-of-the-art, disclosing new calcium phosphate compositions and proposing new approaches to process the powders and to mimic the structure, the mineral composition and the properties of bone in order to develop reliable synthetic bone grafts. The as developed materials have shown good mineralization properties when immersed in SBF, and in interesting *in vitro* biocompatibility in cell culture tests. However, much work still needs to be done by testing the materials in animal models to confirm their suitability for the intended applications in bone regeneration and maxillofacial surgeries. The *in vivo* performance of the new calcium phosphate compositions and of the hybrid BL-HA/PLGA composites needs to be compared to draw more sound conclusions about the design of better bone graft substitutes. Moreover, the hybrid BL-HA/PLGA composites offer new opportunities to design biomaterials with new functionalities, namely, that can act as synthetic bone graft substitutes and as controlled drug delivery systems. However, to achieve this goal, plenty of future work needs to be carried out to access the interactions between the drug and the inorganic and organic components, study the release kinetics and set the drug concentrations and the suitable experimental and chirurgical procedures. All of these future works need to be done in close collaborations with professional experts from hospitals.